

# PACIFIC EARTHQUAKE ENGINEERING RESEARCH CENTER

## A Full-Scale, Single-Column Bridge Bent Tested by Shake-Table Excitation

**Matthew J. Schoettler**

Department of Civil and Environmental Engineering  
University of California, Berkeley

**José I. Restrepo**

**Gabriele Guerrini**

**David E. Duck**

Department of Structural Engineering  
University of California, San Diego

**Francesco Carrea**

Tecnomare S.p.A

PEER Report No. 2015/02

Pacific Earthquake Engineering Research Center  
Headquarters at the University of California, Berkeley

@Seismicisolation

### Disclaimer

The opinions, findings, and conclusions or recommendations expressed in this publication are those of the author(s) and do not necessarily reflect the views of the study sponsor(s) or the Pacific Earthquake Engineering Research Center.

# **A Full-Scale, Single-Column Bridge Bent Tested by Shake-Table Excitation**

**Matthew J. Schoettler**

Department of Civil and Environmental Engineering  
University of California, Berkeley

**José I. Restrepo**

Department of Structural Engineering  
University of California, San Diego

**Gabriele Guerrini**

Department of Structural Engineering  
University of California, San Diego

**David E. Duck**

Department of Structural Engineering  
University of California, San Diego

**Francesco Carrea**

Tecnomare S.p.A

PEER Report No. 2015/02

Pacific Earthquake Engineering Research Center  
Headquarters at the University of California, Berkeley

March 2015

**@Seismicisolation**

@Seismicisolation

## **ABSTRACT**

A landmark test of a reinforced concrete bridge column was conducted on the George E. Brown, Jr. Network for Earthquake Engineering Simulation's shake table at the University of California, San Diego. This was the first full-scale bridge column, designed to current US seismic design provisions, to be tested under dynamic conditions on a shake-table. Caltrans seismic design guidelines were followed for the design and detailing of the 1.22-m- (4-ft-) diameter, 7.32-m- (24-ft-) tall column. The flexure-dominated specimen was subjected to ten significant ground motions and tested to impending collapse. The results can provide the basis for comparison with a small-scale shake table test to evaluate the reliability of small scale testing and significance of scale effects under dynamic conditions and also provide a unique dataset that can be used to validate nonlinear computational models. The column exhibited a ductile response with a well-formed plastic hinge within one column diameter from the base. Concrete spalling was observed after a simulated design-level earthquake. Longitudinal bar buckling, longitudinal bar fractures, and concrete core crushing were mechanisms of deteriorating strength and stiffness, but were induced in the later stages of testing after stable response to repeated demands well beyond the design-level event.

@Seismicisolation

## **ACKNOWLEDGMENTS**

This project was sponsored by the Pacific Earthquake Engineering Research Center's Program of Applied Earthquake Engineering Research of Lifelines Systems supported by the California Energy Commission, California Department of Transportation, and the Pacific Gas and Electric Company. Additional support was provided from the Federal Highway Administration (FHWA) contract DTFH61-07-C-00031.

This work made use of the Earthquake Engineering Research Centers Shared Facilities supported by the National Science Foundation (NSF), under award number EEC-9701568 through the Pacific Earthquake Engineering Research Center (PEER).

Any opinions, findings, and conclusions or recommendations expressed in this material are those of the authors and do not necessarily reflect those of NSF or the FHWA.

@Seismicisolation

## CONTENTS

<b>ABSTRACT</b> .....	iii
<b>ACKNOWLEDGMENTS</b> .....	v
<b>TABLE OF CONTENTS</b> .....	vii
<b>LIST OF TABLES</b> .....	ix
<b>LIST OF FIGURES</b> .....	xi
<b>1 INTRODUCTION</b> .....	1
<b>2 LITERATURE REVIEW</b> .....	3
<b>3 DESIGN OF THE EXPERIMENT</b> .....	5
<b>4 TEST SET-UP</b> .....	9
<b>4.1 Column</b> .....	11
<b>4.2 Footing</b> .....	11
<b>4.3 Superstructure Mass</b> .....	12
<b>5 MATERIAL PROPERTIES</b> .....	13
<b>5.1 Concrete</b> .....	13
<b>5.2 Reinforcing Steel</b> .....	15
<b>5.3 Footing and Superstructure Materials</b> .....	17
<b>6 TEST PROTOCOL</b> .....	19
<b>7 INSTRUMENTATION AND DATA PROCESSING</b> .....	27
<b>7.1 Strain Gauges</b> .....	27
7.1.1 Longitudinal Strain Gauges .....	27
7.1.2 Transverse Strain Gauges .....	27
7.1.3 Safety Restraint Strain Gauges .....	27
<b>7.2 Linear Voltage Displacement Transducers</b> .....	28
<b>7.3 String Potentiometers</b> .....	31
<b>7.4 Accelerometers</b> .....	33
<b>7.5 GPS System</b> .....	33
<b>7.6 Video Cameras</b> .....	33
<b>7.7 Data Acquisition System</b> .....	34

7.8	Control System.....	34
7.9	Data Processing .....	35
8	TEST RESULTS .....	37
8.1	Test EQ1 .....	37
8.2	Test EQ2 .....	43
8.3	Test EQ3 .....	49
8.4	Test EQ4 .....	55
8.5	Test EQ5 .....	60
8.6	Test EQ6 .....	65
8.7	Test EQ7 .....	70
8.8	Test EQ8 .....	75
8.9	Test EQ9 .....	81
8.10	Test EQ10 .....	85
9	SUMMARY AND CONCLUSIONS .....	91
9.1	Summary.....	91
9.2	Conclusions.....	99
	REFERENCES.....	101
	APPENDIX A        INSTRUMENTATION LAYOUT .....	103

## LIST OF TABLES

Table 5.1	Column as-built concrete mix proportions per cubic yard of concrete.....	13
Table 5.2	Column concrete compressive strength.....	14
Table 5.3	Measured reinforcement strengths.....	16
Table 6.1	Idealized, monotonic response of the analytical model.....	20
Table 6.2	Idealized, monotonic response of the analytical model in normalized units.....	20
Table 6.3	Ground motion selections and scale factors.....	20
Table 6.4	Ground motion peak ground parameters.....	21
Table 6.5	Ground motion selection and scale factors for extended testing.....	21
Table 6.6	Ground motion peak ground parameters for extended testing.....	21
Table 7.1	Shake table capacities.....	34
Table 9.1	Peak response quantities.....	91
Table 9.2	Dynamic properties from white-noise tests.....	94

@Seismicisolation

## LIST OF FIGURES

Figure 3.1	Column reinforcing details.....	6
Figure 3.2	Bundled hoops with alternating butt-welds.....	7
Figure 4.1	Test specimen.....	10
Figure 4.2	Collapse restraint mechanism.....	10
Figure 4.3	Test set-up.....	11
Figure 5.1	Column concrete stress-strain relationship of individual samples.....	15
Figure 5.2	Column longitudinal reinforcement stress-strain relationship.....	16
Figure 5.3	Column transverse hoop reinforcement stress-strain benchmarking.....	17
Figure 6.1	Desired ground motions in terms of (a) pseudo-acceleration and (b) displacement response spectra at 5% damping ratio.....	23
Figure 6.2	EQ1 (a) pseudo-acceleration and (b) displacement response spectra at 5% damping ratio.....	24
Figure 6.3	EQ2 and EQ4 (a) pseudo-acceleration and (b) displacement response spectra at 5% damping ratio.....	24
Figure 6.4	EQ3 and EQ6 (a) pseudo-acceleration and (b) displacement response spectra at 5% damping ratio.....	25
Figure 6.5	EQ5 (a) pseudo-acceleration and (b) displacement response spectra at 5% damping ratio.....	25
Figure 6.6	EQ7 (a) pseudo-acceleration and (b) displacement response spectra at 5% damping ratio.....	26
Figure 6.7	EQ8, EQ9, and EQ10 (a) pseudo-acceleration and (b) displacement response spectra at 5% damping ratio.....	26
Figure 7.1	Curvature, shear, and fixed-end rotation LVDTs on the (a) South and (b) North faces.....	28
Figure 7.2	Column-to-top mass LVDTs.....	29
Figure 7.3	Bond-slip bracket installation: (a) assembly, (b) placed on longitudinal bars, (c) encapsulated with debonding foam, and (d) final installation.....	30
Figure 7.4	Dilation LVDT installation: (a) target welded to a transverse hoop, (b) LVDT assembly, and (c) locations on the West face.....	31

Figure 7.5	Horizontal string potentiometer locations.....	32
Figure 7.6	Inclined string potentiometer locations.....	32
Figure 8.1	Column displacement during Test EQ1.....	37
Figure 8.2	Column base East face during Test EQ1 at (a) peak West displacement, (b) peak East displacement, and (c) post-test.....	38
Figure 8.3	Column response during Test EQ1 in terms of base moment and curvature.....	40
Figure 8.4	Column response during Test EQ1 in terms of base shear and drift ratio.....	40
Figure 8.5	Longitudinal reinforcement tensile strain demand during Test EQ1.....	41
Figure 8.6	Longitudinal reinforcement bond slip during Test EQ1.....	41
Figure 8.7	Transverse hoop reinforcement tensile strain demand during Test EQ1.....	42
Figure 8.8	Curvature profile at peak and residual displacements during Test EQ1.....	43
Figure 8.9	Column displacement during Test EQ2.....	44
Figure 8.10	Column base East face during Test EQ2 at (a) peak West displacement, (b) East positive displacement, and (c) post-test .....	44
Figure 8.11	Column response during Test EQ2 in terms of base moment and curvature.....	45
Figure 8.12	Column response during Test EQ2 in terms of base shear and drift ratio. ....	45
Figure 8.13	Longitudinal reinforcement tensile strain demand during Test EQ2.....	47
Figure 8.14	Longitudinal reinforcement bond slip during Test EQ2.....	47
Figure 8.15	Transverse hoop reinforcement tensile strain demand during Test EQ2.....	48
Figure 8.16	Curvature profile at peak and residual displacements during Test EQ2.....	48
Figure 8.17	Column displacement during Test EQ3.....	49
Figure 8.18	Column base East face during Test EQ3 at (a) peak West displacement, (b) peak East displacement, and (c) post-test.....	50
Figure 8.19	Column base West face after Test EQ3.....	50
Figure 8.20	Column response during Test EQ3 in terms of base moment and curvature.....	52
Figure 8.21	Column response during Test EQ3 in terms of base shear and drift ratio. ....	52
Figure 8.22	Longitudinal reinforcement tensile strain demand during Test EQ3.....	53
Figure 8.23	Longitudinal reinforcement bond slip during Test EQ3.....	53
Figure 8.24	Transverse hoop reinforcement tensile strain demand during Test EQ3.....	54
Figure 8.25	Curvature profile at peak and residual displacements during Test EQ3.....	54
Figure 8.26	Column displacement during Test EQ4.....	55
Figure 8.27	Column base East face during Test EQ4 at (a) peak West displacement, (b) peak East displacement, and (c) post-test.....	56

Figure 8.28	Column response during Test EQ4 in terms of base moment and curvature.....	56
Figure 8.29	Column response during Test EQ4 in terms of base shear and drift ratio. ....	57
Figure 8.30	Longitudinal reinforcement tensile strain demand during Test EQ4.....	58
Figure 8.31	Longitudinal reinforcement bond slip during Test EQ4.....	58
Figure 8.32	Transverse hoop reinforcement tensile strain demand during Test EQ4.....	59
Figure 8.33	Curvature profile at peak and residual displacements during Test EQ4.....	59
Figure 8.34	Column displacement during Test EQ5.....	61
Figure 8.35	Column base East face during Test EQ5 at (a) peak West displacement, (b) peak East displacement, and (c) post-test.....	61
Figure 8.36	Column response during Test EQ5 in terms of base moment and curvature.....	62
Figure 8.37	Column response during Test EQ5 in terms of base shear and drift ratio. ....	62
Figure 8.38	Longitudinal reinforcement tensile strain demand during Test EQ5.....	63
Figure 8.39	Longitudinal reinforcement bond slip during Test EQ5.....	63
Figure 8.40	Transverse hoop reinforcement tensile strain demand during Test EQ5.....	64
Figure 8.41	Curvature profile at peak and residual displacements during Test EQ5.....	64
Figure 8.42	Column displacement during Test EQ6.....	66
Figure 8.43	Column base East face during Test EQ6 at (a) peak West displacement, (b) peak East displacement, and (c) post-test.....	67
Figure 8.44	Column response during Test EQ6 in terms of base moment and curvature.....	67
Figure 8.45	Column response during Test EQ6 in terms of base shear and drift ratio. ....	68
Figure 8.46	Longitudinal reinforcement tensile strain demand during Test EQ6.....	68
Figure 8.47	Longitudinal reinforcement bond slip during Test EQ6.....	69
Figure 8.48	Transverse hoop reinforcement tensile strain demand during Test EQ6.....	69
Figure 8.49	Curvature profile at peak and residual displacements during Test EQ6.....	70
Figure 8.50	Column displacement during Test EQ7.....	71
Figure 8.51	Column base East face during Test EQ7 at (a) peak West displacement, (b) peak East displacement, and (c) post-test.....	72
Figure 8.52	Column response during Test EQ7 in terms of base moment and curvature.....	72
Figure 8.53	Column response during Test EQ7 in terms of base shear and drift ratio. ....	73
Figure 8.54	Longitudinal reinforcement tensile strain demand during Test EQ7.....	73
Figure 8.55	Longitudinal reinforcement bond slip during Test EQ7.....	74
Figure 8.56	Transverse hoop reinforcement tensile strain demand during Test EQ7.....	74
Figure 8.57	Curvature profile at peak and residual displacements during Test EQ7.....	75

Figure 8.58	Column displacement during Test EQ8.....	77
Figure 8.59	Column base East face during Test EQ8 at (a) peak West displacement, (b) peak East displacement, and (c) post-test.....	77
Figure 8.60	Column response during Test EQ8 in terms of base moment and curvature.....	78
Figure 8.61	Column response during Test EQ8 in terms of base shear and drift ratio.....	78
Figure 8.62	Longitudinal reinforcement tensile strain demand during Test EQ8.....	79
Figure 8.63	Longitudinal reinforcement bond slip during Test EQ8.....	79
Figure 8.64	Transverse hoop reinforcement tensile strain demand during Test EQ8.....	80
Figure 8.65	Curvature profile at peak and residual displacements during Test EQ8.....	80
Figure 8.66	Column displacement during Test EQ9.....	82
Figure 8.67	Column base East face during Test EQ9 at (a) peak West displacement, (b) peak East displacement, and (c) post-test.....	82
Figure 8.68	Column response during Test EQ9 in terms of base moment and curvature.....	83
Figure 8.69	Column response during Test EQ9 in terms of base shear and drift ratio.....	83
Figure 8.71	Transverse hoop reinforcement tensile strain demand during Test EQ9.....	84
Figure 8.72	Curvature profile at peak and residual displacements during Test EQ9.....	85
Figure 8.73	Column displacement during Test EQ10.....	86
Figure 8.74	Column base East face during Test EQ10 at (a) peak West displacement, (b) peak East displacement, and (c) post-test.....	87
Figure 8.75	Column response during Test EQ10 in terms of base moment and curvature.....	87
Figure 8.76	Column response during Test EQ10 in terms of base shear and drift ratio.....	88
Figure 8.77	Longitudinal reinforcement strain demand during Test EQ10.....	88
Figure 8.78	Transverse hoop reinforcement strain demand during Test EQ10.....	89
Figure 9.1	Drift ratios achieved during tests.....	92
Figure 9.2	Displacement components at peak displacements.....	93
Figure 9.3	Column dilation.....	94
Figure 9.4	Dynamic properties from white-noise tests.....	95
Figure 9.5	Column base East face post test: (a) EQ1, (b) EQ2, (c) EQ3, (d) EQ4, (e) EQ5, (f) EQ6, (g) EQ7, (h) EQ8, (i) EQ9, and (j) EQ10.....	96
Figure 9.6	Extracted longitudinal reinforcement.....	97
Figure 9.7	South face of the column post-test.....	98
Figure A.1	Longitudinal strain gauge locations on the East face of the column.....	105

Figure A.2	Longitudinal strain gauge locations on the West face of the column .....	106
Figure A.3	Transverse strain gauge locations on the East face of the column. ....	107
Figure A.4	Transverse strain gauge locations on the West face of the column.....	108
Figure A.5	Curvature and fixed-end rotation LVDT locations on the South face of the column.....	109
Figure A.6	Curvature and fixed-end rotation LVDT locations on the North face of the column.....	110
Figure A.7	Inclined shear LVDT locations on the South face of the column.....	111
Figure A.8	Horizontal shear LVDT locations on the South face of the column.....	112
Figure A.9	Transverse hoop LVDT locations on the East face of the column. ....	113
Figure A.10	Transverse hoop LVDT locations on the West face of the column. ....	114
Figure A.11	Horizontal spring potentiometer and GPS antennae locations. ....	115
Figure A.12	Inclined spring potentiometer and column-to-top mass LVDT locations. ....	116
Figure A.13	Footing and table accelerometer locations and reference GPS antenna. ....	117
Figure A.14	Column and mass block accelerometer locations. ....	118
Figure A.15	Mass block accelerometer and wire pot locations for tests on 9/20/2010. ....	119
Figure A.16	Mass block accelerometer and wire pot locations for tests on 9/21/2010. ....	120
Figure A.17	Bond-slip LVDT locations and instrumentation locations on the inclined safety restraints. ....	121

@Seismicisolation

# 1 Introduction

Bridge failures during earthquakes in the 1970s through 1990s generated substantial investigations into the causes of unacceptable performance [Penzen and Clough 1971; Mellon 1988; Abolhassan et al. 1989; Housner et al. 1994; and Kawashima 1995]. Experimental investigations sought and identified successful retrofit techniques [Priestley et al. 1996], which were duly implemented through Caltrans' Seismic Retrofit Program. In parallel, seismic design guidelines evolved with these advances. A major philosophical change occurred as designs adopted a ductility approach to achieve certain performance objectives [Unjoh et al. 2002; Marquez 2010].

To achieve the desired performance levels, designs incorporate details to ensure plastic deformations are sustainable under cyclic loading. Experimental investigations have and continue to provide much needed evidence as to what constitutes safe and sustainable levels. Shen et al. [2006] asserted: "The advancing of seismic design methodology and specifications is closely associated with findings and verifications produced by laboratory testing." These experiments are the basis for empirically-based design equations and confidence in the adopted design philosophy.

To provide assurance that the desired and sustainable behavior is achieved through current seismic design guidelines, a 1.22-m- (4-ft-) diameter reinforced concrete (RC) bridge column was tested under dynamic loading conditions with simulated ground motions produced by a shake table. The single cantilevered column had a nonlinear response dominated by flexural yielding at the base. Test-specimen design was based on current Caltrans design specifications [Caltrans 2006a]. To mobilize inertia forces, a concrete block weighing 2.32 MN (521.9 kip) was cast on top of the 7.32-m (24-ft) column.

Test objectives included subjecting the column to lateral displacement demands at targeted values and then monitoring the dynamic response. Seismic performance under current design practices and analysis methods were of primary interest in this project. For a single-column bent supported on a fixed foundation, the design ductility is less than or equal to four for the direction transverse to the bridge deck [Caltrans 2006a]. Resistance to forces generated at this design level was investigated in the third test, EQ3. Experimental results at higher and lower level demands are also presented.

The test specimen was densely instrumented to obtain high-quality response measurements under various ground motions. A total of ten earthquake simulations were conducted. Tests were conducted over a span of two days on the NEES shake table at the

University of California, San Diego's Englekirk Structural Engineering Center. These tests provided a unique dataset that can be used to validate nonlinear computational models. The first six tests served as the benchmark for a blind prediction competition [Terzic et al. 2015]. Predictions of basic demand parameters from forty-one teams showed significant scatter and provided needed insight on the uncertainty quantification in analytical modeling.

## 2 Literature Review

Only one prior test program has reported shake table tests of full-scale bridge columns. Kawashima et al. [2009] investigated the failure mechanism of three full-scale specimens. Of these specimens, only one was designed according to current Japanese standards. An unanticipated failure of this column involved the flow of crushed core concrete through the reinforcing cage. Sasaki and Kawashima [2009] reported shear strength scale effects under dynamic loads utilizing the same test program.

Other full-scale investigations of RC bridges have been limited to *in situ* testing or pseudo-static tests. Douglas and Buckle [1985] performed snap-back tests on two bridges in New Zealand within the elastic range to determine dynamic properties. Eberhard et al. [1993] performed *in situ* cyclic-load testing in the transverse direction of a three-span bridge built before 1984. They noted a large abutment contribution to the system lateral stiffness resulting from the continuous superstructure and bearing details. Gilani et al. [1995] field tested a seismically isolated bridge with snap-back tests and forced vibration. The dynamic properties obtained from these tests were reported to match closely with nonlinear dynamic simulations.

Pseudo-static tests typically included evaluation of specimen designed to earlier design standards and proposed retrofit strategies. Ohtaki et al. [1996] compared a full-scale column built to pre-1971 design standards and a retrofitted specimen.. Stone and Cheok [1989] studied scale effects under pseudo static testing with one-sixth-scale columns for both flexure- and shear-critical scenarios. Gamble et al. [1995] performed pseudo-static testing of full-scale columns to pre-standard details (as-built and retrofitted). Priestley et al. [1992] tested a full-scale column with a lap splice in the critical region.

Significant numbers of small-scale columns have been subjected to shake table testing or pseudo-static loading. Extensive literature reviews of these tests can be found in Lehman et al. [1998] and Hachem et al. [2003].

@Seismicisolation

### 3 Design of the Experiment

The column was designed according to Caltrans Seismic Design Criteria [Caltrans 2006a] and Bridge Design Specifications [Caltrans 2004], and is representative of single-column bents commonly found in California. Uni-axial shake table excitation subjected the test specimen to loading in the table's east-west direction only. Boundary conditions, fixed at the base and free at the top, corresponded to a bent subjected to ground excitation in the transverse direction of the bridge deck. The idealized condition neglects the complexities of system behavior, such as multiple-span interaction through deck coupling, superstructure restraint in the longitudinal direction of the deck, and foundation or abutment response.

The 1.22-m- (4-ft-) diameter column spanned 7.32 m (24 ft) above the footing. With a height-to-diameter aspect ratio of six, the test specimen was intended to respond in the nonlinear range with predominant flexural behavior. A capacity-based design aimed to preclude other failure modes. A design ductility of four was established for the test specimen based on the Seismic Design Criteria [Caltrans 2006a]. For this scenario, the probabilistic design spectrum corresponded to a 5% in 50 years probability of exceedance [Caltrans 2006a] and was obtained through ARS Online [Caltrans 2010].

Longitudinal reinforcement consisted of eighteen, Grade 60 ASTM A706 [2009b], 35.8-mm-diameter (#11) bars concentrically spaced around the column in a single layer. Butt-welded, double, Grade 60 ASTM A706 [2009b], 15.9-mm-diameter (#5) hoops, spaced at 152 mm (6 in.) on-center, were used as transverse reinforcement. The term "double" refers to two hoops bundled together at each 152-mm spacing; see Figure 3.2. Butt-weld locations alternate on opposite sides (north and south) of the column. Clear cover to the hoops was 51 mm (2 in.). Column reinforcement layout and the test specimen's geometry are provided in Figure 3.1. Complete construction drawings are available on the NEEShub data repository website [NEES 2011].

A longitudinal reinforcement ratio,  $\rho_l$ , of 1.55%, typical of current practice, was provided for the column. The transverse reinforcement provided a volumetric confining ratio,  $\rho_s$ , of 0.95%. Reinforcement complied with minimum and maximum requirements [Caltrans 2004; Caltrans 2006a].

The as-built estimated axial load at the column base was 2.53 MN (570 kip). Accounting for the measured concrete strength at day one of testing, this axial load produced an axial load

ratio,  $N/A_g f'_c$ , of 5.3%, where  $N$  is the estimated axial load,  $A_g$  is the gross cross-sectional area of the column, and  $f'_c$  is the concrete strength at day one of testing.

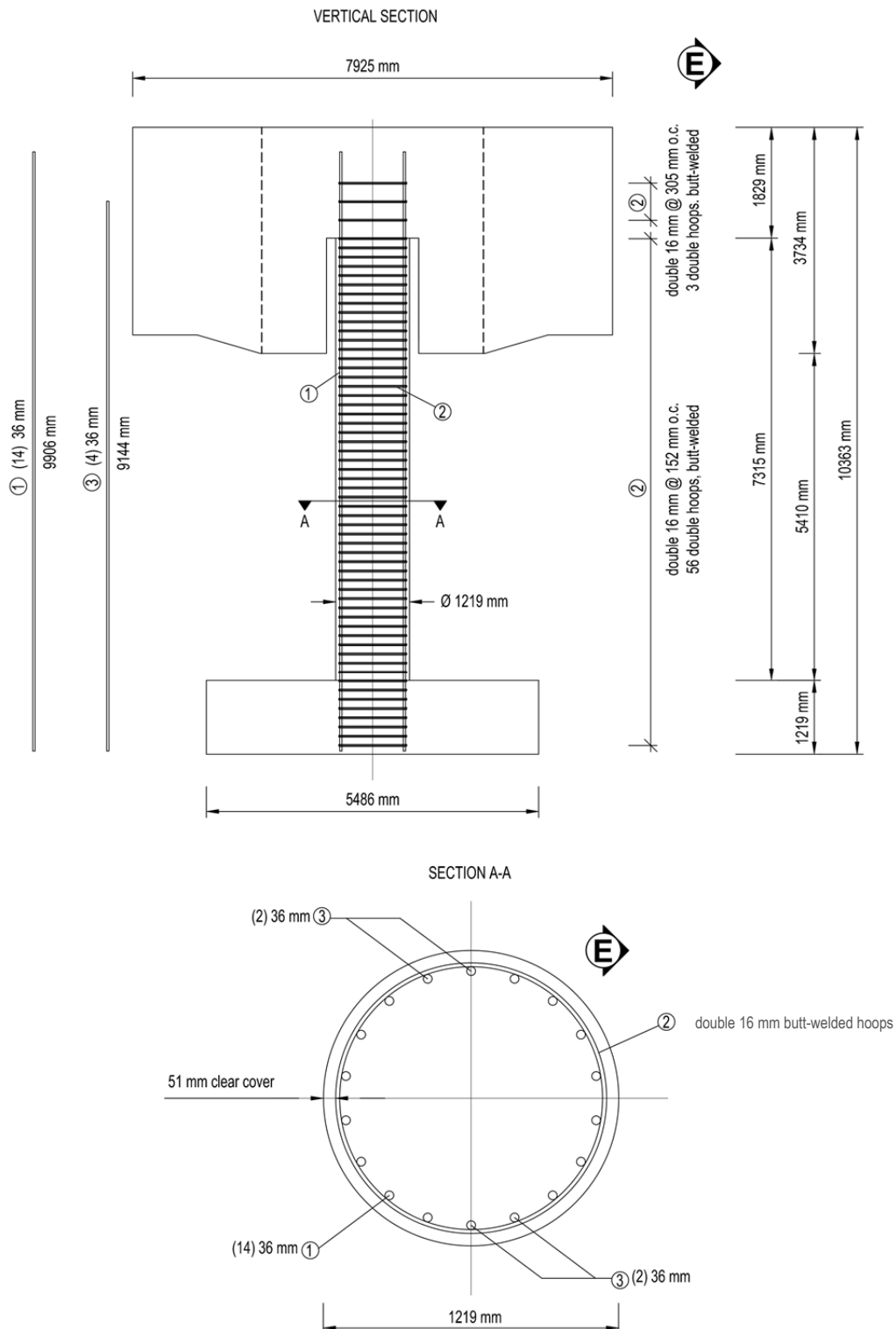


**Figure 3.1 Column reinforcing details.**



**Figure 3.2      Bundled hoops with alternating butt-welds.**

@Seismicisolation

## 4 Test Set-Up

The test specimen included a cantilevered RC column, footing, and superstructure mass; see Figure 4.1. The specimen represented a full-scale bridge column designed to current Caltrans design guidelines, as discussed in Section 3. The footing was secured to the shake table with post-tensioning to prevent decompression under maximum expected overturning moment and provide shear transfer without sliding. A fixed-base test set-up isolated nonlinear response to the element of interest. The superstructure mass provided the targeted column axial load and the inertia mass necessary to generate nonlinear response.

Input excitation consisted of a single horizontal component reproduced by the uni-axial shake table with the following dimensions: 7.6 m (25 ft) wide and 12.2 m (40 ft) long [Van Den Einde et al. 2004]. Safety restraints that were secured to the shake table surrounded the test specimen to provide protection to site personnel and equipment. Two types of restraints were provided: inclined safety columns and arched restraint towers.

Column displacement was limited to a 10% drift ratio. This restriction was imposed by inclined safety columns placed on either side of the test specimen in the direction of shaking, which formed a collapse restraint mechanism, see Figure 4.2. They were inclined 11.6° off-vertical and were designed to contact the angled portion on the underside of the superstructure block at the limiting drift ratio. Safety columns consisted of double W32×302 sections. Headed reinforcing bars were welded to the flanges of the W-sections and anchored in a concrete footing. The W-sections were also embedded 38 mm (1.5 in.) deep in the footing. Although post-tensioned to the shake table, these footings were independent from the column's footing. Large timbers were secured to the top of the safety columns for energy dissipation at impact between the concrete block and safety column.

To preclude out-of-plane motion, the arched safety restraints located at the corners of the specimen were fitted with longitudinal east-west guides. Pairs of steel tubes were aligned in the direction of shaking and welded to the arched safety towers. A clear 6.4-mm (0.25-in.) gap between the guide and concrete block was greased to reduce friction should contact initiate during testing. The complete test set-up including the arched safety restraints is shown in Figure 4.3.



**Figure 4.1** Test specimen.

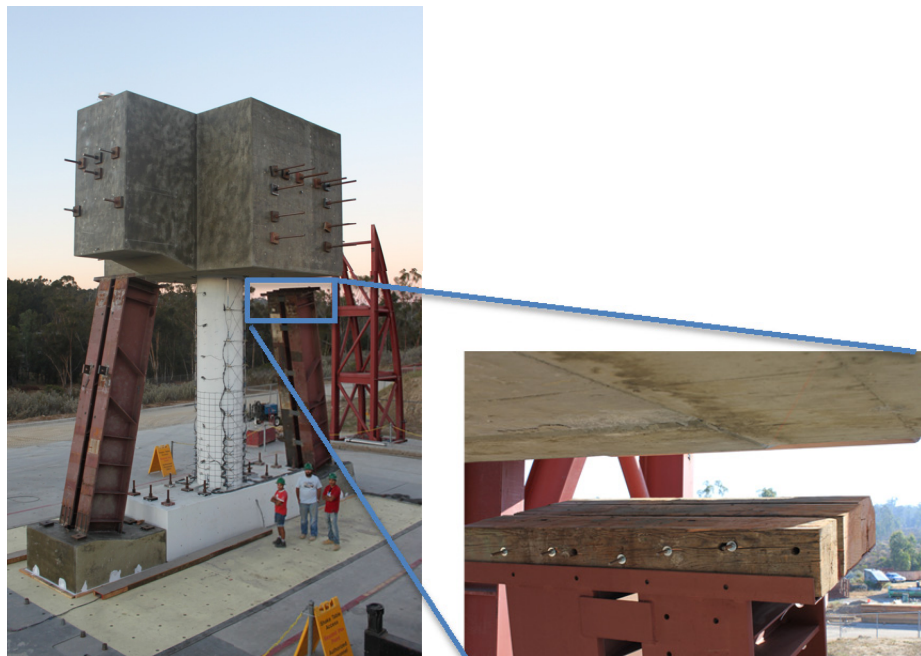


**Figure 4.2** Collapse restraint mechanism.

@Seismicisolation



**Figure 4.3      Test set-up.**

## 4.1    COLUMN

The 1.22-m- (4-ft-) diameter column had a moment-to-shear ratio of  $6.0D$ , where  $D$  is the column's diameter. The free height-to-the-center-of-mass of the superstructure mass measured from the column base was 7.32 m (24 ft). To ensure the column was unencumbered by the inertia mass to the full 7.32 m, a gap was provided between the two of them. This gap is visible in Figure 4.3 where it appears the column is a peg in an oversized socket. However, a full moment-resisting connection was provided at the top of the column where longitudinal reinforcement extended into the superstructure mass. Intentionally roughened construction joints were located at the top of the column and footing.

## 4.2    FOOTING

The footing was designed according to Caltrans Seismic Design Criteria [Caltrans 2006a] and Bridge Design Specifications [Caltrans 2004] guidelines. It consisted of a 5.49-m- (18-ft-) long, 1.83-m- (6-ft-) wide, and 1.22-m- (4-ft-) deep RC block. The moment-resisting connection between the footing and column was designed similar to a superstructure "T" joint [Caltrans 2006a], and was reinforced with Grade 60 ASTM A706 [2009b] reinforcement. The reinforcement consisted of twelve 35.8-mm-diameter (#11) bars top and bottom and 12.7-mm-diameter (#4) transverse stirrups and ties. Reinforcing details can be found in construction

drawings available in the project archive [NEES 2011]. The footing was post-tensioned to the shake table to prevent decompression under maximum expected overturning moment and prevent sliding at maximum shear transfer relative to the shake table.

### 4.3 SUPERSTRUCTURE MASS

The superstructure consisted of five cast-in-place concrete blocks. These blocks were arranged in a cruciform shape to accommodate the placement of the safety restraints on the table. The blocks were post-tensioned together and had a combined estimated weight of 2.32 MN (522 kip). This weight was based on the measured concrete unit weight and the specified geometry, and accounted for block's reinforcement through holes for post-tensioning, and post-tensioning bars. The rotational mass moment of inertia about the center-of-mass was calculated as  $2.50 \times 10^{10}$   $\frac{kNm^2}{g} \left( 3.62 \times 10^6 \frac{\text{kip in.}^2}{g} \right)$ . This calculation relied also on the specified geometry and estimated weight.

Post-tensioning the blocks together ensured that the total mass was mobilized as a single block. It was designed to ensure that decompression would not occur between the blocks under combined gravity and seismic loading. Minimum reinforcement was provided for each block. The reinforcement ratio was assigned per ACI 318 [ACI 2008] requirements, and was distributed as skin reinforcement on each face of the blocks. Specified block dimension and reinforcing details can be found in construction drawings available in the project archive [NEES 2011].

The central block was cast on top of the column and provided anchorage for the column's longitudinal reinforcement for a full moment-resisting connection. The combined block geometry was designed so its center-of-mass coincided with the top of the column. To ensure an unencumbered column height of 7.32 m (24 ft), a block out was provided between the column and the central block for the bottom 1.91 m (6.25 ft) of the block. A 1.52-m- (5-ft-) diameter corrugated pipe embedded in the block resulted in a 152-mm- (6-in.-) gap between the block and the column. The corrugated drainage pipe was utilized as stay-in-place formwork.

# 5 Material Properties

## 5.1 CONCRETE

The specified concrete strength of the column was 27.6 MPa (4.0 ksi) for a targeted axial load ratio of 6.1% based on an expected concrete strength of  $1.3 f'_c$ . Maximum aggregate size for the mix was specified as 25.4 mm (1.0 in.), which conformed to Caltrans' aggregate grading [Caltrans 2006b]. The mix design included type II Portland cement with a water-to-cement ratio of 0.44, including 25% contribution from fly ash, and had an anticipated 102-mm (4.0-in.) slump. Prior to placing the concrete, 0.019 m<sup>3</sup> (5 gallons) of water was added to each delivery truck with 6.1 m<sup>3</sup> (8 yd<sup>3</sup>) of concrete containing 1.03 m<sup>3</sup> (273 gallons) of water. The resulting water to cement ratio was 0.43. Each batch was further supplemented with 1480 ml (50 oz) of superplasticizer to improve workability and achieved a measured slump of 159 mm (6.25 in.) and 165 mm (6.5 in.). Mix proportions, averaged between the two batches, are provided in Table 5.1.

**Table 5.1 Column as-built concrete mix proportions per cubic yard of concrete.**

Material	Proportion
Cement	230 kgf (509 lb)
Fly ash – Class F	77 kgf (169 lb)
Fine aggregate	634 kgf (1400 lb)
Aggregate: 1-1/2 in. × ¾ in.	0 kgf (0 lb)
Aggregate: 1 in. × #4	620 kgf (1368 lb)
Aggregate: 3/8 in. × #8	134 kgf (298 lb)
Water (34.8 gallons)	131 kgf (290 lb)
Entrapped air	1%
Water reducing admixture	600 ml (20.3 oz)
Superplasticizer	185 ml (6.3 oz)
<b>Total</b>	<b>1792 kgf (3952 lb)</b>

At the time of casting, 152-mm- (6-in.-) diameter  $\times$  305-mm (12-in.) high concrete test cylinders were taken. These gave an average concrete unit weight of 23.6 kN/m<sup>3</sup> (150 pcf). Cylinders were tested under monotonic compression in sets of three samples at twenty-one, twenty-nine, forty-two, and forty-three days. The first of the six samples tested at forty-two days was excluded as a low outlier. Commencement of shake table testing corresponded to an age of forty-two days in the column concrete. The concrete age at forty-three days corresponds to the second day of shake table testing. Of the three samples in a set, two samples were taken from the first batch of concrete delivered to the site, and one sample was from the second batch of concrete to emphasize the concrete strength in the plastic hinge region. Table 5.2 summarizes the results of these compression tests. At forty-two and forty-three days, two sets of three samples were tested; however, the first sample at forty-two days was excluded as an outlier.

A complete stress-strain relationship to peak load was obtained for the first sample of each set of cylinders; see Figure 5.1. The strain was obtained as the average measurement from three concrete strain gauges oriented in the longitudinal direction. To emphasize the material within the plastic hinge region, the sample was taken from the first batch of concrete delivered to the site.

As shown in Figure 5.1, the modulus of elasticity of the concrete,  $E_c$ , defined here as the slope of the secant line from the origin to the point at  $0.5 f'_c$ , was obtained from the stress-strain curves tested at forty-two or forty-three days as 22,900 MPa (3320 ksi). This was determined from the average value of three concrete breaks: one from forty-two days and two from forty-three days. This modulus of elasticity is only 79% of the anticipated modulus calculated from equation 3.11 [Caltrans 2006a], based on the expected concrete compressive strength and unit weight.

The unconfined concrete compressive strain at maximum compressive stress,  $\varepsilon_{co}$ , was 0.0026; see Figure 5.1. This was based on an average from the three samples tested with concrete strain gauges at forty-two or forty-three days. This unconfined concrete compressive strain at maximum compressive stress was 30% greater than the 0.002 value specified for design [Caltrans 2006a]. The maximum compressive stress reported in Table 5.2 was based on the average of the samples tested that day. This accounts for the discrepancy between values in Table 5.2 and the maximum compressive stress of the single sample shown in Figure 5.1

**Table 5.2      Column concrete compressive strength.**

Age (days)	$f'_c$ [MPa (ksi)]
21	37.0 (5.4) *
29	40.3 (5.8) *
42	40.9 (5.9) +
43	42.0 (6.1) ‡

\* Average of three samples; + average of five samples; and  
 ‡ average of six samples.

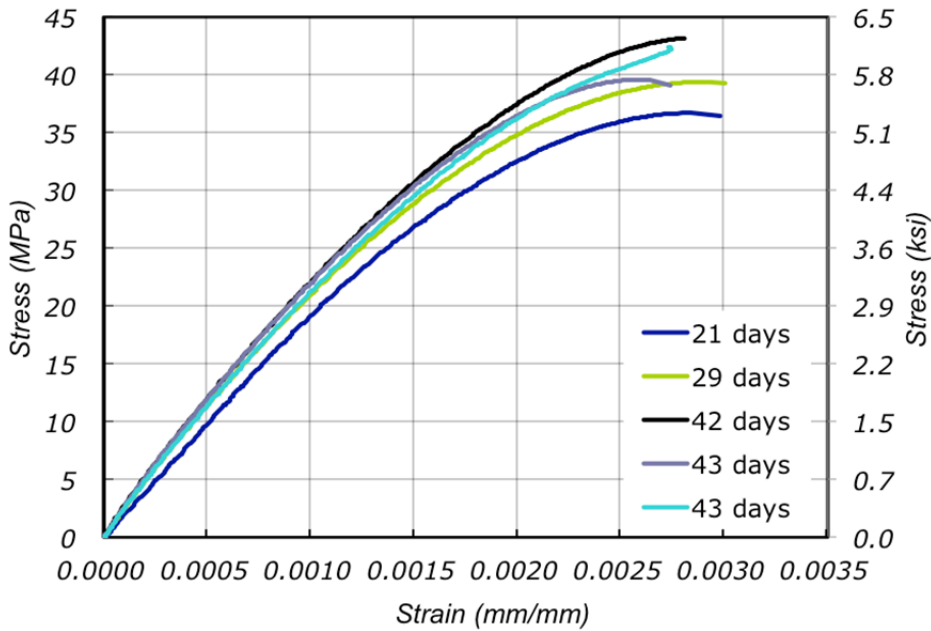


**Figure 5.1** Column concrete stress-strain relationship of individual samples.

## 5.2 REINFORCING STEEL

Column longitudinal and transverse reinforcement were specified as Grade 60 (414 MPa) steel conforming to ASTM A706 [2009]. The 35.8-mm-diameter (#11) longitudinal reinforcement had a yield strength of 519 MPa (75.2 ksi) and an ultimate strength of 707 MPa (102.4 ksi). As shown in Table 5.3, these strengths and other mechanical properties of the reinforcement were obtained from monotonic tension tests. The yield strength is based on the average of two samples, and the ultimate strength is based on the average of three samples. Test coupons were instrumented with a pair of strain gauges to obtain strain measurements. Strain-gauge readings were not recorded for one of the three samples, precluding its yield strain and stress from being included in the estimation, but the sample's ultimate strength was identifiable. A complete stress-strain curve for one sample is provided Figure 5.2.

Five samples taken from the 15.9-mm-diameter (#5) transverse hoops tested under monotonic tension did not exhibit a yield plateau. These samples were cut from three bent hoops outside of the weld-affected region. The butt welds of these hoops were proof tested, and all failed outside of the weld. Yield strength based on the mill cert of the straight bars was expected to be 454 MPa (65.8 ksi), and the ultimate tensile strength was expected to be 600 MPa (87.0 ksi). The ultimate tensile strength based on five samples was 592 MPa (85.9 ksi). Strain was calculated as the average strain recorded by a pair of strain gauges. One gauge was located on the concave side of the bar and the other on the convex side. The stress-strain relationship of the five samples is provided in Figure 5.3. Specimens 1, 2, and 3 had strain gauges that saturated prematurely.

**Table 5.3      Measured reinforcement strengths.**

Reinforcement	$\varepsilon_y$ (%)	$f_y$ MPa (ksi)	$E_s$ MPa (ksi)	$\varepsilon_{sh}$ (%)	$E_{sh}$ MPa (ksi)	$\varepsilon_u^*$ (%)	$f_u$ MPa (ksi)
Longitudinal 35.8-mm diam.	0.26	519 (75.2)	196,000 (28,400)	1.1	5520 (800)	12.2	707 (102.4)
Transverse 15.9-mm diam.	-	338 (54.8)*		-	-	12.5	592 (85.9)

$\varepsilon_u$  is the tensile strain at the peak tensile force,  $f_u$ .

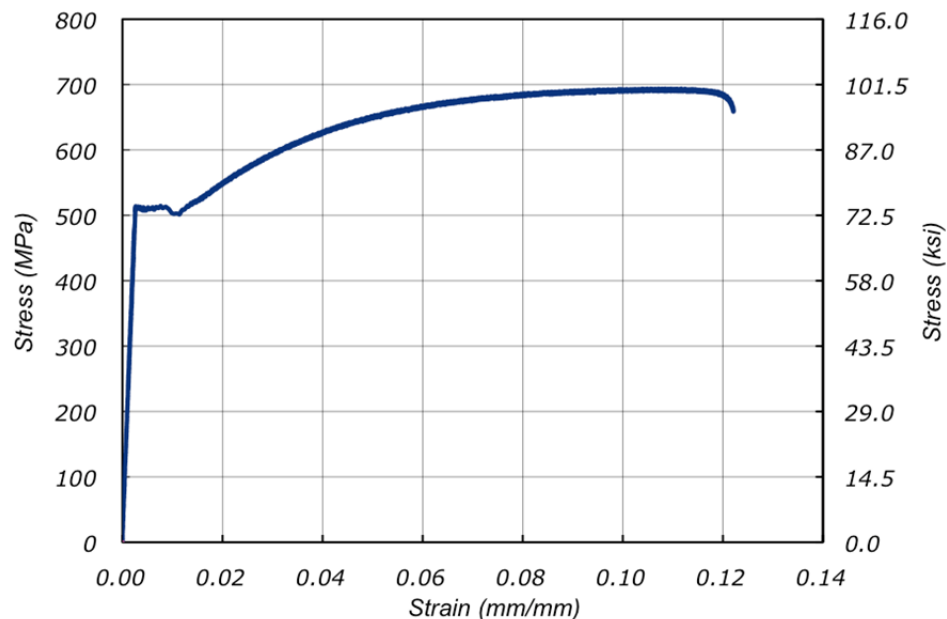


**Figure 5.2      Column longitudinal reinforcement stress-strain relationship.**

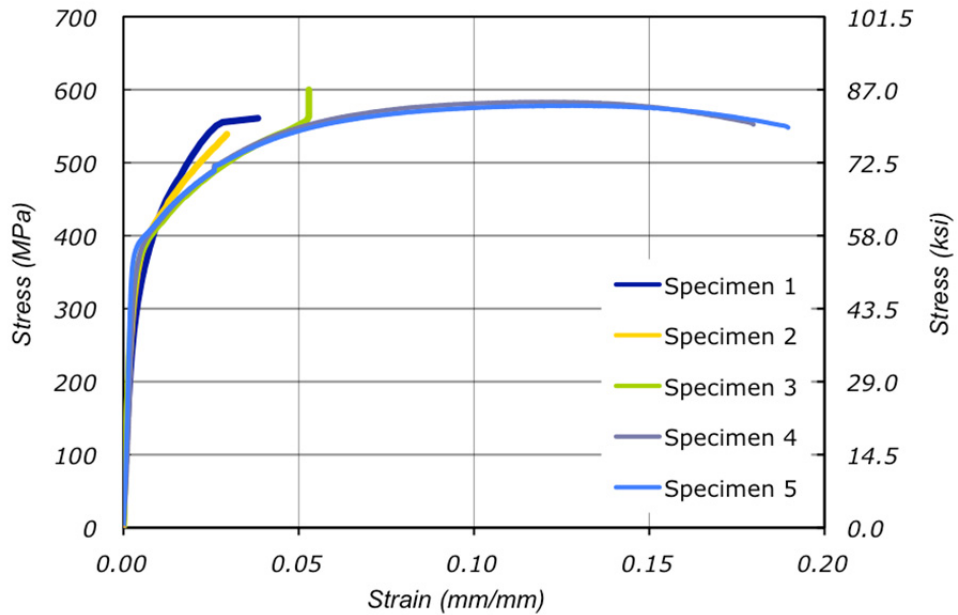


**Figure 5.3 Column transverse hoop reinforcement stress-strain benchmarking.**

### 5.3 FOOTING AND SUPERSTRUCTURE MATERIALS

Footing and superstructure reinforcement were specified as Grade 60 (414 MPa) steel conforming to ASTM A615 [2009]. Normal weight concrete was utilized in both of these components. Samples from each of these provided an average concrete unit weight of 23.5 kN/m<sup>3</sup> (150 pcf) and 23.7 kN/m<sup>3</sup> (151 pcf) for the footing and superstructure, respectively. The concrete in the footing had a specified strength of 27.6 MPa (4.0 ksi), and the mix design was the same as utilized for the column. The concrete strength on the day one of testing was 41.9 MPa (6.1 ksi). The superstructure mass included high early-strength concrete to accommodate the project schedule. The specified strength of this mix design was 35 MPa (5.1 ksi), with an expected strength of 31.3 MPa (4.7 ksi) at seven days.

**@Seismicisolation**

## 6 Test Protocol

Six earthquake simulation tests were planned in the loading protocol. The test objectives were to achieve desired column lateral displacement demands at the center-of-mass of the inertia mass block. The displacements were selected in terms of target displacement ductilities as 1, 2, 4, and 8. However, to investigate the effects of lower intensity aftershocks, the test sequence was not conducted with continually increasing demands. The protocol included a repetition of the target ductility of 2 and 4 after subsequent testing at a higher ductility demand. The resulting protocol called for tests with input motions capable of producing target ductilities in the following sequence: 1, 2, 4, 2, 8, and 4. Tests conducted at a repeated target ductility used the same input motion as the initial trial. This provided the opportunity to investigate the effect of damping and damage accumulation.

The test specimen design was not based on a prototype bridge and test objectives did not rely on a seismic hazard; therefore, a bridge location in San Francisco, California, was adopted. The site considered, latitude 37.77 and longitude -122.42, had stiff soil with an average small strain shear-wave velocity,  $V_{s30}$ , of 350 m/sec (1,170 ft/sec) in the upper 30 m (98 ft) of the soil column. Considering the site location, earthquake recordings from a strike-slip fault mechanism were given preference. The selection of input table motions relied on the Pacific Earthquake Engineering Research (PEER) Center's strong motion database [PEER 2007]. Preference was also given to records that could produce the desired response without scaling. Ground motion selections were based initially on their 2% damped, elastic response spectrum. The equal displacement concept, displacement response spectrum, and analytically based fundamental period were used to identify possible candidates for the targeted ductility ratios. Displacement ductility was based on an idealized yield displacement determined analytically as 88 mm (3.47 in. which corresponds to a drift ratio of 1.2%) [Carrea 2010].

Based on nonlinear dynamic time history analyses [Carr 2002; Carrea 2010], possible input motions were further reassessed. The lumped plasticity model, with which the yield displacement was calculated, was calibrated against a full-scale, pseudo-static test by Stone and Cheok [1989], which had similar design properties. The idealized moment-curvature response was refined to account for measured material properties such as a lower than anticipated concrete modulus. The resulting idealized monotonic behavior can be characterized by the parameters shown in Table 6.1 and presented in normalized units in Table 6.2.

After analyzing possible candidates, four historical earthquake recordings were selected as shake table input motions. Three input motions were selected from the 1989 Loma Prieta earthquake. The fourth record was sourced from the Takatori station during the 1995 Kobe earthquake. These records are identified in Table 6.3 and peak parameters recorded during the tests provided in Table 6.4. Analytical predictions indicated the Takatori record was stronger than necessary to achieve the target ductility and exceeded the safety limit imposed due to ratcheting when run in sequence with the other motions. Therefore, the amplitude was reduced and polarity inverted as indicated in Table 6.3.

**Table 6.1      Idealized, monotonic response of the analytical model.**

Limit state	Curvature (rad/m)	Moment (kN-m)	Displacement (mm)	Shear force (kN)
First cracking	$2.93 \times 10^{-4}$ ( $7.43 \times 10^{-6}$ rad/in.)	839 (619 kip-ft)	4 (0.17 in.)	97 (21.8 kip)
Nominal or idealized yield	$4.73 \times 10^{-3}$ ( $1.20 \times 10^{-4}$ rad/in.)	5790 (4270 kip-ft)	88 (3.47 in.)	782 (176 kip)
Ultimate	$7.56 \times 10^{-2}$ ( $1.92 \times 10^{-3}$ rad/in.)	6280 (4630 kip-ft)	506 (20.0 in.)	705 (159 kip)

**Table 6.2      Idealized, monotonic response of the analytical model in normalized units.**

Limit state	Curvature ( $\phi D$ )	Moment ( $M/D^3 f'_c$ )	Displacement ( $\Delta/H$ )	Shear force ( $V/A_g f'_c$ )
First cracking	0.0004	0.011	0.0006	0.077
Nominal or idealized yield	0.0058	0.079	0.0120	0.621
Ultimate	0.0922	0.085	0.0694	0.530

**Table 6.3      Ground motion selections and scale factors.**

Test	Earthquake	Date	Moment magnitude	Station	Component	Scale factor
EQ1	Loma Prieta	10/18/1989	6.9	Agnew State Hospital	090	1.0
EQ2	Loma Prieta	10/18/1989	6.9	Corralitos	090	1.0
EQ3	Loma Prieta	10/18/1989	6.9	LGPC	000	1.0
EQ4	Loma Prieta	10/18/1989	6.9	Corralitos	090	1.0
EQ5	Kobe	01/16/1995	6.9	Takatori	000	-0.8
EQ6	Loma Prieta	10/18/1989	6.9	LGPC	000	1.0

With significant structural integrity after the planned test sequence, the scope was expanded and an additional four tests conducted. These tests utilized the Takatori ground motion from the Kobe earthquake at different amplitudes; see Table 6.5. The scale factors for the ground motions in the extended test sequence are provided in Table 6.6.

**Table 6.4      Ground motion peak ground parameters.**

Test	Station	Target displacement ductility	Table PGA (g)	Table PGV (m/sec)
EQ1	Agnew State Hospital	1.0	-0.199	0.16 (6 in./sec)
EQ2	Corralitos	2.0	0.409	0.37 (15 in./sec)
EQ3	LGPC	4.0	0.526	0.89 (35 in./sec)
EQ4	Corralitos	2.0	0.454	0.39 (15 in./sec)
EQ5	Takatori	8.0	-0.533	0.95 (38 in./sec)
EQ6	LGPC	4.0	-0.512	0.87 (34 in./sec)

**Table 6.5      Ground motion selection and scale factors for extended testing.**

Test	Earthquake	Date	Moment magnitude	Station	Component	Scale factor
EQ7	Kobe	01/16/1995	6.9	Takatori	000	1.0
EQ8	Kobe	01/16/1995	6.9	Takatori	000	-1.2
EQ9	Kobe	01/16/1995	6.9	Takatori	000	1.2
EQ10	Kobe	01/16/1995	6.9	Takatori	000	1.2

**Table 6.6      Ground motion peak ground parameters for extended testing.**

Test	Station	Target displacement ductility	Table PGA (g)	Table PGV (m/sec)
EQ7	Takatori	Not applicable	0.646	1.14 (45 in./sec)
EQ8	Takatori	Not applicable	-0.829	1.34 (53 in./sec)
EQ9	Takatori	Not applicable	0.819	1.35 (53 in./sec)
EQ10	Takatori	Not applicable	0.851	1.40 (55 in./sec)

The response spectra of the desired ground motions were obtained after filtering and scaling the selected records found in the PEER Ground Motion Database [PEER 2007]; see Figure 6.1. The records were band-pass filtered using an FIR filter of order 5000 with cut-off frequencies of 0.25 and 25 Hz. Table acceleration feedback is the recorded table motion and input to the test specimen since the shake table does not reproduce exactly the desired motion. The table acceleration feedback was also band-pass filtered using the same FIR filter before obtaining the response spectra.

The elastic pseudo-acceleration and displacement response spectra for the ten tests are provided in Figure 6.2–Figure 6.7. These contain both the desired motion and table feedback. For comparison, the 975-year return period probabilistic seismic hazard for the San Francisco site considered is also provided in Figure 6.1–Figure 6.7. The response spectra for EQ1 are provided in Figure 6.2. Tests EQ2 and EQ4 are repetitions of the same ground motion and are plotted together in Figure 6.3. Similarly, Figure 6.4 contains the response spectra of both EQ3 and EQ6. The response spectra of EQ5 and EQ7 are provided in Figure 6.5 and Figure 6.6, respectively. Tests EQ8, EQ9, and EQ10 utilized the same ground motion so their response spectra are all contained in Figure 6.7.

Before the first earthquake simulation, two, five-minute-long, white noise table motions were conducted. The first white noise table motion with 0.03g root mean square amplitude was used to check the instrumentation for quality control assurance. The same five-minute-long white-noise motion was repeated before testing commenced and then repeated between subsequent earthquake tests. This was implemented to observe the period shift and mode shape changes caused by damage accumulation.

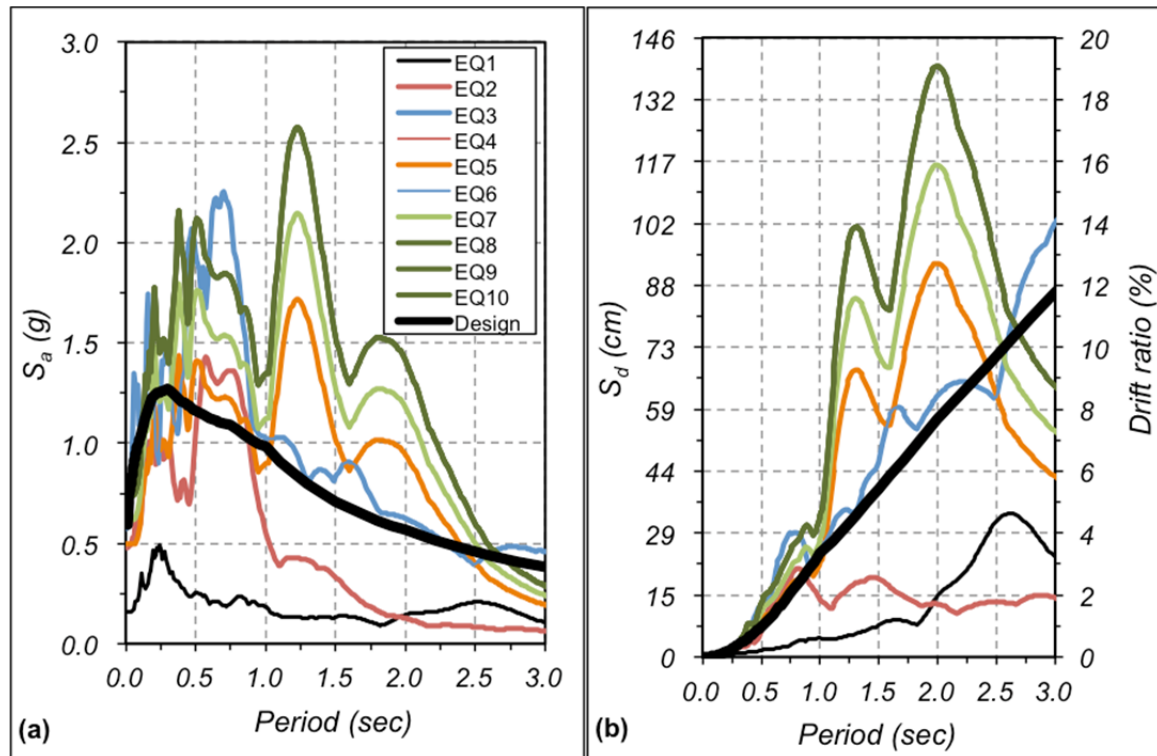


**Figure 6.1** Desired ground motions in terms of (a) pseudo-acceleration and (b) displacement response spectra at 5% damping ratio.

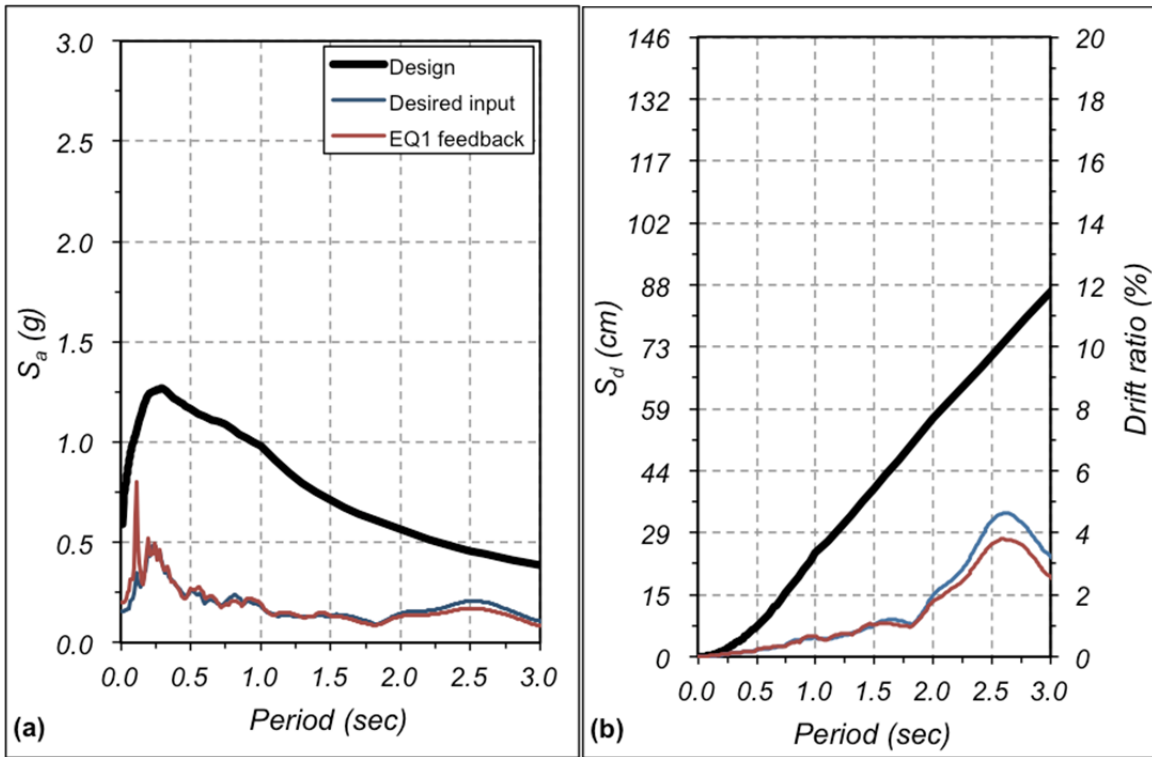


**Figure 6.2** EQ1 (a) pseudo-acceleration and (b) displacement response spectra at 5% damping ratio.

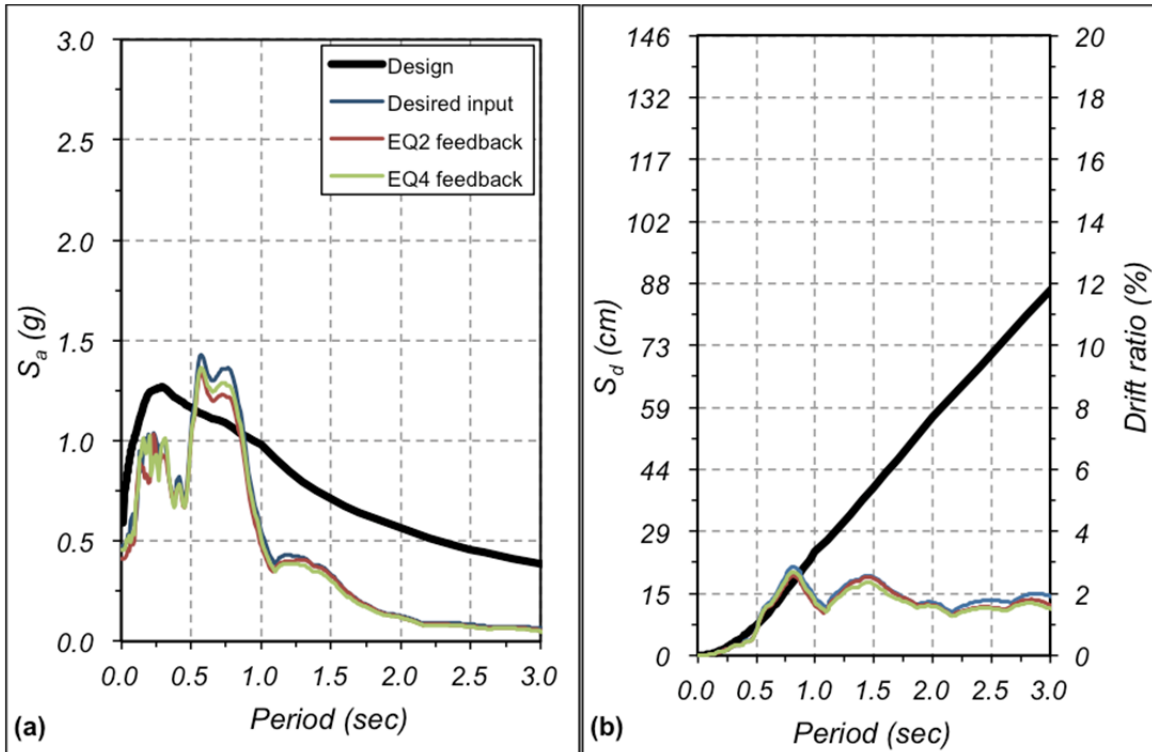


**Figure 6.3** EQ2 and EQ4 (a) pseudo-acceleration and (b) displacement response spectra at 5% damping ratio.

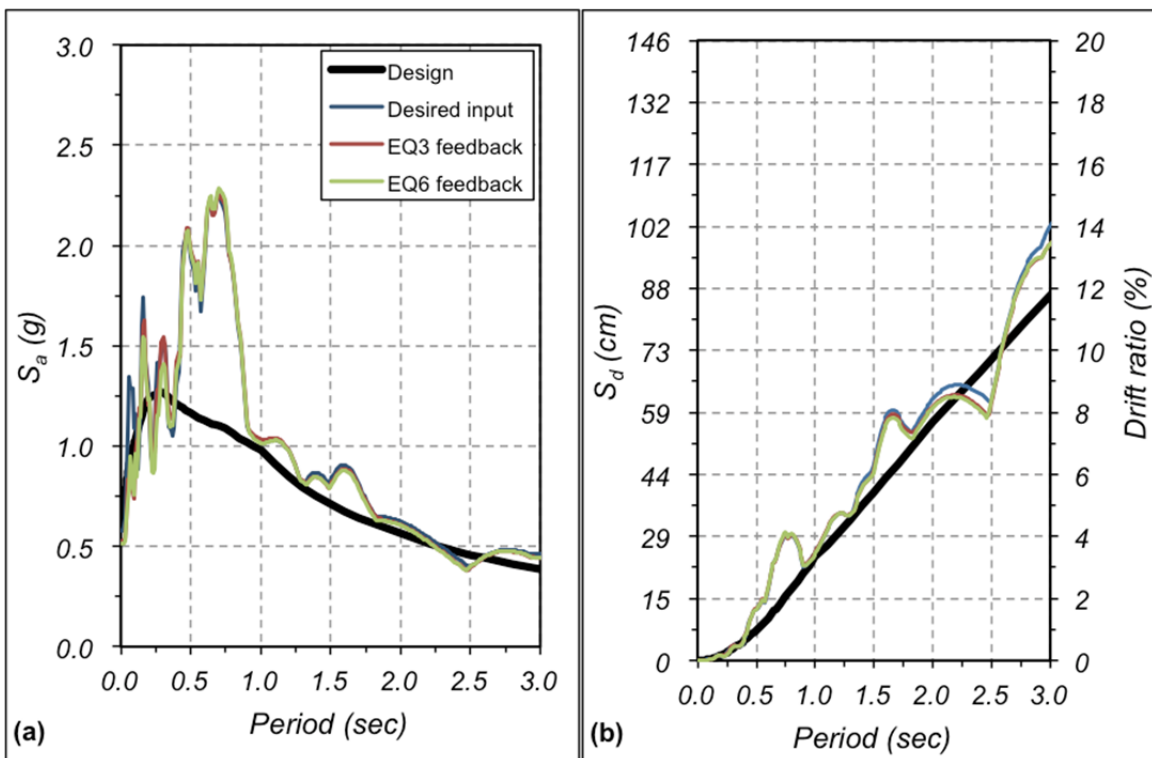


**Figure 6.4** EQ3 and EQ6 (a) pseudo-acceleration and (b) displacement response spectra at 5% damping ratio.

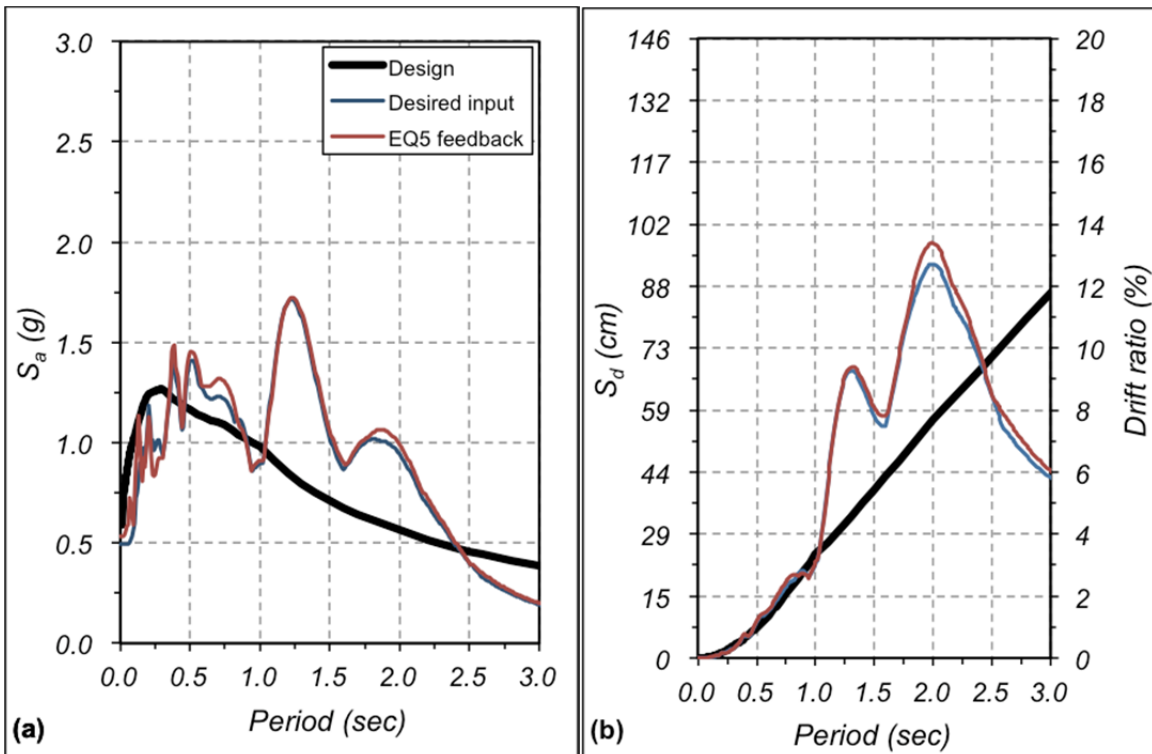


**Figure 6.5** EQ5 (a) pseudo-acceleration and (b) displacement response spectra at 5% damping ratio.

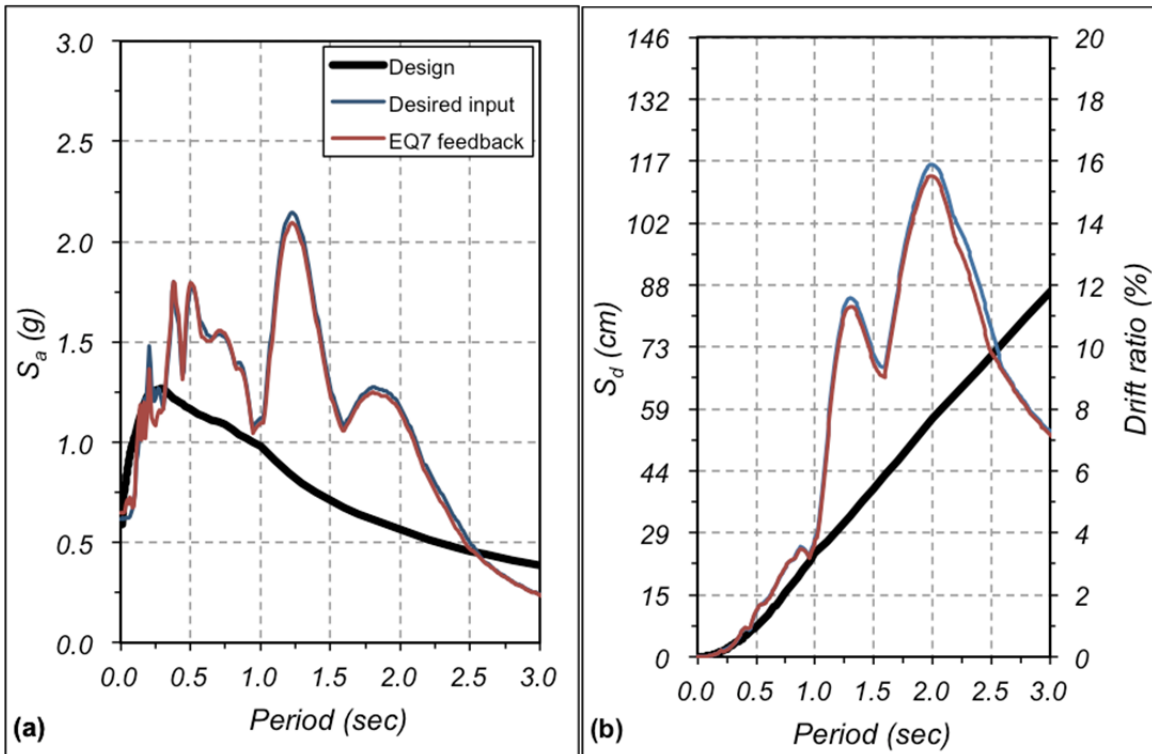


**Figure 6.6** EQ7 (a) pseudo-acceleration and (b) displacement response spectra at 5% damping ratio.

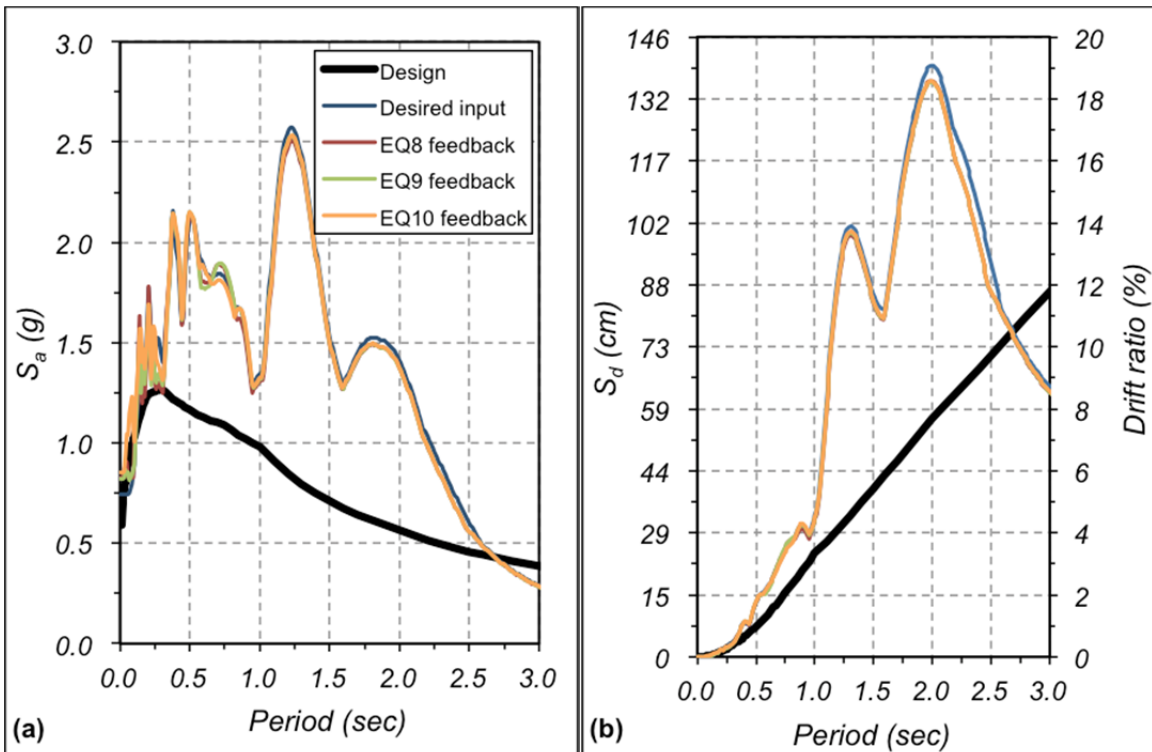


**Figure 6.7** EQ8, EQ9, and EQ10 (a) pseudo-acceleration and (b) displacement response spectra at 5% damping ratio.

# 7 Instrumentation and Data Processing

The test specimen was densely instrumented with 278 channels of data acquisition. These included strain gauges, linear and string potentiometers, accelerometers, and Global Positioning System (GPS) receivers to measure internal, local, and global deformations during testing. Detailed instrumentation plans are provided in Appendix A and available at the project space on the NEEShub data repository website [NEES 2011].

## 7.1 STRAIN GAUGES

### 7.1.1 Longitudinal Strain Gauges

Electrical resistance strain gauges were symmetrically installed on two longitudinal reinforcing bars at both East and West faces of the column to monitor axial strains. These gauges were placed in pairs on both sides of each bar in the direction of shaking to monitor any bending in the bar. In total, sixty-four gauges with a 5 mm (0.2 in.) gauge length were installed on the four longitudinal bars. Prior to installation of the gauges, the steel reinforcement was filed to expose a smooth surface free of mill scale and deformations.

### 7.1.2 Transverse Strain Gauges

Strain gauges were installed on the exterior face of the transverse hoops on the East and West sides of the column. Twenty-two foil resistance strain gauges with a 5 mm (0.2 in.) gauge length were installed; 11 gauges were located on either side. The purpose of these gauges was to monitor the hoops' axial elongation caused by radial dilation of the concrete core and longitudinal bars buckling. Prior to installation of the gauges, the steel reinforcement was filed to expose a smooth surface free of mill scale and deformations

### 7.1.3 Safety Restraint Strain Gauges

Eight strain gauges were installed on the flanges of the four inclined steel columns used as safety restraints. Two gauges per steel column were installed as pairs on opposite flanges; one on the East and one on the West. These gauges were intended to estimate the impact force should the column reach a 10% drift ratio.

## 7.2 LINEAR VOLTAGE DISPLACEMENT TRANSDUCERS

Linear displacement sensors with either a 50-mm (2-in.) or 100-mm (4-in.) stroke were installed externally to monitor column deformations; they are referred to as curvature Linear Variable Differential Transformers (LVDTs) or shear deformation LVDTs. These potentiometers were mounted on 9.5-mm (3/8-in.) threaded rods cast horizontally in the column in the North-South direction perpendicular to the direction of shaking. This removed the LVDTs from regions of potential spalling to decrease the likelihood of sensor damage. The rods were placed parallel and as close as possible to the expected neutral axis position to move them from the region of potential spalling and prevent dislocation during concrete crushing. They were encased in a rubber hose to debond them from the concrete core and disable their contribution as shear reinforcement. Debonded, threaded couplers encased in the concrete cover accommodated extension of the threaded rods to mount the LVDTs once the steel form was removed.

The rods were vertically spaced at 203 mm (8-in.) starting 50.8 mm (2 in.) above the column base and extending one column diameter. Above this, 610-mm (24-in.) and 787-mm (31-in.) spacings were used. Both curvature and shear LVDTs were installed on the South face of the column, whereas only curvature LVDTs were mounted on the North face; see Figure 7.1. Four vertical spring-loaded LVDTs were installed to determine the fix-end rotation of the column at its base. They were mounted on the curvature rods located 51mm (2 in.) above the column-footing interface and they targeted the top of the footing as shown in Figure 7.1.

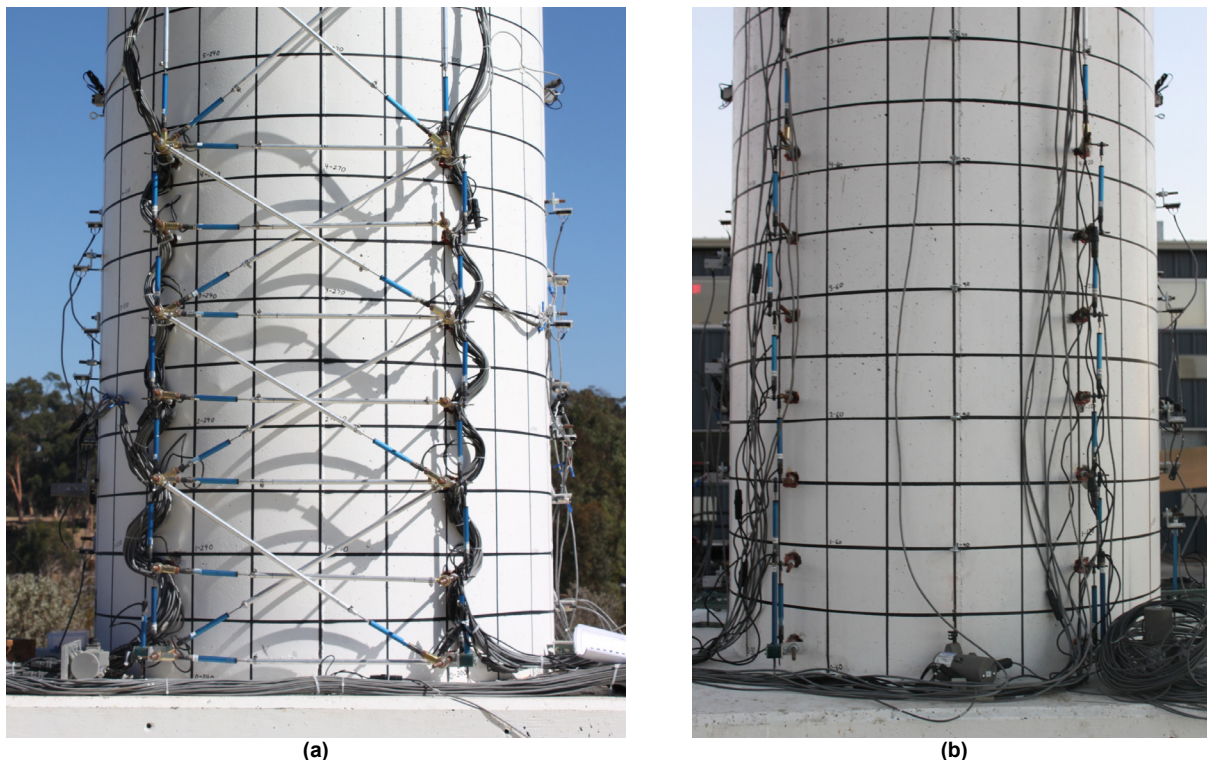


**Figure 7.1 Curvature, shear, and fixed-end rotation LVDTs on the (a) South and (b) North faces.**

Two horizontal spring-loaded LVDTs were installed to monitor the relative rotation between the column and the superstructure mass. Mounted on the lower face of the central block, these sensors targeted the East and West faces of the column; see Figure 7.2.

Vertical LVDTs were installed to measure bond slip between the longitudinal bars and the concrete of the footing. One bar on both East and West faces of the column was monitored. As shown in Figure 7.3, steel brackets were clamped on these bars using three sharpen screws. Brackets were placed just below the column-footing interface. Two concave steel targets were welded to each bracket to prevent slipping of the LVDT. The distances from the center of the longitudinal bar to the center of each target were 119 mm (4.7 in.) and 208 mm (8.2 in.). Epoxy filled the gap between the bracket's collar and the longitudinal bar, and the screws were ground flush to the exterior of the collar. The assembly was encapsulated in expansive foam to debond it from and allow movement within the surrounding concrete; see Figure 7.3(c). The LVDTs were placed on a rigid support bolted to the footing away from the column. Access to the bracket was made possible by removing the expansive foam after casting the footing. Two LVDTs were used to capture the rotation and vertical movement of the bracket.

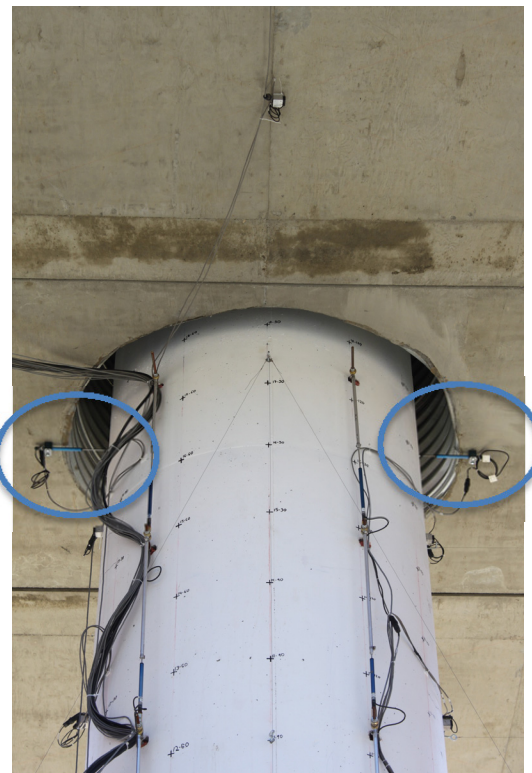
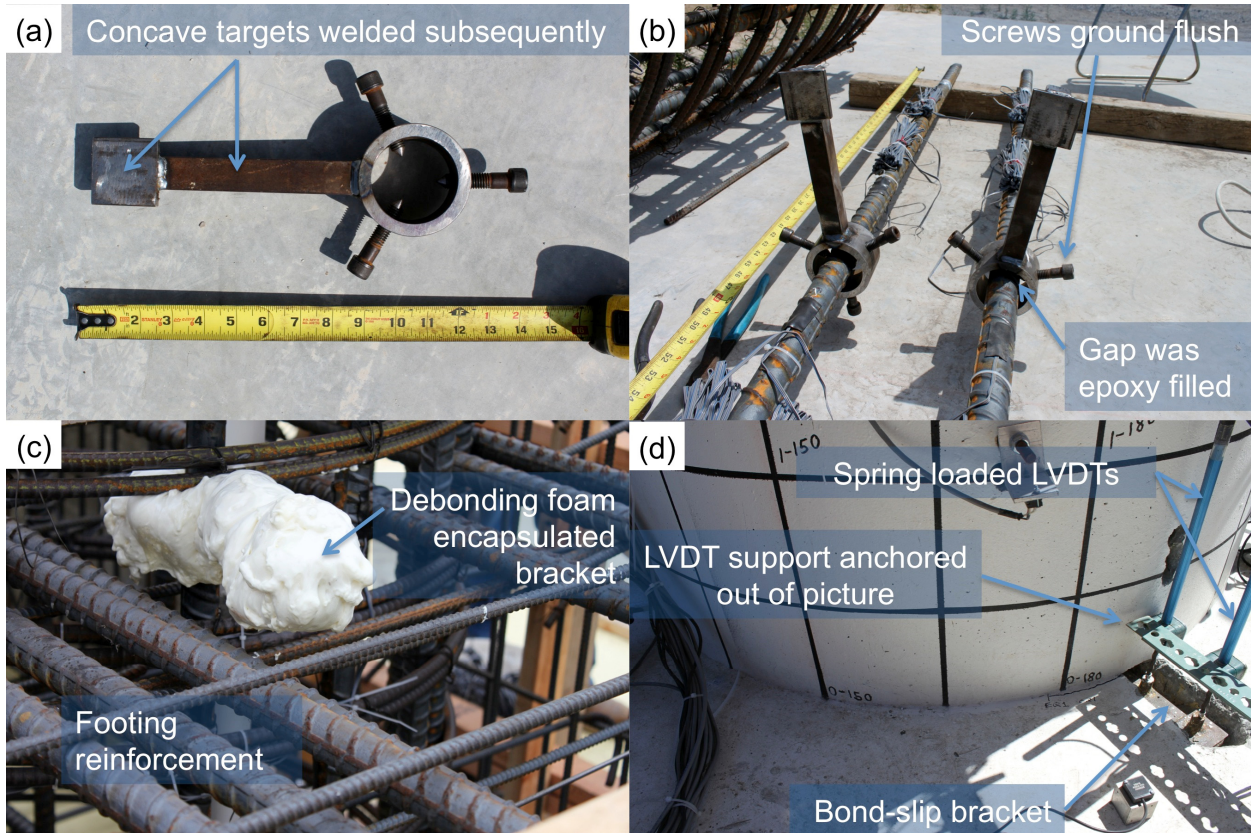


Figure 7.2      Column-to-top mass LVDTs.



**Figure 7.3** Bond-slip bracket installation: (a) assembly, (b) placed on longitudinal bars, (c) encapsulated with debonding foam, and (d) final installation.

Spring-loaded linear displacement sensors with a 25.4-mm (1-in.) stroke were installed to measure the radial dilation of the concrete core in the plastic-hinge region; they are referred to as dilation LVDTs (see Figure 7.4). These potentiometers were mounted on steel rods that were cast into the column. The rods passed horizontally through the column along the diameter of its cross section. They were encased in steel pipes to inhibit bond with the surrounding concrete. However, a 127-mm- (5-in.-) long segment at the rod's center remained exposed to fix the rods in a stable area of the column cross section. These sensors were aligned to concave steel targets that were welded to the exterior face of the transverse reinforcement; see Figure 7.4(a).

A 25.4-mm- (1-in.-) stroke LVDT was installed to monitor shear slip between the base of the column and the footing along their interface. This potentiometer was placed on the column-footing interface at the South side. In total, 107 LVDTs were installed on the column.

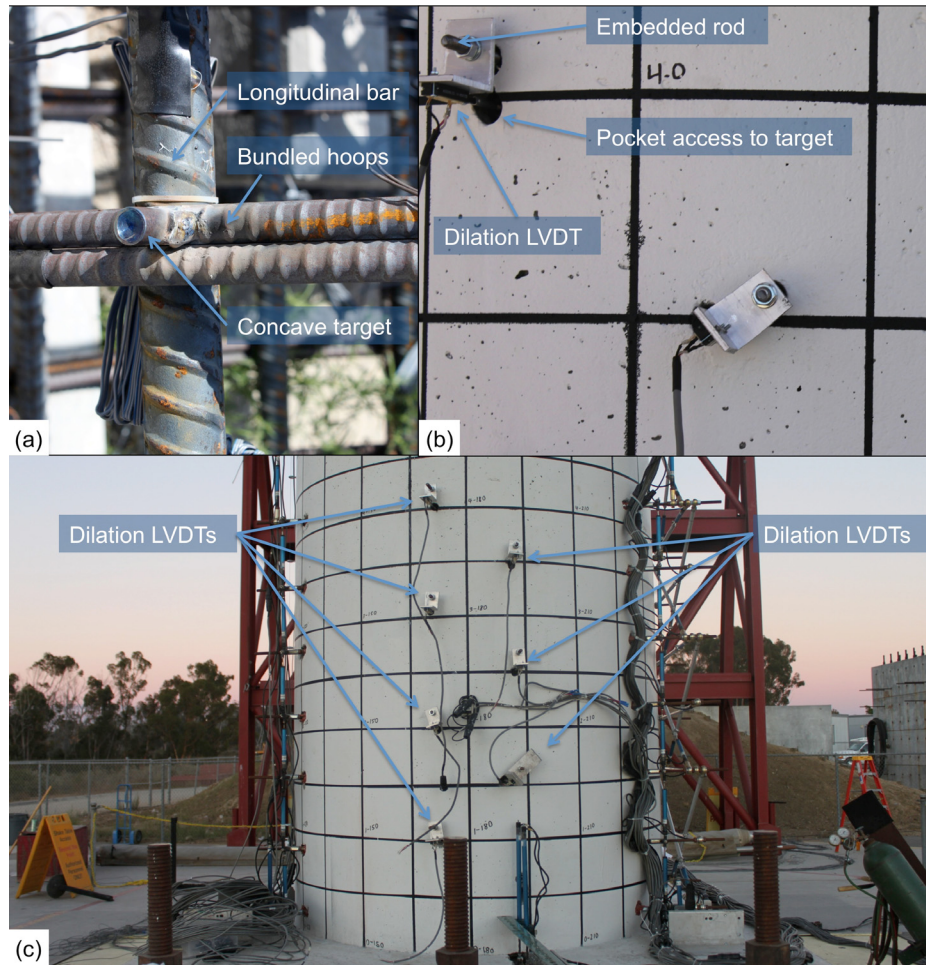


**Figure 7.4** Dilation LVDT installation: (a) target welded to a transverse hoop, (b) LVDT assembly, and (c) locations on the West face.

### 7.3 STRING POTENTIOMETERS

The relative horizontal displacement between the shake table and the column was measured at different heights using five cable-extension position transducers; they are referred to as horizontal string potentiometers. These instruments were mounted to steel plates connecting the two steel safety restraint columns on the West side of the specimen; they are highlighted in Figure 7.5. Because the upper portion of the column was embedded in the superstructure, four string potentiometers were installed between the restraining towers and the side blocks to measure the relative horizontal displacement of the column top. The horizontal string potentiometer layout is shown in Figure 7.5; only one of the four string potentiometers between the arched safety restraint and the mass block is visible. In tests up to and including the white-noise test after EQ3, the string potentiometers measuring top block displacement at the elevation of the top of the column were located on the four corners of the block. For the remaining tests, the potentiometers on the East side of the block were relocated to the West side and placed in series with the potentiometers on this side. This was done to ensure adequate stroke in the combined sensors at the maximum drift.

Three sensors were installed to monitor the relative displacement of the column at 5.41 m (17.75 ft) above the top of the footing. They were placed on the North side of the column: one was vertical, whereas the others two were inclined, as shown in Figure 7.6. This configuration allows the computation of the column elongation.



**Figure 7.5** Horizontal string potentiometer locations.

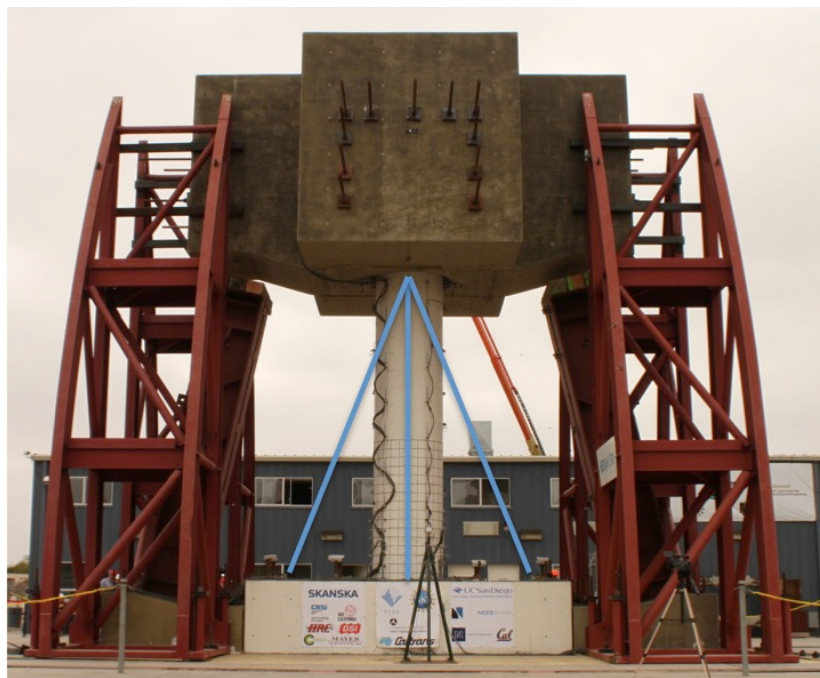


**Figure 7.6** Inclined string potentiometer locations.

## **7.4 ACCELEROMETERS**

Twenty-three accelerometers were installed to monitor the dynamic response of the specimen. These sensors measured vertical and horizontal accelerations of the specimen and safety restraints. They were DC coupled, silicone MEMS, uniaxial accelerometers with  $\pm 5g$  dynamic range.

Accelerometers were installed on the East and West faces of the column in different locations along its height. Since the column tip was embedded in the superstructure, two vertical and two horizontal accelerometers were placed on the North and South faces of the superstructure to measure the center-of-mass acceleration. The horizontal acceleration at the base of the column was measured using two accelerometers placed on the footing at North and South sides. The data obtained from these sensors allowed computation of the inertia forces generated on the specimen from the base excitation.

Vertical accelerometers were installed on the platen and on the footing to monitor the possible rotation of the shake table and column foundation in the shaking direction. Vertical and horizontal accelerometers were mounted on the superstructure mass to monitor its longitudinal, transverse, and rotational response.

The possible impact between the superstructure and the wood blocks located atop of the steel safety columns was measured by eight accelerometers and the four strain gauges; see Section 7.1.3. Two accelerometers were mounted on each of the four steel sections; one accelerometer was mounted horizontally and one vertically.

The column's lateral displacement was measured relative to the arched restraining towers, which were anchored to the shake table. The towers' responses are therefore included in the reported lateral displacement of the test specimen. While these towers were assumed to be rigid, four horizontal accelerometers were installed to measure their response.

## **7.5 GPS SYSTEM**

A network of three NAVCOM ANT-2004T antennae provided global displacement monitoring. Two GPS antennae were mounted on top of the superstructure mass, and one was used as a reference on the ground. These measured global displacement of the test specimen in three dimensions. The GPS acquisition system was separate from the table's data acquisition system. The dedicated standalone computer allowed continuous monitoring via three NAVCOM NTC-2030M receivers operating at 50 Hz.

## **7.6 VIDEO CAMERAS**

Six video cameras were mounted on the shake table observing the plastic hinge region: four were secured to the footing pointing to the East and West faces of the column, and two were installed on rigid supports bolted to the platen pointing to the North and South faces of the column. These cameras were connected to a PC based digital video recording system synchronized with the data

acquisition system. Several independent video cameras were installed outside the shake table to record the tests from different angles.

## 7.7 DATA ACQUISITION SYSTEM

A data acquisition system, operating at 240 Hz, was used to interpret signals from the instrumentation channels and to convert them into a digital format. It consisted of eight PXI chassis (or nodes). Each chassis was loaded with an embedded controller based on Windows XP running Lab View applications and eight SCXI-1520 signal conditioning modules. With this configuration, each chassis had a total capability of sixty-four channels. All eight chassis were triggered to record simultaneously before the command signal was sent by the control system. Therefore, there is a time lag between the data acquisition system recordings and the control system feedback data.

## 7.8 CONTROL SYSTEM

Base excitation was applied using the NEES@UCSD shake table located at the Englekirk Structure Engineering Center. The  $7.6 \times 12.2$  m (25×40 ft) shake table allowed testing of the column under a wide range of ground motions, starting with low-intensity shaking and bringing the column progressively towards near-collapse conditions. Table 7.1 summarizes the shake table's performance parameters such as peak velocity and acceleration, stroke and force capacity of actuators, maximum gravity payload and overturning moment, and frequency bandwidth [Van Den Einde et al. 2004]. Table command and feedback data operated at a sampling rate of 256 Hz.

**Table 7.1 Shake table capacities.**

Test		Metric	US Customary
Platen dimensions		7.6 m×12.2 m	25 ft×40 ft
Peak acceleration	Bare table	4.2g	
	400 ton payload	1.2g	
Peak velocity		1.8 m/sec	70.9 in./sec
Stroke		±0.75 m	±29.5 in.
Payload capacity		20 MN	2250 tons
Overturning moment capacity	Bare table	35 MN-m	25,800 kip-ft
	400 ton payload	50 MN-m	36,900 kip-ft
Frequency bandwidth		0–33 Hz	

## 7.9 DATA PROCESSING

Experimental measurements were filtered to present data within the range of frequencies capable of being produced by the shake table. Spurious recordings outside the useable frequency range of the shake table were filtered out. Acceleration data were band-pass filtered using an FIR filter with an order of 5000. The cut-off frequencies were 0.25 and 25 Hz. To retain the residual measurements from linear voltage displacement transducers and string potentiometers, the data from these instruments were low-pass filtered, with a cut-off frequency of 25 Hz and an FIR filter with an order of 5000.

Lateral displacement of the test specimen was measured with string potentiometers mounted horizontally to the arched safety restraint towers. String potentiometers were located at an elevation consistent with the top of the column, which coincided with the center-of-mass of the superstructure. The horizontal displacement was computed as the average of measurements from string potentiometers on the North and South sides of the column. The arched safety restraints were mounted on the shake table, providing measurement of the relative displacement between the top of the column and the shake table. No corrections were made in this horizontal displacement to account for the response of the towers, which were assumed to be rigid. A positive column displacement was considered to the East.

MEMS accelerometers were installed in pairs on opposite sides of the test specimen for redundancy. The average recording of this pair was utilized as the acceleration at the accelerometers' elevation. Horizontal accelerations considered at the top of the column relied on accelerometers located at the corresponding elevation, but were mounted on the North and South faces of the superstructure block because the block itself restricted access to the column at this elevation. Vertical and horizontal accelerometers on the top of the superstructure block were used to compute the rotational acceleration of the superstructure.

Column shear forces were obtained from the inertial forces computed from measured accelerations and the tributary mass associated with each accelerometer pair. The tributary mass for the superstructure block included its estimated mass and one-half of the column's mass that was recessed in the superstructure block. Tributary mass for column accelerometers accounted for the one half of the column length between adjacent accelerometer pairs and the estimated column mass per unit length. The selected sign convention generated a positive shear force consistent with a column displacement to the East.

The bending moment anywhere along the column height was computed as the contribution of three components; (1) lateral inertia forces generated by the superstructure and column masses; (2) rotational mass moment of inertia of the superstructure mass; and (3)  $P\Delta$  moment generated by the laterally displaced superstructure and column masses. The selected sign convention generated positive moments when the column was displaced to the East, which was considered a positive displacement. The moment generated by inertial forces relied on the inertial force itself and the average measured elevation of the accelerometer pair above the top of the footing. The moment generated by the superstructure rotational inertia was computed from the mass moment of inertia and the rotational acceleration. The mass moment of inertia was based on the specified block geometry—accounting for blockouts—and the estimated weight.

The rotational acceleration was obtained by calculating the average of three accelerometer pairs mounted either vertically or horizontally on the superstructure block, and the distance between the accelerometer pair. The  $P\Delta$  moment was computed from the estimated weight of the superstructure block and column, and horizontal displacements recorded by string potentiometers. This did not include variations in axial load due to induced vertical accelerations.

The column axial force was calculated from contributions of the superstructure mass and column. Vertical accelerometers were mounted on the East and West faces of the column, and on the top of the superstructure mass coinciding with the column centroid. Vertical accelerations, including gravitational acceleration, were multiplied by a tributary mass.

The average column section curvature was calculated over the accessible column height. The curvature was smeared over the gauge length of the LVDTs, which increased along the column height. At the base of the column, six 203 mm (8 in.) (one-sixth column diameter) gauge lengths were used from 51 mm (2 in.) to 1270 mm (50 in.) above the footing. The gauge length was then increased to 610 mm (24 in.) for four regions and increased again to 787 mm (31 in.) for two regions. Measurements from LVDTs located at the four corners of the column were divided by their initial gauge length to obtain average strain. The horizontal, East-West distance between the vertical LVDTs on North side of the column was used to calculate the curvature from the strain measurements on this side. The same calculation was performed for the South side of the column, and the mean value of these two curvatures was retained.

# 8 Test Results

## 8.1 TEST EQ1

The objective of this test was to induce a displacement ductility of 1.0. The peak displacement achieved, defined as the magnitude of the maximum displacement in the East or West direction, was 62 mm (2.44 in.), corresponding to a 0.85% drift ratio with no plastic deformation occurring. Figure 8.1 shows the displacement time history with initial, peak, and residual quantities indicated. The residual displacement was 1 mm (0.03 in.) or a 0.01% residual drift ratio. Figure 8.2(a) and (b) show the East face of the column base at maximum displacement in the West and East directions, respectively.

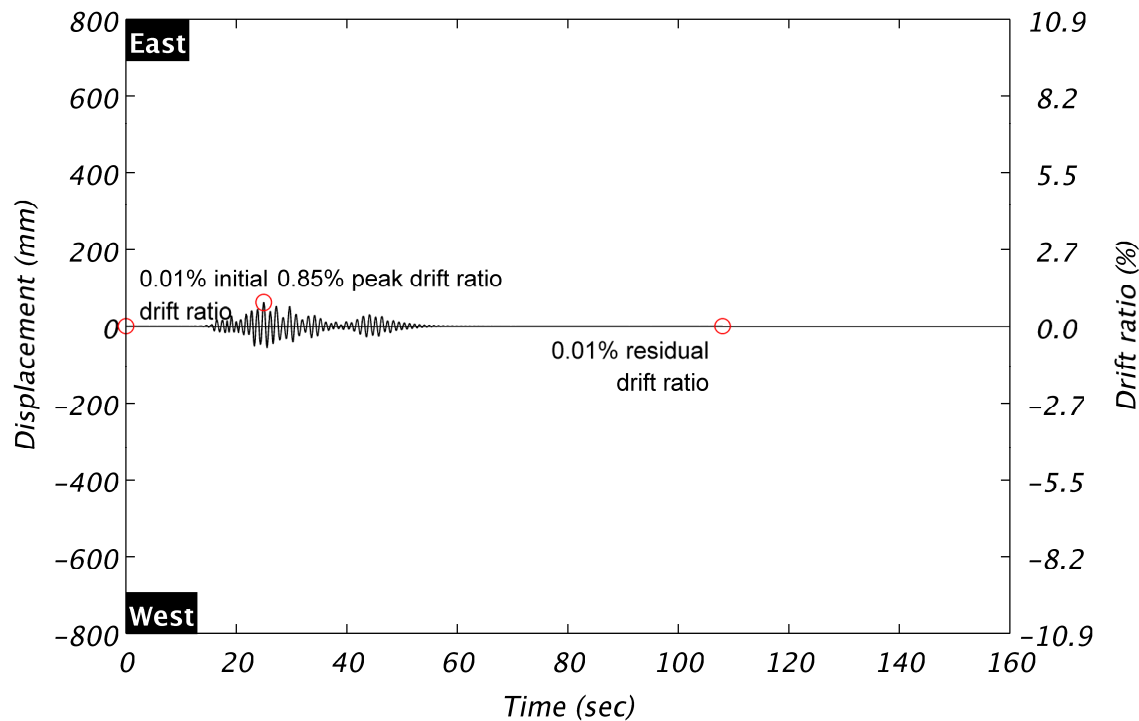
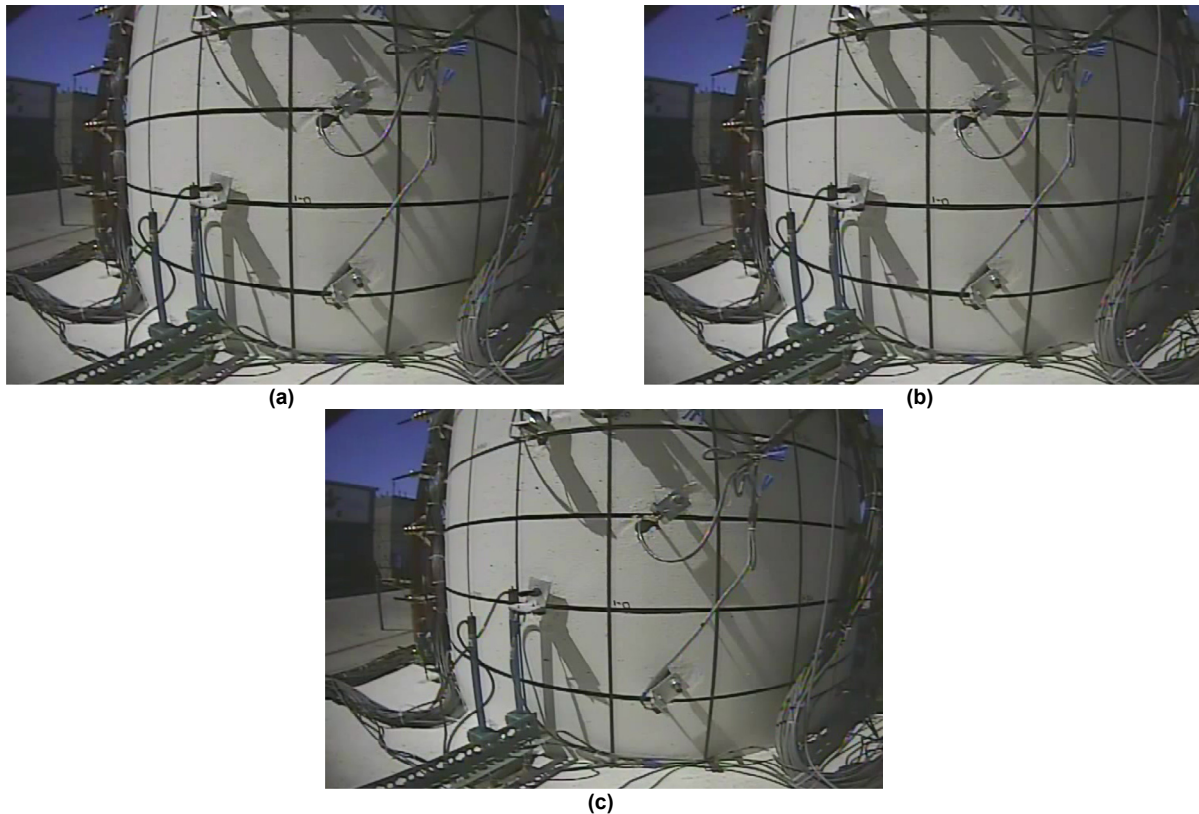


Figure 8.1 Column displacement during Test EQ1.



**Figure 8.2 Column base East face during Test EQ1 at (a) peak West displacement, (b) peak East displacement, and (c) post-test.**

There was no observable damage in the column post-test. Hairline cracks, defined here as less than 0.1 mm (0.004-in), were found at the column to footing interface. The cracks were discontinuous on the East and West sides of the column. No other cracks were observed in the test specimen. A post-test view of the East face of the column base is shown in Figure 8.2(c).

An essentially linear elastic moment-curvature response was obtained from the derived moment at the column base and the average curvature calculated near the column base; see Figure 8.3. The curvature was calculated over a 406 mm (16 in.) (one-third column diameter) gauge length from 51 mm (2 in.) to 457 mm (18 in.) above the footing. The peak column base moment was 3950 kN-m (2910 kip-ft).

The idealized backbone curves shown in Figure 8.3 and Figure 8.4; subsequent similar plots are the monotonic response from the analytical tool developed in the ground motion selection process. The analytical prediction was significantly more stiff in terms of moment curvature. For this reason, an experimental yield curvature is defined as:

$$\phi_{ye} = \frac{M_y}{EI_e} = 8.36 \times 10^3 \frac{\text{rad}}{m} \left( 2.12 \times 10^{-4} \frac{\text{rad}}{\text{in.}} \right) \quad (8.1)$$

where  $M_y$  is the nominal moment capacity from the analytical model, and  $EI_e$  is the average of the secant slope to maximum and minimum moment-curvature response obtained in Test EQ1.

This is the basis for defining curvature ductility hereafter. The experimental yield curvature can be defined in normalized terms as:

$$\phi_{ye} D = 0.010 \text{ rad} \quad (8.2)$$

or

$$\frac{\phi_{ye} D}{\varepsilon_y} = 3.91 \text{ rad} \quad (8.3)$$

Column base shear was derived from inertia forces in the superstructure block and column. The peak shear force was 500 kN (112 kip). The lateral shear force and displacement response shown in Figure 8.4 exhibits a linear elastic behavior influenced by a higher mode. Better agreement was achieved between analytical and experimental stiffness in terms of force-displacement response. The experimental idealized yield displacement,  $D_{ye}$ , is defined as:

$$\Delta_{ye} \frac{V_y}{K_e} = 90 \text{ mm (3.54 in.)} \quad (8.4)$$

where  $V_y$  is the nominal shear capacity, and  $K_e$  is the average of the secant slope to maximum and minimum shear-displacement response. This is the basis for defining displacement ductility throughout the test program. The corresponding experimental yield drift ratio is 1.23%.

Localized yielding may have occurred in the longitudinal reinforcement. Peak recorded strains were averaged from pairs of strain gauges and reached 0.0022 mm/mm; see Figure 8.5. This corresponds to  $0.85 \varepsilon_y$ , where  $\varepsilon_y$  is the longitudinal yield strain of 0.0026 mm/mm obtained from material testing. Although localized yielding may have occurred outside of the monitored locations, a plastic hinge did not form. Both the pair's average response and the corresponding individual gauge readings are shown with error bars. These are indistinguishable in Figure 8.5.

Longitudinal bar strain provides the local response quantity to compare with the longitudinal bar's bond slip. The bond-slip bracket is described in Section 7.2 and depicted in Figure 7.3. For this comparison, the longitudinal bar strain at the top of the footing was selected. This was measured by the longitudinal strain gauges located a few inches above the bond-slip bracket. The responses of both bars instrumented with a bracket (East and West) are presented. Positive bar displacement and strain correspond with tensile demands. Figure 8.6 shows the hysteretic response obtained. The responses during Test EQ1 have minor hysteresis with peak bond slip on the order of 1 mm (0.04 in.) in the West longitudinal bar. In compression, the bars slipped less than 0.254 mm (0.01 in.).

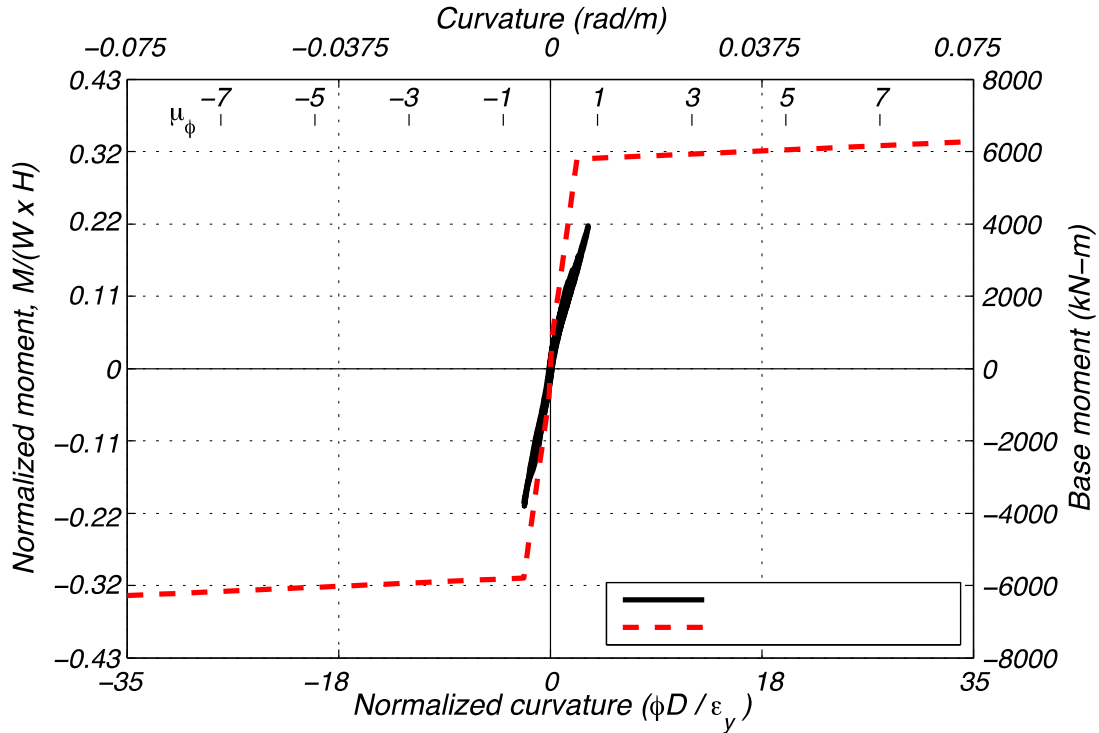


**Figure 8.3** Column response during Test EQ1 in terms of base moment and curvature.

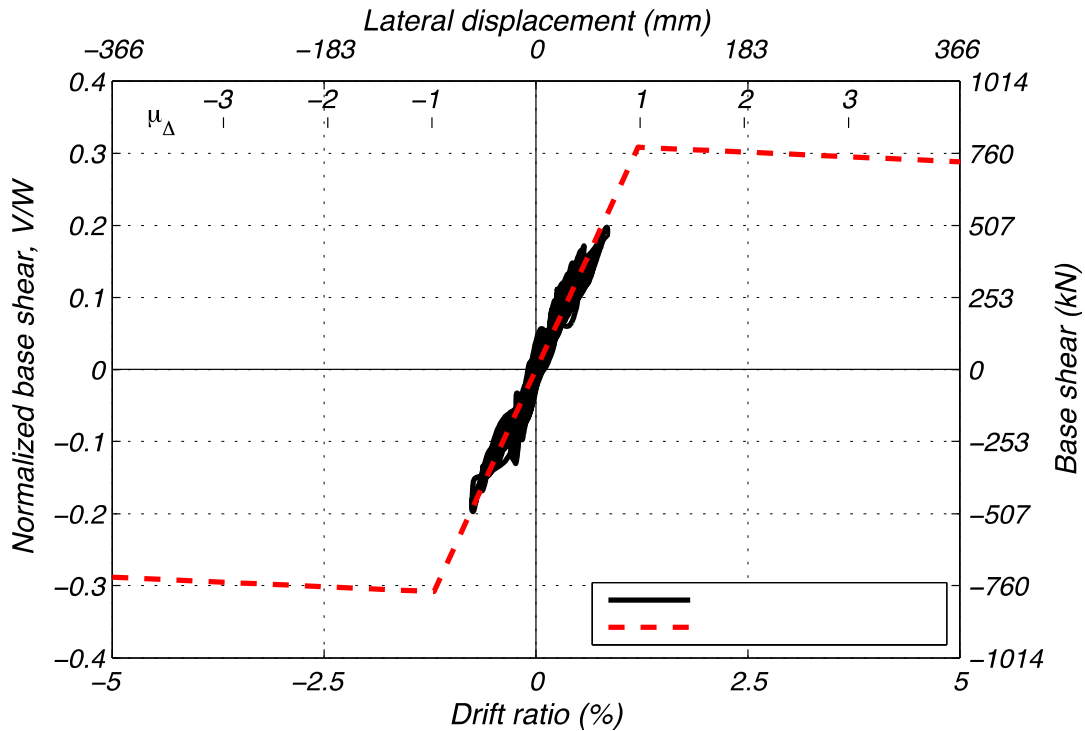


**Figure 8.4** Column response during Test EQ1 in terms of base shear and drift ratio.

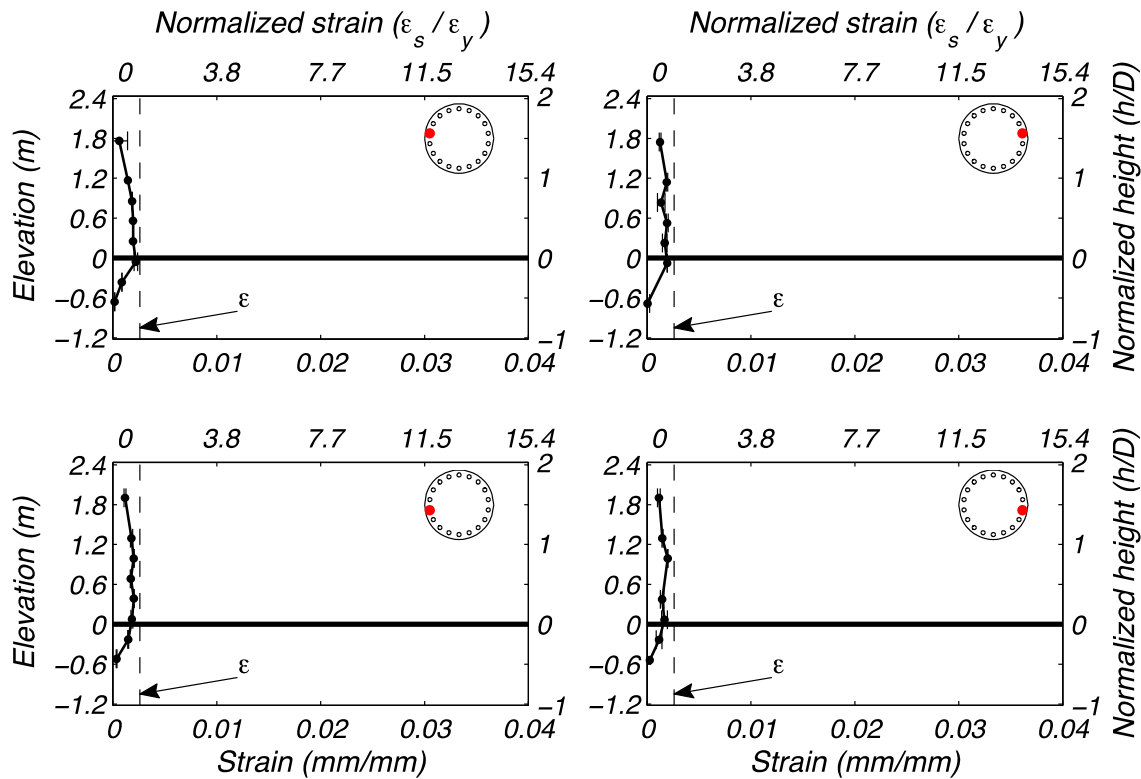


**Figure 8.5** Longitudinal reinforcement tensile strain demand during Test EQ1.

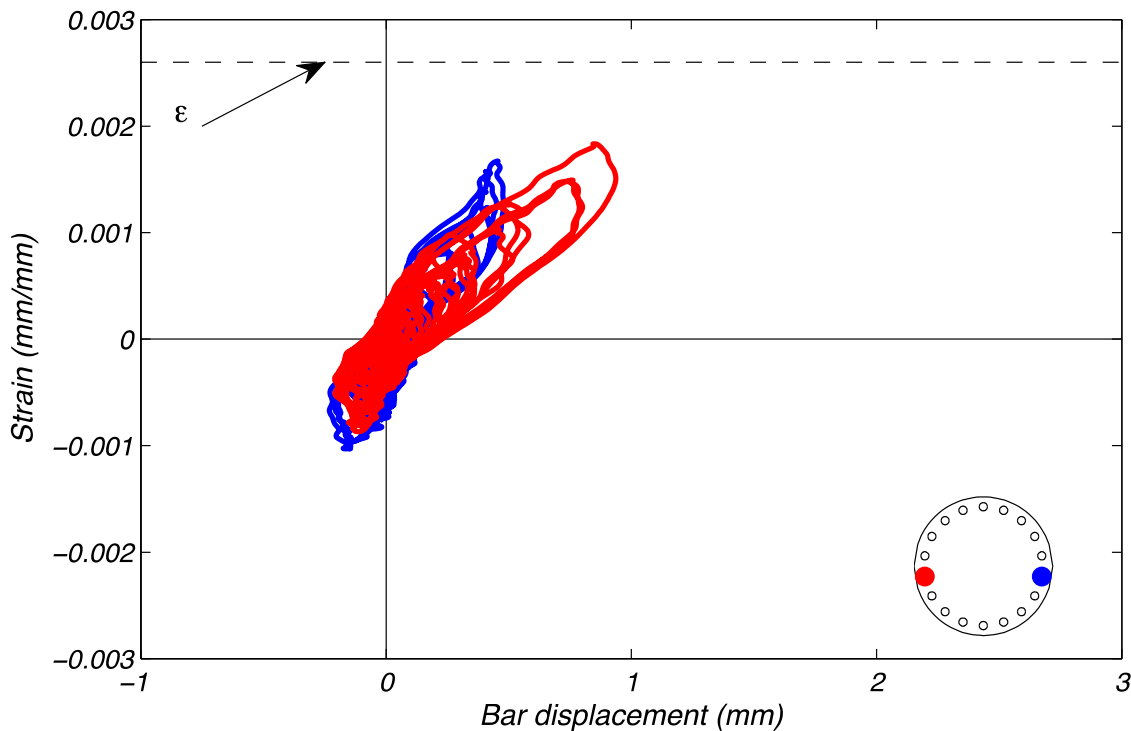


**Figure 8.6** Longitudinal reinforcement bond slip during Test EQ1.

Transverse hoop strains on the East and West faces of the column remained elastic. A single strain gauge was located on the outside of one of the bundled hoops on the East and West sides of the column. Figure 8.7 shows the maximum tensile values obtained in the instrumented hoops were larger on the West face, with values approaching yield at elevations between 0.25 and 0.5 times the column diameter. Negligible strain increases were recorded on the East face.

Figure 8.8 shows the smeared curvature profile of the column over the height; it was measured during instances of peak column displacement, East and West, and post-test. Peak curvature values were below the experimental idealized curvature over the height. The lowermost region instrumented—between 51 mm (2 in.) and 254 (10 in.) above the footing—captured negligible curvature and is not distinguishable in the figure. The residual curvature profile is shown in red and indicates no residual curvature after Test EQ1.

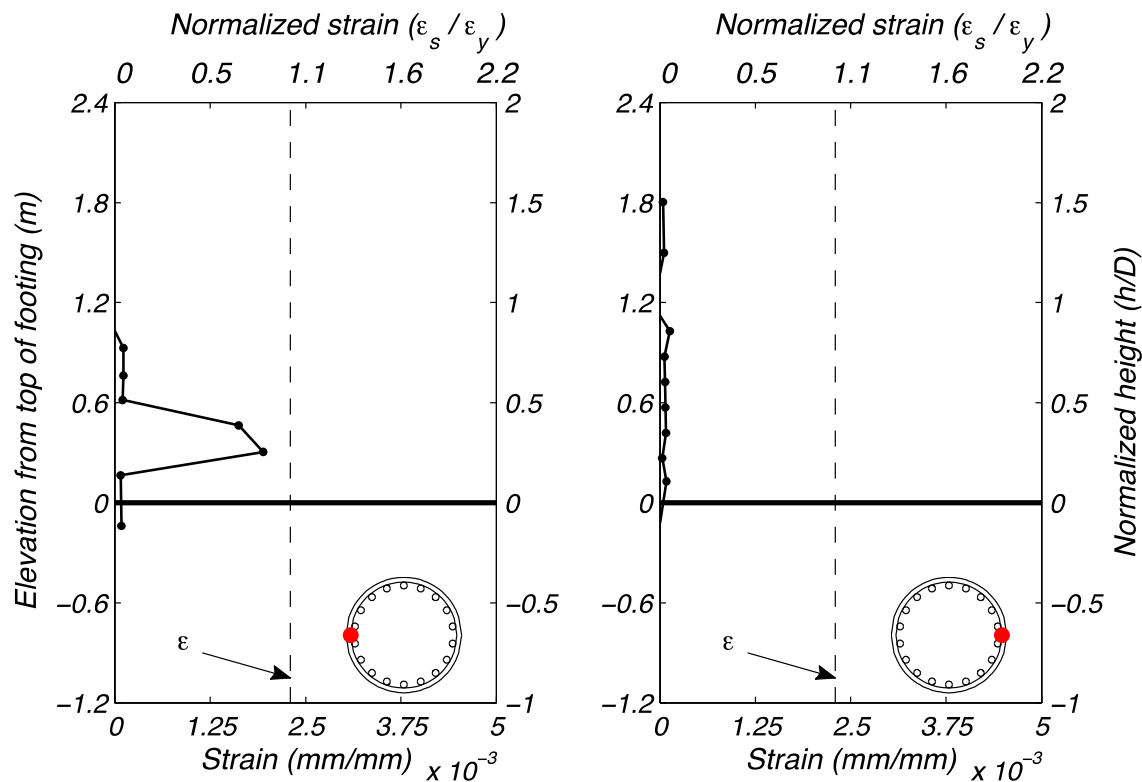


**Figure 8.7 Transverse hoop reinforcement tensile strain demand during Test EQ1.**

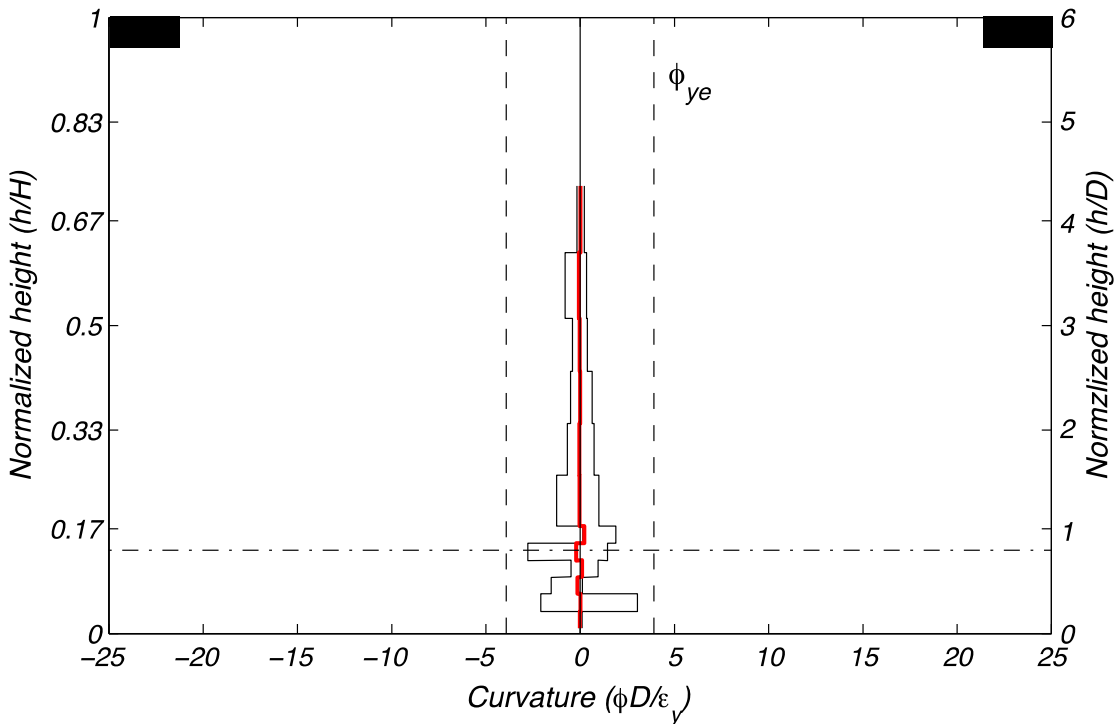


**Figure 8.8 Curvature profile at peak and residual displacements during Test EQ1.**

## 8.2 TEST EQ2

A displacement ductility of two was the target ductility for Test EQ2. The earthquake simulation produced a displacement ductility of 1.48 at the peak displacement of 133 mm (5.23 in.). This corresponds to a drift ratio of 1.82%. The residual displacement was a negligible 4 mm (0.16 in.) or 0.05% residual drift ratio. These values are indicated in the displacement time history of the top of the column in Figure 8.9, corresponding to the center-of-mass of the superstructure. Figure 8.10(a) and (b) show the East face of the column base at peak displacement in the West and East directions, respectively. A tensile crack is visible in Figure 8.10(a) approximately 254 mm (10 in.) above the footing. A post-test view of the East face of the column base is shown in

Figure 8.10(c). The video snapshot was taken before crack marking, so cracks are not visible in this figure.

Residual crack widths remained at hairline width after this test. Crack propagation occurred at the column to footing interface and additional cracks formed. Discontinuous hairline cracks spaced between 152 mm (6 in.) and 305 mm (12 in.) were found in the column from its base to about 1.68 m (5.5 ft). Additional cracks were found between 3.91 m (12.5 ft) and 4.97 m (16.3 ft).

A nonlinear response was obtained in the moment-curvature relationship; see Figure 8.11. The peak column base moment was 5900 kN-m (4350 kip-ft), and peak shear force was 699 kN (157 kip). The lateral shear force and displacement response is shown in Figure 8.12.

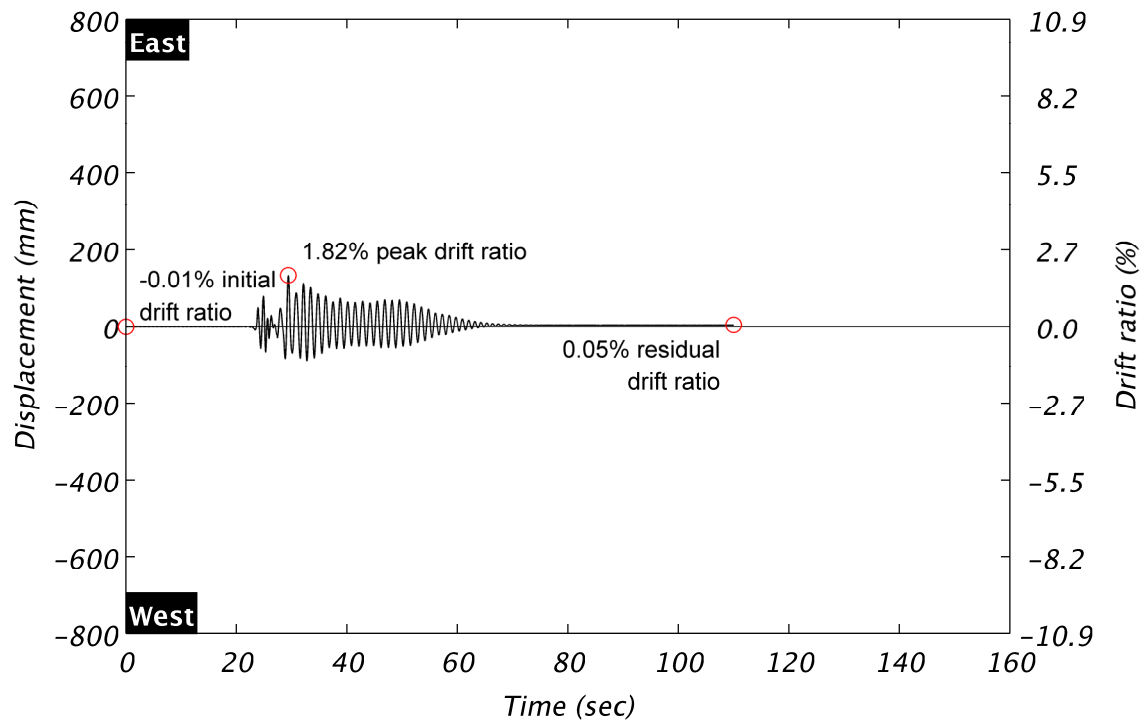


**Figure 8.9      Column displacement during Test EQ2.**

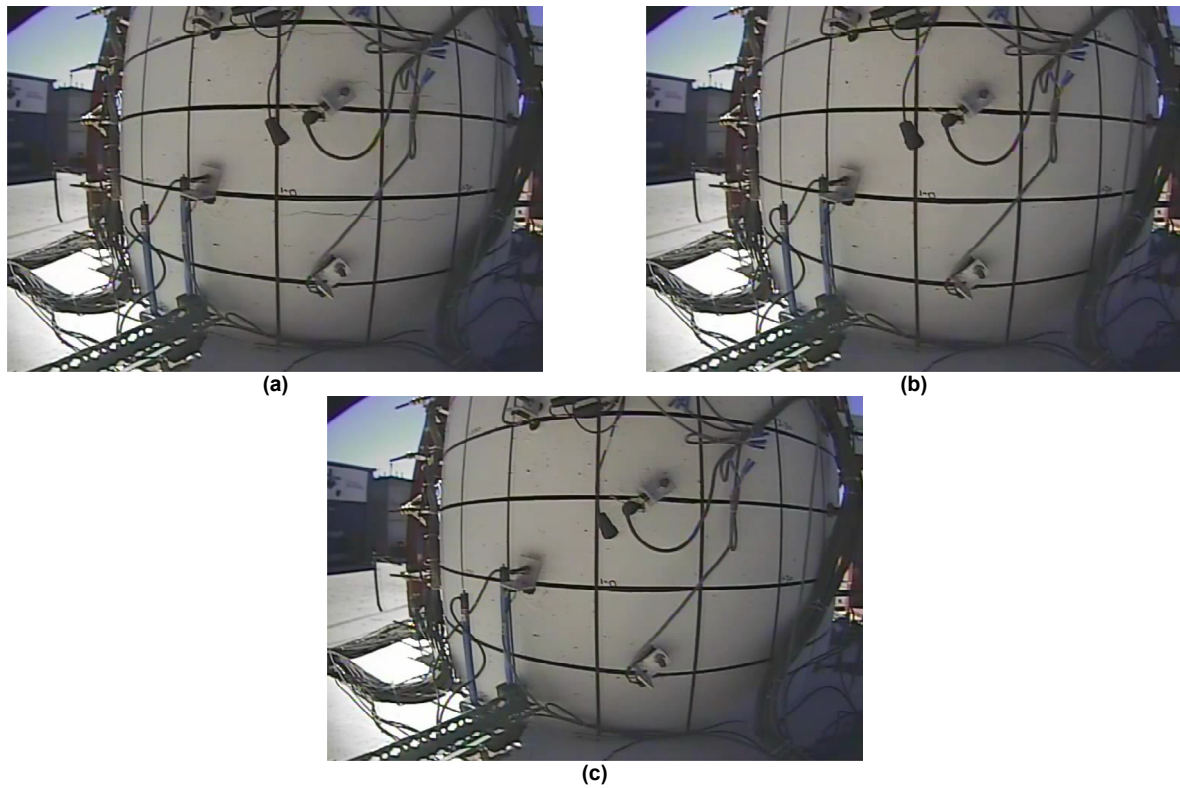


**Figure 8.10      Column base East face during Test EQ2 at (a) peak West displacement, (b) East positive displacement, and (c) post-test.**

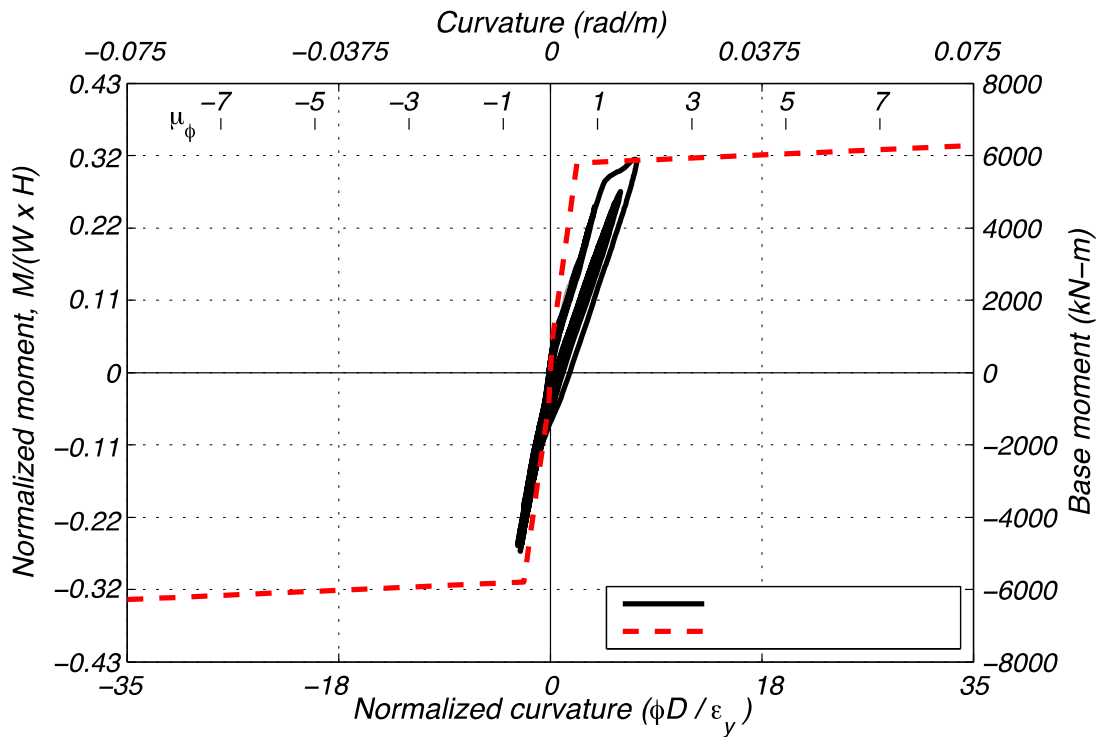


**Figure 8.11** Column response during Test EQ2 in terms of base moment and curvature.

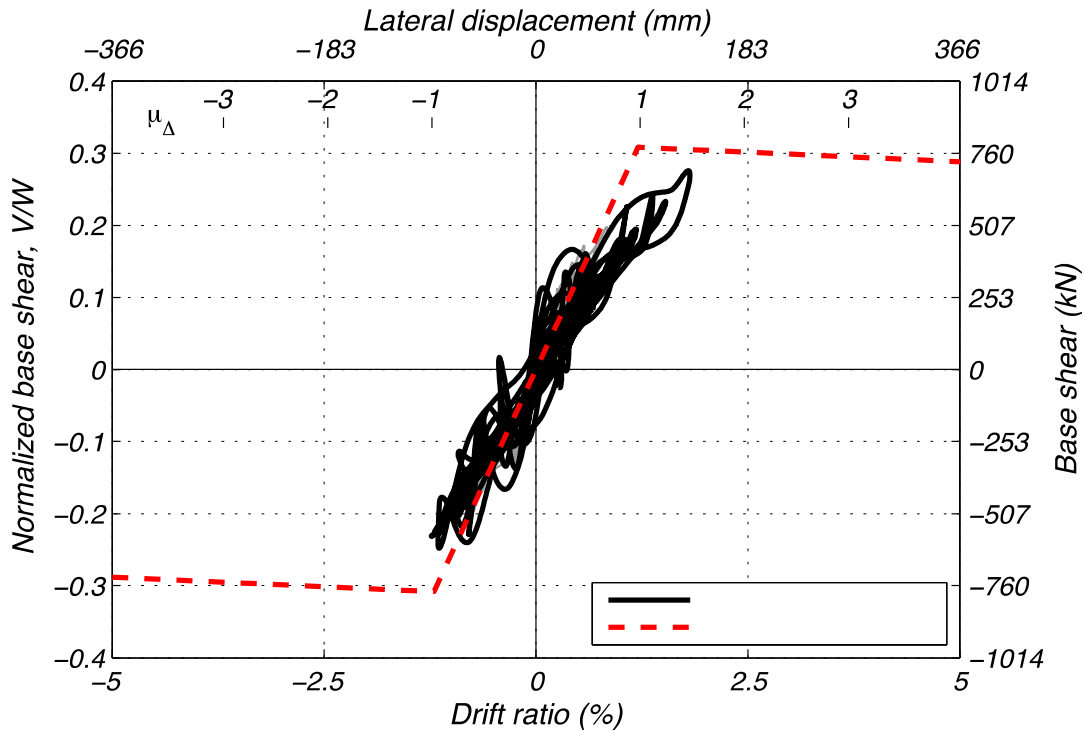
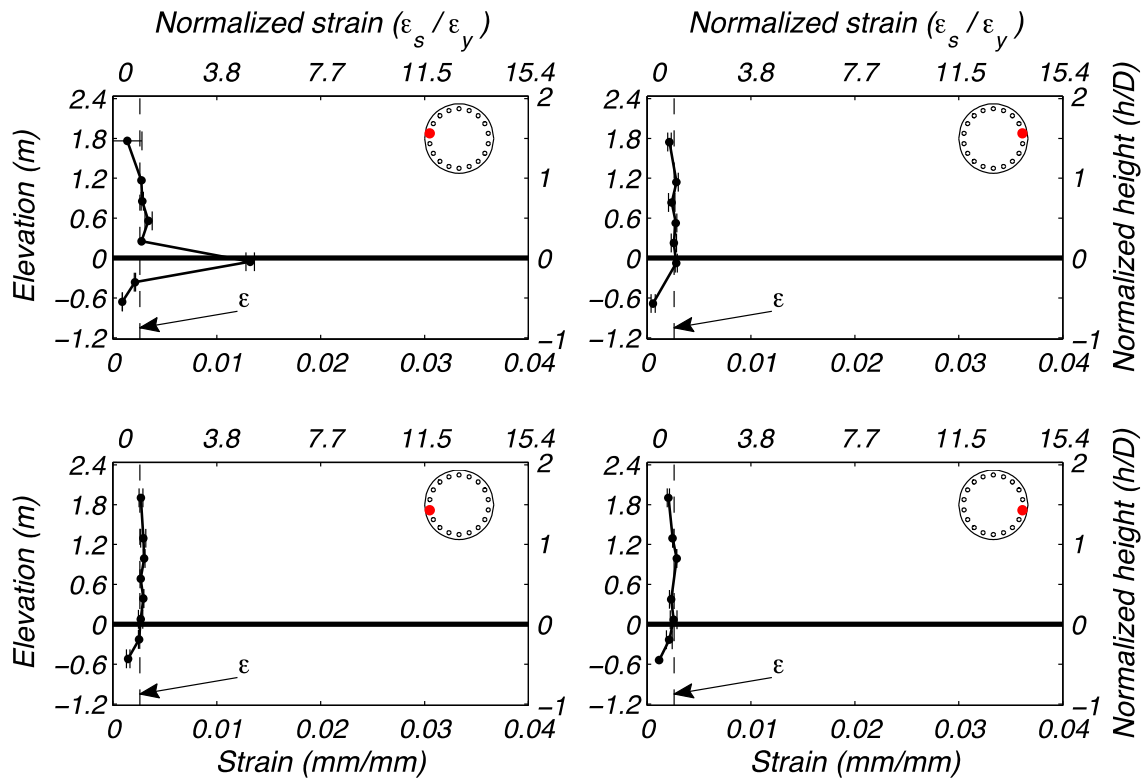


**Figure 8.12** Column response during Test EQ2 in terms of base shear and drift ratio.

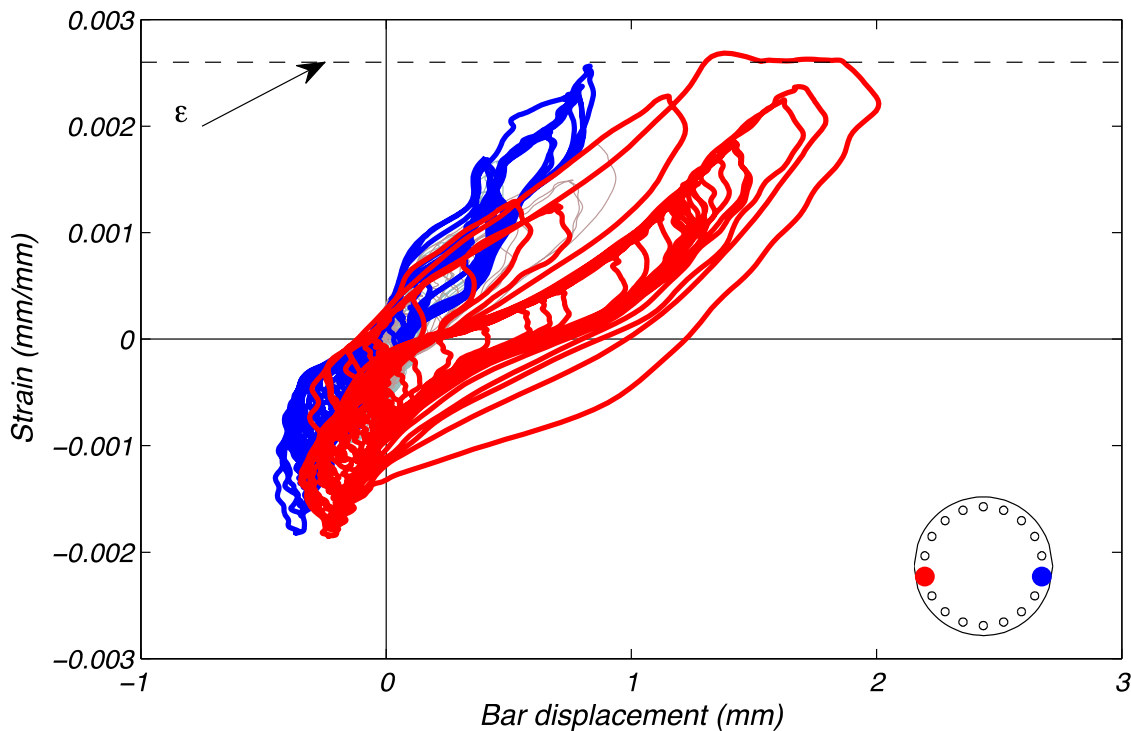
Localized yielding was measured by strain gauges near the column-to-footing interface; see Figure 8.13. Maximum tensile strain was  $0.0132 \text{ mm/mm}$  or  $5.1 \varepsilon_y$ . All four instrumented bars achieved peak tensile strains on the order of yielding within one column diameter from the top of the footing. Although localized yielding occurred, a plastic hinge did not form, as suggested by limited cracking and the lack of plastic displacement; see Figure 8.12. Transverse hoop strains exceeded their yield strain at elevations between 0.25 and 0.5 times the column diameter on the West face; see Figure 8.15. Strains demands on the opposite face were minor.

Figure 8.16 shows the smeared curvature profile of the column over the height measured during instances of peak column displacement, East and West, and post-test. The maximum curvature exceeded the idealized curvature only within the region between 254 mm (10 in.) and 457 mm (18 in.). The lowermost region instrumented, between 51 mm (2 in.) and 254 (10 in.) above the footing, captured negligible curvature and is not distinguishable in the figure. The residual curvature profile after Test EQ2 is shown in red and shows negligible post-test curvature.

Longitudinal bar strain at the top of the footing provides the local response quantity to compare with the longitudinal bar's bond slip. Longitudinal strain gauges were located a few inches above the bond-slip bracket; see Section 7.2. The responses of both bars instrumented with a bracket (East and West) are presented. Positive bar displacement and strain correspond with tensile demands. Figure 8.14 shows the hysteretic responses during Test EQ2. The bar on the West face of the column had larger tensile demands imposed resulting in bond slip on the order of 2 mm (0.08 in.). Both bars uplifted twice the demand imposed by Test EQ1, which is included in a lighter line weight and color. There is a marked increase in uplift [1.3 to 2.0 mm (0.05 in. to 0.08 in.)] in the bar on the West face without an increase in strain, indicating bond slip within the footing.



**Figure 8.13** Longitudinal reinforcement tensile strain demand during Test EQ2.



**Figure 8.14** Longitudinal reinforcement bond slip during Test EQ2.

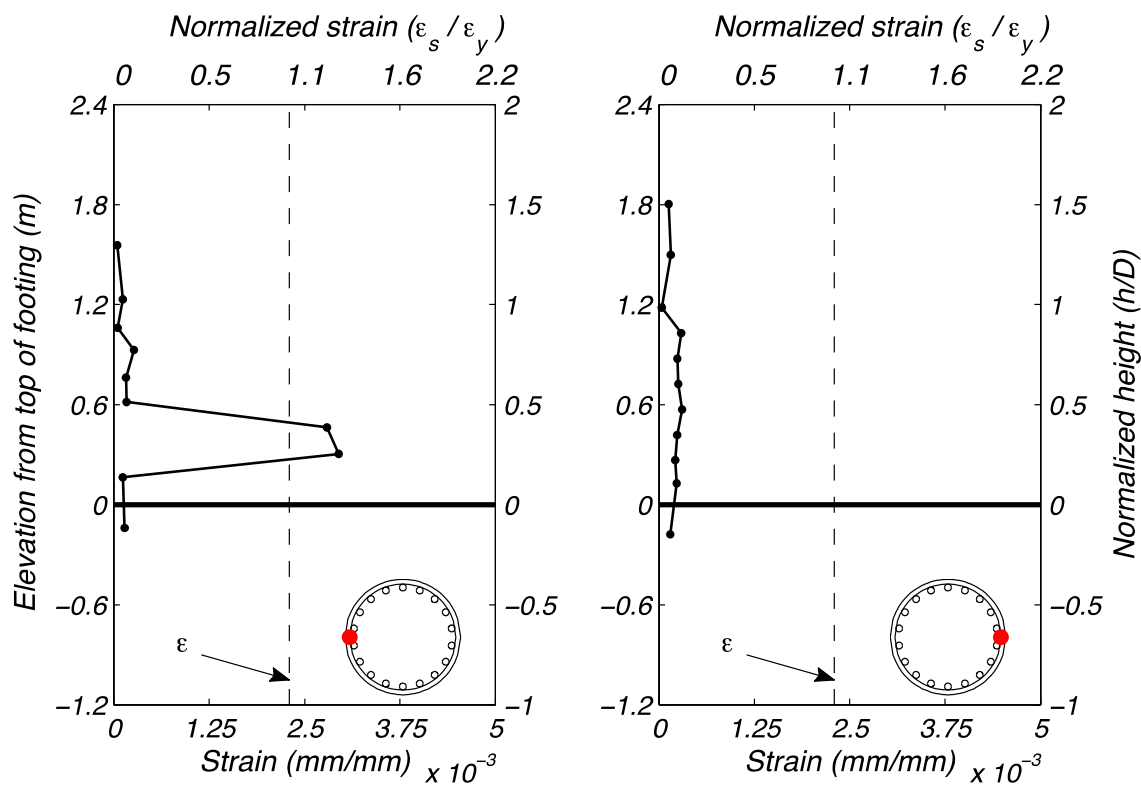


**Figure 8.15 Transverse hoop reinforcement tensile strain demand during Test EQ2.**

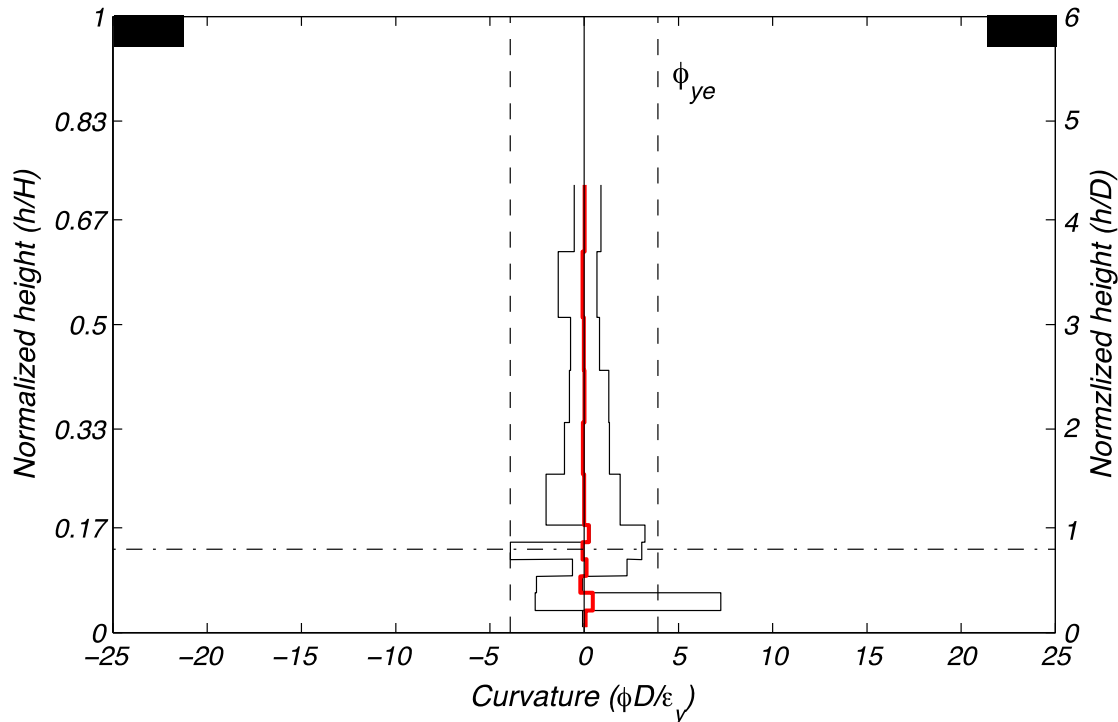


**Figure 8.16 Curvature profile at peak and residual displacements during Test EQ2.**

### 8.3 TEST EQ3

Test EQ3 represents a simulation of a design level earthquake. The target displacement ductility of four was achieved with only cosmetic damage. A peak displacement of 361 mm (14.2 in.) was measured at the top of the column. This corresponds to a displacement ductility of 4.01 or a drift ratio of 4.93%. A residual drift ratio of -0.87% or -63mm (-2.49 in.) resulted from the nonlinear response. These values are indicated in the displacement time history shown in Figure 8.17. This was the first instance of residual drift. Figure 8.18(a) and (b) show the East face of the column base at peak displacement in the West and East directions, respectively. A residual displacement after Test EQ3 denotes that target displacement ductilities are not relevant to subsequent tests. Target displacement ductilities used in the ground motion selection process were based on cracked section properties and zero initial displacement. No attempts were made to straighten or repair the column between tests.

Spalling of the concrete cover was initiated at this level of testing. Spalling occurred on the West face of the column; see in Figure 8.19. The maximum residual crack width near the base of the column was 1.4 mm (0.055 in.). Significant cracking developed at the base of the column; see the post-test views of the East and West column faces in Figure 8.18(c) and Figure 8.19, respectively. The snapshot in this figure was taken before cracks had been marked, but the crack pattern and concrete flaking are visible.

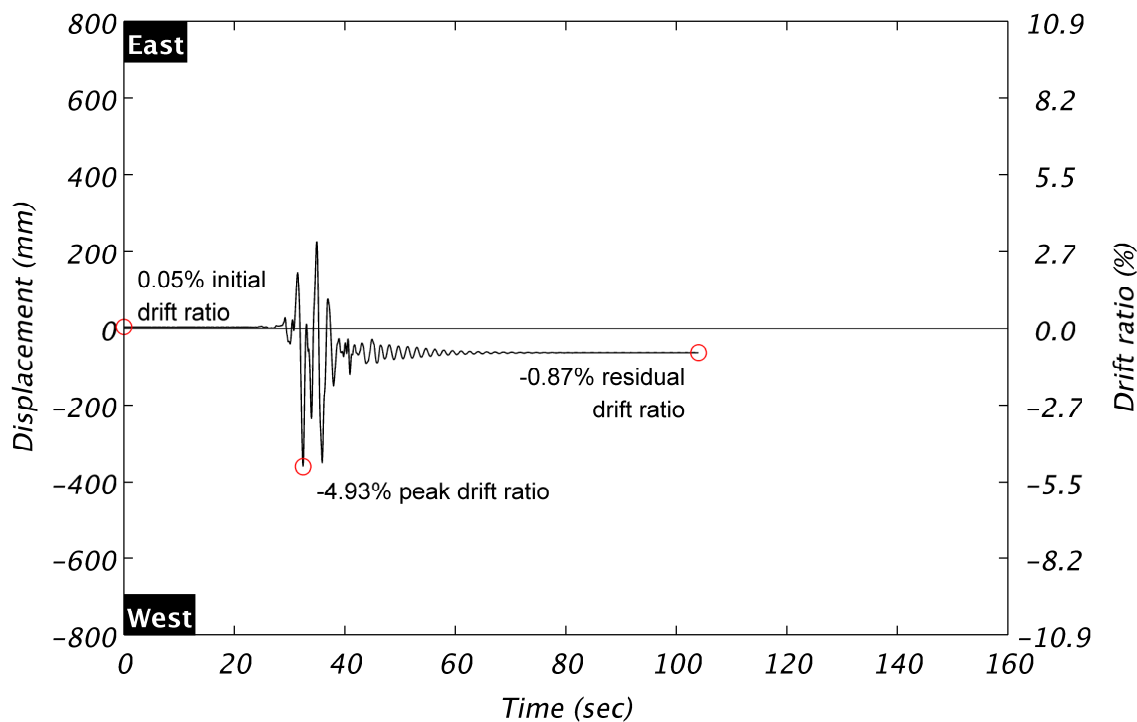
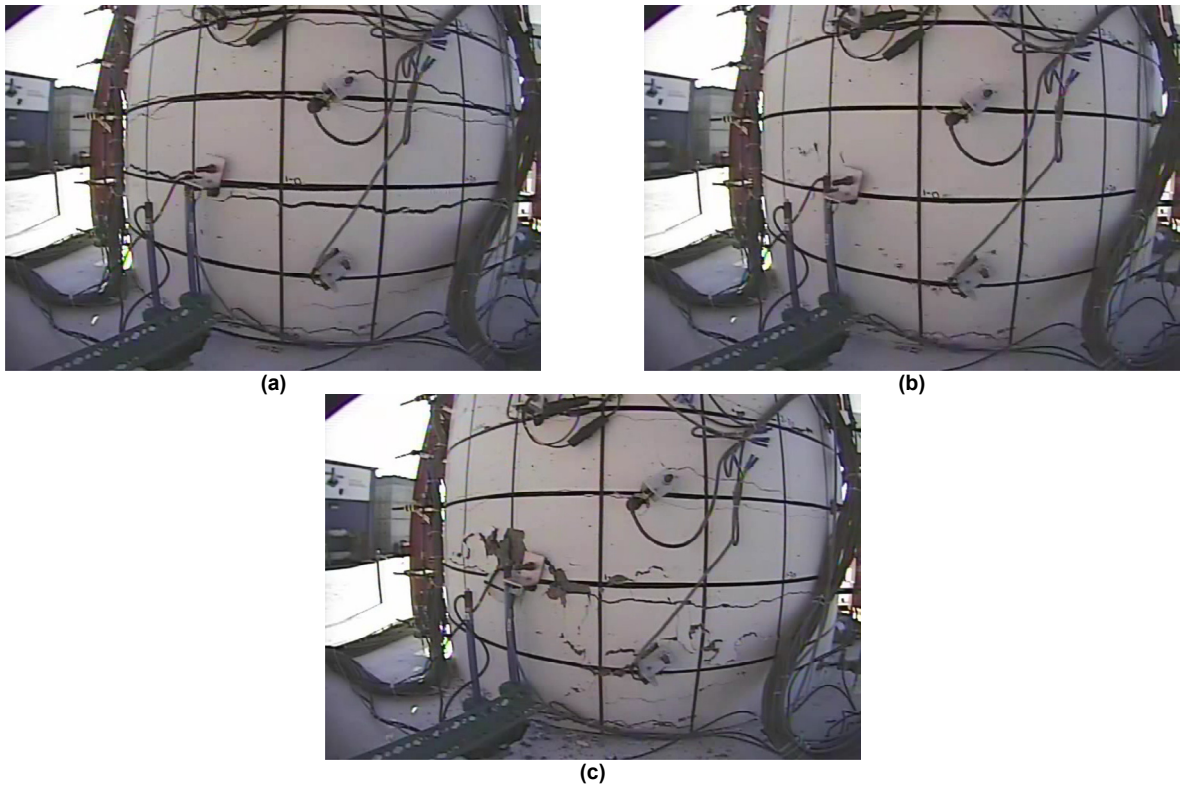


Figure 8.17 Column displacement during Test EQ3.



**Figure 8.18** Column base East face during Test EQ3 at (a) peak West displacement, (b) peak East displacement, and (c) post-test.



**Figure 8.19** Column base West face after Test EQ3.

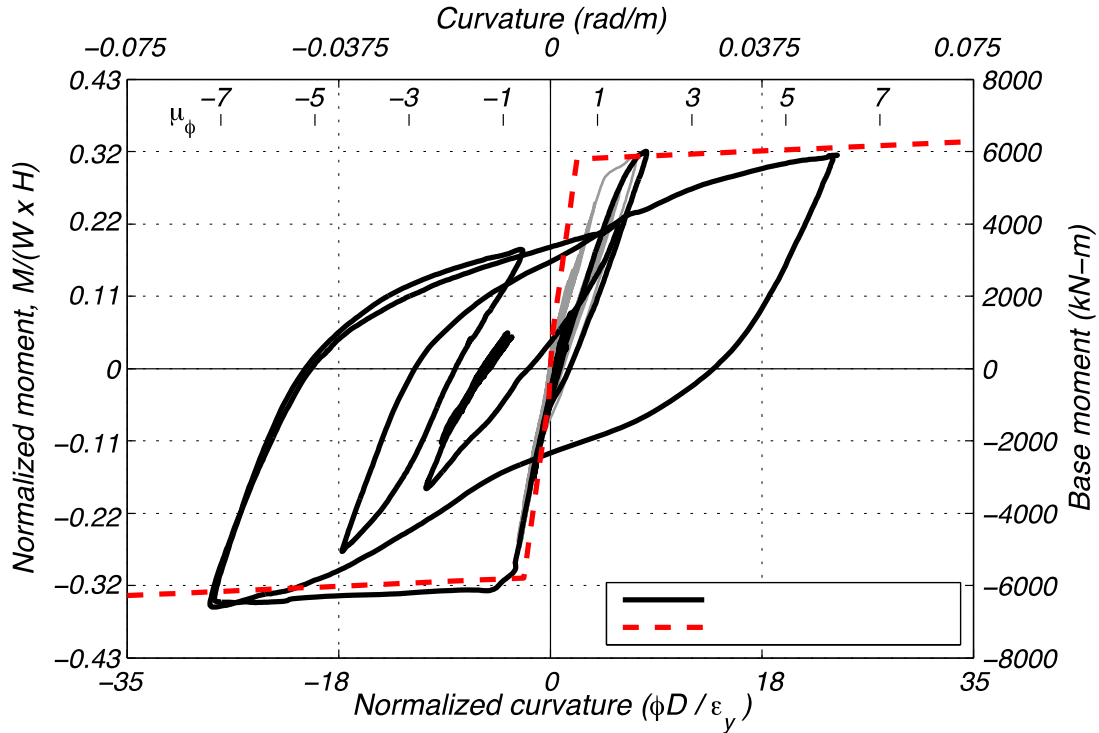
Significant nonlinearity was obtained in the moment-curvature response; see Figure 8.20. The peak column base moment was 6590 kN-m (4860 kip-ft). The peak shear force was 888 kN (200 kip); this was the largest shear force obtained in any of the tests. The lateral shear force and displacement response is shown in Figure 8.21. Contributions from a higher mode are evident in this figure.

Significant yielding was captured by strain gauges on all four instrumented longitudinal bars; see Figure 8.22. This occurred within one column diameter from the footing interface. The maximum tensile strain was 0.0298 mm/mm or  $11.5 \varepsilon_y$ . In this test, gauge pairs began to exhibit variation as evident in the error bars at some locations. Strain penetration into the footing is apparent, but demands were below yield at a depth below the footing of  $\frac{1}{2}D$  or  $17 d_b$ .

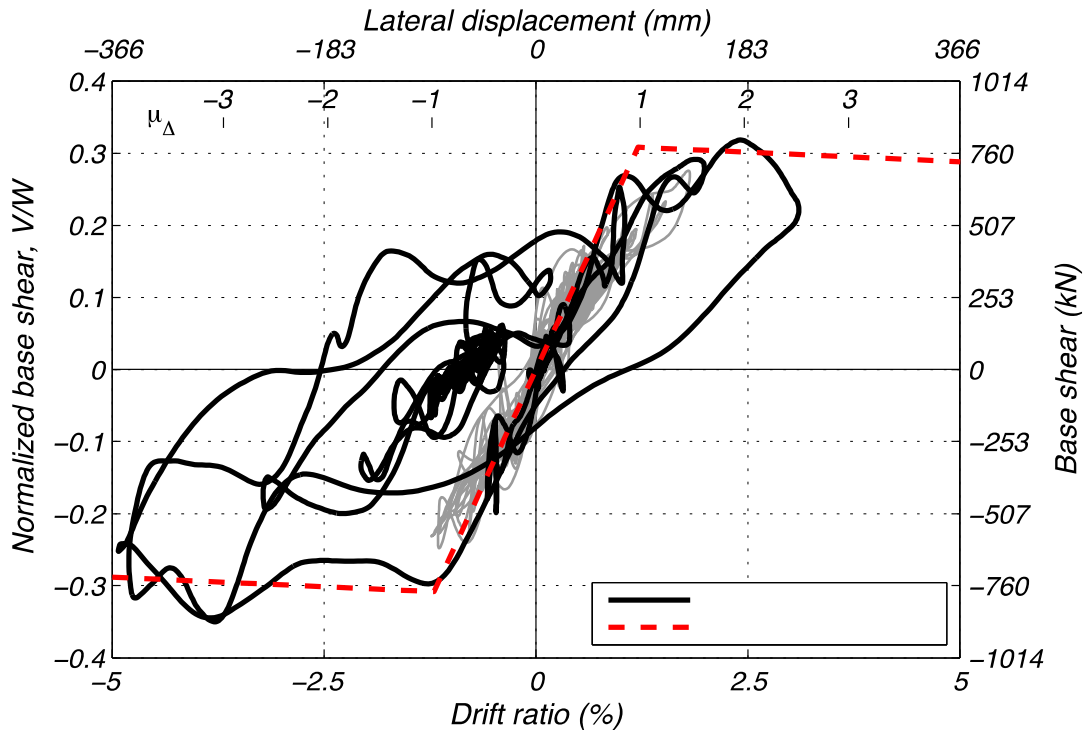
Peak transverse strain demands on the West face were consistent with demands from the prior test. Only two hoops on the West face of the column exceeded yield, see Figure 8.24. Hoop demands elsewhere increased but were below yield. Despite only modest transverse strain demand increases, the plastic hinge was fully formed as evident in the nonlinear moment and shear responses, longitudinal strain demands, and observed damage.

Figure 8.25 shows the smeared curvature profile of the column over the height measured during instances of peak column displacement, East and West, and post-test. The experimental idealized curvature was exceeded over a 1.07 m (42 in.) height, nearly one column diameter, above the footing. The lowermost region instrumented, which indicated negligible curvature in prior tests, generated a peak, smeared curvature just above idealized yield. The maximum curvature produces a curvature ductility of approximately six and occurs at a height above the footing between 254 mm (10 in.) and 457 mm (18 in.). The residual curvature profile is shown in red with negligible residual curvature above one column diameter, but a value slightly larger than yield between 254 mm (10 in.) and 660 mm (26 in.).

Longitudinal bar strain at the top of the footing provides the local response quantity to compare with the longitudinal bar's bond slip. Longitudinal strain gauges were located a few inches above the bond-slip bracket; see Section 7.2 and Figure 7.3. The responses of both bars instrumented with a bracket (East and West) are presented. Positive bar displacement and strain correspond with tensile demands. Figure 8.23 shows the hysteretic responses during Test EQ3. An LVDT attached to the bracket on the West face of the column slipped off its target during this test before significant bond slip or yielding was captured. Uplift in the bar on the East face of the column exceeded 4 mm (0.16 in.), and bar displacement in compression was consistent with prior tests on the order of 0.5 mm (0.02 in.). In this bar, a residual uplift of 1 mm (0.04 in.) remained post-test.



**Figure 8.20** Column response during Test EQ3 in terms of base moment and curvature.



**Figure 8.21** Column response during Test EQ3 in terms of base shear and drift ratio.

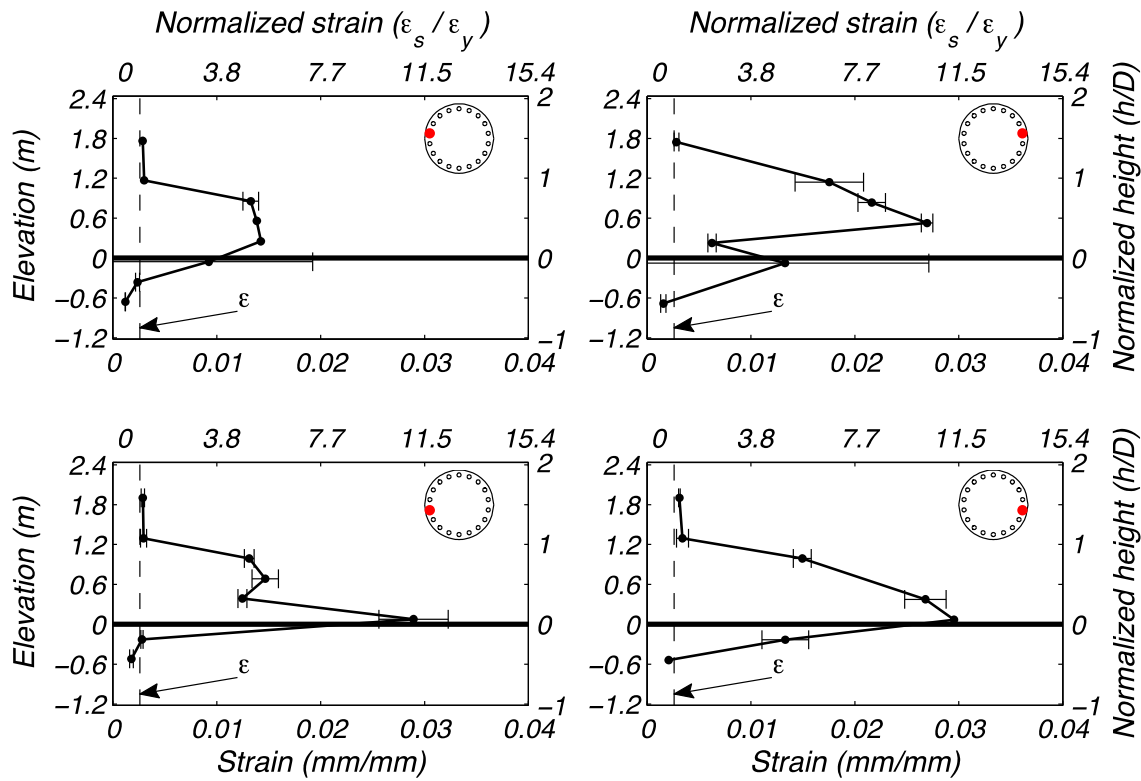


**Figure 8.22** Longitudinal reinforcement tensile strain demand during Test EQ3.

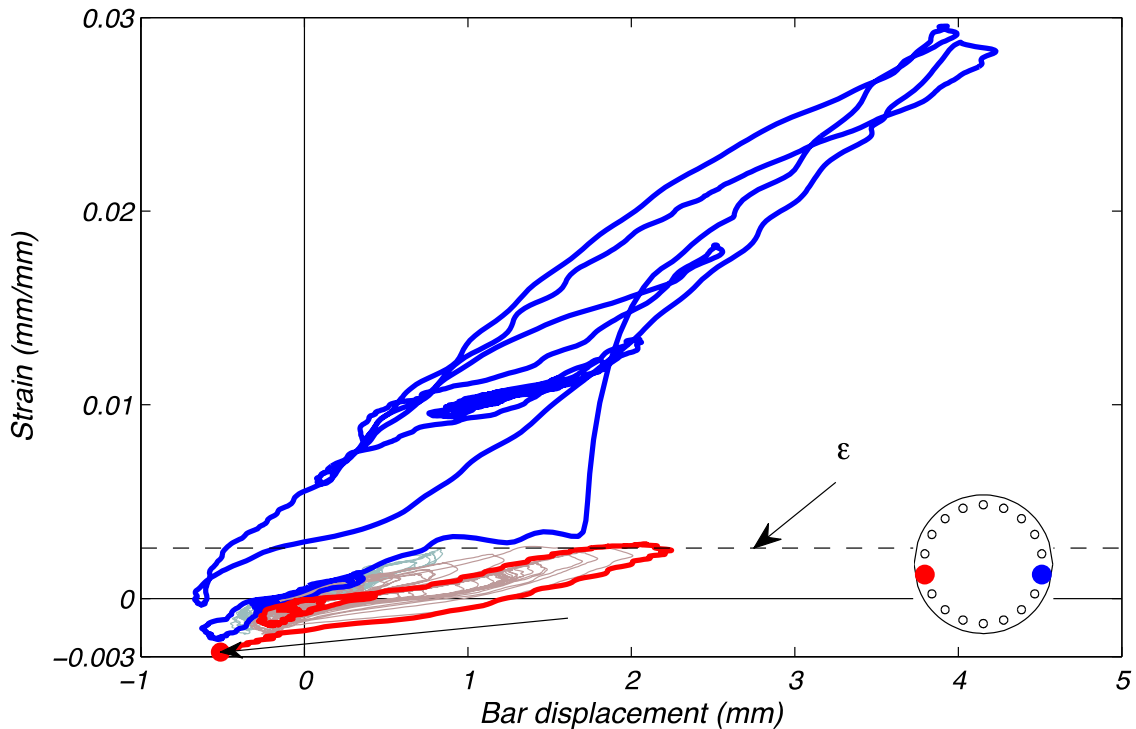


**Figure 8.23** Longitudinal reinforcement bond slip during Test EQ3.

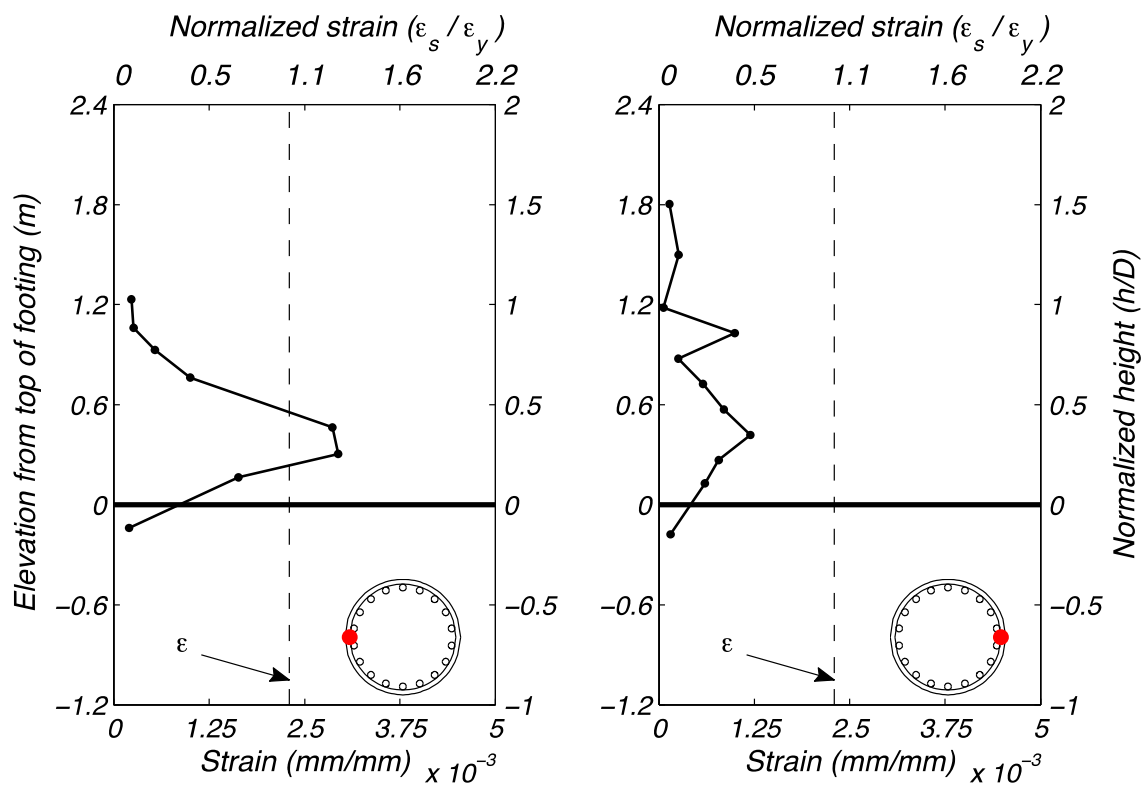


Figure 8.24 Transverse hoop reinforcement tensile strain demand during Test EQ3.

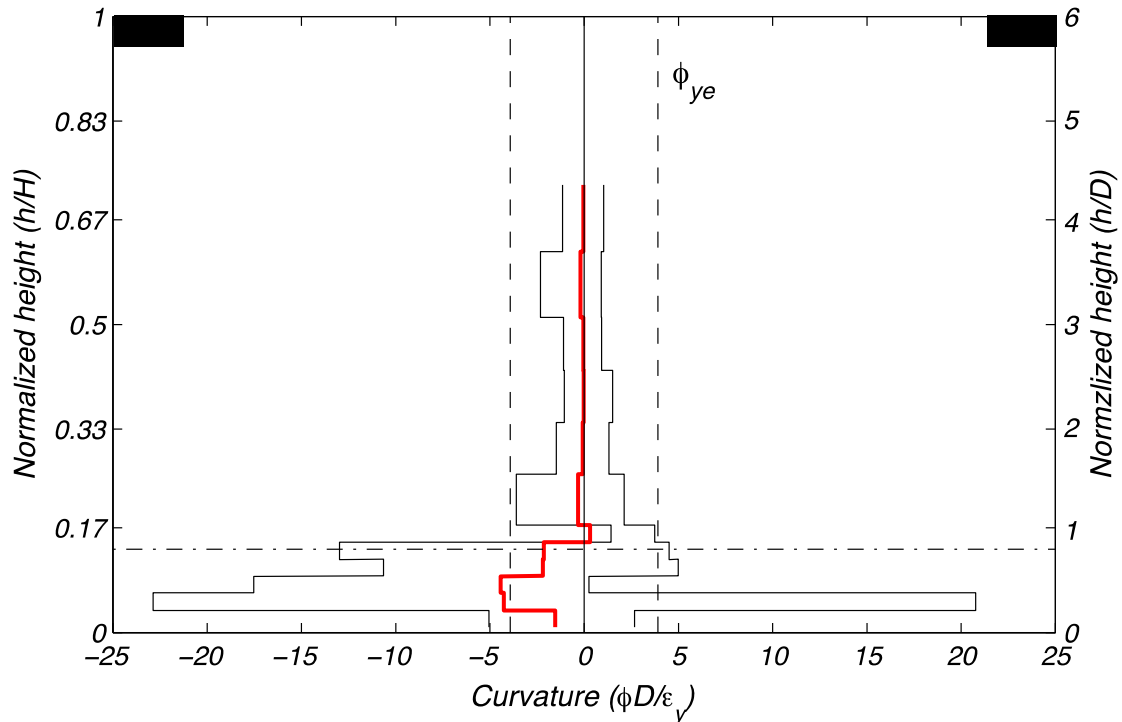


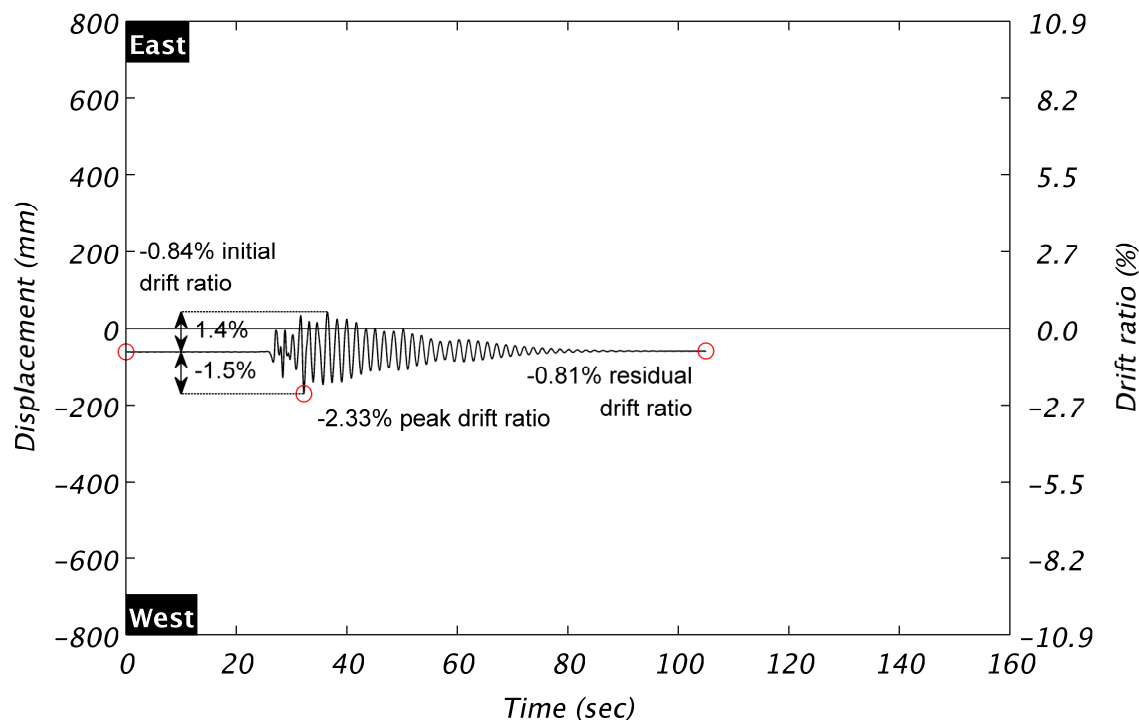
Figure 8.25 Curvature profile at peak and residual displacements during Test EQ3.

## 8.4 TEST EQ4

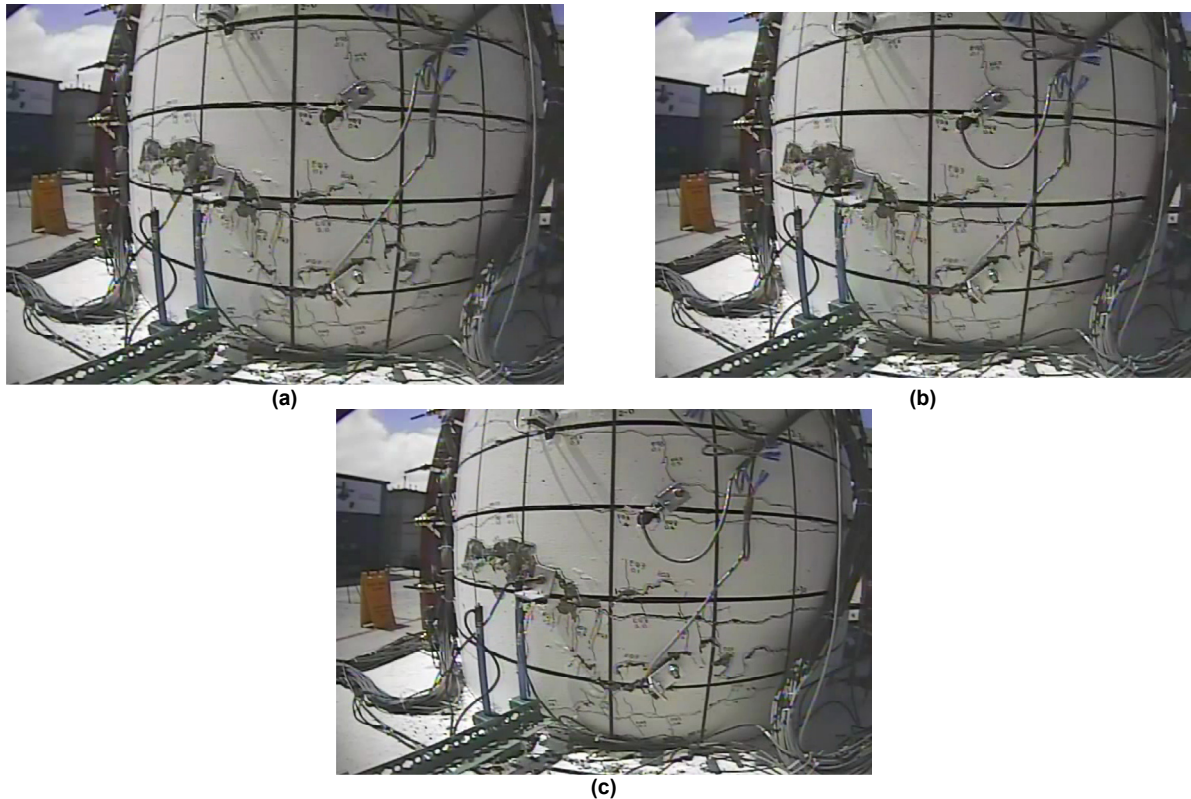
Test EQ4 simulated an aftershock to the design level event of EQ3. A residual displacement from the prior test remained as an initial offset. The input motion was the same as Test EQ2. The aftershock simulation achieved a peak displacement of 170 mm (6.71 in.) or 2.33% drift ratio. A residual displacement, consistent with the residual from the prior test, of -59 mm (-2.33 in.) remained post-test. The displacement time history of the top of the column is shown in Figure 8.26.

Figure 8.27(a) and (b) show the East face of the column base at peak displacement in the West and East directions, respectively. Residual cracks were not marked post-test due to testing time constraints. Regions with spalling caused by Test EQ3 enlarged, but damage was less severe than that induced by EQ3. A post-test view of the East face of the column base is shown in Figure 8.27(c).

A nearly linear response was obtained in terms of moment-curvature, see Figure 8.28. This curve is offset along the curvature axis due to the residual deformation of Test EQ3. The peak column base moment was 3750 kN-m (2760 kip-ft). The peak shear force was 401 kN (90 kip). The lateral shear force and displacement response is shown in Figure 8.29. This figure also shows an offset along its horizontal axis and contains contributions from a higher mode.



**Figure 8.26 Column displacement during Test EQ4.**



**Figure 8.27 Column base East face during Test EQ4 at (a) peak West displacement, (b) peak East displacement, and (c) post-test.**

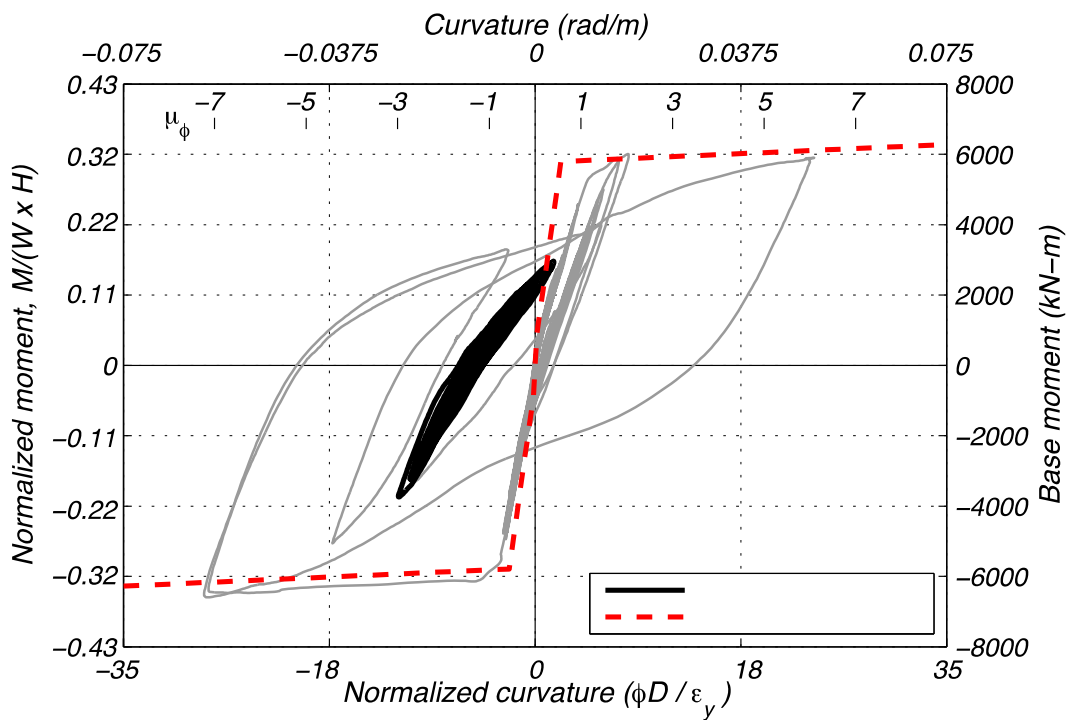


**Figure 8.28 Column response during Test EQ4 in terms of base moment and curvature.**

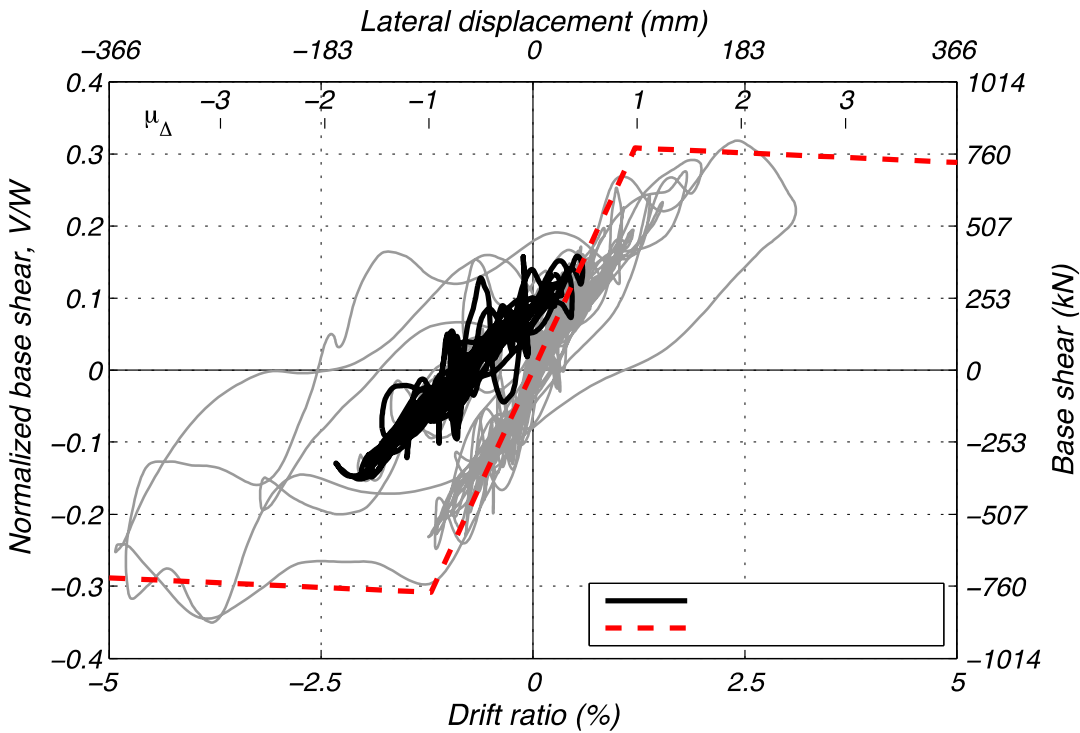


**Figure 8.29 Column response during Test EQ4 in terms of base shear and drift ratio.**

Strain gauges on longitudinal reinforcement measured a maximum tensile strain of  $0.0144 \text{ mm/mm}$  or  $5.5 \varepsilon_y$ , see Figure 8.30. These strains were largely influenced by the residual from the prior test. Demands in this test were on the order of  $0.005 \text{ mm/mm}$  above the prior residual.

Longitudinal bar strain at the top of the footing provides the local response quantity to compare with the longitudinal bar's bond slip. Longitudinal strain gauges were located a few inches above the bond-slip bracket; see Section 7.2 and Figure 7.3. The responses of both bars instrumented with a bracket (East and West) are presented with prior test results indicated with a lighter line width and color. Positive bar displacement and strain correspond with tensile demands. Figure 8.31 shows the hysteretic responses during Test EQ4. During the prior test, an LVDT attached to the bracket on the West face of the column slipped off its target, and no correction was made to the data after replacing the sensor on its target. It is unknown whether the large offset in this bar was due to residual uplift from the prior test or re-attaching the sensor with its target. Only minor hysteretic response is observed in this test.

Figure 8.32 shows transverse strain demands were below yield with larger demands on the West face where spalling initiated in the prior test. Figure 8.33 shows the smeared curvature profile of the column over the height it was measured during instances of peak column displacement, East and West, and post-test. Peak values are similar to those obtained in Test EQ2, and the residual curvature profile is similar to that resulting from the prior test, EQ3. Significant yielding or plastic hinge elongation did not occur as a consequence of the lower amplitude aftershock scenario.

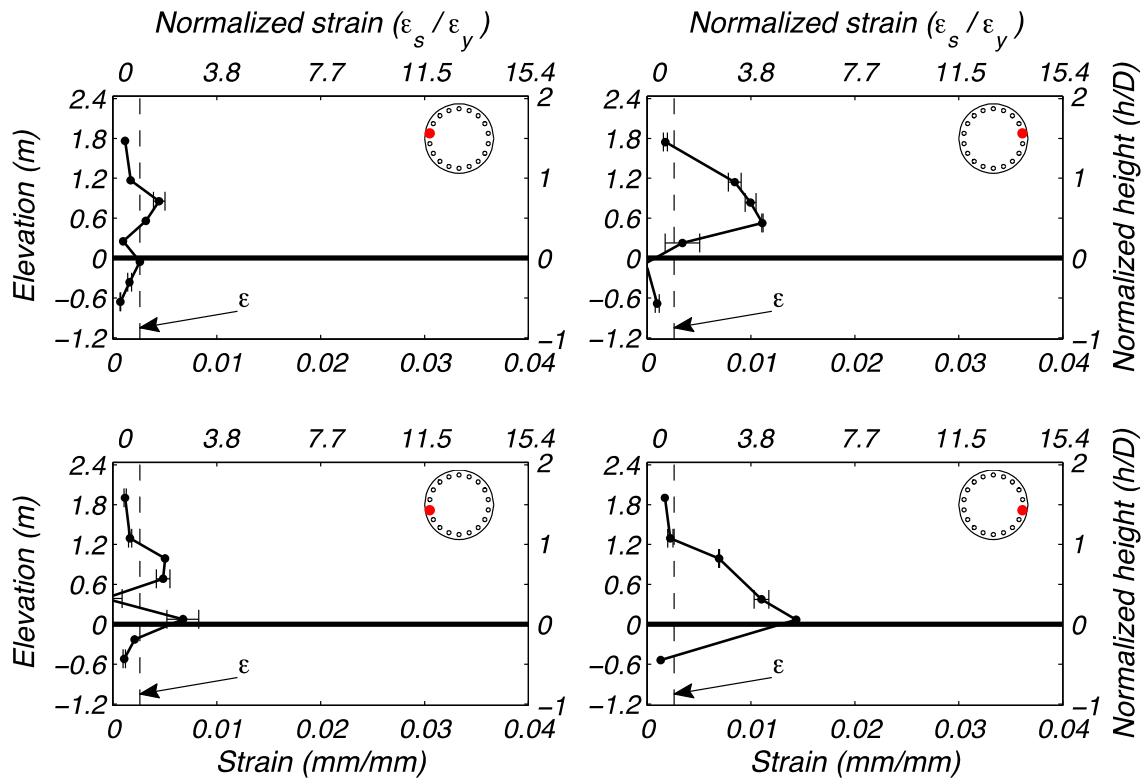


**Figure 8.30** Longitudinal reinforcement tensile strain demand during Test EQ4.

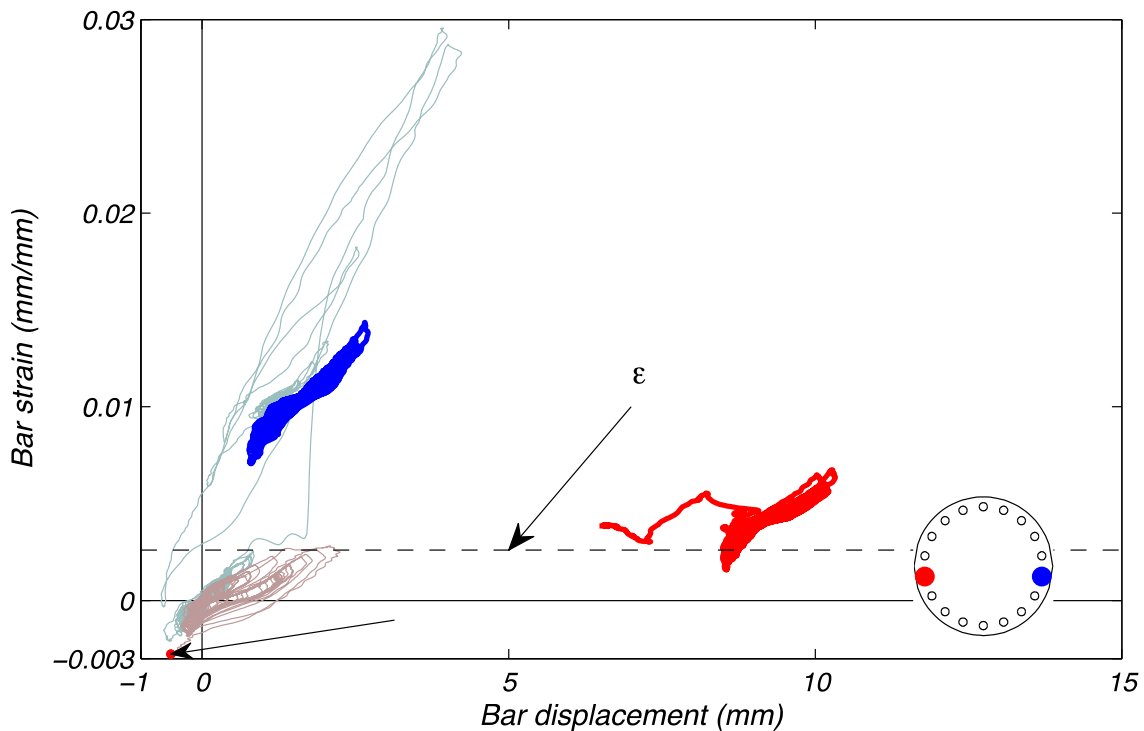


**Figure 8.31** Longitudinal reinforcement bond slip during Test EQ4.

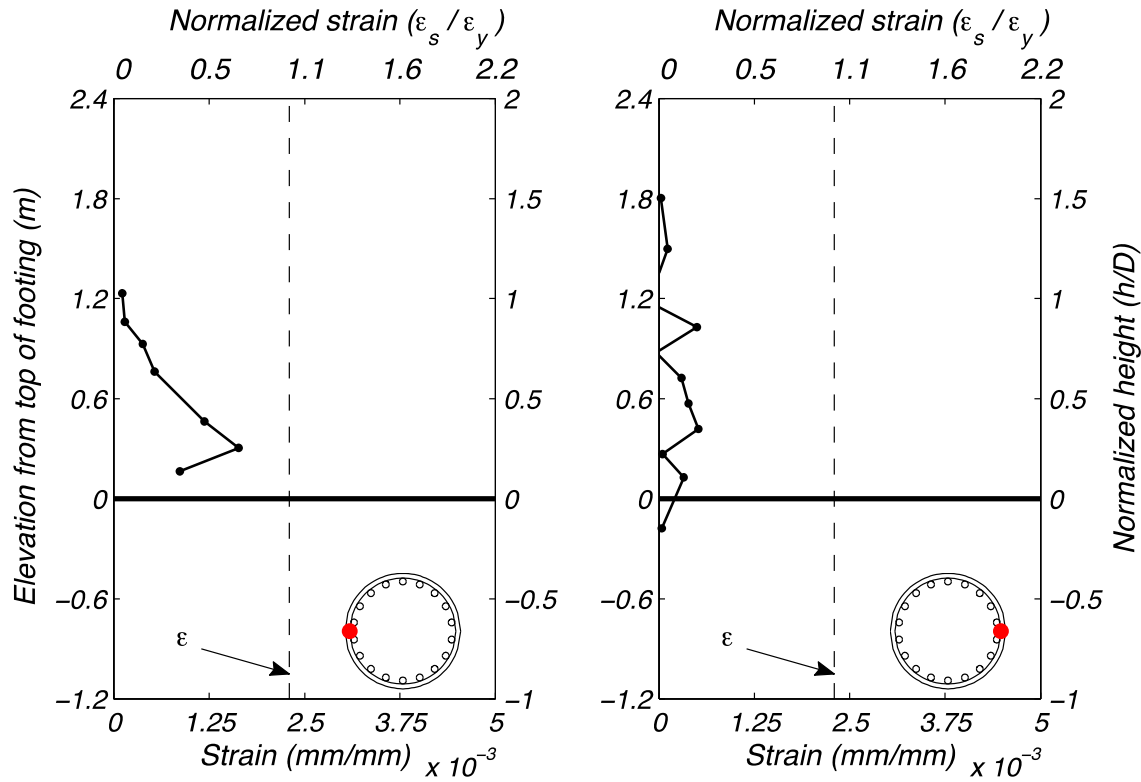


**Figure 8.32 Transverse hoop reinforcement tensile strain demand during Test EQ4.**

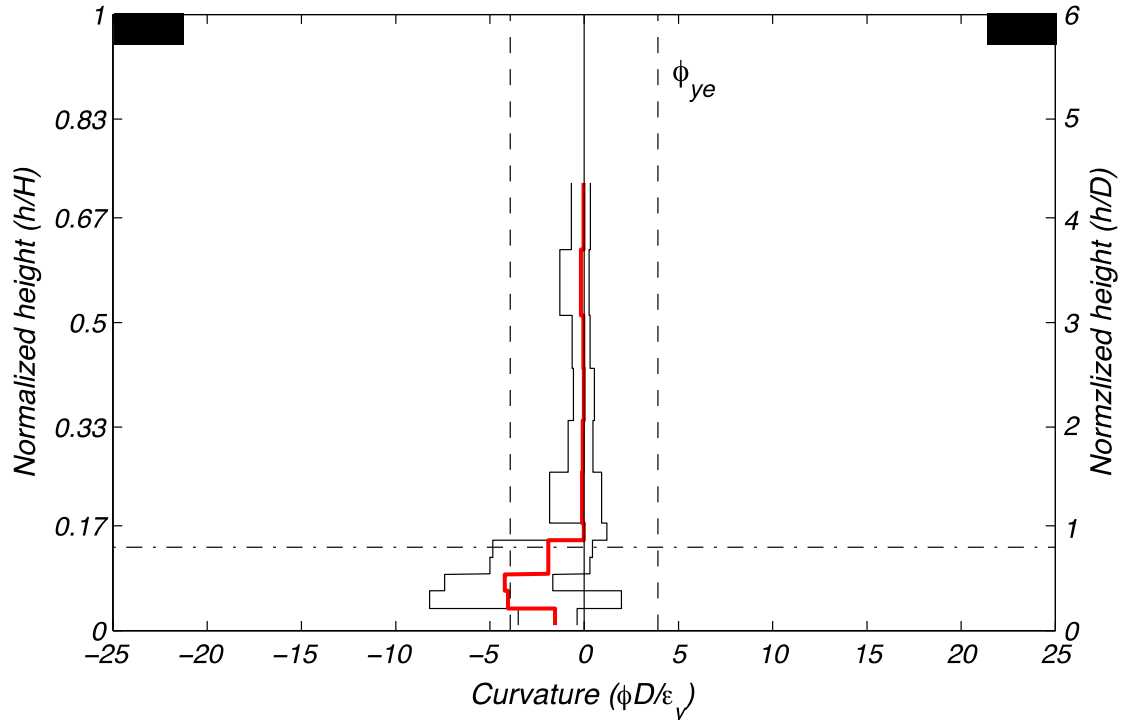


**Figure 8.33 Curvature profile at peak and residual displacements during Test EQ4.**

## 8.5 TEST EQ5

A peak displacement of 569 mm (22.40 in.) or 7.78% drift ratio was achieved. Displacement ductility at this peak displacement was 6.32. The residual displacement was 104 mm (4.11 in.) corresponding to 1.43% residual drift ratio; see Figure 8.34. The peak and residual drift ratios were to the East, which was opposite the initial drift ratio. Figure 8.35(a) and (b) show the East face of the column base at peak displacement in the West and East directions, respectively.

Continued concrete spalling occurred and extended to 1.07 m (3.5 ft) above the column base. A post-test view of the East face of the column base is shown in Figure 8.35(c). Concrete spalling is evident in this figure to a height of 0.76 m (2.5 ft), or 0.625 column diameters.

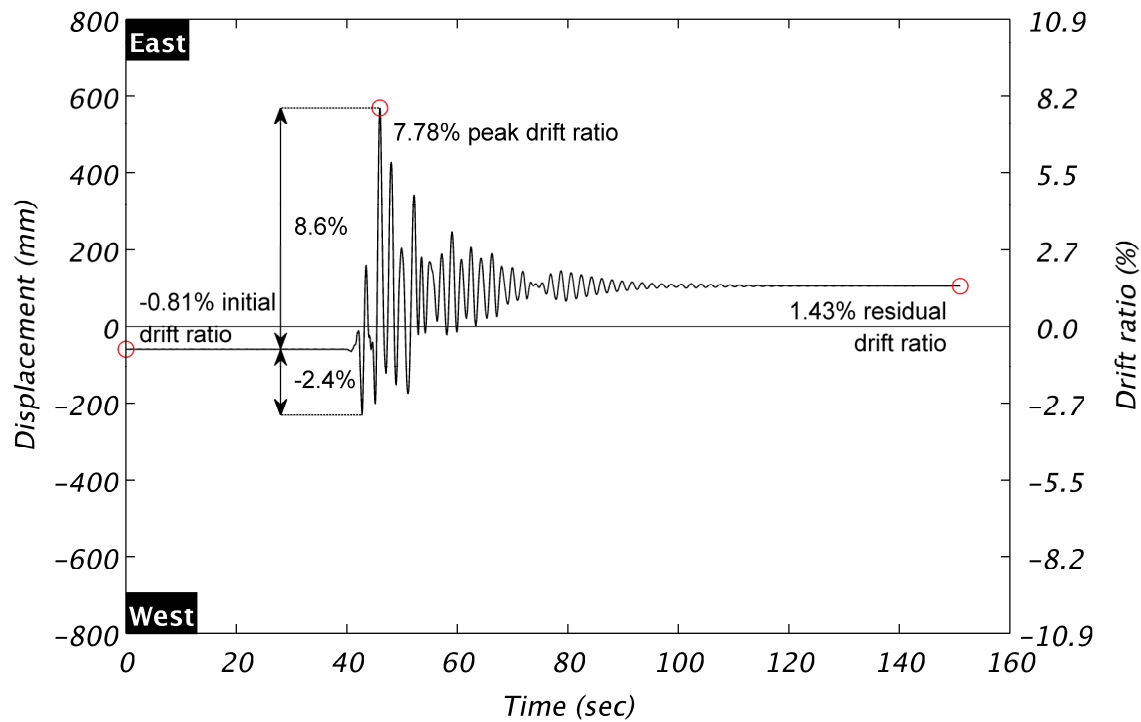
The peak column base moment was 7240 kN-m (5340 kip-ft), which was the second largest demand of any test. The moment-curvature response is shown in Figure 8.36. Large, stable hysteretic loops are evident. The peak shear force was 811 kN (183 kip). The lateral shear force-displacement response is shown in Figure 8.37.

The peak longitudinal strain measured was 0.0466 mm/mm, see Figure 8.38. Error bars indicate measurements from a pair of reliable strain gauges. The absence of error bars means that only one gauge was reliable, and the absence of a solid black circle means neither gauge was viable during the test.

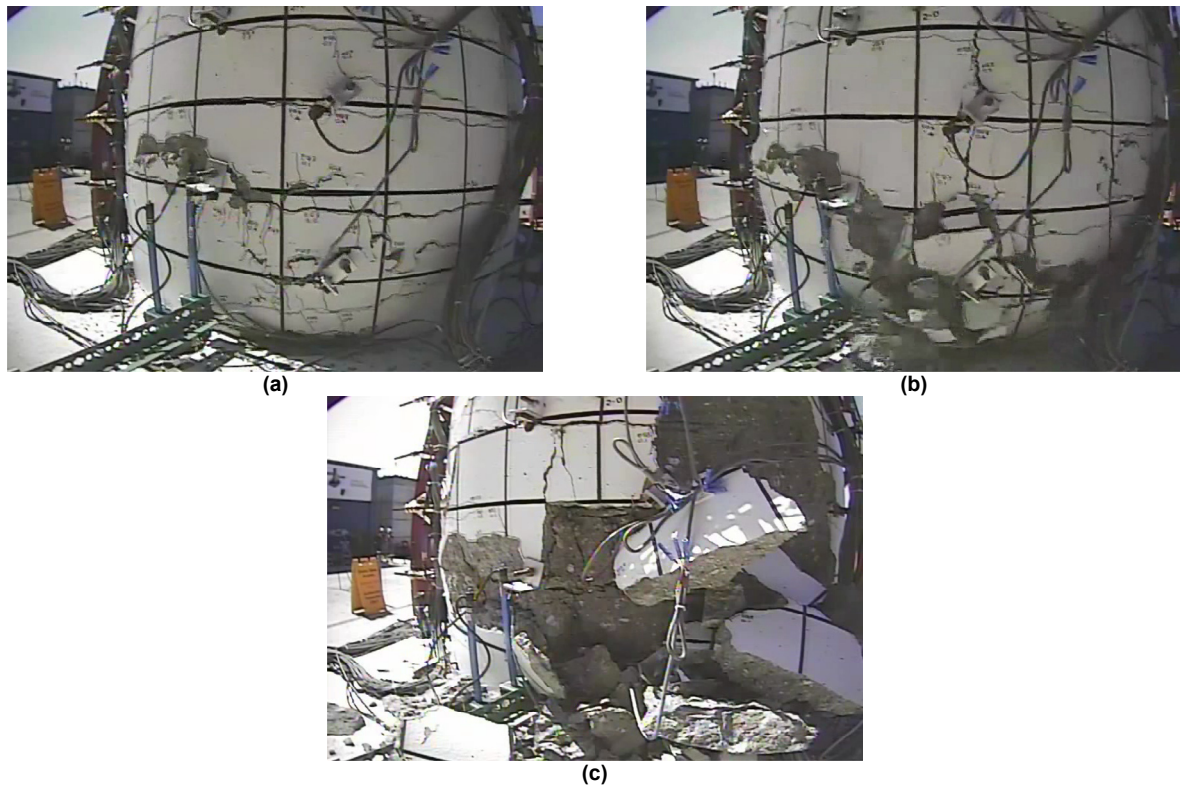
Longitudinal bar strain at the top of the footing provides the local response quantity to compare with the longitudinal bar's bond slip. Longitudinal strain gauges were located a few inches above the bond-slip bracket; see Section 7.2 and Figure 7.3. The responses of both bars instrumented with a bracket (East and West) are presented with prior test results indicated with a lighter line width and color. Positive bar displacement and strain correspond with tensile demands. Figure 8.39 shows the hysteretic responses during Test EQ5 up until the point that LVDTs were knocked off their bracket targets. Uplift to this point was consistent with demands from prior tests. This is the last test for which the bond-slip data is presented for the East bar since strain gauges for this location beyond Test EQ5 were not reliable.

Figure 8.40 illustrates the large demands placed on transvere reinforcement in this test. The peak demand on the West face, 0.025 mm/mm, was the largest of any test. However, nonlinear demands were all contained within 0.76 m (30 in.) or 0.63D from the column base.

Figure 8.41 shows the smeared curvature profile of the column over the height it was measured during instances of peak column displacement, East and West, and post-test. The experimental idealized curvature was exceeded over a height of 1.5 column diameters above the footing. The lowermost region instrumented generated the largest curvature corresponding to a curvature ductility of 6.9. The residual curvature profile is shown in red with values at or above yield for locations within a height of 864 mm (34 in.) above the footing.



**Figure 8.34    Column displacement during Test EQ5.**



**Figure 8.35    Column base East face during Test EQ5 at (a) peak West displacement, (b) peak East displacement, and (c) post-test.**

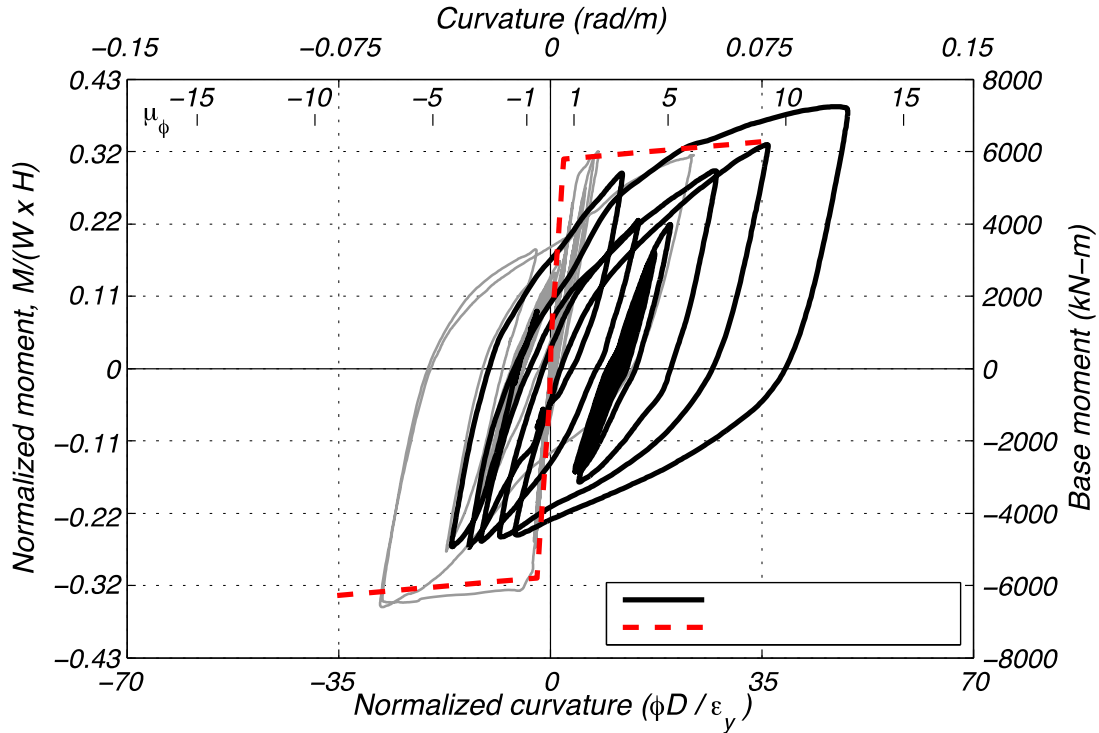


**Figure 8.36** Column response during Test EQ5 in terms of base moment and curvature.

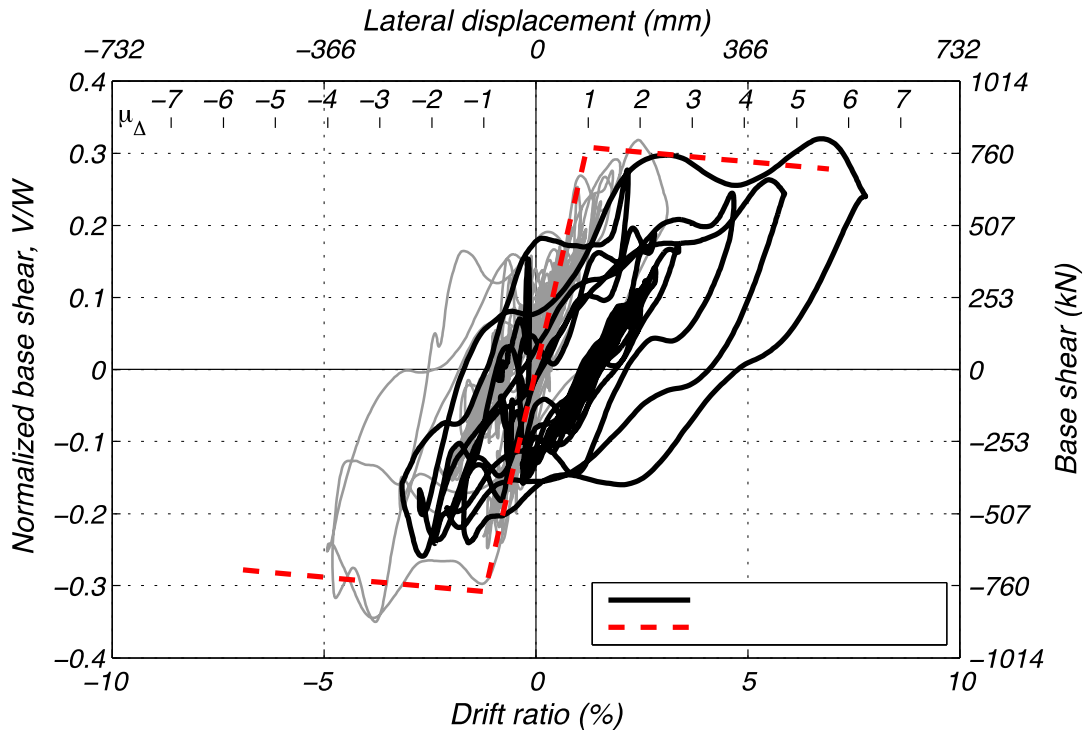


**Figure 8.37** Column response during Test EQ5 in terms of base shear and drift ratio.

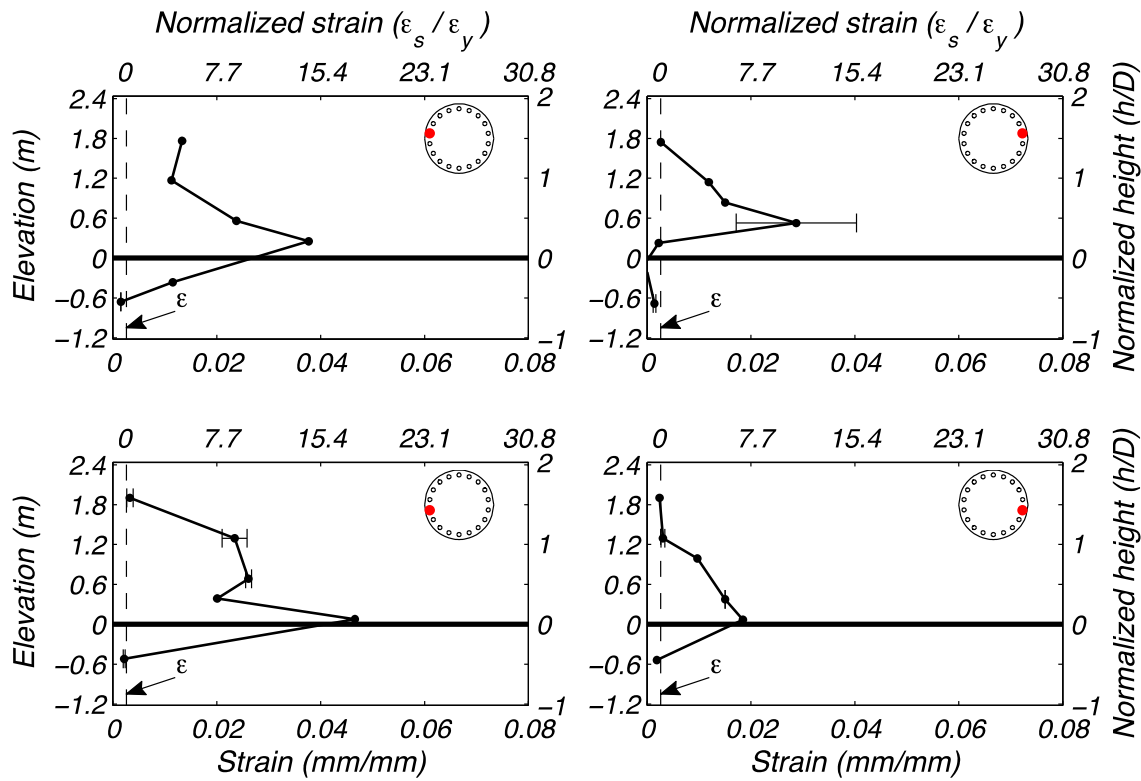


**Figure 8.38** Longitudinal reinforcement tensile strain demand during Test EQ5.

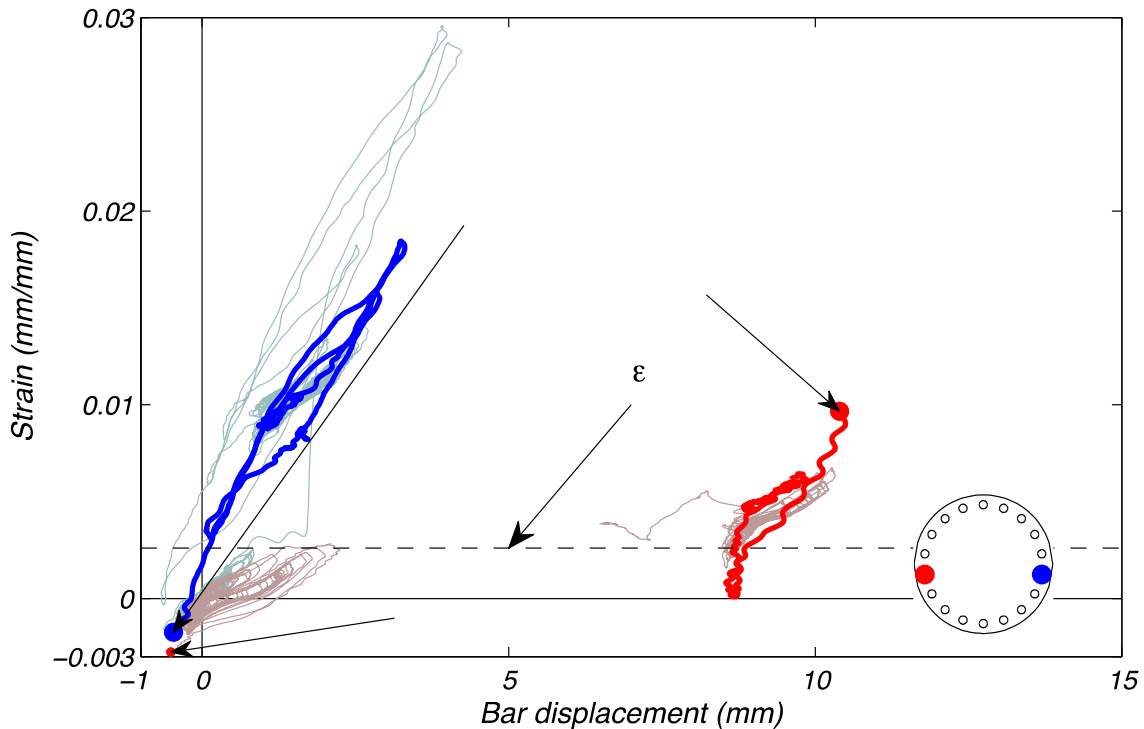


**Figure 8.39** Longitudinal reinforcement bond slip during Test EQ5.

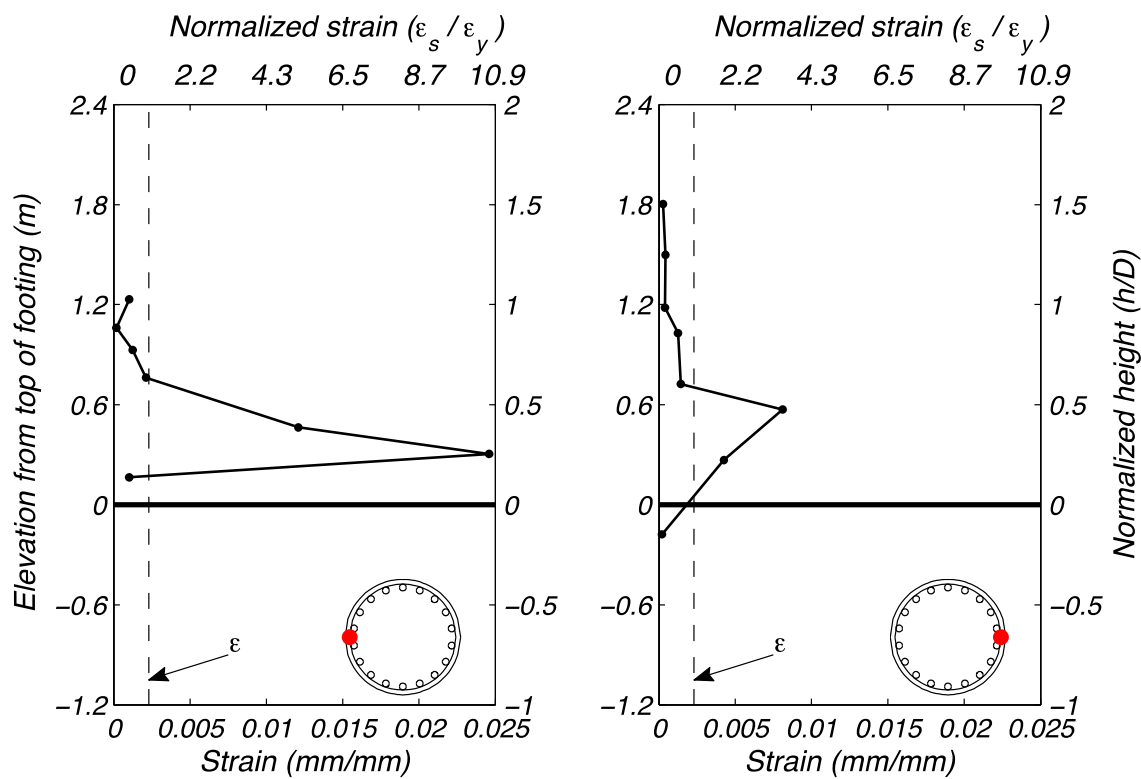


**Figure 8.40 Transverse hoop reinforcement tensile strain demand during Test EQ5.**

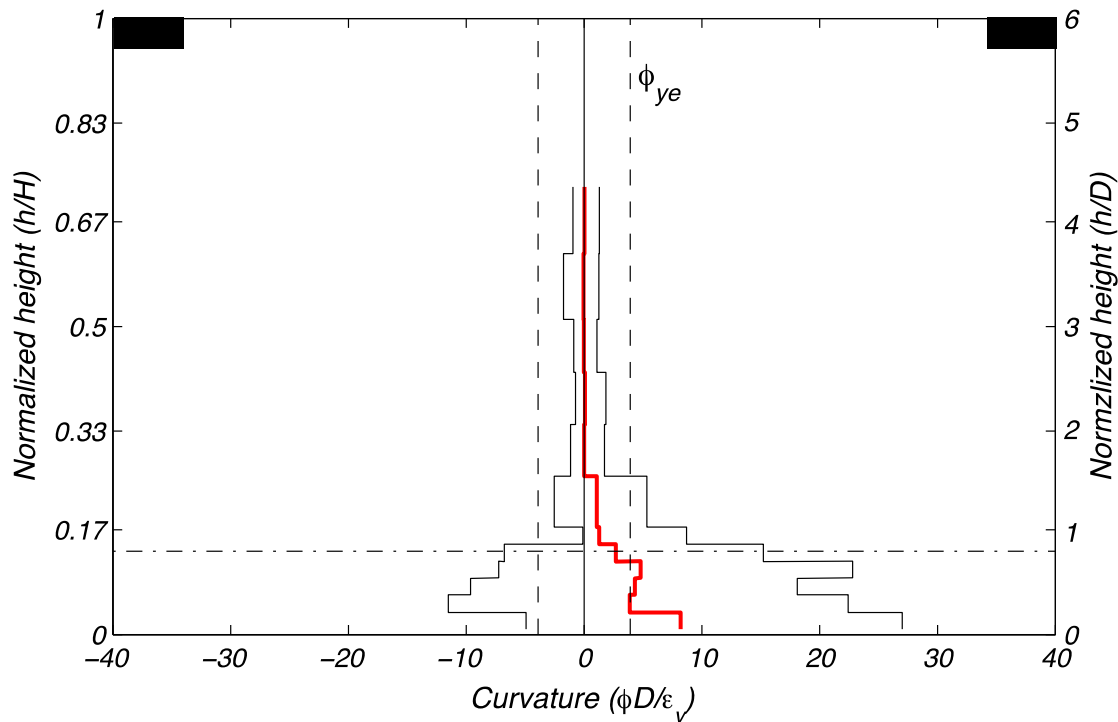


**Figure 8.41 Curvature profile at peak and residual displacements during Test EQ5.**

## 8.6 TEST EQ6

A repeat of Test EQ3, the Los Gatos Presentation Center record from the Loma Prieta earthquake, was the last planned test in the loading protocol. It resulted in a displacement ductility of 5.44. The peak displacement was 490 mm (19.3 in.) or a 6.69% drift ratio. Post-test, a residual displacement of 50 mm (1.97 in.) remained. This corresponds to 0.68% residual drift ratio, but the test began with an initial drift ratio of 1.41%. The displacement time history of the top of the column is shown in Figure 8.42. Figure 8.43(a) and (b) show the East face of the column base at peak displacement in the West and East directions, respectively.

A post-test view of the East face of the column base is shown in Figure 8.43(c). Concrete spalling and longitudinal reinforcement are visible, but spalling did not extend beyond the damage caused by Test EQ5. The primary difference between Figure 8.43(c) and Figure 8.35(c) is the removal of spalled and loose concrete before Test EQ6. The concrete core remained intact.

The peak column base moment was 6500 kN-m (4790 kip-ft). Stable hysteretic loops are present in the moment-curvature response of Figure 8.44. The peak shear force was 771 kN (173 kip). The lateral shear force and displacement response is shown in Figure 8.45.

Strain profiles are presented in Figure 8.46 for longitudinal reinforcement. Strains were on the same order of magnitude as the prior test. Longitudinal strains beyond the elastic limit were measured at 1.8 m (71 in.) or 1.5 column diameters above the footing. This was the highest elevation monitoring longitudinal bar strains. Longitudinal gauges at a depth of 0.6 m (24 in.) in the footing remained elastic.

Longitudinal bar strain at the top of the footing provides the local response quantity to compare with the longitudinal bar's bond slip. Longitudinal strain gauges were located a few inches above the bond-slip bracket; see Section 7.2 and Figure 7.3. The response of the West bar instrumented with a bracket is presented with prior test results indicated with a lighter line width and color. Positive bar displacement and strain correspond with tensile demands. Figure 8.47 shows the hysteretic responses during Test EQ6. During the prior test, an LVDT slipped off its target. No correction was made to the data after replacing the sensor on its target before Test EQ6. It is unknown whether the offset between this test and the prior one was due to residual uplift from the prior test or re-attaching the sensor with its target. The 10.6-mm (0.42-in.) uplift was the largest reliable measurement of bond slip.

Strain profiles for transverse reinforcement are presented in Figure 8.48. Strains were on the same order of magnitude as the prior test. The profiles illustrate transverse reinforcement yielding above the footing between 0.15 and 0.5 times the column diameter. However, fewer transverse gauges remained viable during this test.

Figure 8.49 shows the smeared curvature profile of the column over the height it was measured during instances of peak column displacement, East and West, and post-test. The experimental idealized curvature was exceeded over a height above the footing corresponding to 1.5 column diameters. Demands were consistent with those obtained from the prior test, EQ5. The lowermost region instrumented generated the largest curvature corresponding to a curvature

ductility of 6.6. The residual curvature profile is shown in red with values below that corresponding to yield at all locations except for the lowermost.

Test EQ6 was the last test intended in the loading protocol. However, damage up to this point was limited to concrete spalling. This provided the opportunity to extend the scope of testing.

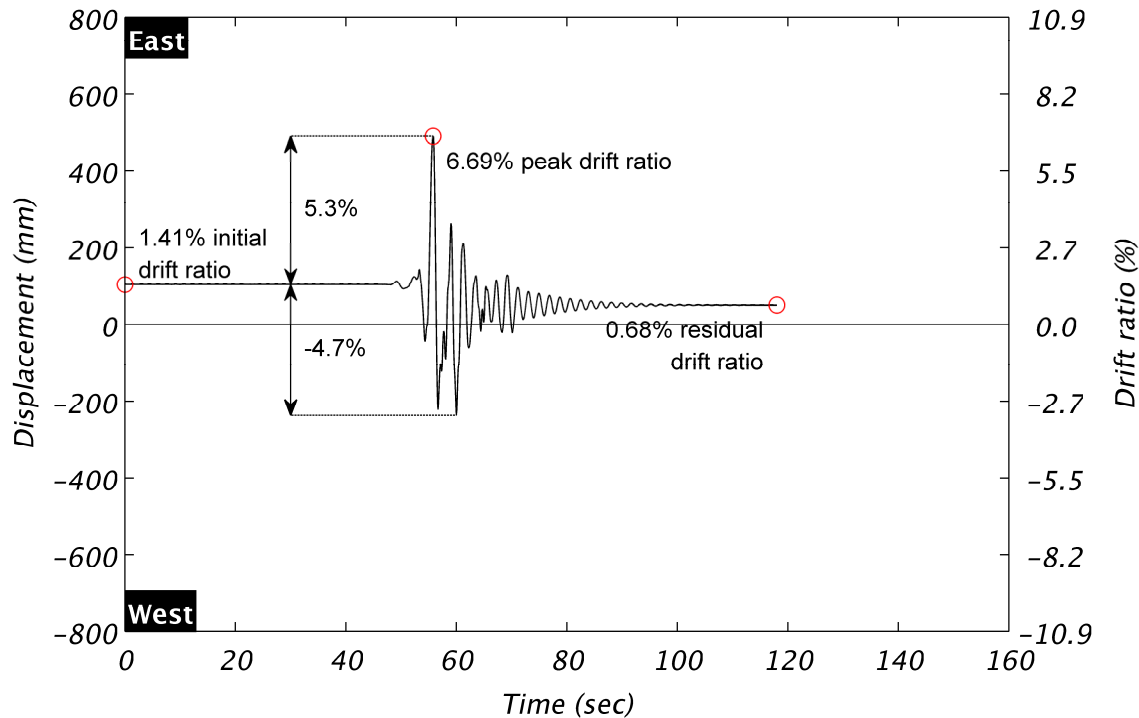


**Figure 8.42    Column displacement during Test EQ6.**

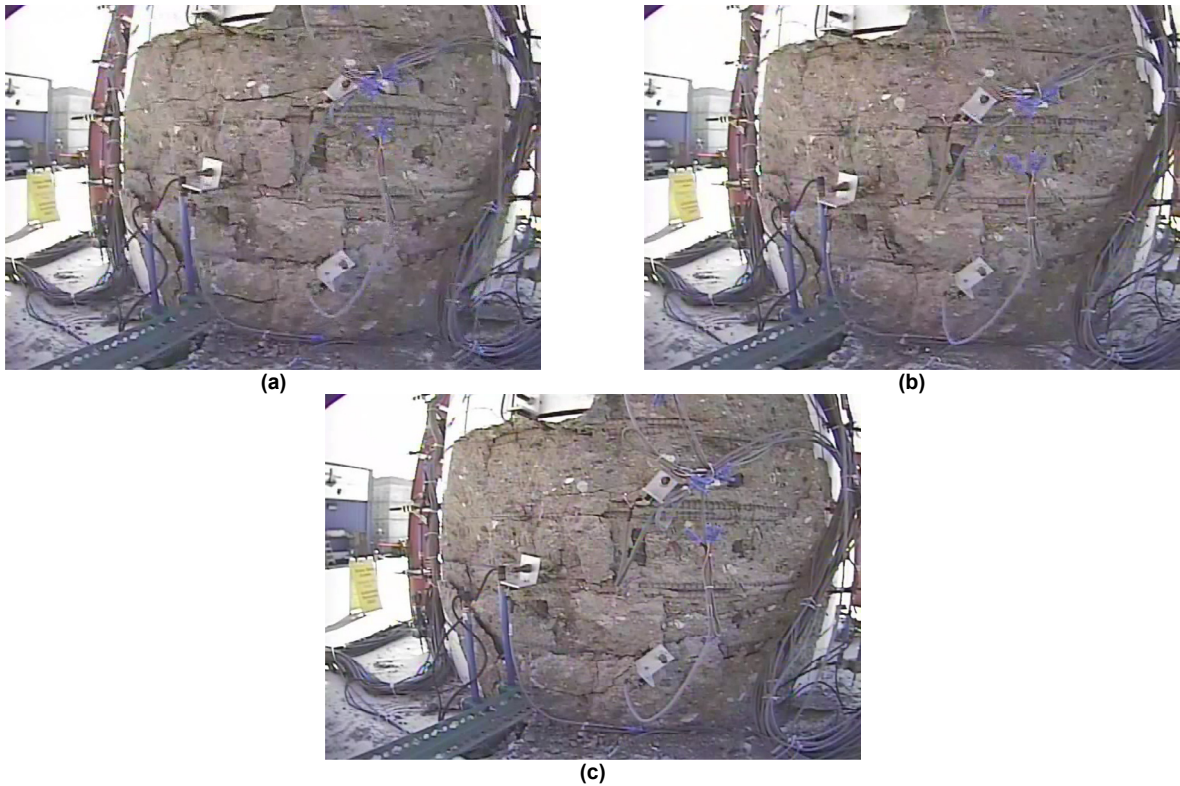


**Figure 8.43 Column base East face during Test EQ6 at (a) peak West displacement, (b) peak East displacement, and (c) post-test.**

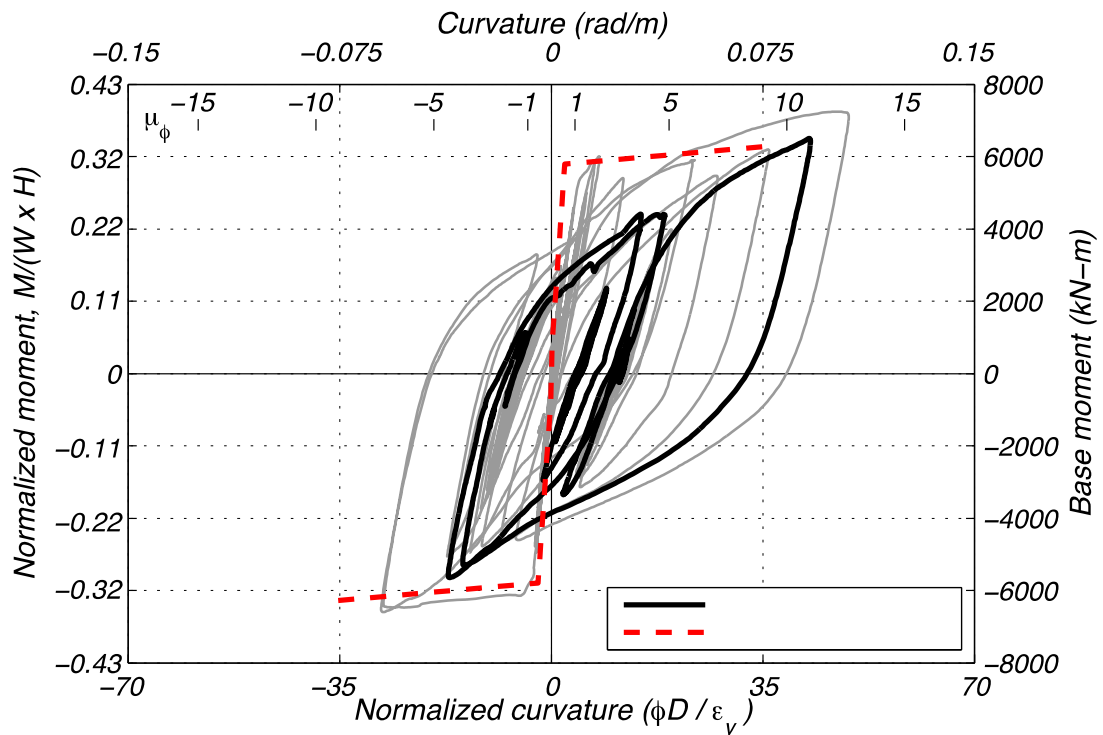


**Figure 8.44 Column response during Test EQ6 in terms of base moment and curvature.**

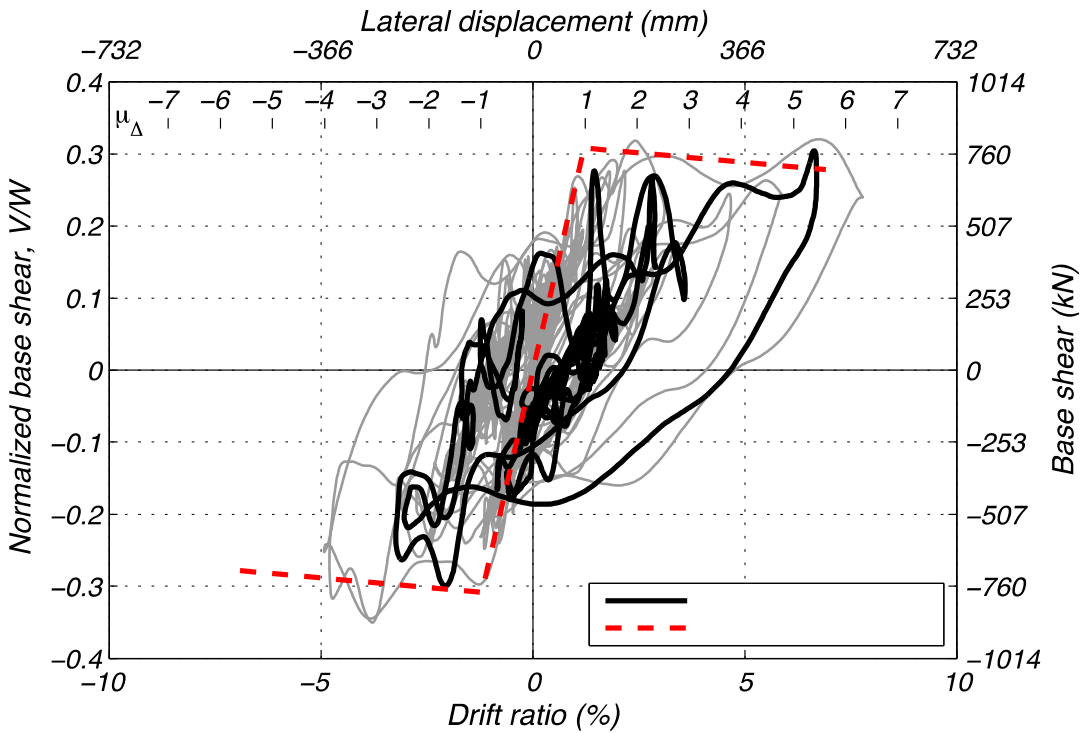


**Figure 8.45** Column response during Test EQ6 in terms of base shear and drift ratio.

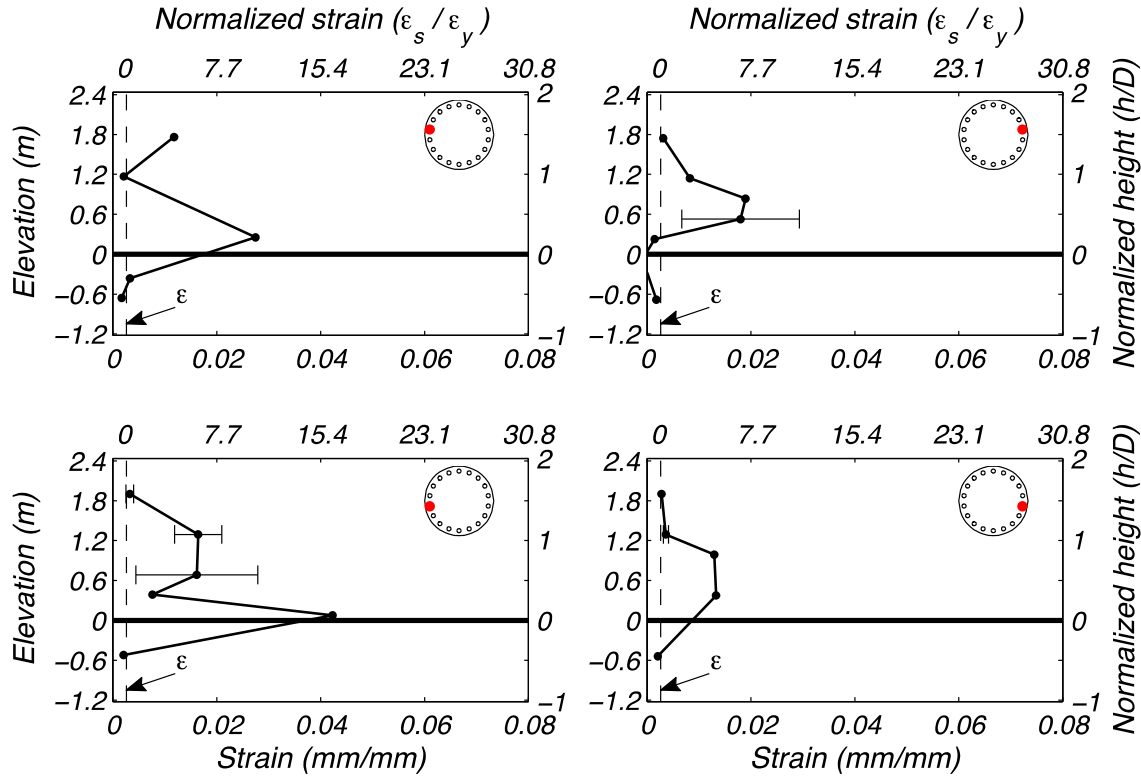


**Figure 8.46** Longitudinal reinforcement tensile strain demand during Test EQ6.

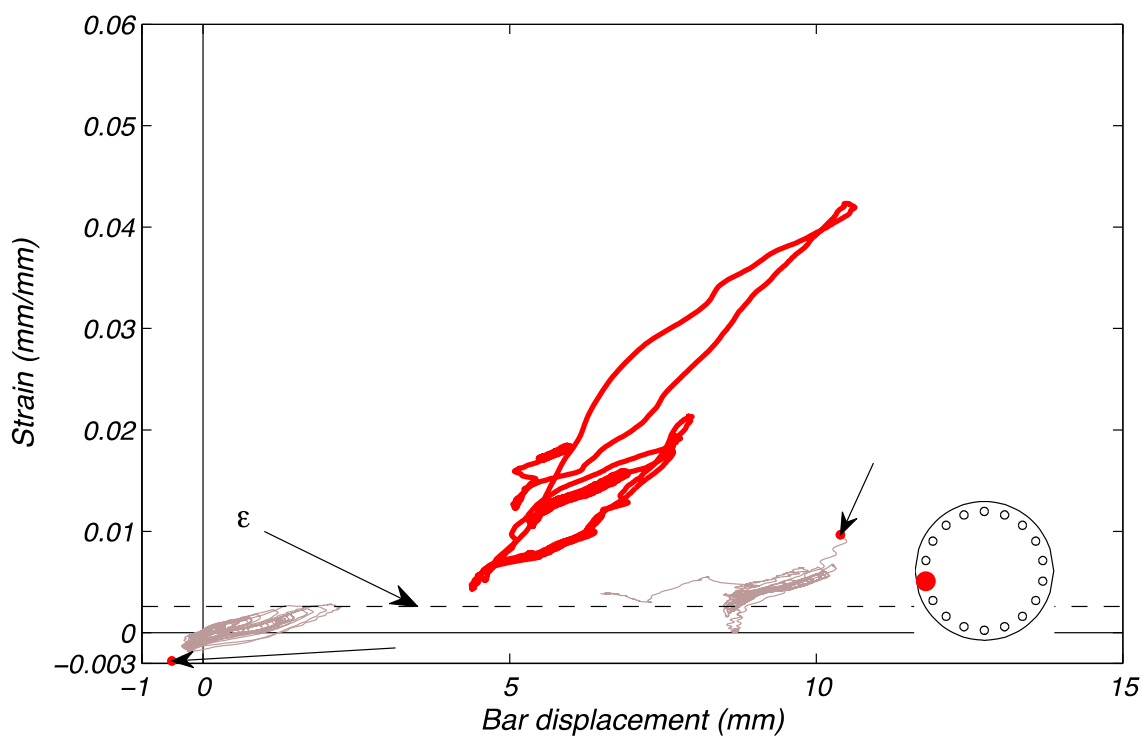


**Figure 8.47 Longitudinal reinforcement bond slip during Test EQ6.**

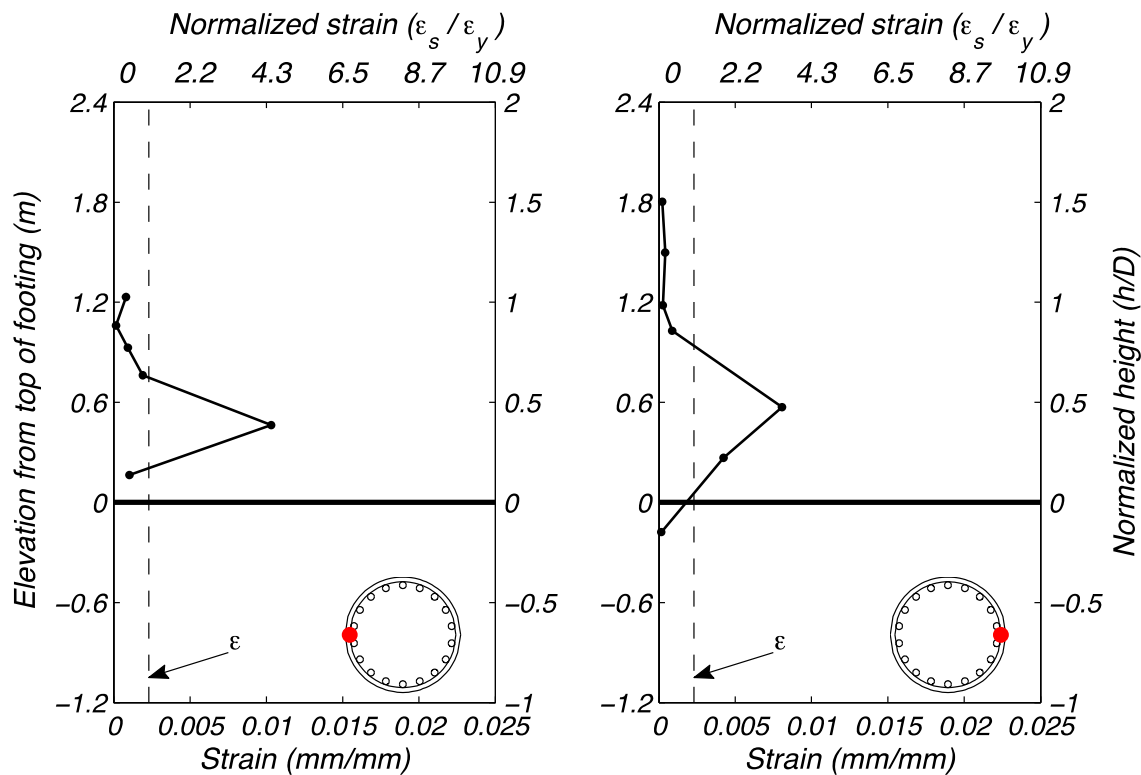


**Figure 8.48 Transverse hoop reinforcement tensile strain demand during Test EQ6.**

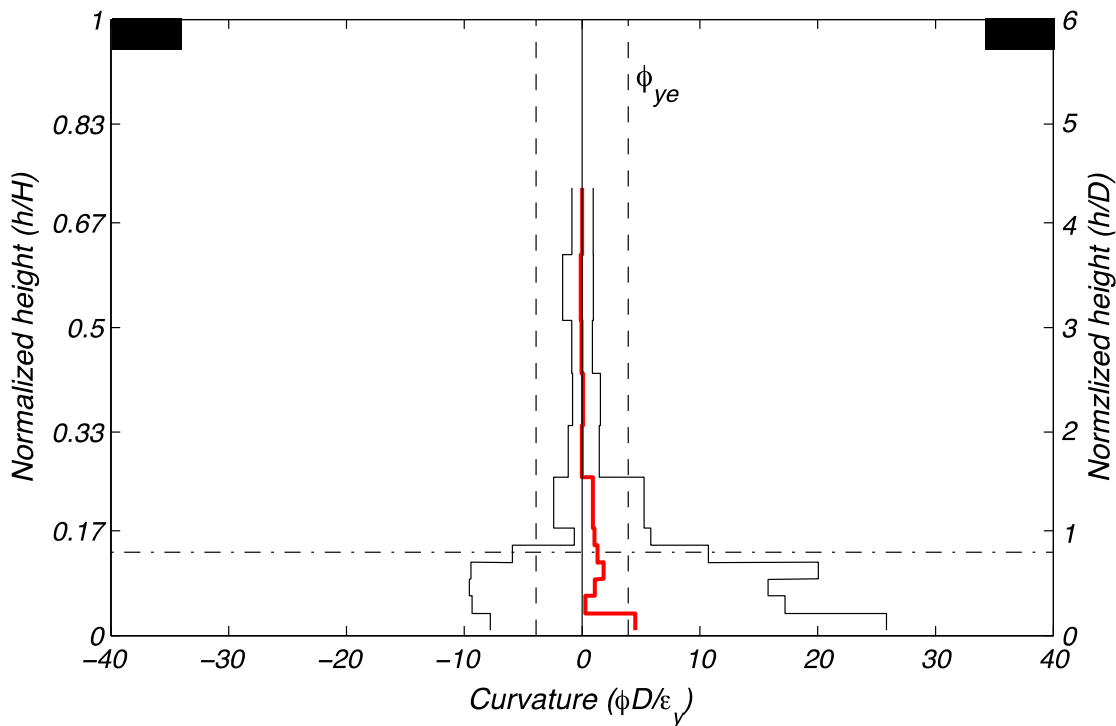


**Figure 8.49 Curvature profile at peak and residual displacements during Test EQ6.**

## 8.7 TEST EQ7

For extended testing, the Takatori record from the Kobe earthquake was utilized at different amplitudes to bring the column to near collapse. In Test EQ7, the Takatori motion was utilized at 100% of the original record, resulting in a peak displacement of 553 mm (21.8 in.) or a 7.56% drift ratio. This corresponds to a displacement ductility of 6.15. A residual drift ratio of -1.98%, or -145 mm (-5.7 in.) column displacement, remained post-test, see Figure 8.50. Figure 8.51 (a) and (b) show the East face of the column base at peak displacement in the West and East directions, respectively.

A post-test view of the East face of the column base is shown in Figure 8.51(c). Further spalling was induced and more of the longitudinal bars were exposed as the spalling penetrated deeper into the face of the column. The loss of bond with the longitudinal bars in this figure and video footage indicate the onset of bar buckling.

The peak column base moment was 7390 kN-m (5450 kip-ft). This was the maximum overturning moment obtained in any of the tests, see Figure 8.52. The peak shear force was 812 kN (183 kip); the second largest shear force obtained in any of the tests. The lateral shear force and displacement response is shown in Figure 8.53.

Longitudinal strains, in terms of peak tensile demand, are shown in Figure 8.54. Unfortunately, only one gauge was reliable at each location in Figure 8.54(c), so buckling onset cannot be confirmed in this bar with these sensors.

Longitudinal bar strain at the top of the footing provides the local response quantity to compare with the longitudinal bar's bond slip. Longitudinal strain gauges were located a few inches above the bond-slip bracket; see Section 7.2 and Figure 7.3. The response of the West bar instrumented with a bracket is presented in Figure 8.47. Prior tests are indicated with a lighter line width and color. Positive bar displacement and strain correspond with tensile demands. The peak bond slip was 8.5 mm (0.33 in.).

Transverse strain demands were similar to the prior test with the largest demands occurring at 0.6 m (24 in.) above the footing. The strain profile is depicted in Figure 8.56. Peak strain demands were similar on both East and West faces of the column.

Figure 8.57 shows the smeared curvature profile of the column over the height it was measured during instances of peak column displacement, East and West, and post-test. The experimental idealized curvature was exceeded over a height above the footing corresponding to 1.5 column diameters. Peak demands were on the same order with those obtained from the prior two tests, EQ5 and EQ6, but in the opposite direction. The region between 660 mm (26 in.) and 864 mm (34 in.) generated the largest smeared curvature and corresponded to a curvature ductility of 6.6. The residual curvature profile is shown in red with values close to the idealized experimental yield below one column diameter.

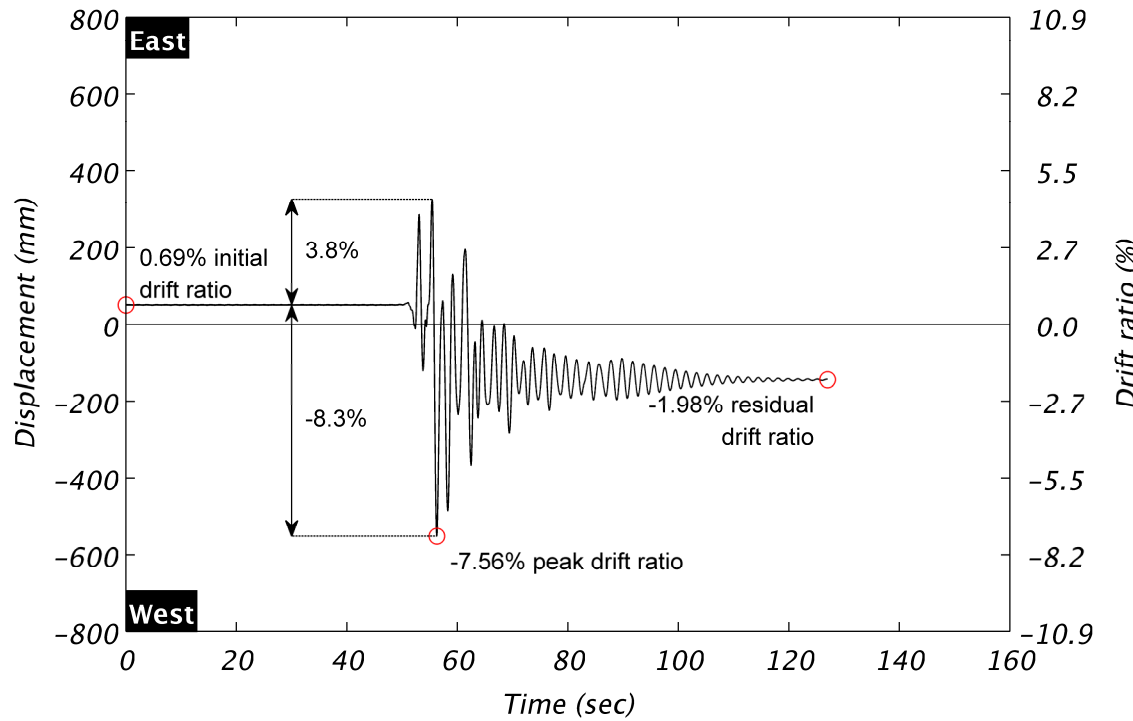


**Figure 8.50    Column displacement during Test EQ7.**

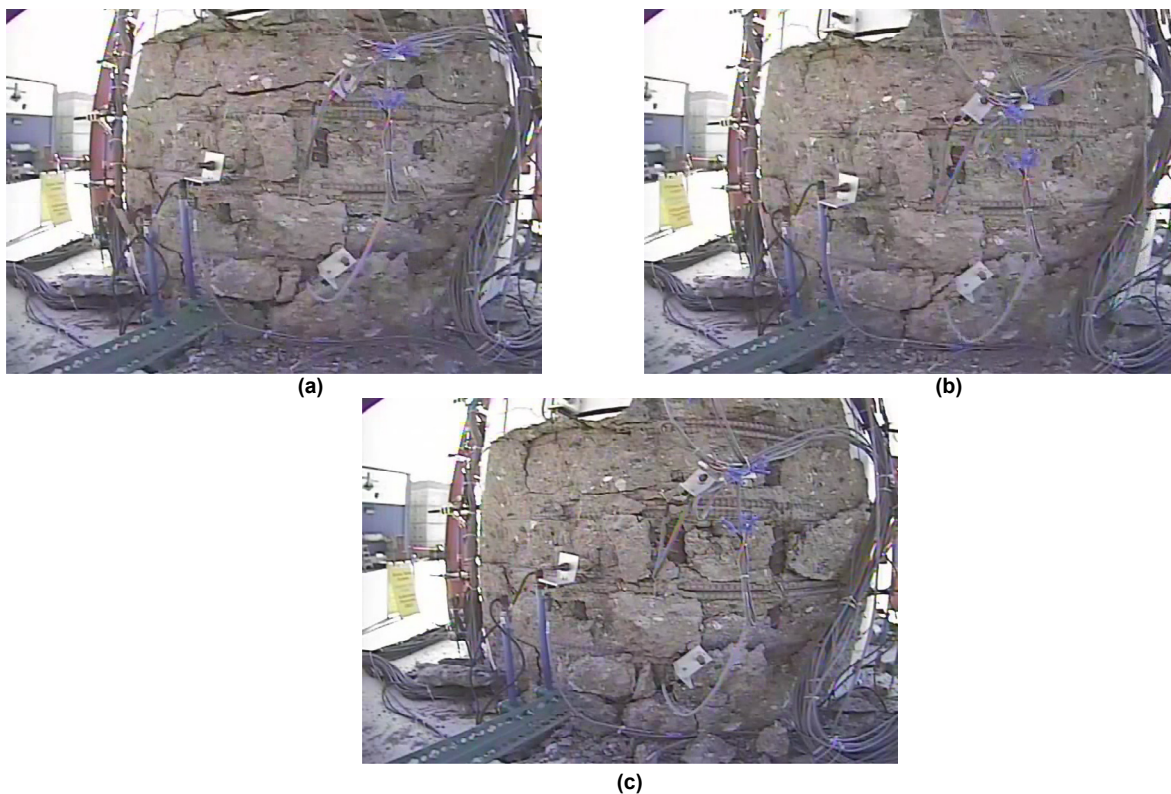


**Figure 8.51 Column base East face during Test EQ7 at (a) peak West displacement, (b) peak East displacement, and (c) post-test.**

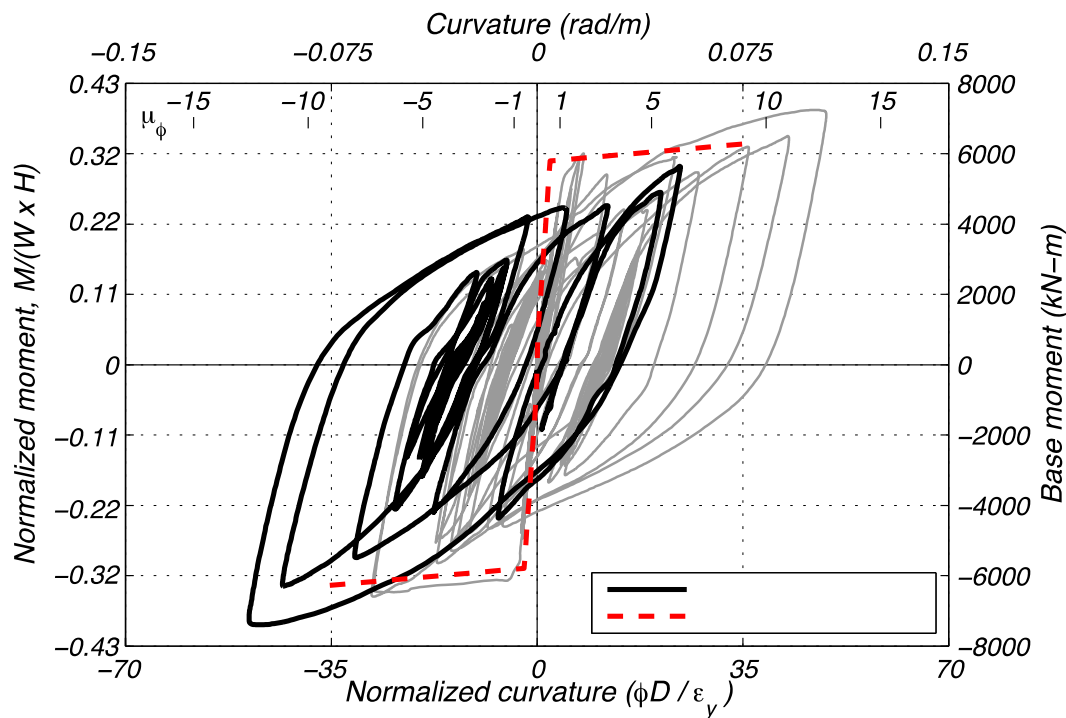


**Figure 8.52 Column response during Test EQ7 in terms of base moment and curvature.**

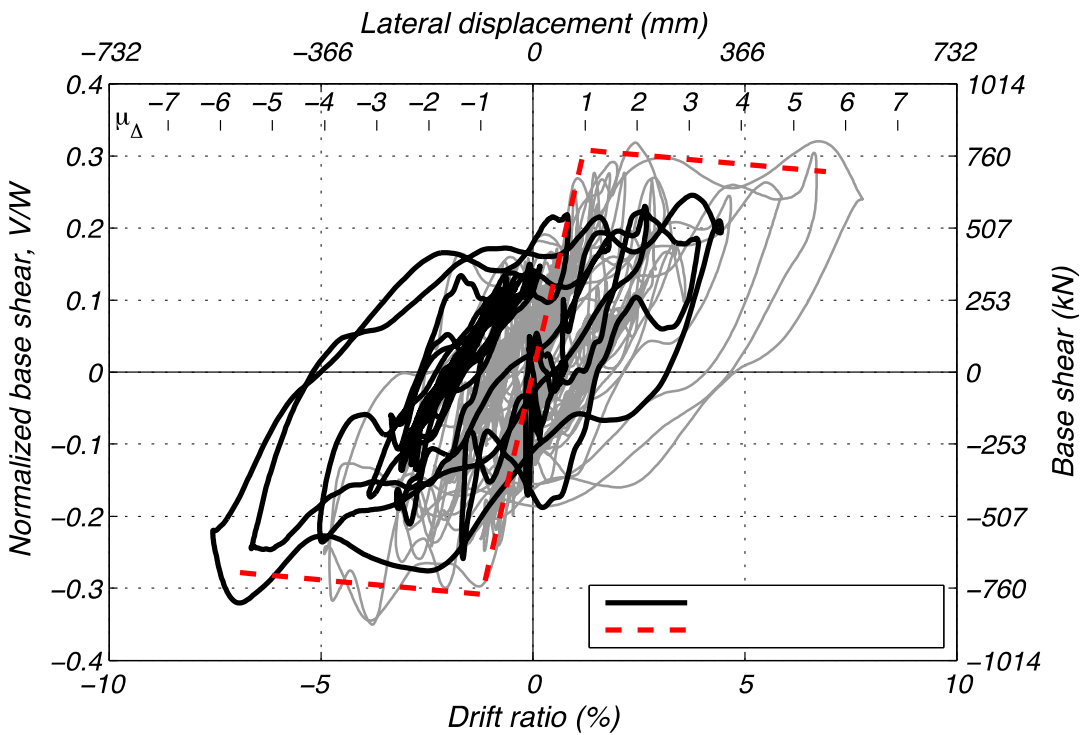


**Figure 8.53** Column response during Test EQ7 in terms of base shear and drift ratio.

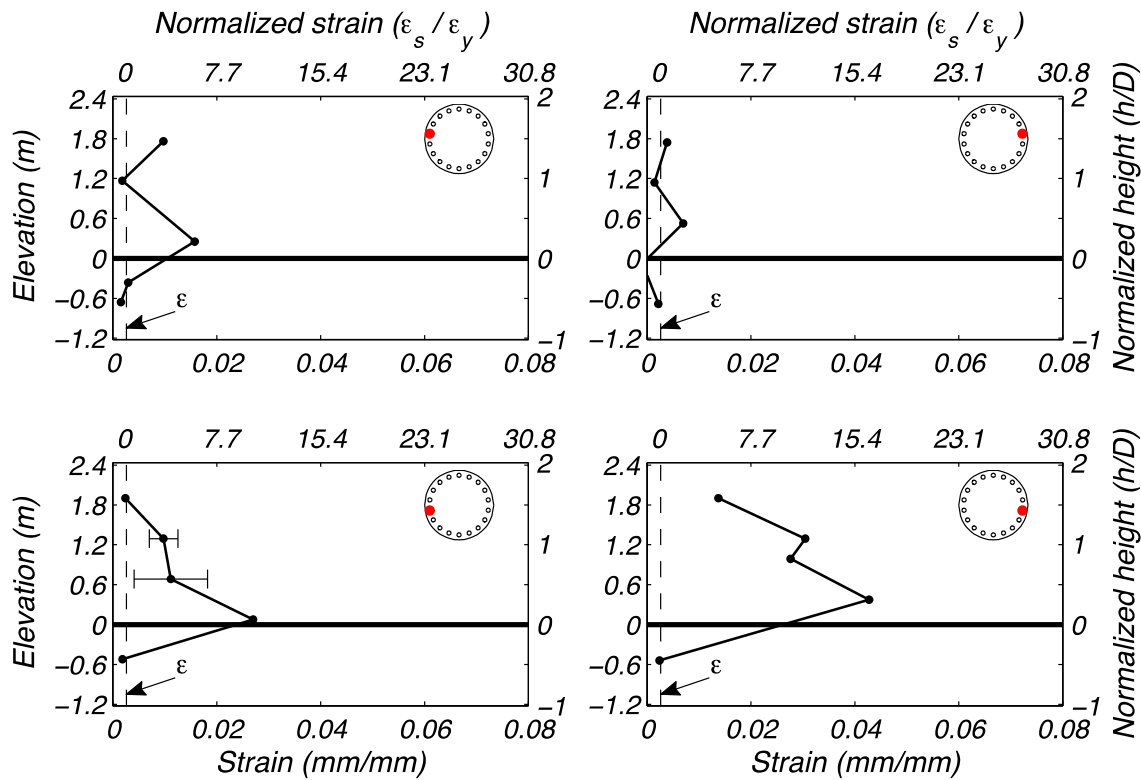


**Figure 8.54** Longitudinal reinforcement tensile strain demand during Test EQ7.

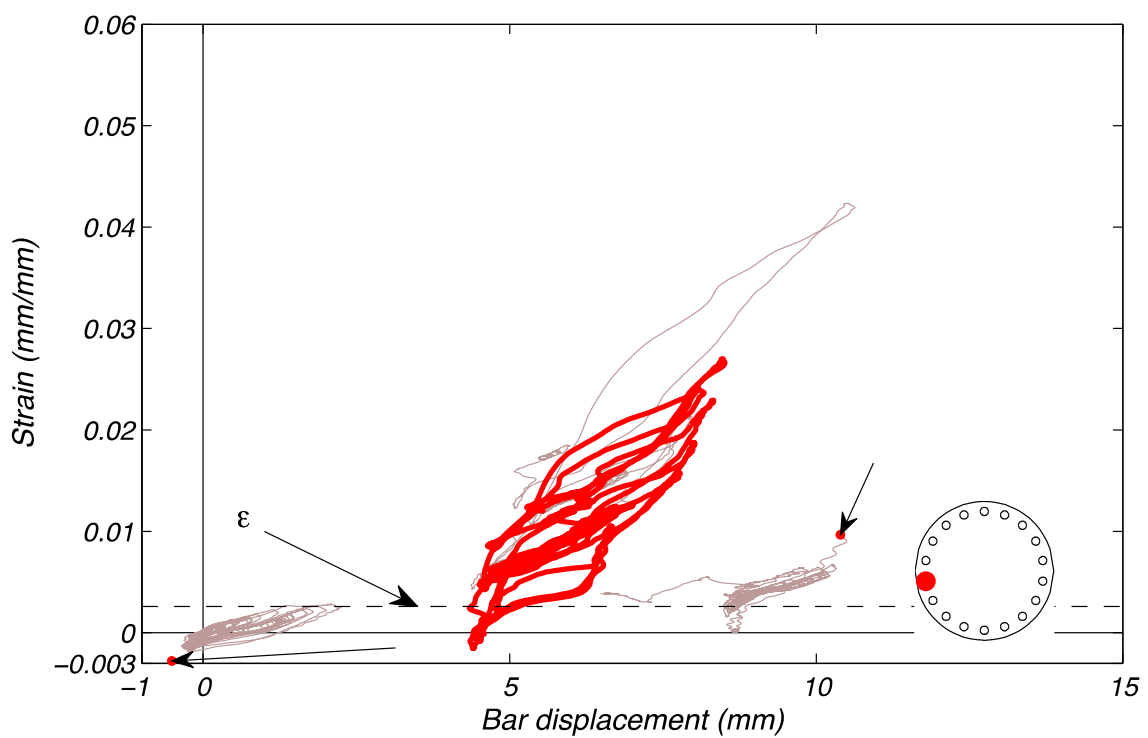


**Figure 8.55 Longitudinal reinforcement bond slip during Test EQ7.**

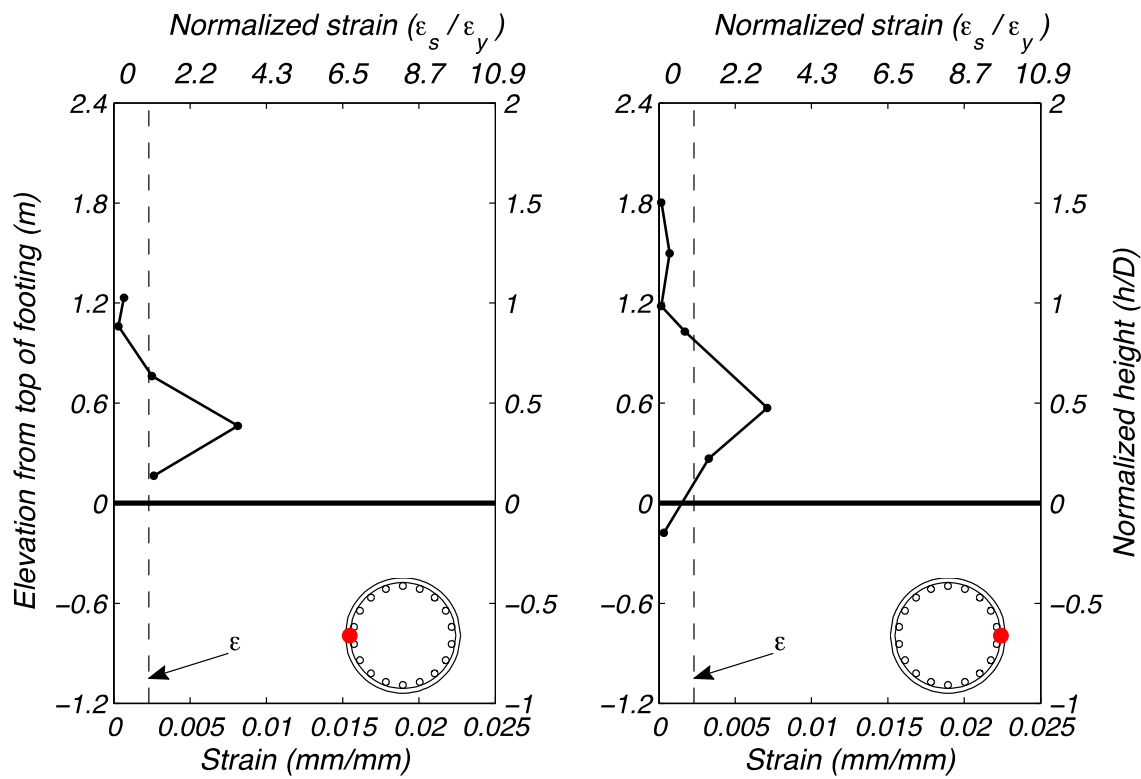


**Figure 8.56 Transverse hoop reinforcement tensile strain demand during Test EQ7.**

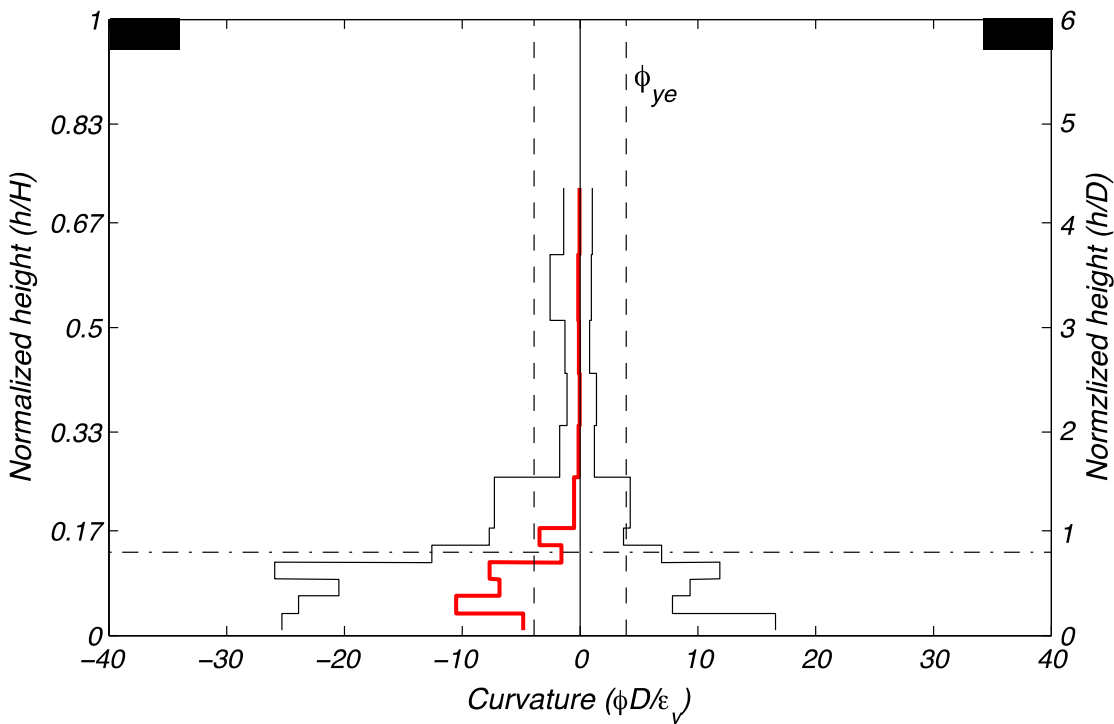


**Figure 8.57 Curvature profile at peak and residual displacements during Test EQ7.**

## 8.8 TEST EQ8

With the robustness observed in the prior test and drift demands still shy of the 10% limit, the prior signal was repeated and amplified. A scale factor of -1.2 was used with the original Takatori record. This imposed a displacement ductility of 6.73 at 606 mm (23.9 in.) of column displacement. The corresponding drift ratio was 8.28%. The residual displacement was 97 mm (3.83 in.) at the top of the column. This normalizes to a 1.33% residual drift ratio and was slightly lower than the prior residual drift ratio of 1.98%. The displacement time history is shown in Figure 8.58. Figure 8.59(a) and (b) show the East face of the column base at peak displacement in the West and East directions, respectively.

A post-test view of the East face of the column base is shown in Figure 8.59(c). In this figure, the two exposed longitudinal reinforcing bars on the right side of the column centerline have fractured; the fractures and buckled shapes are readily apparent. This was the first sign of significant damage beyond concrete cracking and spalling induced in the test specimen.

The peak column base moment was 7160 kN-m (5280 kip-ft), see Figure 8.60. Reduced capacity in the reloading cycle beyond a normalized curvature of +35.0 is not due to rebar fracture. Flexural demands put these bars in compression during these cycles, and fractures occurred after this sequence near zero curvature. The peak shear force was 742 kN (167 kip); see Figure 8.61.

Longitudinal strain demands are shown in Figure 8.62. One of the fractured bars was instrumented with strain gauges; see Figure 8.62(c), but tensile demands on this bar occurred early in the loading sequence during negative curvature demands. Tensile strain demands on the diametrically opposite bar were the largest yet recorded and occurred at the column-to-footing interface; see Figure 8.62(b).

Longitudinal bar strain at the top of the footing provides the local response quantity to compare with the longitudinal bar's bond slip. Longitudinal strain gauges were located a few inches above the bond-slip bracket; see Section 7.2 and Figure 7.3. The response of the West bar instrumented with a bracket is presented in Figure 8.63. Prior test results are indicated with a lighter line width and color. Positive bar displacement and strain correspond with tensile demands. The peak bond slip was 12.8 mm (0.50 in.), which is the largest obtained in the loading protocol thus far. This is the last test for which bond slip is reported. Subsequent tests lack reliable strain gauge data for comparisons.

In this test, peak transverse strain demands were similar to prior tests; see Figure 8.64. On both column faces, strain gauges on the hoop where maximum stain had previously been measured were no longer providing viable readings. Eleven of the twenty transverse gauges were reliable at this level of testing.

Figure 8.65 shows the smeared curvature profile of the column over the height it was measured during instances of peak column displacement, East and West, and post-test. The experimental idealized curvature was exceeded over a height above the footing corresponding to 1.5 column diameters. Peak demands exceeded those of prior tests and a curvature ductility of 9.0 was obtained at the lowermost region instrumented. Curvature demands below one column diameter were large in both East and West directions. The residual curvature profile is shown in red with values close to the idealized experimental yield below one column diameter.

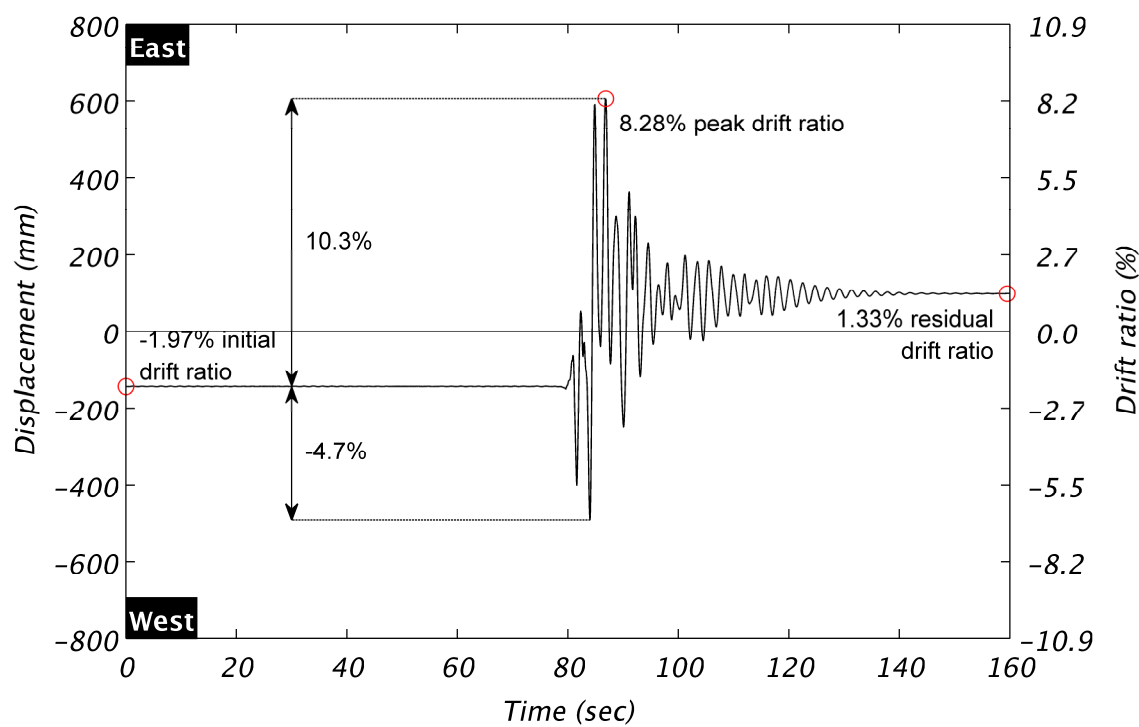


**Figure 8.58    Column displacement during Test EQ8.**

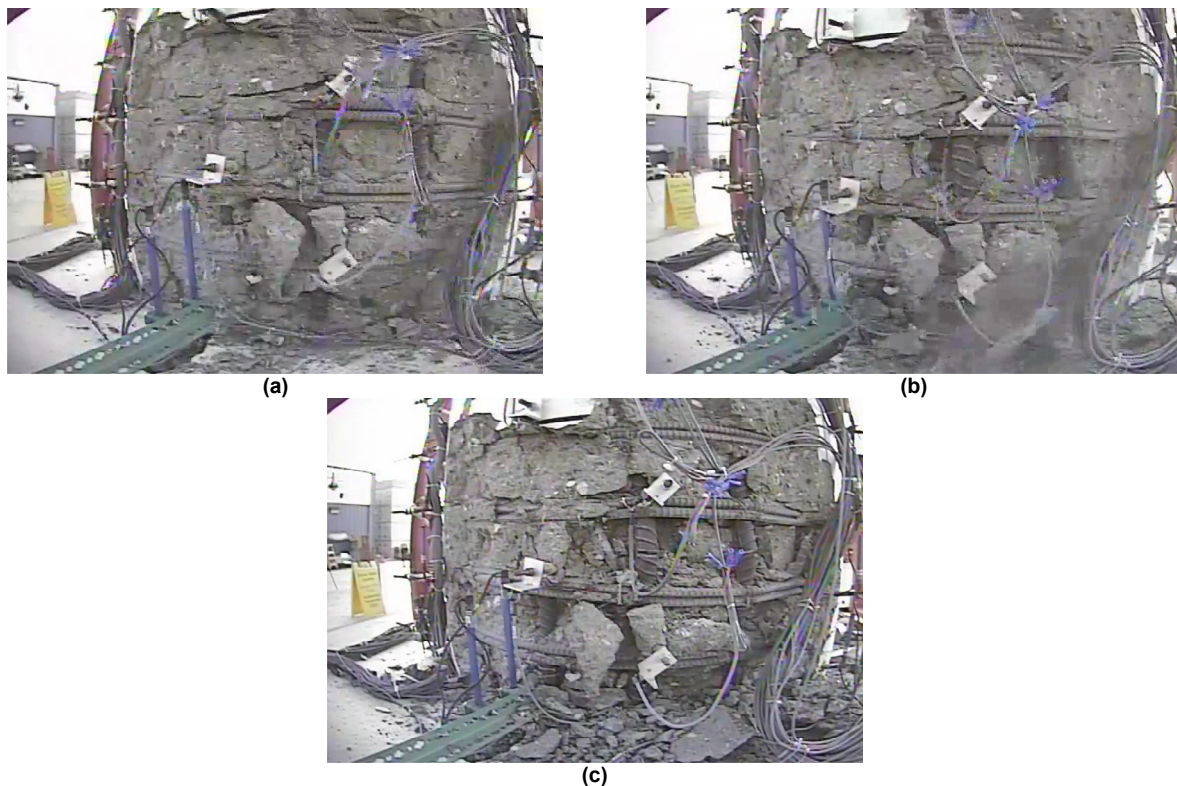


**Figure 8.59    Column base East face during Test EQ8 at (a) peak West displacement, (b) peak East displacement, and (c) post-test.**

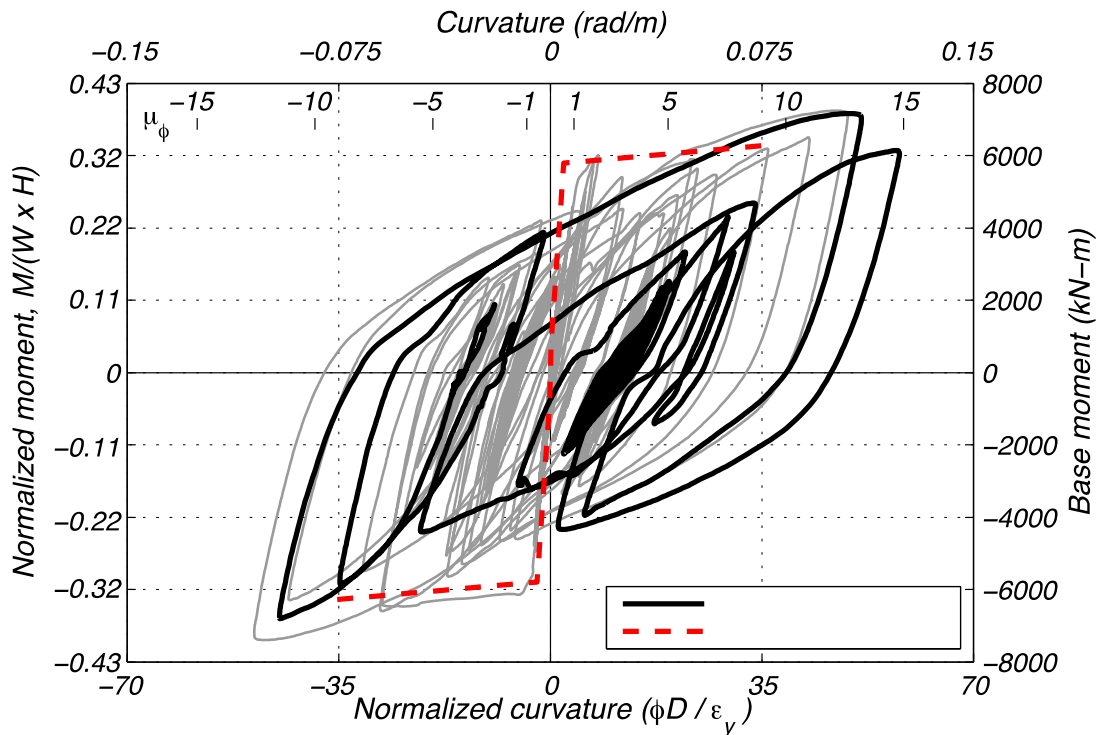


**Figure 8.60** Column response during Test EQ8 in terms of base moment and curvature.

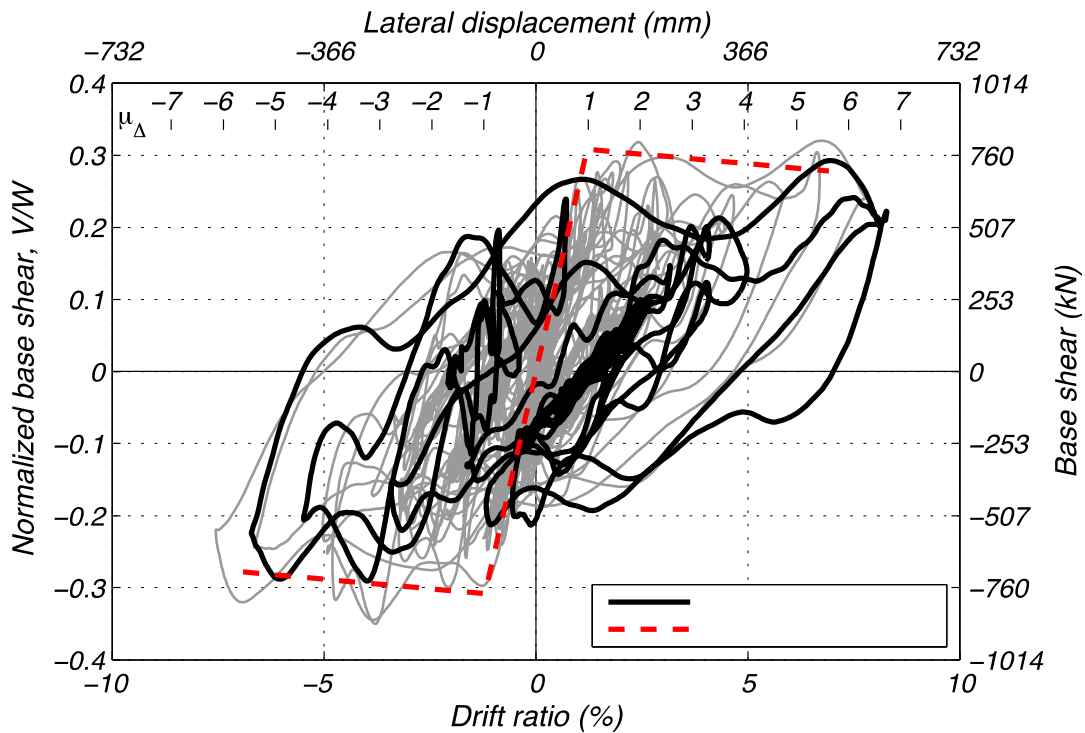


**Figure 8.61** Column response during Test EQ8 in terms of base shear and drift ratio.

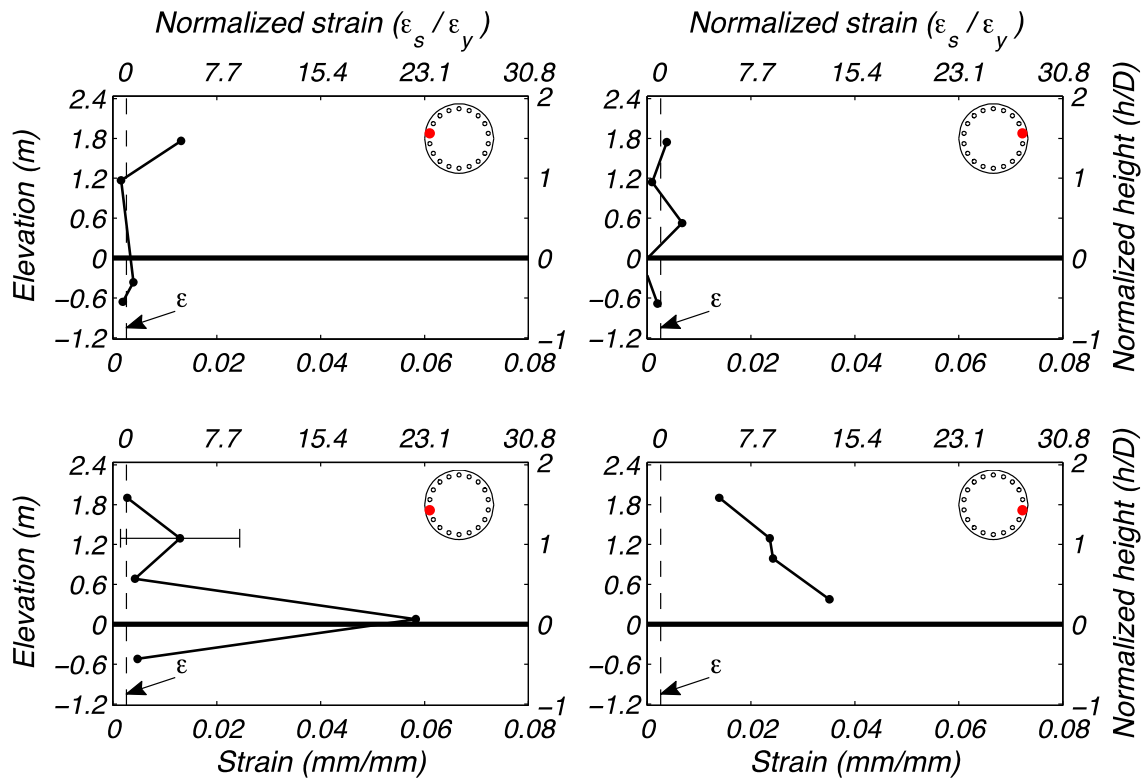


**Figure 8.62** Longitudinal reinforcement tensile strain demand during Test EQ8.

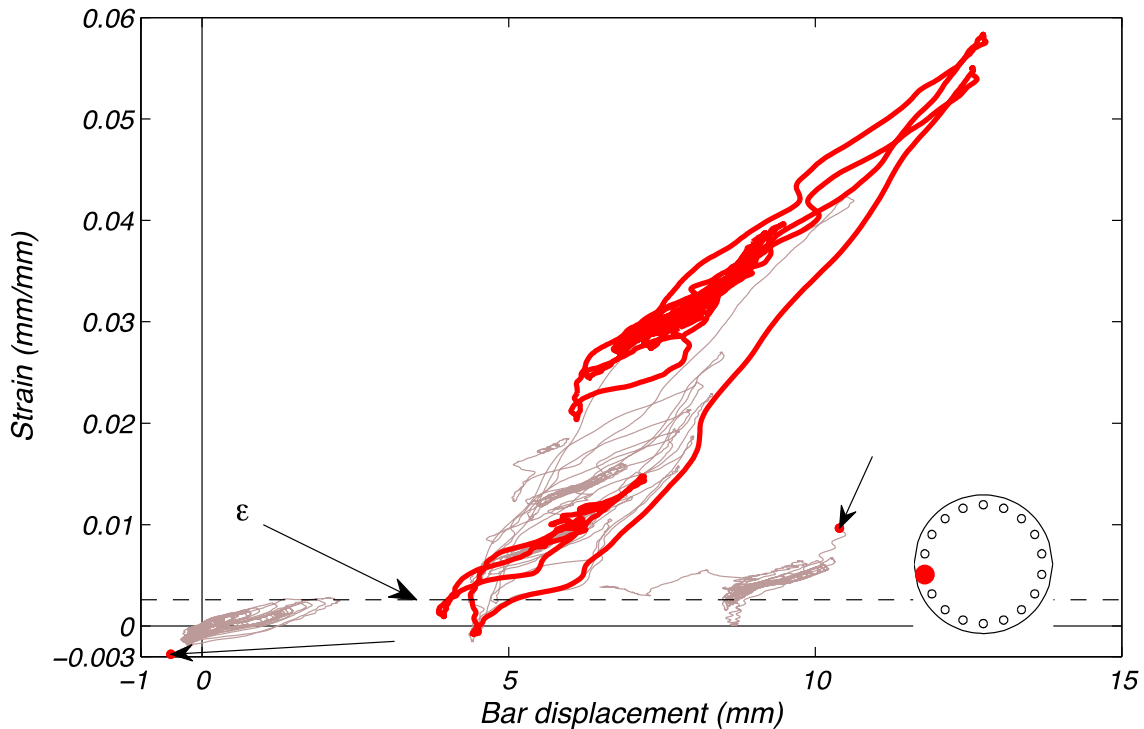


**Figure 8.63** Longitudinal reinforcement bond slip during Test EQ8.

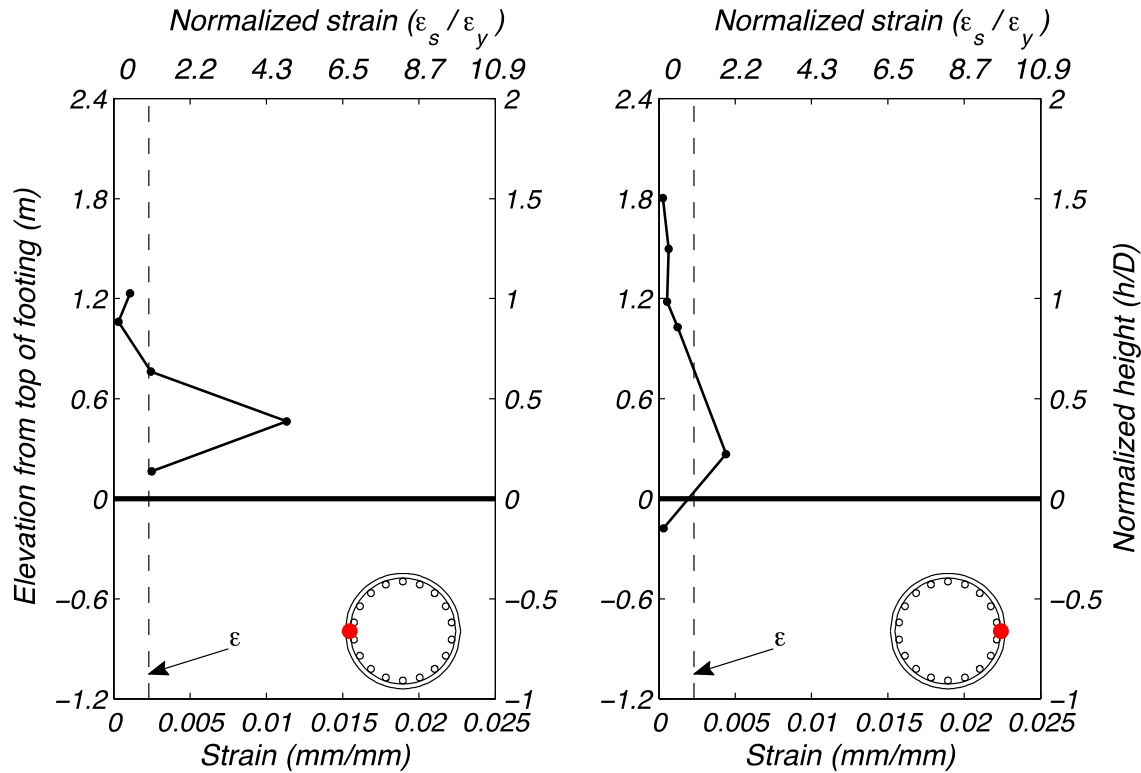


**Figure 8.64 Transverse hoop reinforcement tensile strain demand during Test EQ8.**

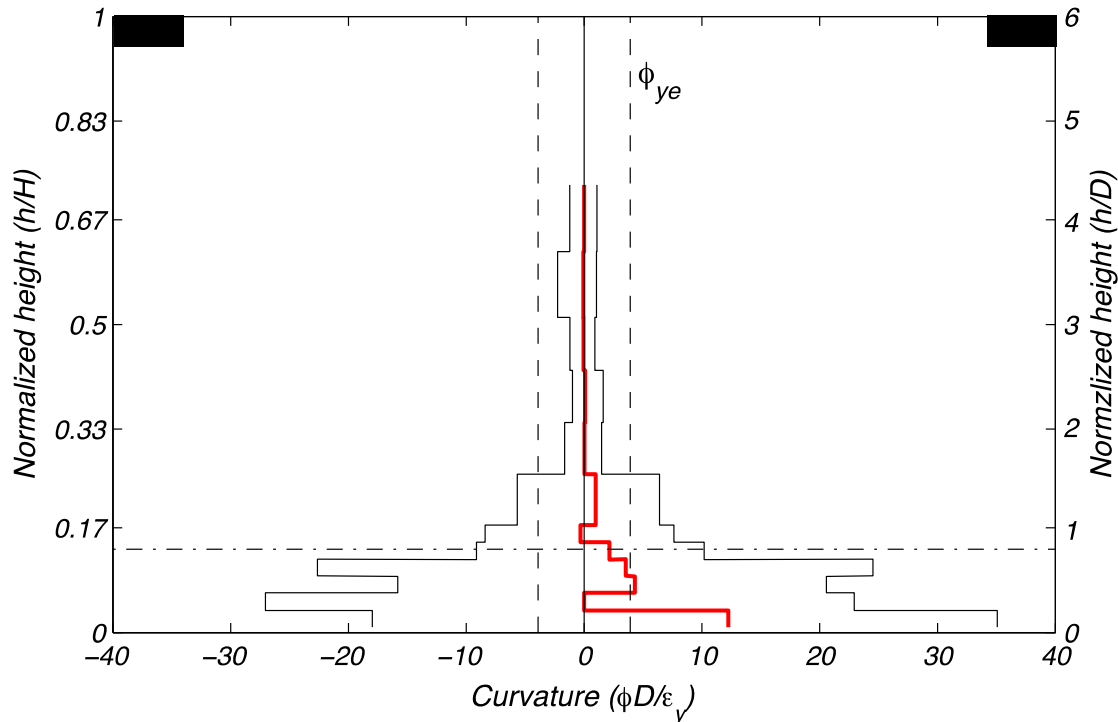


**Figure 8.65 Curvature profile at peak and residual displacements during Test EQ8.**

## 8.9 TEST EQ9

Reversing the polarity of the previous test, a scale factor of +1.2 was used with the original Takatori record for Test EQ9. Despite the reversed polarity, the column accumulated further residual displacement to the East; see Figure 8.66. Early in the time history, a third longitudinal reinforcing bar fractured on the East face of the column. A post-test view of the East face of the column base is shown in Figure 8.67(c), but the new fracture is not apparent. Two reinforcing bars fractured on the West face during this test. This is evident as a drop in moment capacity at about 0.11 rad/m (0.0028 rad/in.) in the moment-curvature relationship of Figure 8.68.

The peak column displacement was 635 mm (25.0 in.), corresponding to a drift ratio of 8.69%. The displacement ductility achieved was 7.06. A residual displacement of 225 mm (8.9 in.), or 3.07% residual drift ratio, remained post-test, as indicated in the displacement time history of Figure 8.66. Figure 8.67(a) and (b) show the East face of the column base at peak displacement in the West and East directions, respectively.

The peak column base moment was 6160 kN-m (4540 kip-ft). This is 83% of the peak moment achieved in Test EQ7. Stiffness degradation is apparent in the moment-curvature response, see Figure 8.68. The peak shear force of 755 kN (170 kip) was largely a product of the mass moment of inertia of the superstructure that induced an inflection point at approximately 75% of the column height. The consequence is a relatively low overturning moment demand, approximately 4000 kN-m (2950 kip-ft), that produced the peak shear force. The lateral shear force-displacement response is shown in Figure 8.69.

Only thirteen of sixty-four longitudinal strain gauges remained intact for this test. These are shown in Figure 8.70; note that the bar in Figure 8.70(c) had fractured in the prior test and the bars in (a) and (d) fractured during this test. The largest longitudinal strain, 6.4%, recorded during any test was obtained in a bar on the West face just above the footing, see Figure 8.70(b). Transverse strain demands remained consistent with demands imposed in the prior five tests, see Figure 8.71.

Figure 8.72 shows the smeared curvature profile of the column over the height it was measured during instances of peak column displacement, East and West, and post-test. The experimental idealized curvature was exceeded over a height above the footing corresponding to 1.5 column diameters. Peak demands exceeded those of prior tests and a curvature ductility of 9.7 was obtained at the lowermost region instrumented. Curvature demands below one column diameter were large in both East and West directions. The residual curvature profile is shown in red with fluctuating values exceeding yield below a height of 864 mm (34 in.).

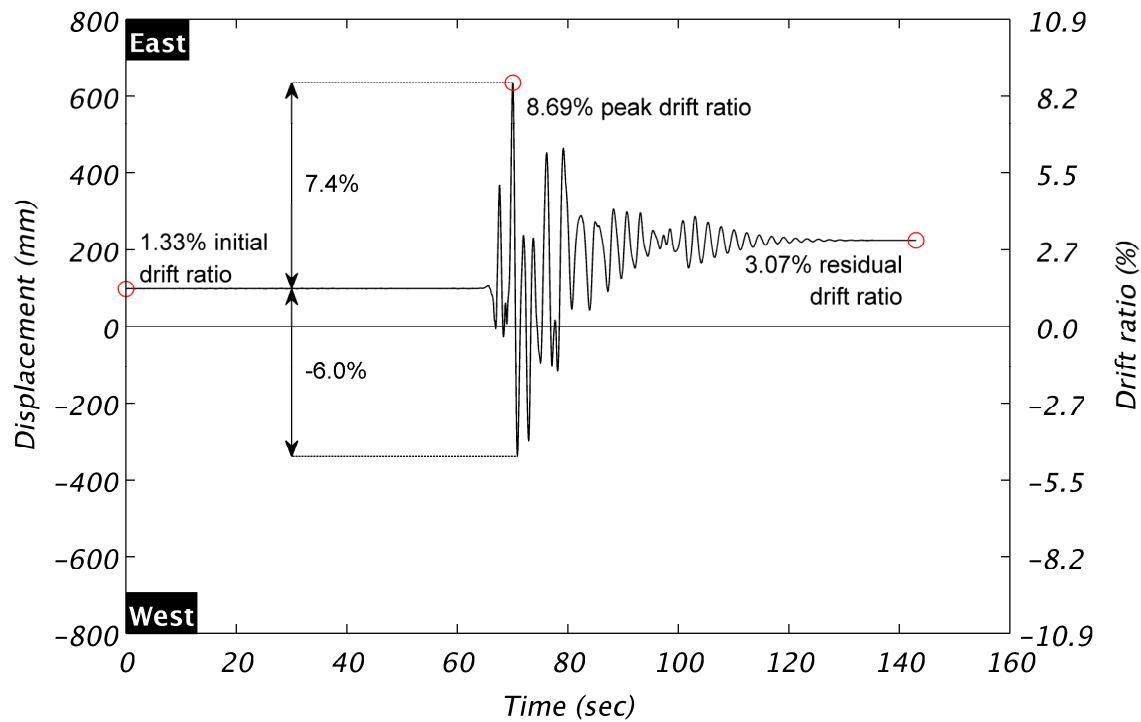


**Figure 8.66    Column displacement during Test EQ9.**

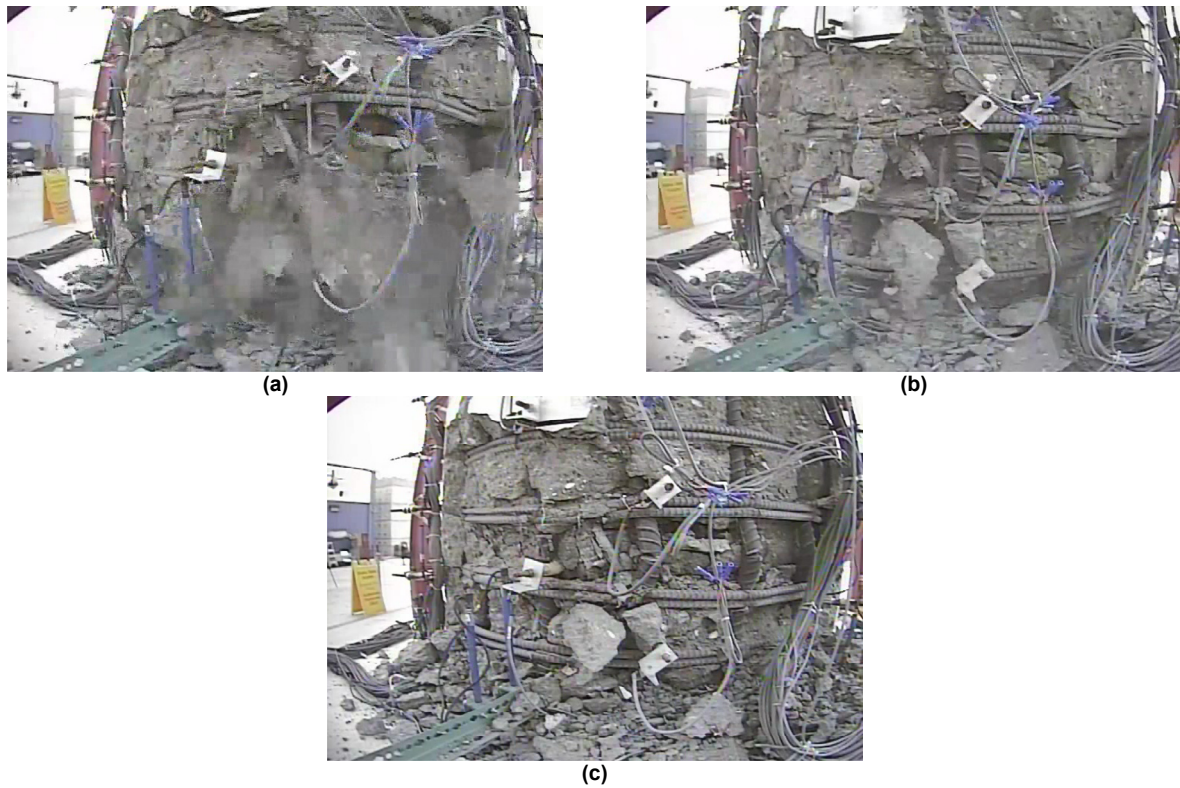


**Figure 8.67    Column base East face during Test EQ9 at (a) peak West displacement, (b) peak East displacement, and (c) post-test.**

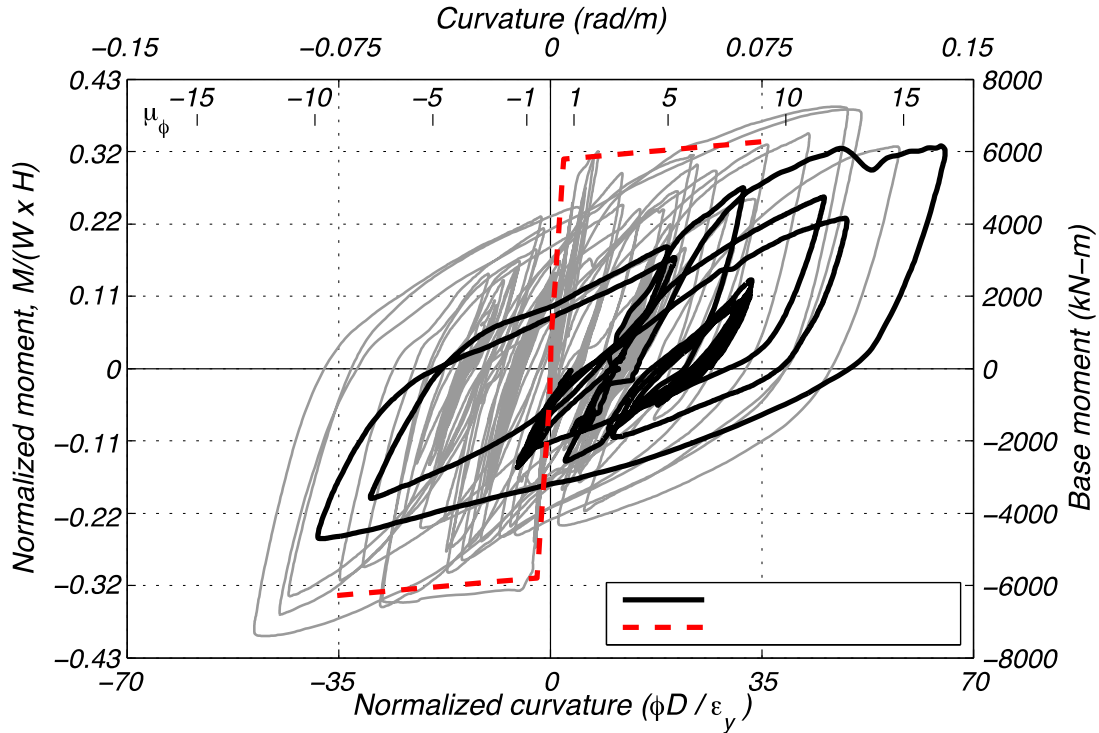


**Figure 8.68 Column response during Test EQ9 in terms of base moment and curvature.**

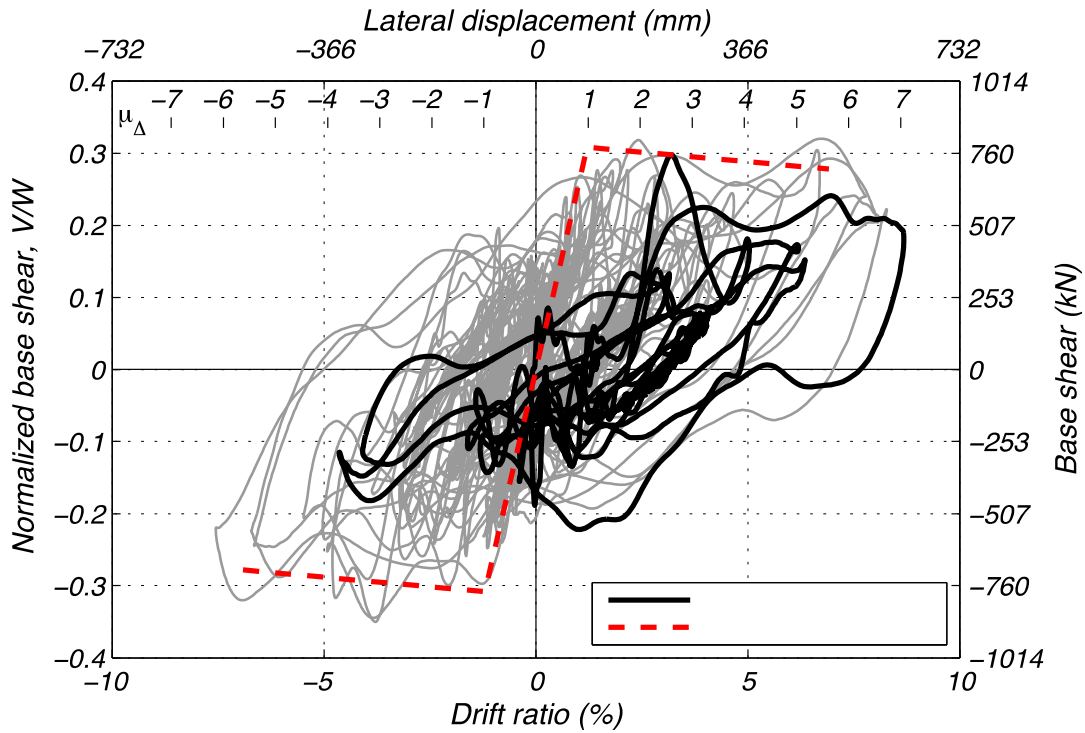


**Figure 8.69 Column response during Test EQ9 in terms of base shear and drift ratio.**

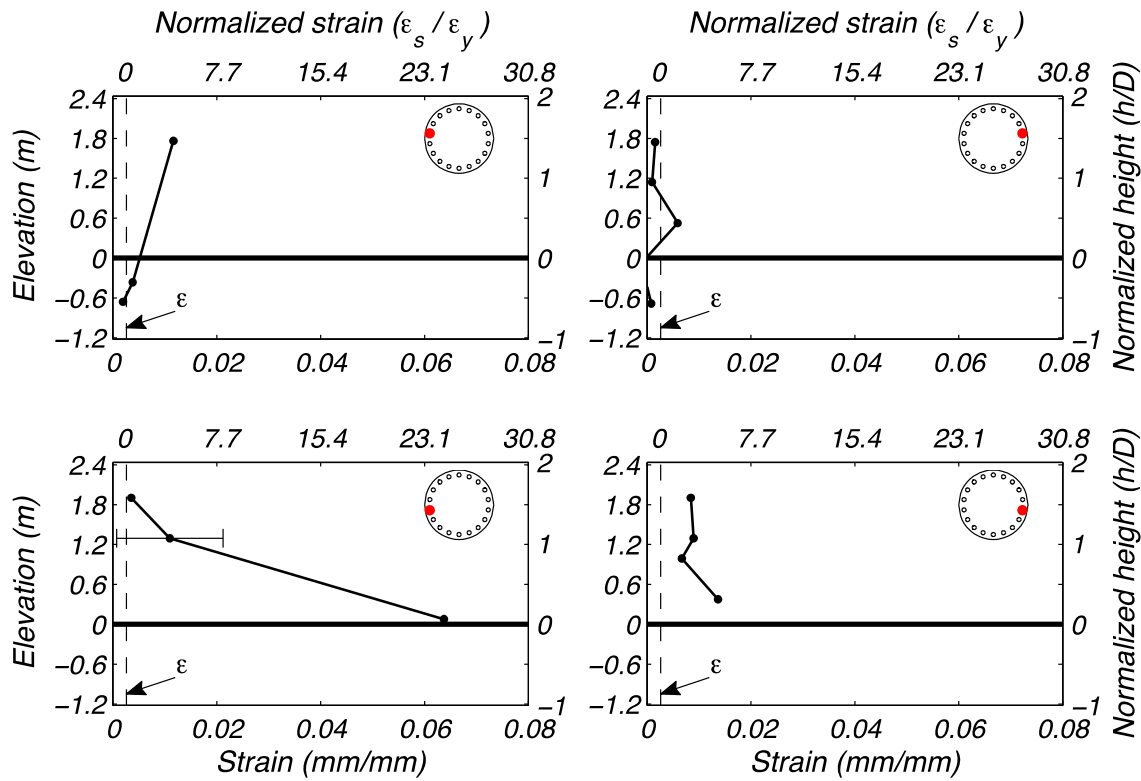


Figure 8.70 Longitudinal reinforcement tensile strain demand during Test EQ9.

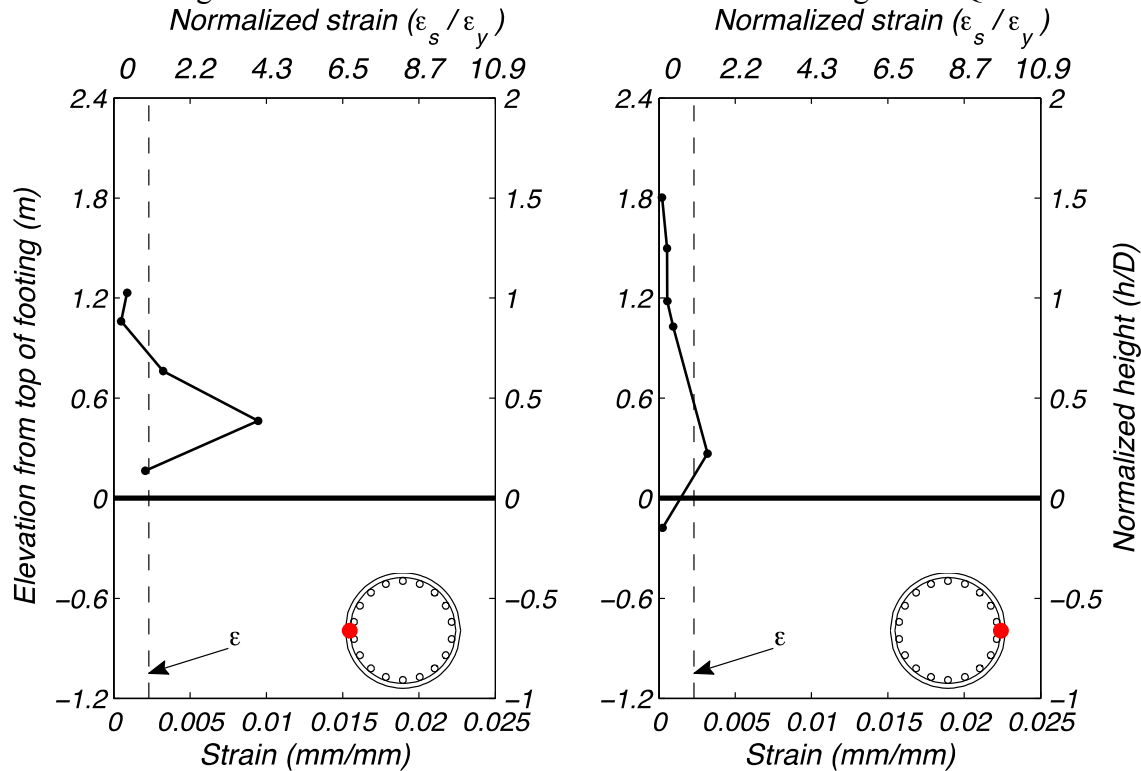
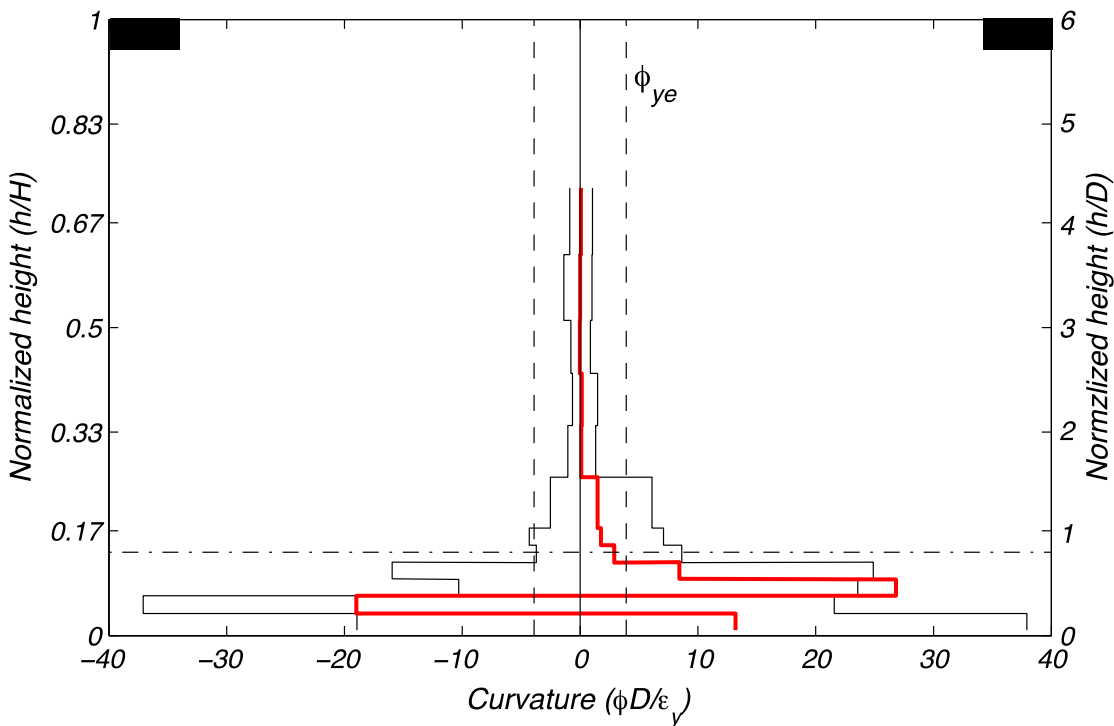


Figure 8.71 Transverse hoop reinforcement tensile strain demand during Test EQ9.



**Figure 8.72 Curvature profile at peak and residual displacements during Test EQ9.**

## 8.10 TEST EQ10

Prior earthquake simulation tests resulted in a reduced column capacity caused by the fracture of five longitudinal bars, buckling of others, and crushing of the concrete core. Continued testing at this point was aimed at pushing the column to the imposed drift limit of 10%. For this purpose, the same scale factor of 1.2 was utilized with the Takatori record consistent with the prior test. A sixth longitudinal reinforcing bar fractured during this test. This was the fourth bar to fracture on the East face of the column. However, the superstructure mass impacted the East safety column before this fracture occurred. During impact, the column displaced 757 mm (29.8 in.). The drift ratio at impact was 8.69. The displacement time history is shown in Figure 8.73. Figure 8.74(a) and (b) show the East face of the column base at peak displacement in the West and East directions, respectively. A post-test view of the East face of the column base is shown in Figure 8.74(c). Vertical offset of the transverse hoops caused by the buckled longitudinal reinforcement is evident in this figure, but transverse reinforcement did not fracture. Exposed longitudinal reinforcement was hot to the touch post-test. Cracks in the top of the footing surrounding the column were present post-test. Their onset was not identifiable due to debris, but they extended radially 0.61 m (24 in.) from the column face.

The derived moment and shear force were heavily influenced by the impact due to their calculation from inertial forces; see Figure 8.75 and Figure 8.76, respectively. Figure 8.75 shows the overturning moment-curvature response, but calculated curvature was not corrected for the influence of curvature rod movement within the crushed concrete core. Hoop dislocation caused

by buckled longitudinal reinforcement disturbed vertical LVDT measurements as evident in videos footage of the North and South faces.

Longitudinal strain gauge readings in Figure 8.77 contain results from three bars that fractured in prior tests. Figure 8.77(b) contains the only bar that was not visually identified as having fractured previously. As shown in Figure 8.78, transverse strain demands were lower than prior tests. This is likely attributed to reduced shear capacity, prior fractures of buckled longitudinal bars, and concrete core crushing.

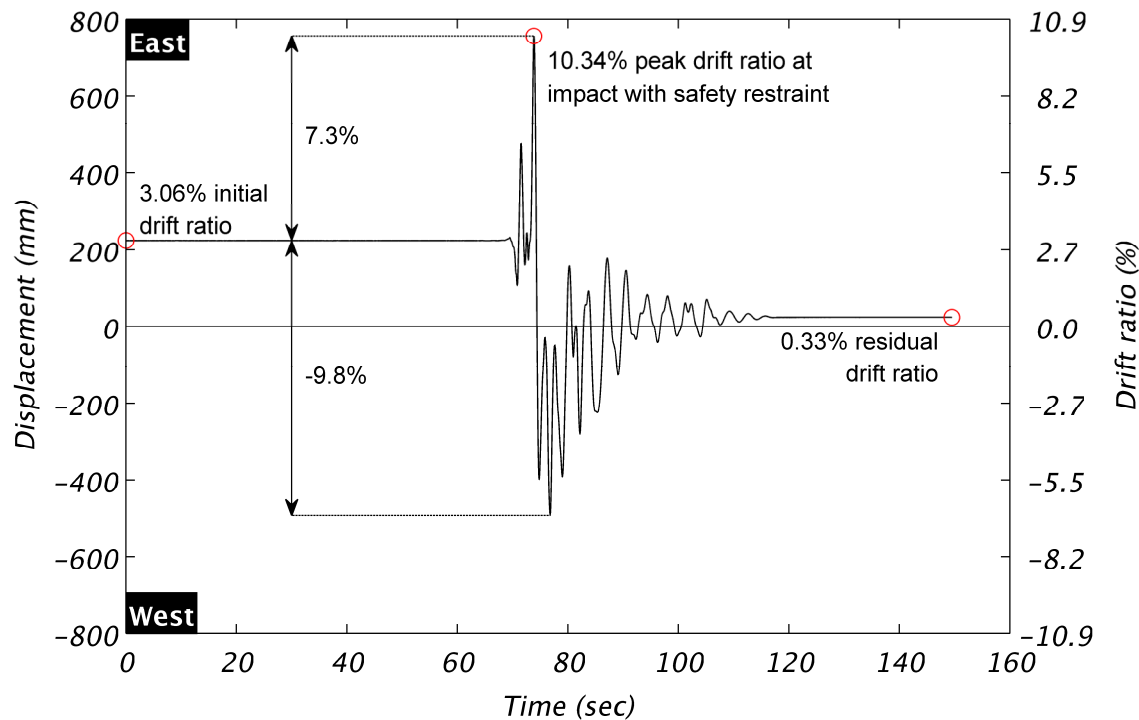


**Figure 8.73    Column displacement during Test EQ10.**

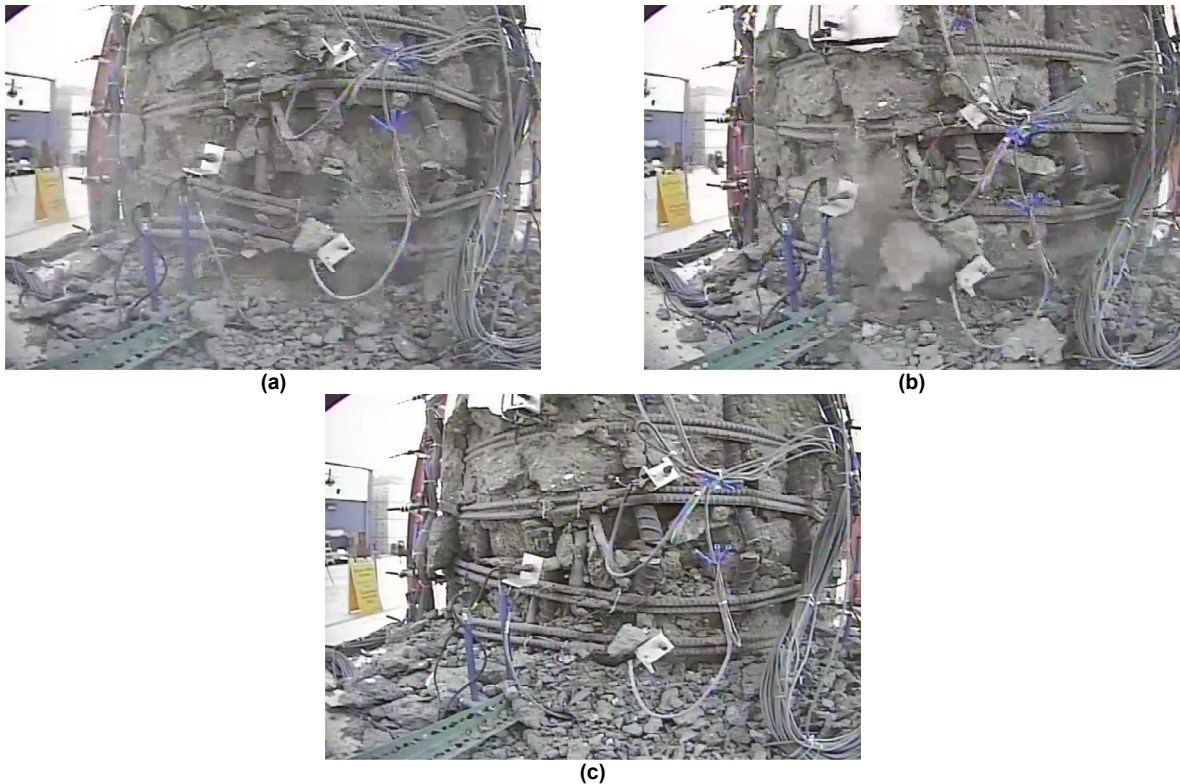


**Figure 8.74 Column base East face during Test EQ10 at (a) peak West displacement, (b) peak East displacement, and (c) post-test.**

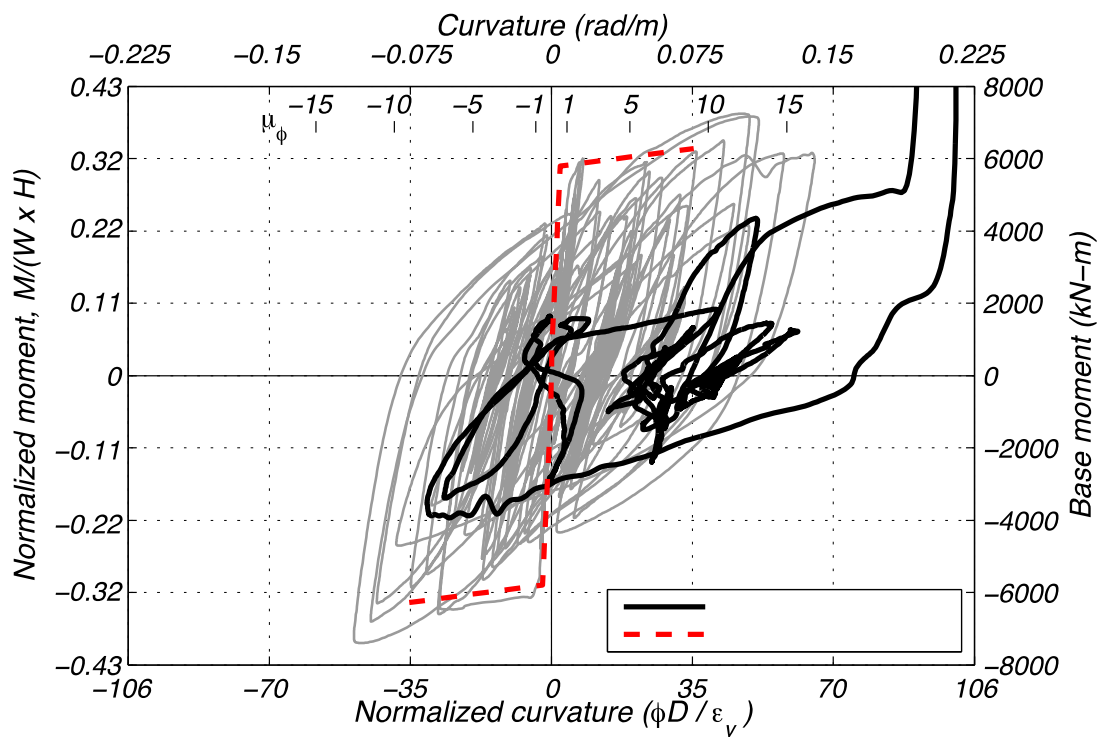


**Figure 8.75 Column response during Test EQ10 in terms of base moment and curvature.**

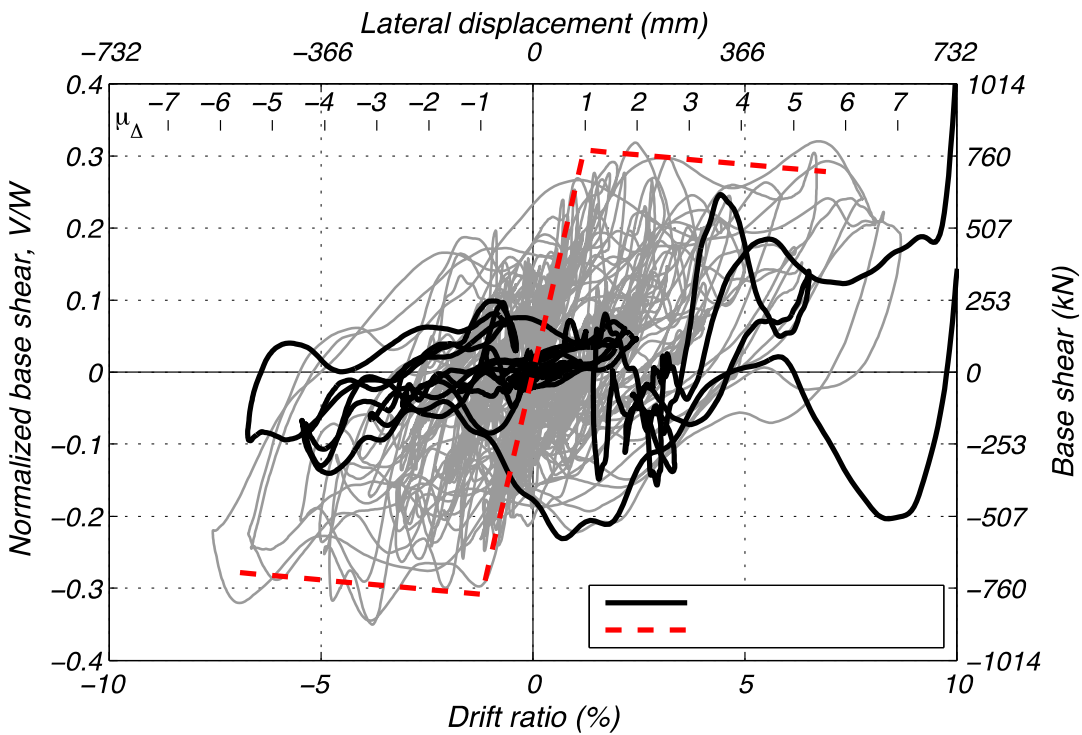


**Figure 8.76    Column response during Test EQ10 in terms of base shear and drift ratio.**

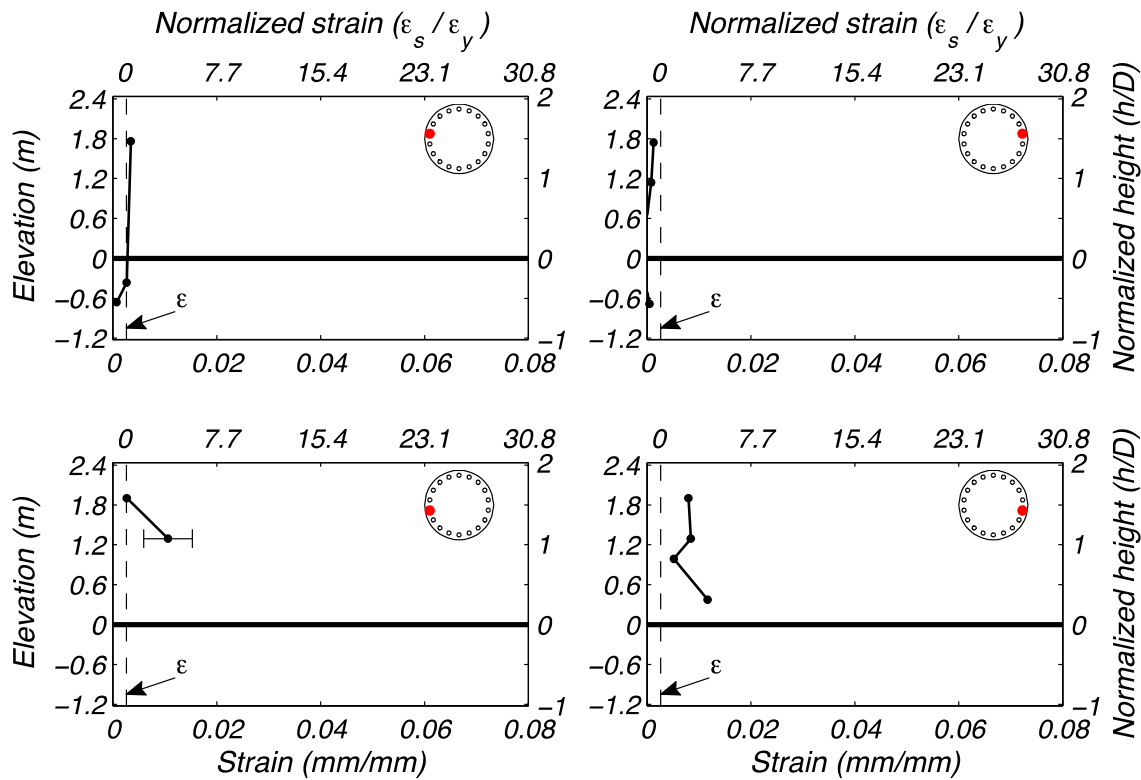


**Figure 8.77    Longitudinal reinforcement strain demand during Test EQ10.**

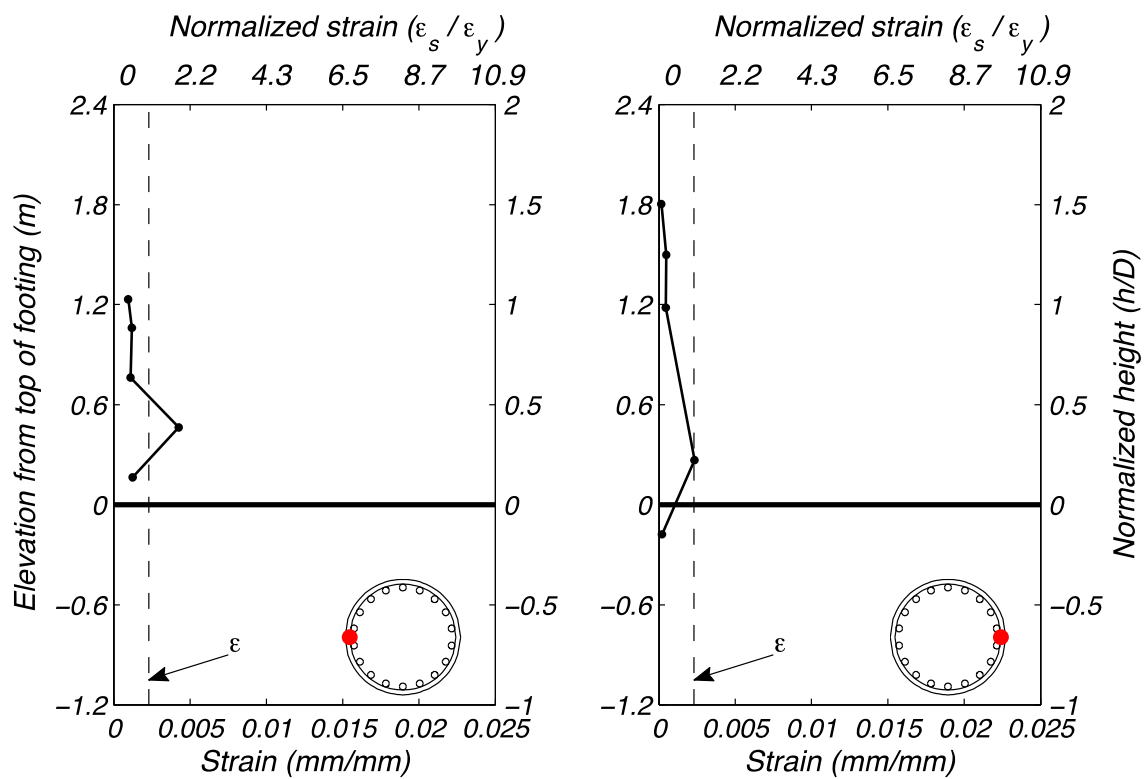


**Figure 8.78 Transverse hoop reinforcement strain demand during Test EQ10.**

@Seismicisolation

# 9 Summary and Conclusions

## 9.1 SUMMARY

Ten earthquake simulations were conducted on a full-scale bridge column built to current Caltrans design specifications. The column exhibited ductile behavior and achieved a maximum displacement ductility of 7.06, where the experimental yield displacement was calculated as 90 mm (3.54 in.). Table 9.1 contains a summary of response quantities from each of the tests.

**Table 9.1 Peak response quantities.**

Test	Displacement ductility	Peak drift ratio (%)	Peak longitudinal strain (%)	Peak moment (MN-m)	Peak shear (kN)	Peak curvature (rad/km)
EQ1	0.69	0.85	0.22	3.95	500	7
EQ2	1.48	1.82	1.32	5.90	699	16
EQ3	4.01	4.93	2.98	6.59	888	61
EQ4	1.89	2.33	1.44	3.75	401	25
EQ5	6.32	7.78	4.66	7.24	811	105
EQ6	5.44	6.69	4.23	6.50	771	92
EQ7	6.15	7.56	4.28	7.39	812	105
EQ8	6.73	8.28	5.84	7.16	742	123
EQ9	7.06	8.69	6.38	6.16	755	140
EQ10*	8.41	10.34	1.16	-	-	214

\* Impacted the East safety column at peak displacement.

Test EQ1 demonstrated the column's elastic behavior. Test EQ2 initiated nonlinear response with limited ductility demands. Design-level demands were imposed by Test EQ3, with a displacement ductility of 4.0. Concrete spalling was the extent of visible damage, and peak longitudinal strains were less than 3%. Damage was repairable and the residual drift ratio was less than 0.9%. The largest shear demand was generated in this design-level test. Test EQ4 represented an aftershock, which resulted in linear column response. Tests EQ5 represented a beyond-design-level scenario, followed by a repeat of the design-level event in EQ6. Structural

integrity remained after the intended protocol with concrete spalling as the extent of damage. Remaining tests were added successively with the aim of inducing failure. Test EQ7 triggered bar buckling and generated the largest overturning moment of any test. Two longitudinal bar fractures occurred in EQ8, which was the fifth consecutive test to impose drift ratio demands greater than 6.5%. Bar fracture corresponded with onset of concrete core crushing. Test EQ9 induced bar fracture in three additional longitudinal bars and caused further core crushing. Moment capacity reduced to 83% of the maximum obtained in EQ7. Subsequent testing brought the specimen to near collapse and impact with the safety restraint. This prompted the conclusion of the test program. Just before impact, the moment capacity was reduced to 69% of the maximum obtained during Test EQ7.

Figure 9.1 illustrates the peak drift ratio achieved during testing with the residual drift ratio superimposed on top. The largest residual drift ratio was 3.1% after Test EQ9. A residual drift ratio of 0.9% remained after the design-level scenario of Test EQ3. Repeated demands beyond the design level demonstrate the durability and ductility of the seismic details provided. Lateral displacements were mainly contributed to by flexure; see Figure 9.2. Flexure accounted for 70% or more of the measured column displacement in nearly all tests. A fixed-end rotation of approximately 15% was the secondary contribution, which was consistent throughout testing. A minor contribution due to shear deformation was computed as 5% or less in all tests.

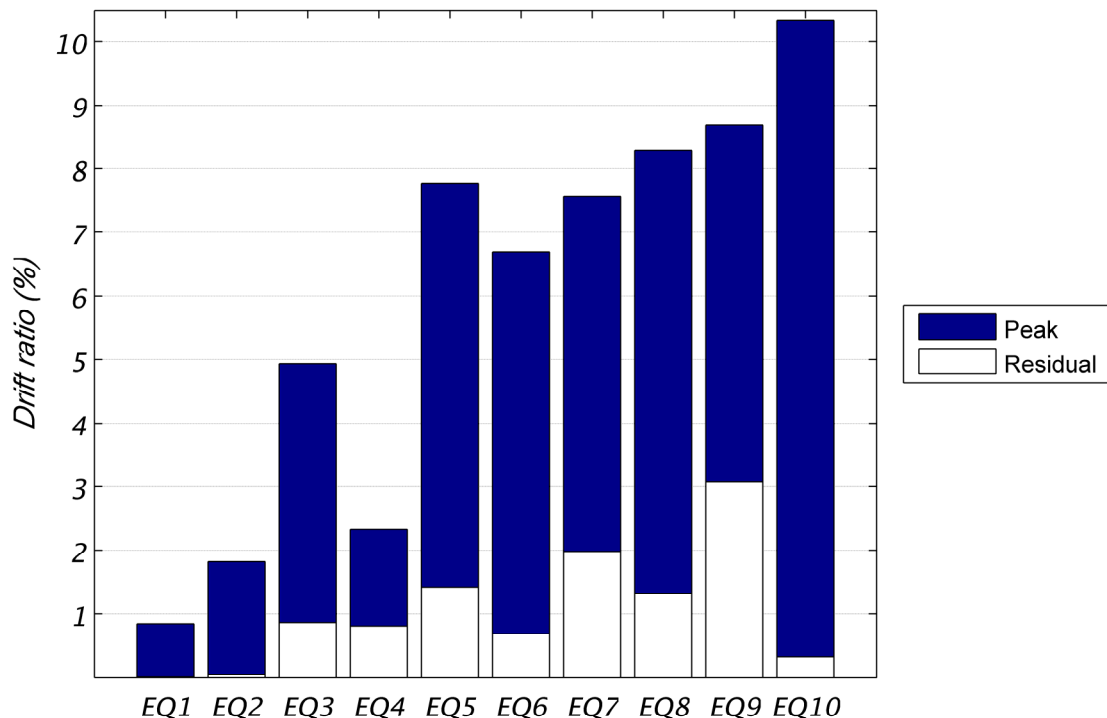


**Figure 9.1      Drift ratios achieved during tests.**

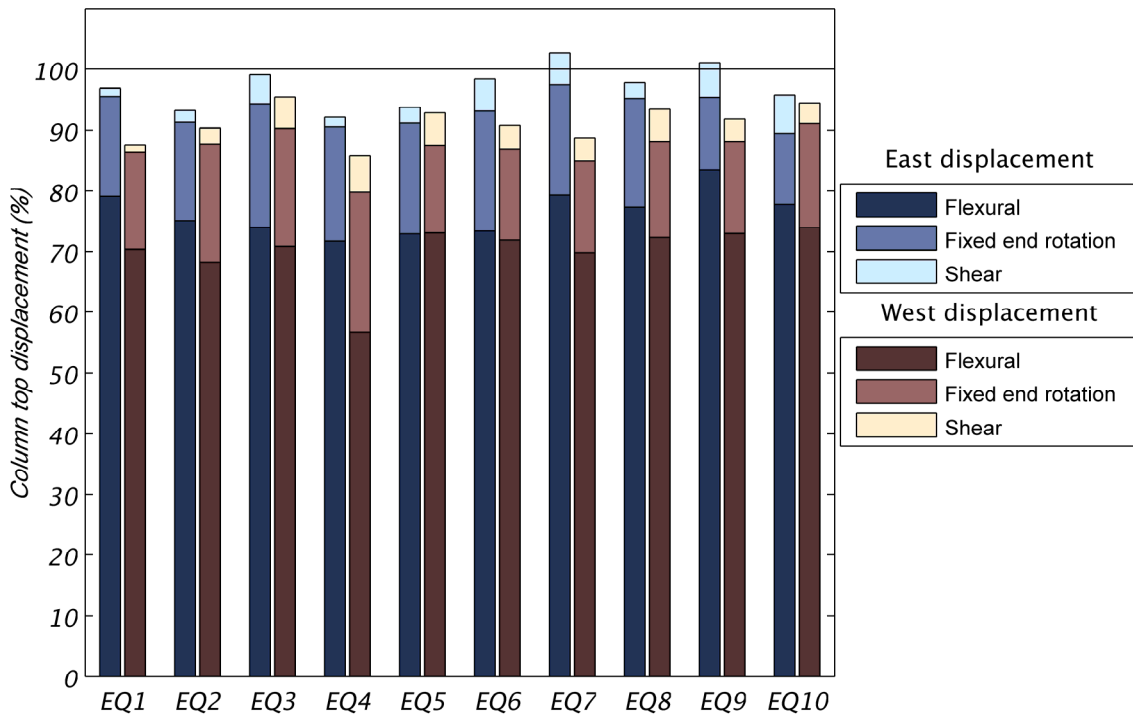


**Figure 9.2 Displacement components at peak displacements.**

Column dilation was captured via spring loaded linear displacement sensors; see Section 7.2. These captured concrete core dilation as the sensor target was welded to the transverse reinforcement. Peak dilation values are reported at discrete points between 0.2 and 1.0 column diameter above the footing; see Figure 9.3. During the design-level event, the maximum dilation was between 1.4 mm (0.05 in.) and 3.4 mm (0.13 in.). The maximum dilation obtained was 10.3 mm (0.40 in.), which occurred during Test EQ9.

Dynamic properties for the first and second modes of vibration were obtained from white-noise tests conducted before each earthquake simulation. Analysis of these tests identified the frequency and equivalent viscous damping ratio for both modes. Mode one corresponds to the lateral deformation of the column at the center-of-mass of the superstructure, and mode two results from the rotational inertia of the superstructure. The dynamic properties are summarized in Table 9.2 and Figure 9.4, and were identified from the transmissibility ratio. Linear viscous damping was bounded between 2% and 4.3% for mode one and between 1.3% and 5.3% for mode two. Period elongation was most pronounced as a consequence of Test EQ3, which represented the design-level event.

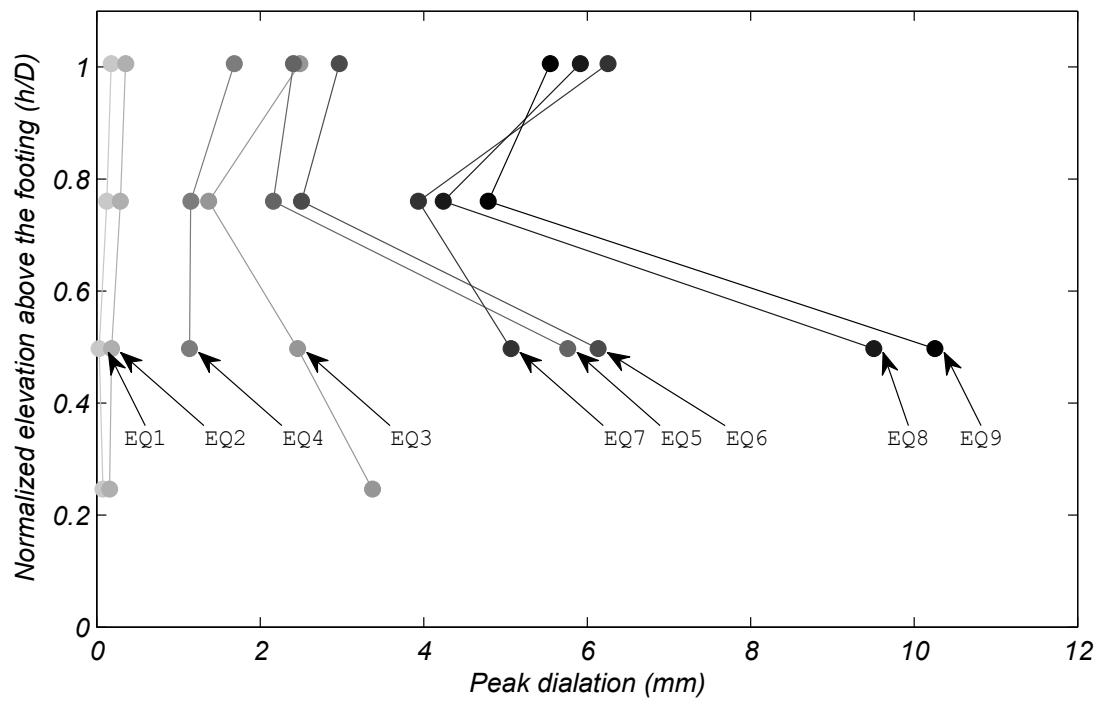


**Figure 9.3      Column dilation.**

**Table 9.2      Dynamic properties from white-noise tests.**

Test	Mode 1		Mode 2	
	Period (sec)	Damping ratio (%)	Period (sec)	Damping ratio (%)
Pre-EQ1	0.88	4.3	0.17	1.3
Pre-EQ2	0.91	4.0	0.17	1.4
Pre-EQ3	1.12	3.3	0.19	1.5
Pre-EQ4	1.67	2.3	0.22	2.3
Pre-EQ5	1.67	2.0	0.22	2.3
Pre-EQ6	1.83	2.5	0.23	3.3
Pre-EQ7	1.88	2.7	0.24	3.3
Pre-EQ8	1.92	2.2	0.24	3.3
Pre-EQ9	2.20	2.9	0.26	5.3

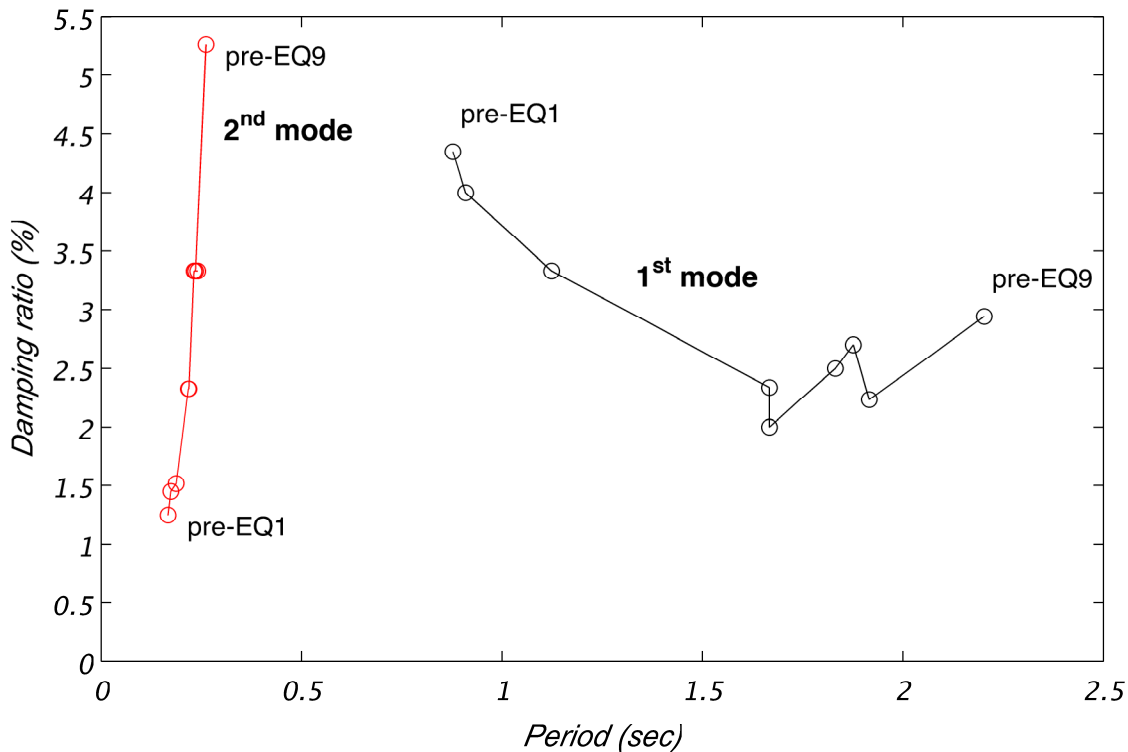


**Figure 9.4      Dynamic properties from white-noise tests.**

The progressive damage is shown chronologically Figure 9.5 as the post-test state of the column's East face. The images show the column base up to 0.61 m (24 in.) or one-half the column's diameter. After the design-level earthquake, only cracks are evident in Figure 9.5(c), but spalling had initiated on the opposite face. The damage state at this level was cosmetic and easily repairable. This was the same scenario after a simulated aftershock. The onset of bar buckling did not occur until a third test at or beyond the design-level event (Test EQ7).

Damage occurred in a localized plastic hinge region at the base of the column. The response was flexure-dominant, and shear capacity was maintained throughout testing. Column cracks extended throughout the entire accessible height of the column by testing completion. However, concrete spalling, longitudinal bar buckling, and longitudinal bar fracture were located within 1.22 m (4 ft), or one column diameter, of the base of the column. Footing cracks were evident in the top of the footing after Test EQ10 due to cone pullout from strain penetration.

After testing, all of the exposed longitudinal bars exhibited buckling deformation. Four longitudinal bars on the East face of the column fractured. Three longitudinal bars on the West face fractured and an additional two bars developed cracks, which did not propagate through the bar diameter. During demolition, the longitudinal bars were cut from the specimen for inspection. Photos of the extracted bars are arranged radially from their location in the column in Figure 9.6. Thirteen out of the eighteen bars were buckled. The typical buckled length was 300 mm (12 in.) or twice the hoop spacing.

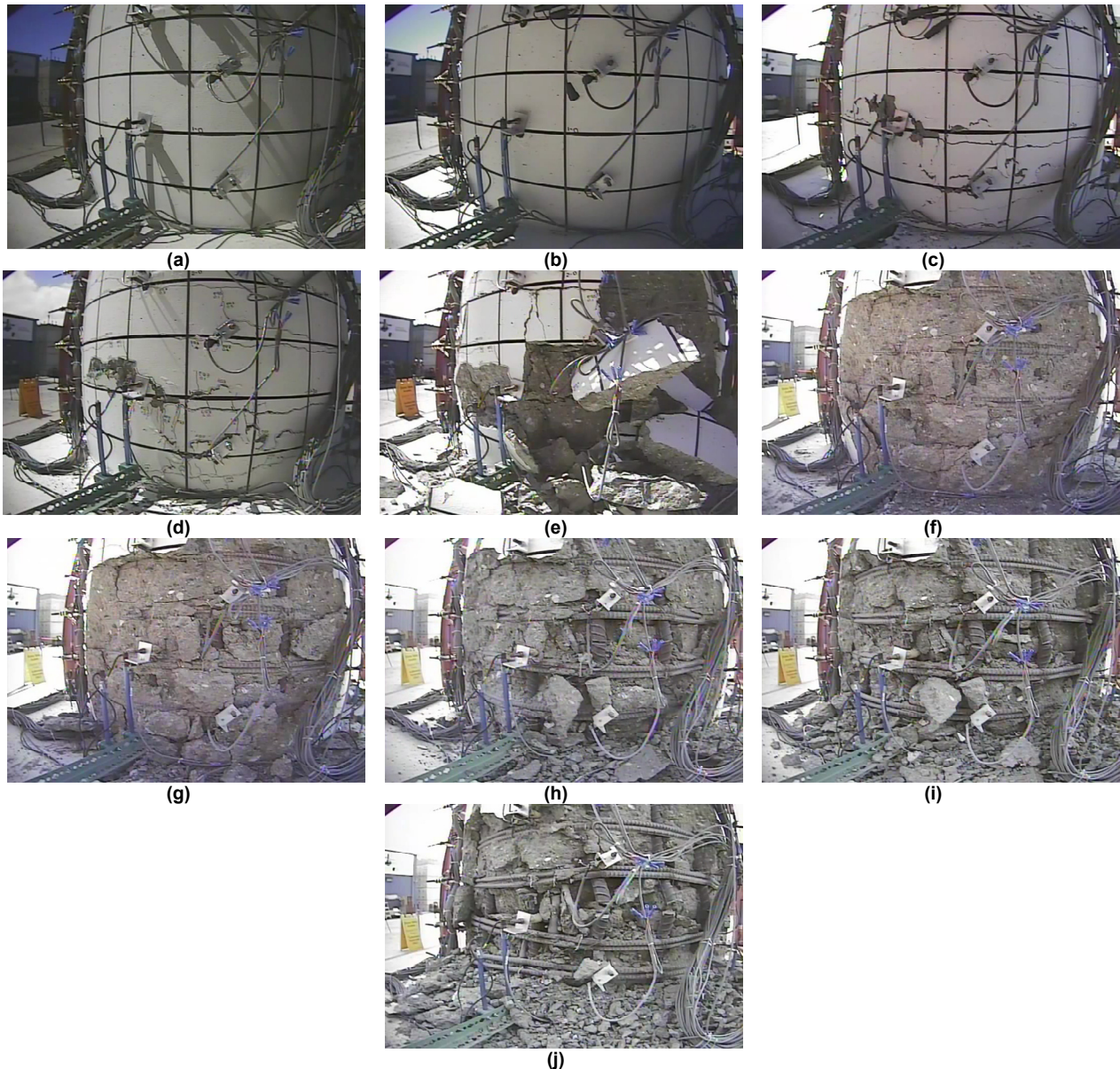


**Figure 9.5      Column base East face post test: (a) EQ1, (b) EQ2, (c) EQ3, (d) EQ4, (e) EQ5, (f) EQ6, (g) EQ7, (h) EQ8, (i) EQ9, and (j) EQ10.**

A necking phenomenon was not apparent in the fractured bars because fracture initiated with a crack on the concave side of the buckled segment. This crack originated from stress concentration around bar deformations in compression. However, some of the buckling deformation was induced after bar fracture when fractured ends came in contact with each other during a compression cycle. During Test EQ9 the peak longitudinal strain measured by strain gauges was 6.4%.

Of the seven fractured bars, video evidence identified when fracture occurred for six of the bars: two on the West face during Test EQ8, one on West face and two on the East face during Test EQ9, and one on the East face during Test EQ10. The last fracture on the West face

may have occurred near impact with the safety restraint during Test EQ10, but this could not be confirmed from the videos or data.

Transverse hoops did not fracture despite the nonlinear demands imposed by concrete dilation and longitudinal bar buckling. Redundancy provided by bundled hoops may have been beneficial and kept transverse strains low, but strain gauges were not installed on both of the bundled hoops. Because only one gauge was installed per bundle, the redundancy provided cannot be quantified. The maximum strain in any test, measured during Test EQ5, was 2.5%, and the maximum strain demand in all other tests was less than 1.2%. Demands imposed on the hoops from shear transfer and concrete dilation were within the strain capacity of the hoops.

Vertical offset of the transverse hoops caused by the buckled longitudinal reinforcement is evident in Figure 9.7. Buckling is clearly seen in this figure as occurring across multiple spacings of transverse reinforcement. The region of the column requiring enhanced lateral confinement per section 7.6.3 of the Seismic Design Criteria [Caltrans 2006a] was 1.5 times the column diameter for this test set-up, but no change in reinforcement detailing was made up the column height. This plastic hinge region,  $L_{pr}$ , is indicated in Figure 9.7 and extends 0.61 m (24 in.) or  $\frac{1}{2}D$  above the extent of spalling.

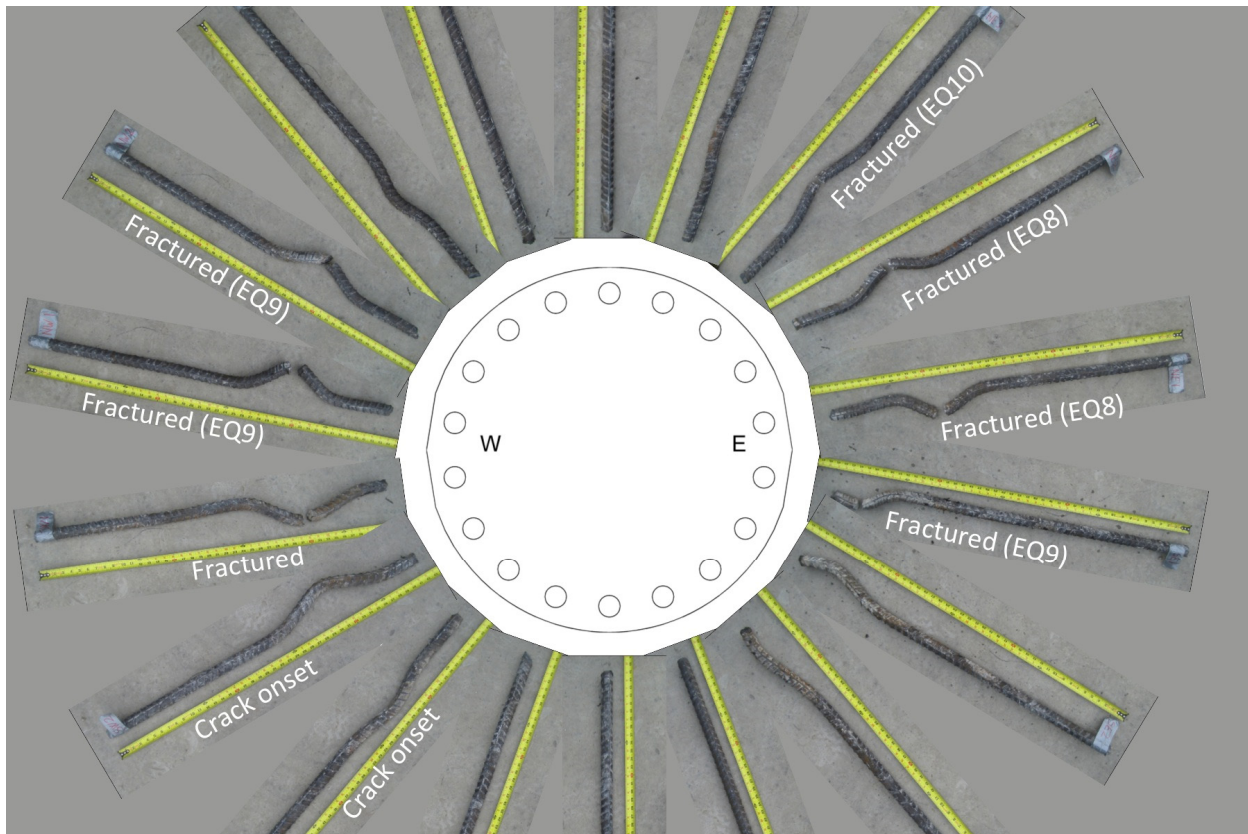


**Figure 9.6      Extracted longitudinal reinforcement.**



Figure 9.7      South face of the column post-test.

## 9.2 CONCLUSIONS

The 1.22-m (4-ft) diameter and 7.32-m (24-ft) tall column was the largest column tested in the U.S. under dynamic loading conditions. Significant nonlinear response was induced during the uniaxial shake table tests. Durability and ductility of the structure were demonstrated by repeated cycles beyond the design level with strength degradation only after rebar fractures (Test EQ8). Conformity to the design philosophy was observed with ductile a plastic hinge forming at the base of the cantilevered column. The concentrated hinge developed concrete spalling up to one column diameter from its base. This was within the code specified region for enhanced confinement of 1.5 column diameters.

Concrete spalling initiated during the simulated design-level earthquake (Test EQ3). This damage was cosmetic and repairable. For classification as a Caltrans Ordinary Bridge, the seismic performance criteria were exceeded: damage was limited and collapse was not imminent. A residual drift ratio of 0.9%, however, is significant as it may necessitate replacement rather than repair. Difficulty repairing bridges in Japan after the 1995 Kobe earthquake led the Japan Road Association [2002] to adopt seismic design guidelines that limit residual drift ratios to 1%. For this reason and because the seismic hazard was defined as a 975-year return period for an Ordinary Bridge (and not at the functional and safety seismic hazards for a Caltrans' defined Important Bridge), it is difficult to assess if this specimen would have satisfied the performance criteria of an Important Bridge.

As anticipated, a higher-mode contribution from the rotational inertia of the superstructure is evident in base shear response. This contribution is present in real bridges not just an artifact of the test set-up. Its effect should be considered in design where analytical modeling or dynamic amplification factors can be used as a remedy.

The provisions for anti-buckling restraint in the Seismic Design Criteria [Caltrans 2006a] were successful at the design level. These guidelines anticipate the prevention of buckling between layers of transverse reinforcement, but the observed buckling mode during later stages of testing (initiated during Test EQ7) was across adjacent layers. Furthermore, transverse hoops were spaced 25% closer than the maximum allowed; specified spacing was 0.15 m (6 in.) versus 0.20 m (8 in.) maximum allowed. The reduced spacing may have played a role in the buckling onset, but an alternate loading sequence would have had a more pronounced influence.

By the conclusion of testing, some crushing of the core concrete occurred at the exterior. However, this was limited and the core remained largely intact. A flow of core concrete spilling through the cage, as observed by Kawashima et al. [2009], did not occur.

Test objectives to induce and monitor nonlinear lateral demands at targeted deformations were achieved. These demands were imposed at and beyond the design level, and achieved the objective of assessing current design practices. While this validation holds only for the case investigated, the design philosophy and methodology appear sound. Scale effects can be assessed once published results on a replica model have been made available. Based on a blind prediction competition of this test specimen, analysis methods require further development to gain sufficient confidence in the reliable prediction of response quantities across platforms.

@Seismicisolation

## REFERENCES

- Abolhassan A., Bertero V.V., Bolt B.A., Mahin S.A., Moehle J.P., Seed, R.B. (1989). Preliminary report on the seismological and engineering aspects of the October 17, 1989 Santa Cruz (Loma Prieta) Earthquake, *Report No. UCB/EERC-89/14*, Earthquake Engineering Research Center, University of California, Berkeley, CA.
- ACI 318 (2008). *Building Code Requirements for Structural Concrete and Commentary*, American Concrete Institute, Farmington Hills, MI.
- ASTM (2009a). *Standard Specification for Deformed and Plain Carbon-Steel Bars for Concrete Reinforcement, ASTM A615*, American Society for Testing and Materials International, West Conshohocken, PA.
- ASTM (2009b). *Standard Specification for Low-Alloy Steel Deformed and Plain Bars for Concrete Reinforcement, ASTM A706*, American Society for Testing and Materials International, West Conshohocken, PA.
- Caltrans, (2004). *Bridge Design Specifications*, California Department of Transportation, Sacramento, CA.
- Caltrans (2006a). *Seismic Design Criteria*, California Department of Transportation, Sacramento, CA.
- Caltrans (2006b). *Standard Specifications*, California Department of Transportation, Sacramento, CA.
- Caltrans (2010b). *Caltrans ARS Online*, [http://dap3.dot.ca.gov/shake\\_stable/](http://dap3.dot.ca.gov/shake_stable/).
- Carr A.J. (2002). *Ruaumoko, Volume 2: User Manual for the 2-Dimensional Version, Ruaumoko2D*, Department of Civil Engineering, University of Canterbury, Christchurch, New Zealand.
- Carrea F. (2010). *Shake-Table Test on a Full-Scale Bridge Reinforced Concrete Column*, Tesi di Laurea, Dipartimento di Ingegneria Civile, Ambientale e dei Materiali, Università Bologna, Bologna, Italy.
- Douglas B.M., Buckle, I.G. (1985). Field response studies of two highway bridges subjected to simulated earthquake loads, *Proceedings, Second Joint U.S. – Japan Workshop on Performance and Strengthening of Bridge Structures and the Research Needs*, San Francisco, CA.
- Eberhard M.O., MacLardy J.A., Marsh M.L., Hjartarson, G. (1993). Lateral-load response of a reinforced concrete bridge, Washington State Transportation Center (TRAC), University of Washington, Seattle, WA.
- Gamble W.L., Hawkins N.M., Kaspar, I.I. (1995). Seismic retrofitting of bridge pier columns, *Proceedings, National Seismic Conference on Bridges and Highways, "Progress in Research and Practice,"* Federal Highway Administration, San Diego, CA.
- Gilani A.S., Mahin S.A., Fenves G.L., Aiken I.D., Chavez J.W. (1995). Field testing of bridge design and retrofit concepts, *Report No. UCB/EERC-95/14*, Earthquake Engineering Research Center, University of California, Berkeley, CA.
- Hachem M.M., Mahin S.A., Moehle J.P. (2003). Performance of circular reinforced concrete bridge columns under bidirectional earthquake loading, *PEER Report No. 2003/06*, Pacific Earthquake Engineering Research Center, University of California, Berkeley, CA.
- Housner G.W. et al. (1994). *The Continuing Challenge – The Northridge Earthquake of January 17, 1994*, (Report to Director, California Department of Transportation), Sacramento, CA.
- JRA (2002). *Specifications for Highway Bridges, Part V, Seismic Design*, Japan Road Association. Japan Road Association, Tokyo.
- Kawashima K. (1995). Impact of the Hanshin/Awaji, Japan, earthquake on seismic design and seismic strengthening of highway bridges, *Proceedings, National Seismic Conference on Bridges and Highways, "Progress in Research and Practice,"* Federal Highway Administration, San Diego, CA.
- Kawashima K. et al. (2009). Shake table experiment on RC bridge columns using E-Defense, *Proceedings, 41<sup>st</sup> Panel on Wind and Seismic Effects*, UJNR, Public Works Research Institute, Tsukuba Science City, Japan.
- Lehman D.E., Moehle J.P. (1998). Seismic performance of well-confined concrete bridge columns. *PEER Report No. 1998/01*, Pacific Earthquake Engineering Research Center, University of California, Berkeley, CA.

- Marquez T.M. (2010). *Seismic Design Methodology*, California Department of Transportation, Memo to designers, No. 20-1, pp. 1–15, Sacramento, CA.
- Mellon S. (1988). *Highway Bridge Damage, Whittier Earthquake, October 1, 1987*, California Department of Transportation, Seismic Report / Post earthquake investigation team, Sacramento, CA.
- NEES (2011). *NEES Project Warehouse – Large-Scale Validation of Seismic Performance of Bridge Columns*, <https://nees.org/warehouse/project/987/>, (December 2011).
- Ohtaki T., Benzoni G., Priestley M.J.N. (1996). Seismic performance of a full scale bridge column – As built and as repaired, *SSRP Report 96/07*, Department of Structural Engineering, University of California, San Diego, La Jolla, CA.
- PEER (2007). *PEER Strong Motion Database: Introduction*, Pacific Earthquake Engineering Research Center, University of California, Berkeley, CA, <http://peer.berkeley.edu/smcat/>, (July, 2010).
- Penzien J., Clough R.W. (1971). *Observations on the damages of highway bridge structures, San Fernando, California, earthquake February 9th, 1971*, Report to the Division Structural Engineers, Federal Highway Administration, Sacramento, CA.
- Priestley M.J., Seible F., Calvi G.M. (1996). *Seismic Design and Retrofit of Bridges*, New York, NY: John Wiley.
- Priestley M.J.N., Seible F., Chai Y.H., Wong R. (1992). Santa Monica viaduct retrofit – Full-scale test on column lap splice with #11 [35 mm] reinforcement, *SSRP Report 92/08*, Department of Applied Mechanics and Engineering Sciences, University of California, San Diego, La Jolla, CA.
- Sasaki T., Kawashima K. (2009). Scale effect on the shear strength of reinforced concrete columns with termination of main reinforcements, *Proceedings, 3rd International Conference on Advances in Experimental Structural Engineering*, Paper 2009-10, San Francisco, CA.
- Shen J.J., Yen W.H., O'Fallon J. (2006). FHWA recommendations for seismic performance testing of bridge piers, *Proceedings, 4th International Workshop on Seismic Design and Retrofit of Transportation Facilities*, San Francisco, CA.
- Stone W.C., Cheok G.S. (1989). Inelastic behavior of full-scale bridge columns subjected to cyclic loading, *Report No. NIST/BSS-166*, National Institute of Standards and Technology, U.S. Department of Commerce, Gaithersburg, MD.
- Terzic V., Schoettler M.J., Restrepo J.I., Mahin S.A. (2015). Concrete column blind prediction contest 2010: Outcomes and observations, *PEER Report No. 2015/01*, Pacific Earthquake Engineering Research Center, University of California, Berkeley, CA.
- Unjoh S., Nakatani S., Tamura K., Fukui J., Hoshikuma J. (2002). 2002 seismic design specifications for highway bridges, *Special Publication 987*, pp. 231–240, National Institute of Standards and Technology, Gaithersburg, MD.
- Van Den Einde L., Restrepo J.I., Conte J.P., Luco J.E., Seible F., Filiatrault A., Clark A., Johnson A., Gram M., Kusner D., Thoen B. (2004). "Development of the George E. Brown, Jr. Network for Earthquake Engineering Simulation (NEES) large high-performance outdoor shake table at the University of California, San Diego, *Proceedings, 13th World Conf. on Earthquake Engineering*, Paper No. 3281, Vancouver, B.C., Canada.

## Appendix A Instrumentation Layout

Instrumentation plans included in this appendix identify the Cartesian coordinates of each sensor deployed. The origin of the coordinate system was taken as the centroid of the column at the column-to-footing interface. From the origin, positive is taken as East, North, and up. Other sensor metadata include the channel name, data acquisition system, gauge length if applicable, and sensor orientation. The data acquisition system corresponds to the node to which the sensor was wired. There were six nodes that recorded data, numbered 1, 2, 4, 5, 7, and 8. Electronic versions of these drawings are available in the project's archive at NEEShub [NEES 2011]. Sensor coordinates are also available there in tabulated format in the sensor plans.

Figures A.1 through A.4 contain locations for longitudinal and transverse strain gauges. Figures A.5 through A.10 contain locations of the various LVDT configurations. Figures A.11 through A.12 primarily contain locations for string potentiometers. Figures A.13 through A.16 contain accelerometer locations on the shake table, footing, column, and mass block. Figure A.17 contains locations of sensors on the inclined safety columns and the bond slip LVDTs at the column-to-footing interface.

 @Seismicisolation

TEST DATES: 9/20/2010 – 9/21/2010

## A.1 STRAIN GAUGE LOCATIONS

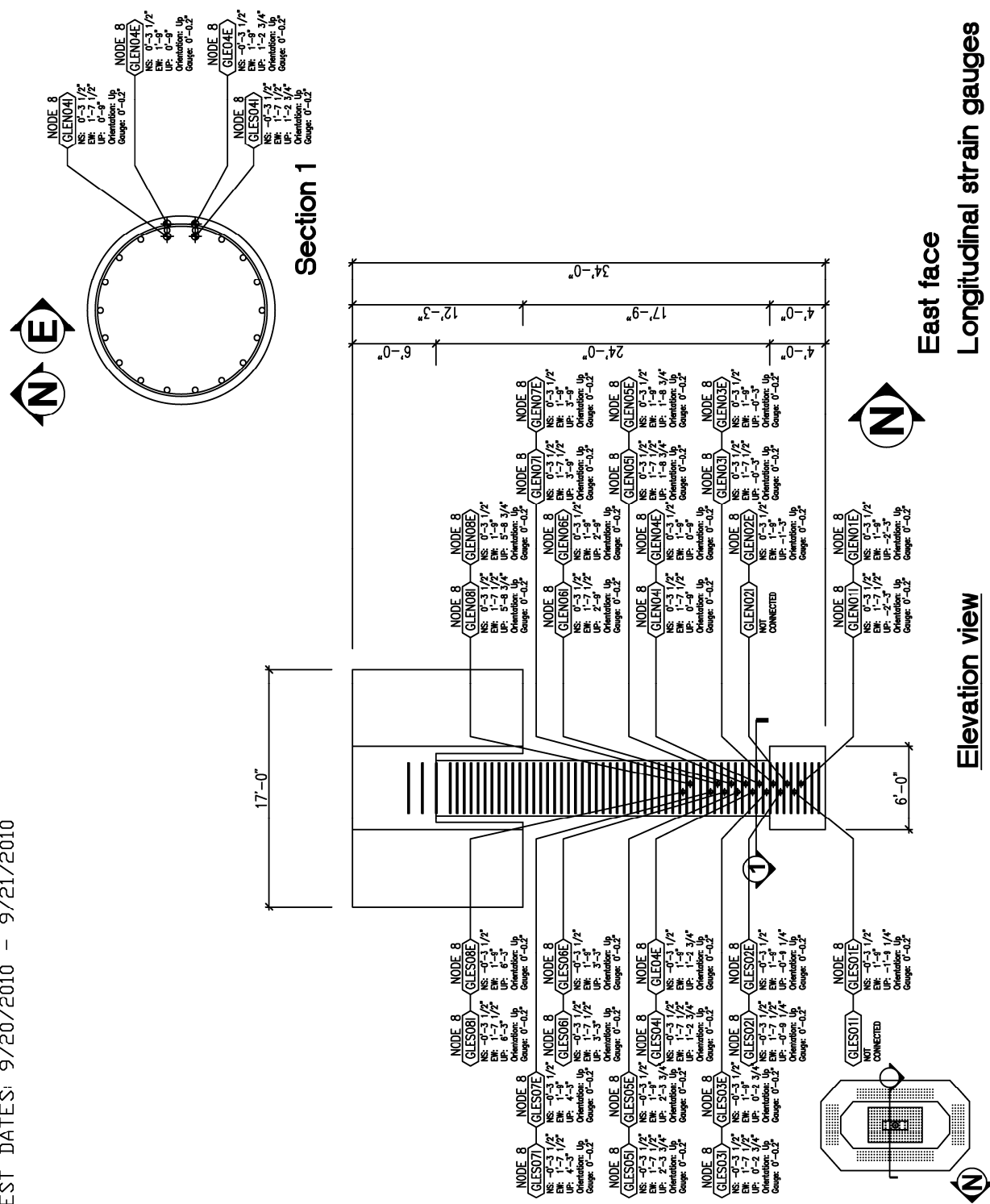
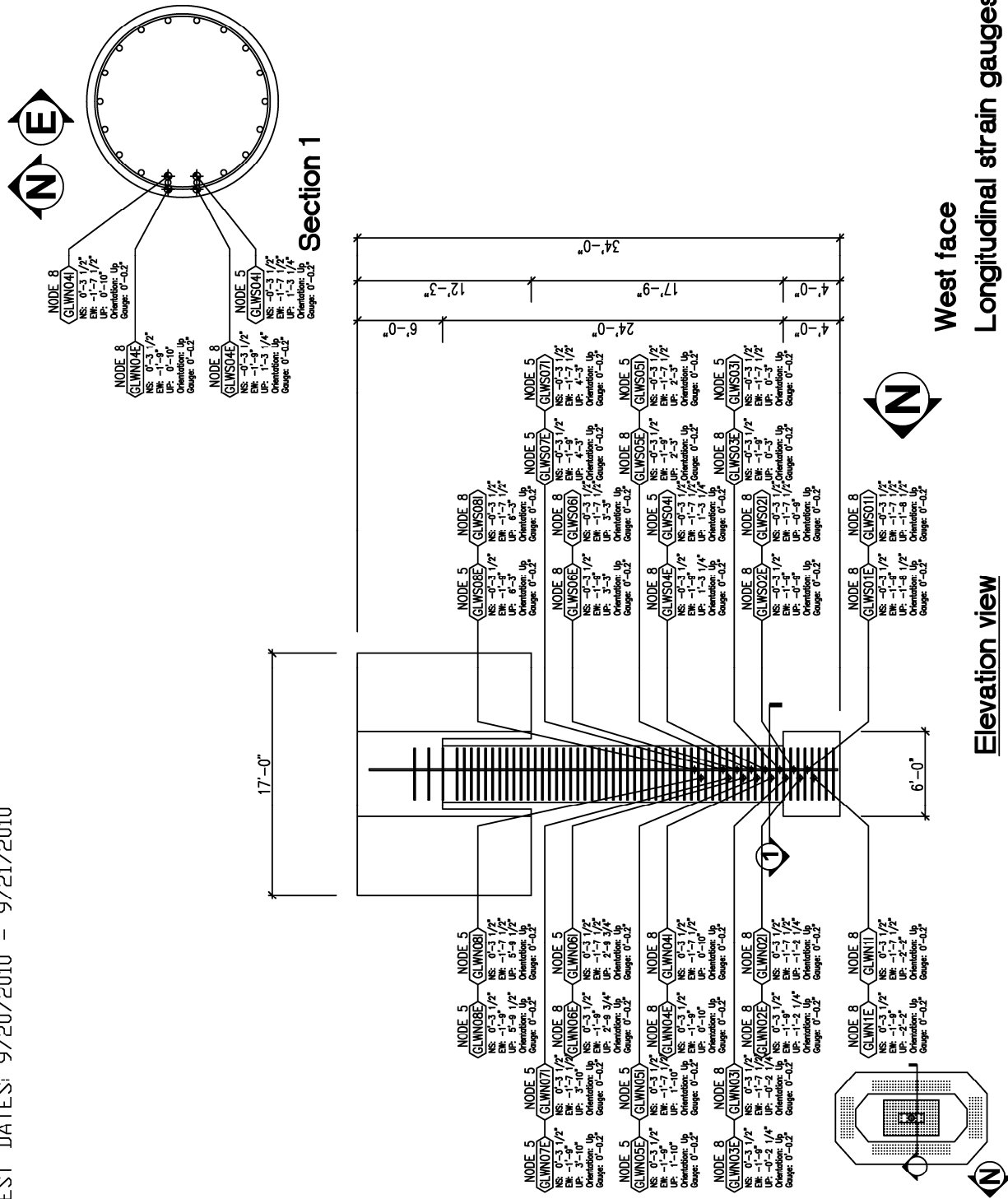


Figure A.1 Longitudinal strain gauge locations on the East face of the column.

TEST DATES: 9/20/2010 - 9/21/2010



**Figure A.2** Longitudinal strain gauge locations on the West face of the column.

TEST DATES: 9/20/2010 - 9/21/2010

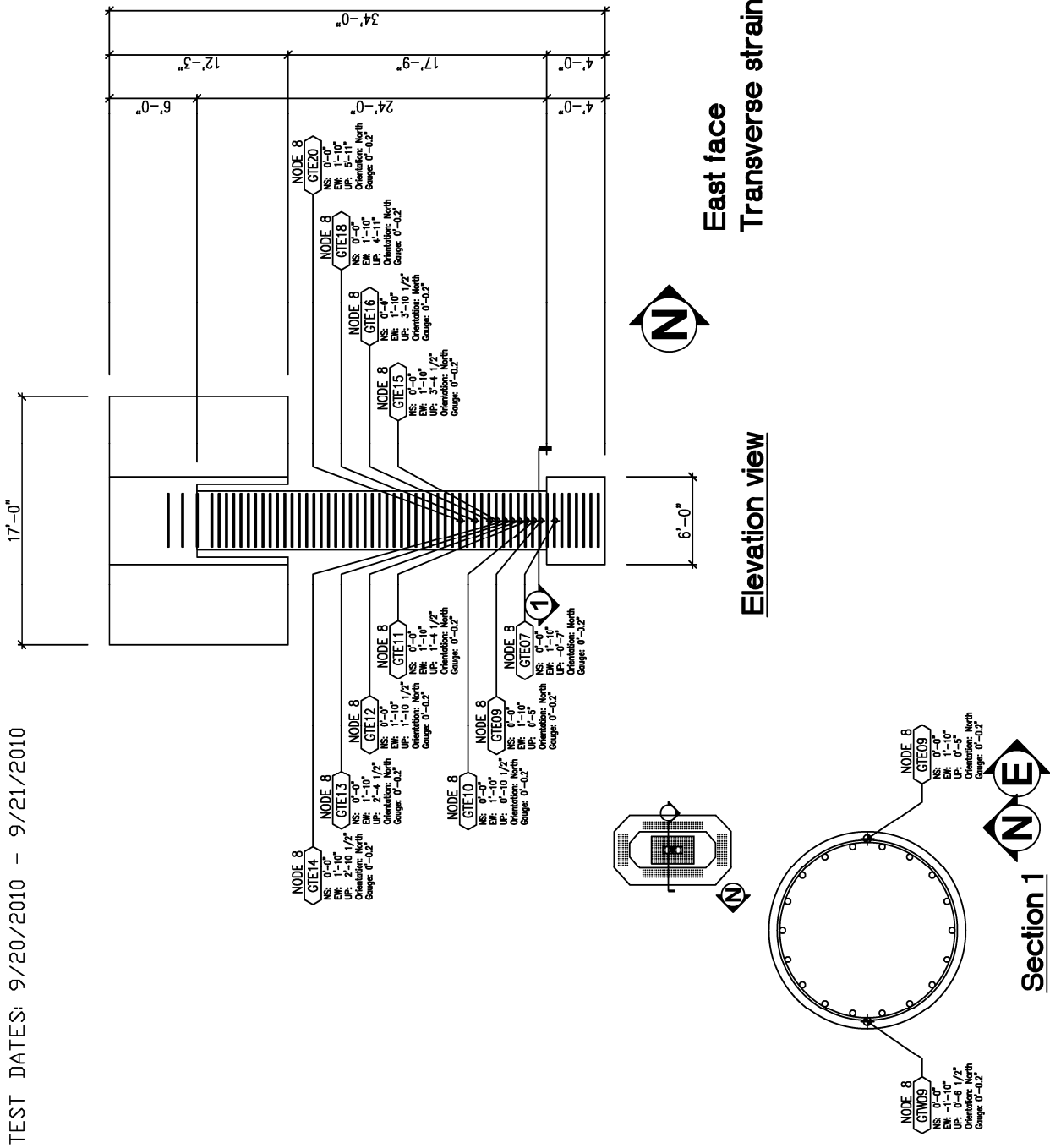
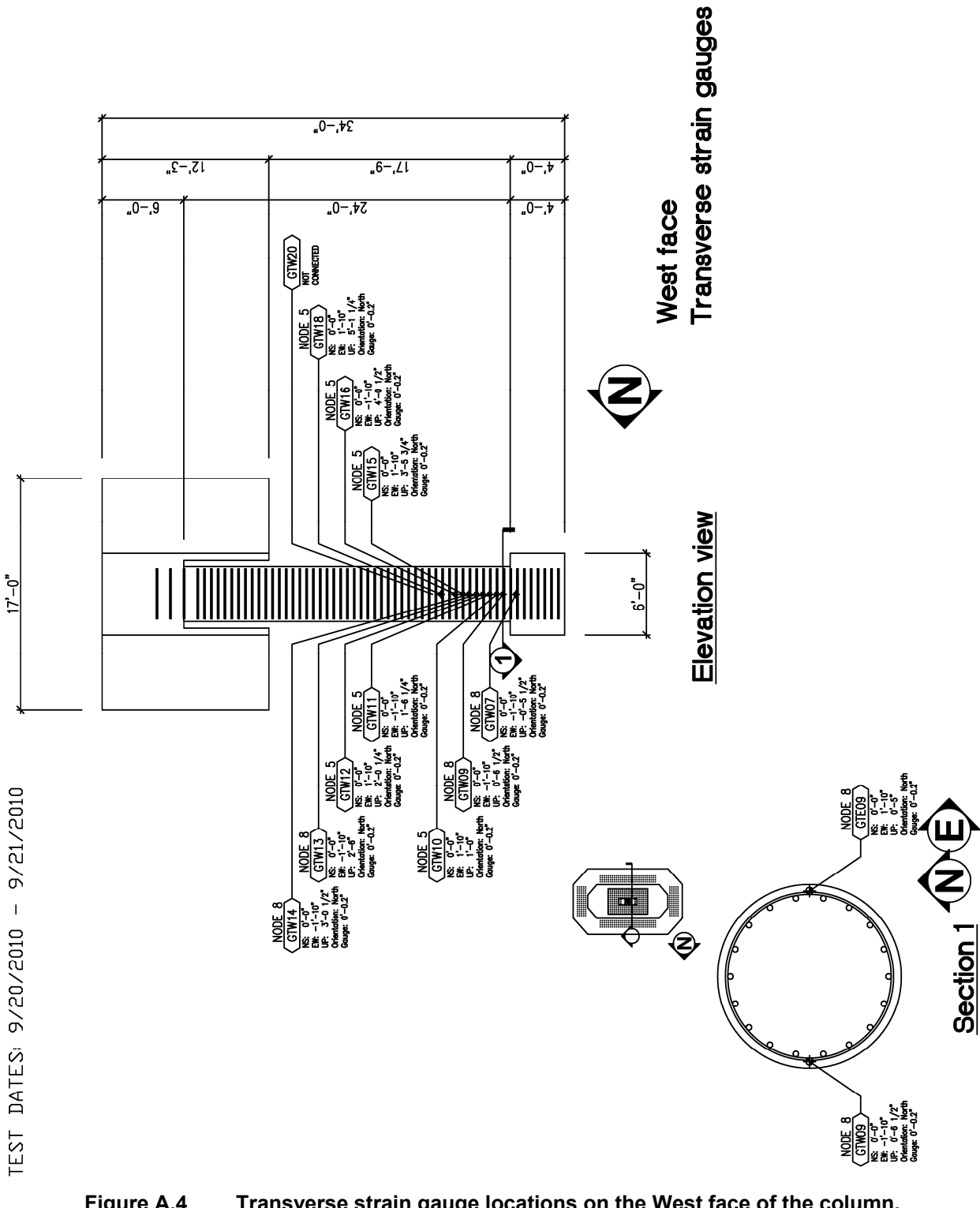


Figure A.3 Transverse strain gauge locations on the East face of the column.

TEST DATES: 9/20/2010 - 9/21/2010



**Figure A.4** Transverse strain gauge locations on the West face of the column.

## A.2 LINEAR VOLTAGE DISPLACEMENT TRANSDUCERS

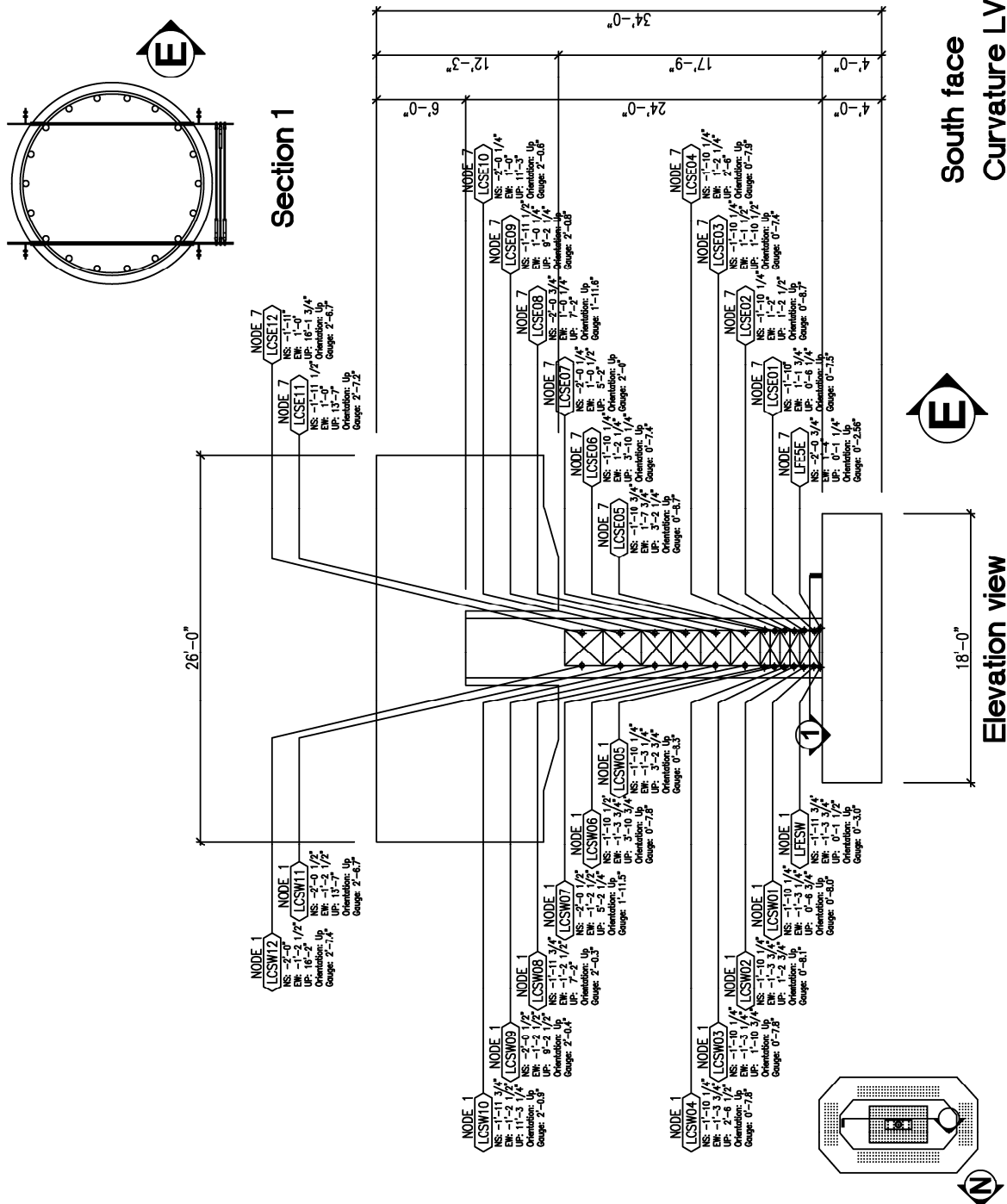


**Figure A.5 Curvature and fixed-end rotation LVDT locations on the South face of the column.**

TEST DATES: 9/20/2010 – 9/21/2010

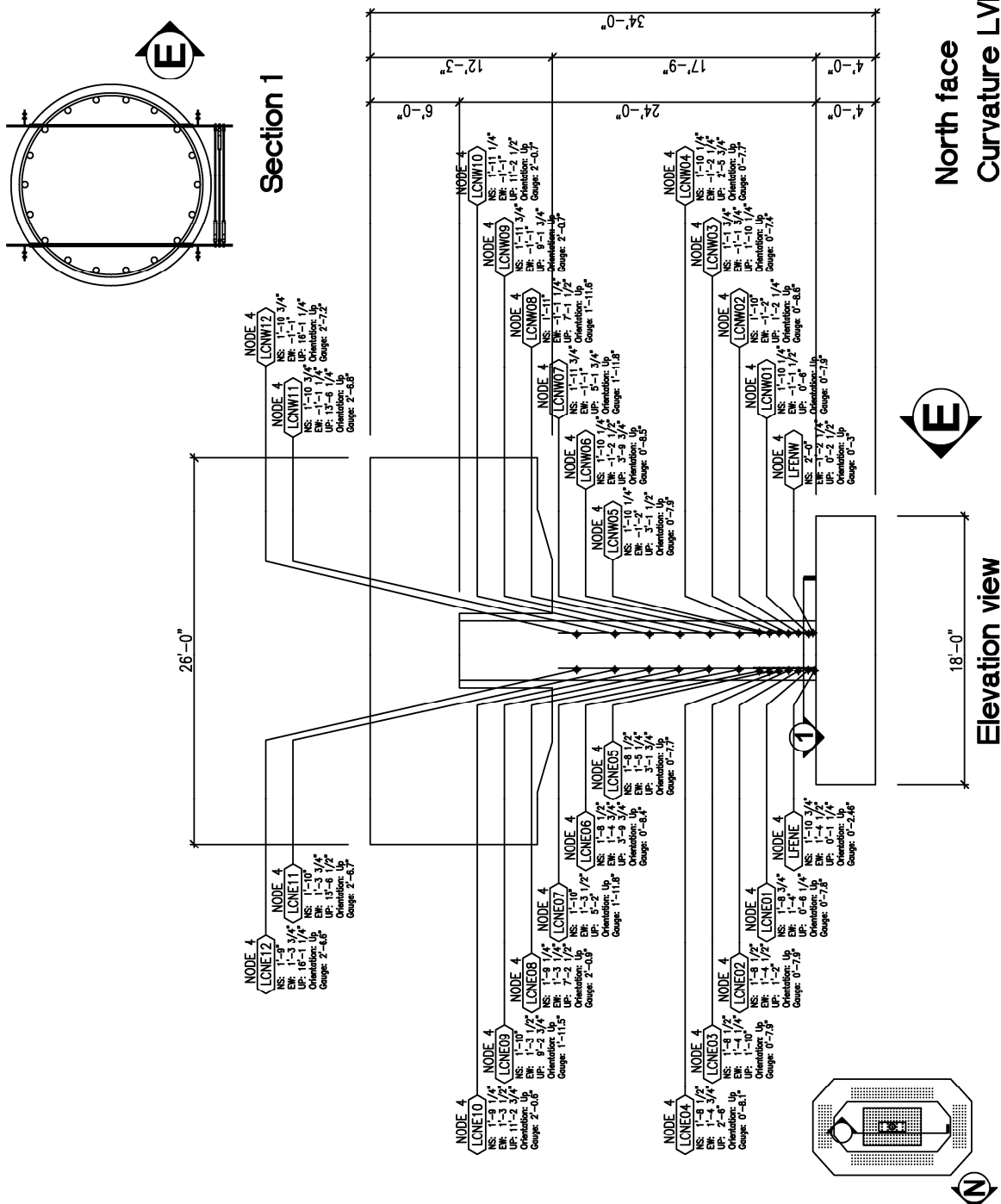


**Figure A.6** Curvature and fixed-end rotation LVDT locations on the North face of the column.

TEST DATES: 9/20/2010 – 9/21/2010

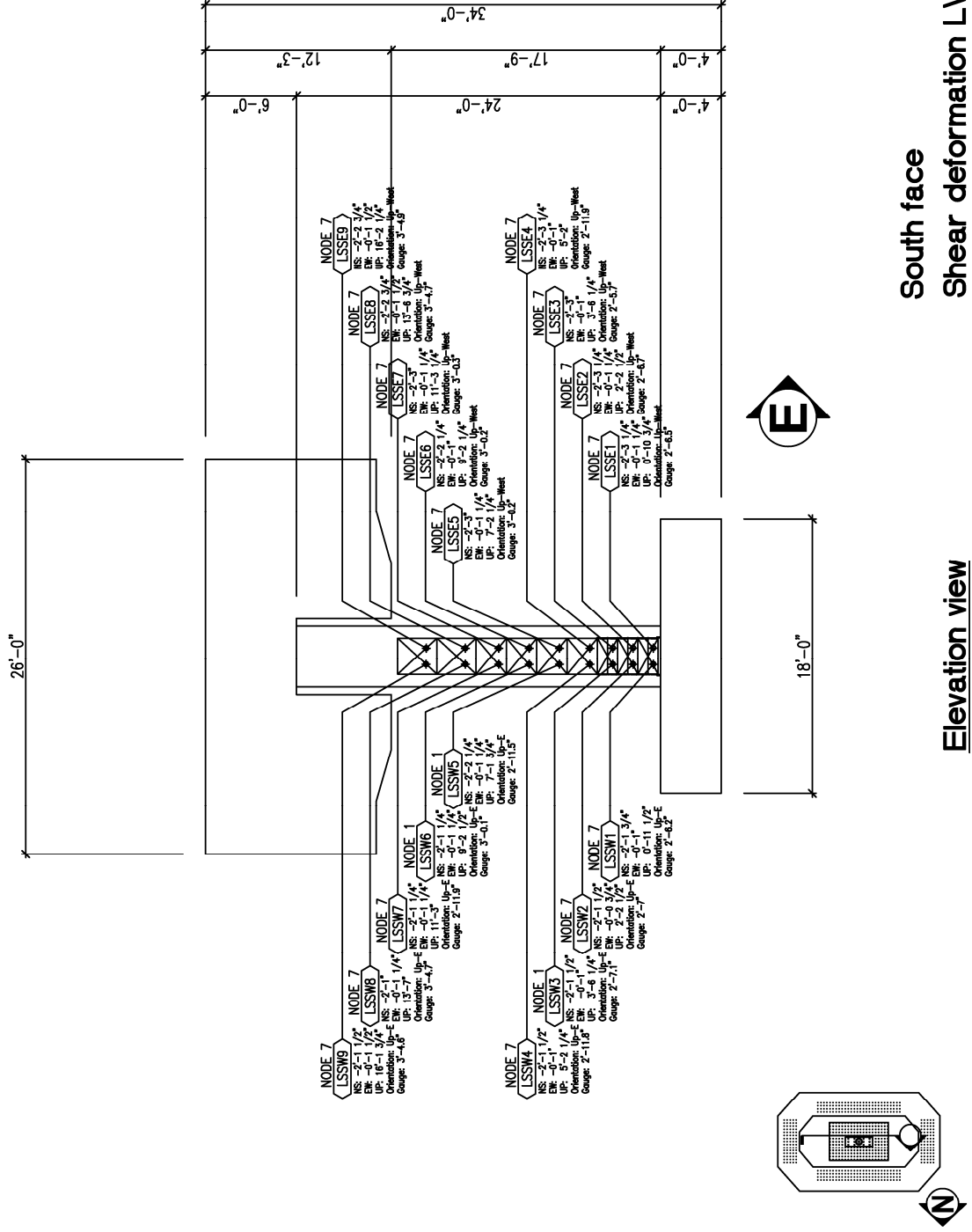


**Figure A.7 Inclined shear LVDT locations on the South face of the column.**

TEST DATES: 9/20/2010 – 9/21/2010

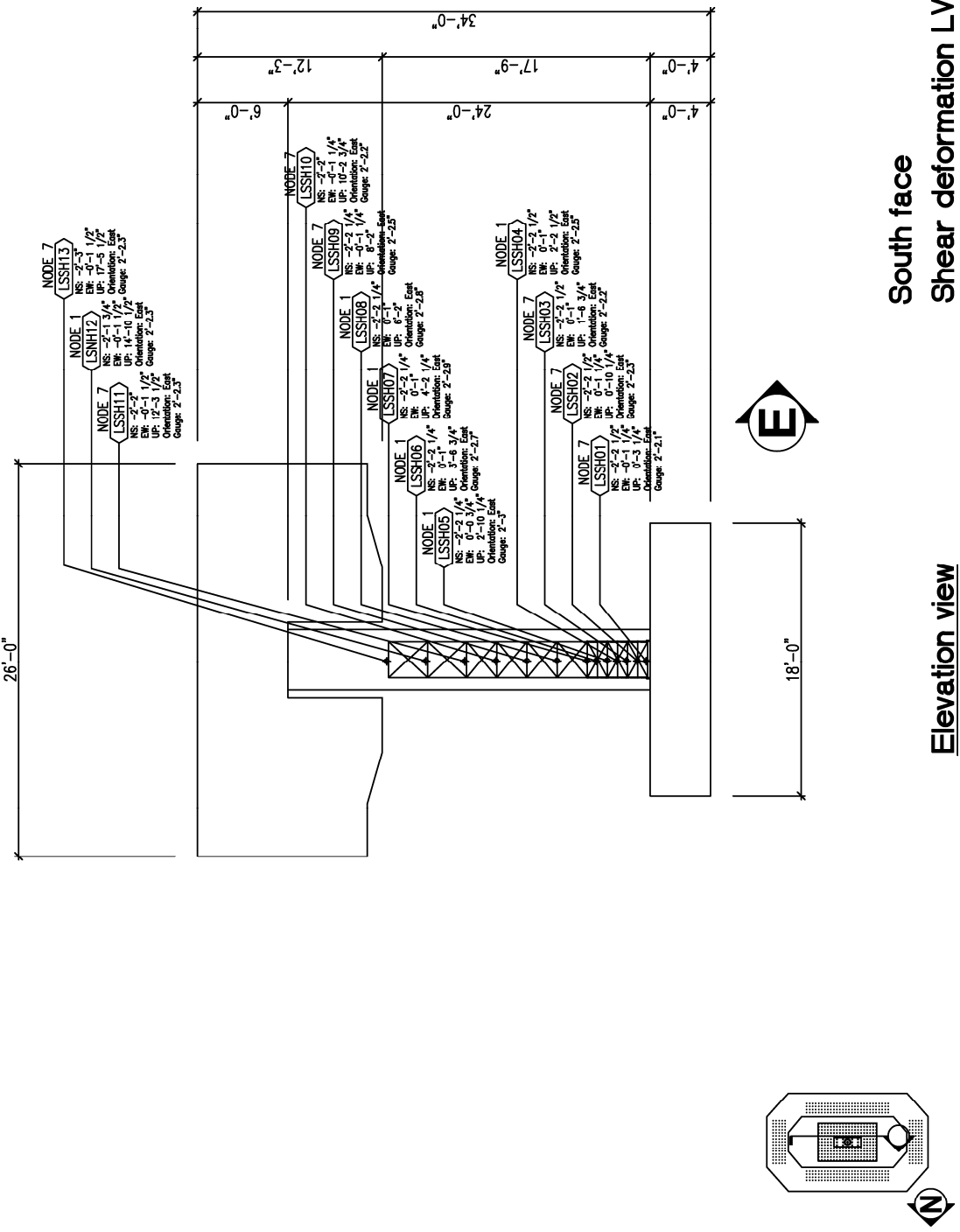
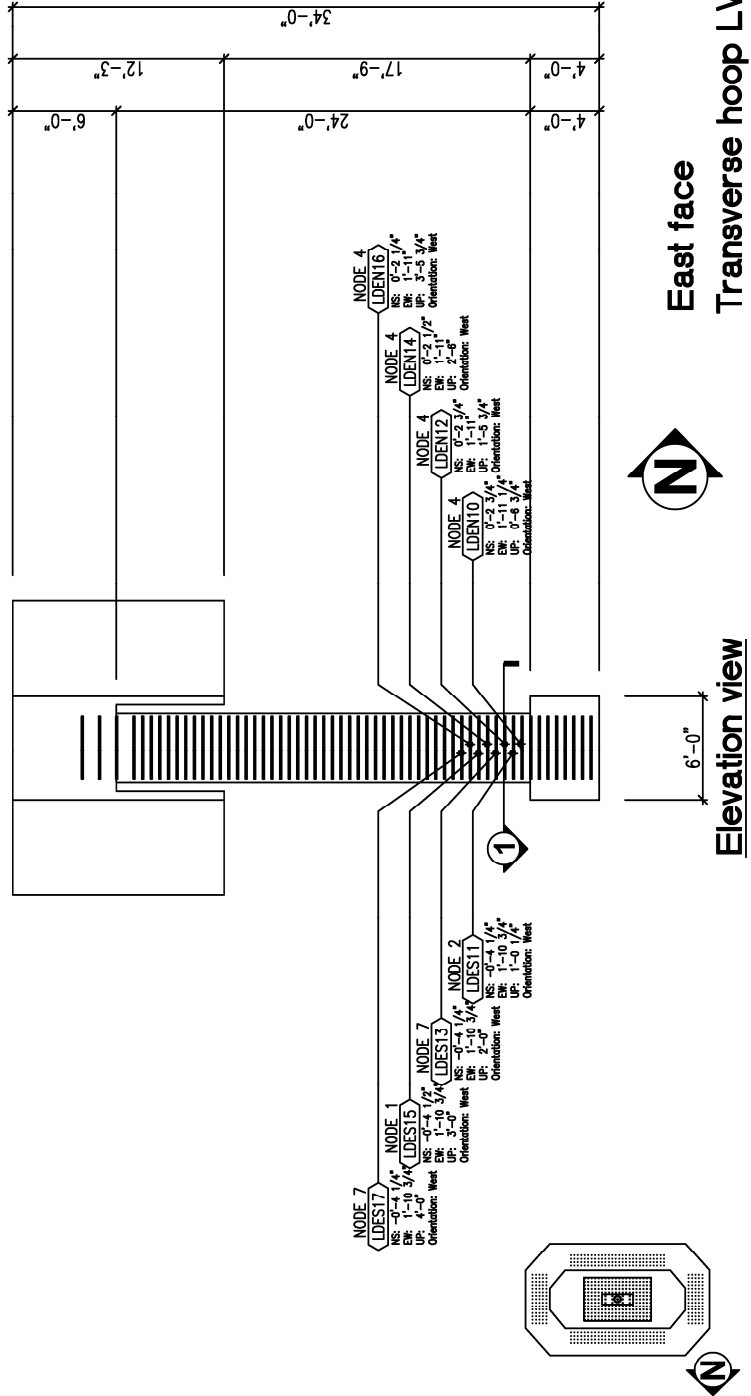


Figure A.8 Horizontal shear LVDT locations on the South face of the column.

TEST DATES: 9/20/2010 - 9/21/2010

17'-0"



### East face Transverse hoop LVDTs

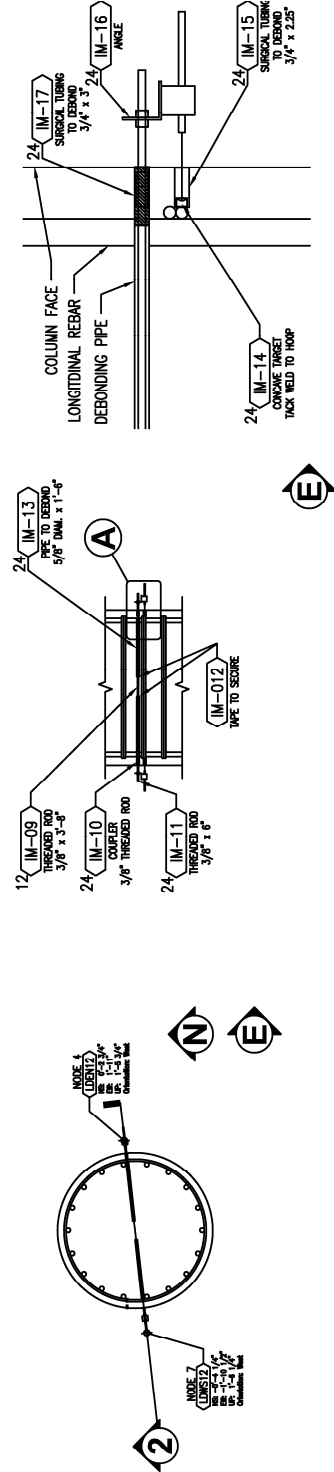
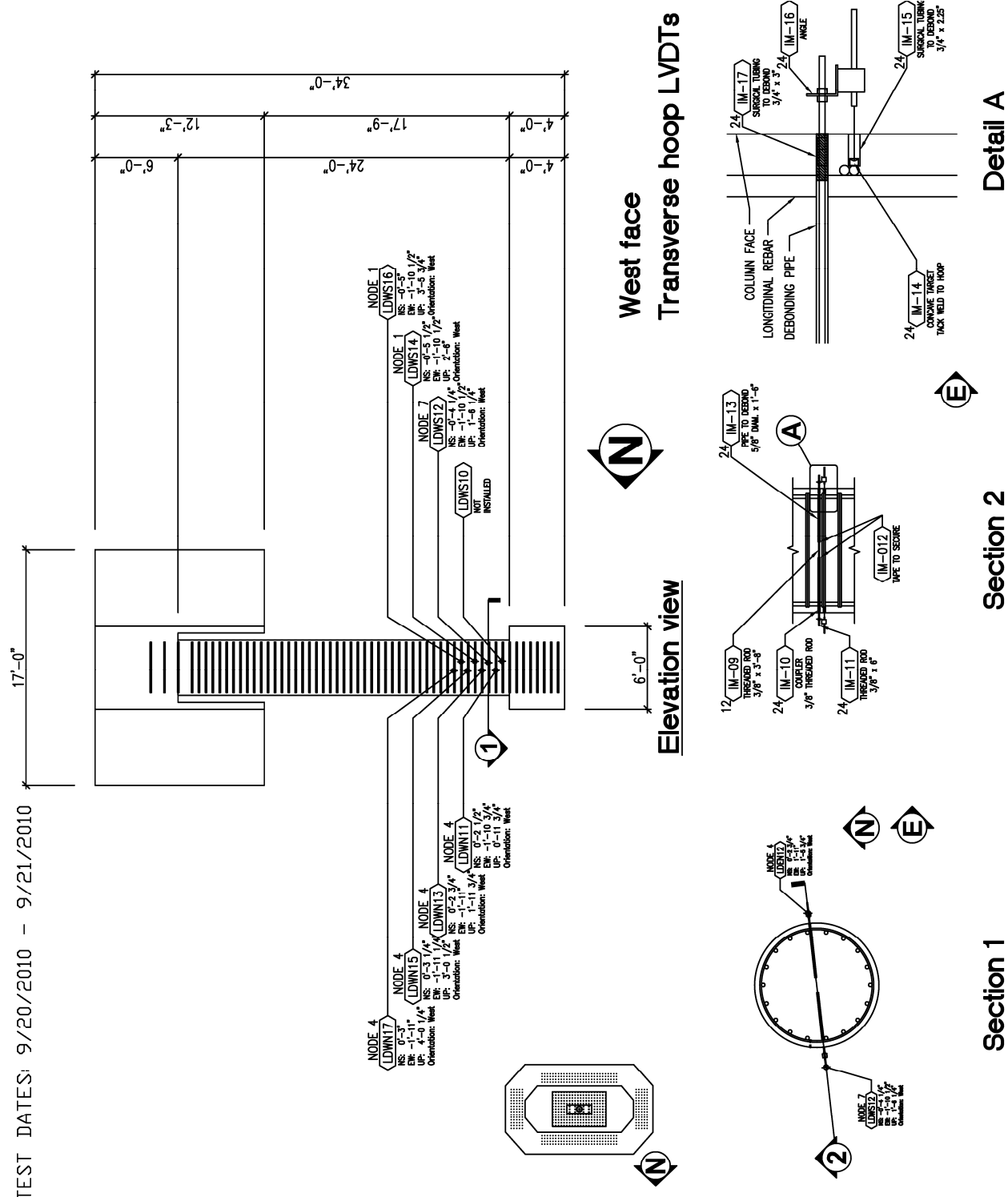


Figure A.9 Transverse hoop LVDT locations on the East face of the column.

TEST DATES: 9/20/2010 - 9/21/2010



**Figure A.10** Transverse hoop LVDT locations on the West face of the column.

TEST DATES: 9/20/2010 – 9/21/2010

### A.3 SPRING POTENTIOMETERS

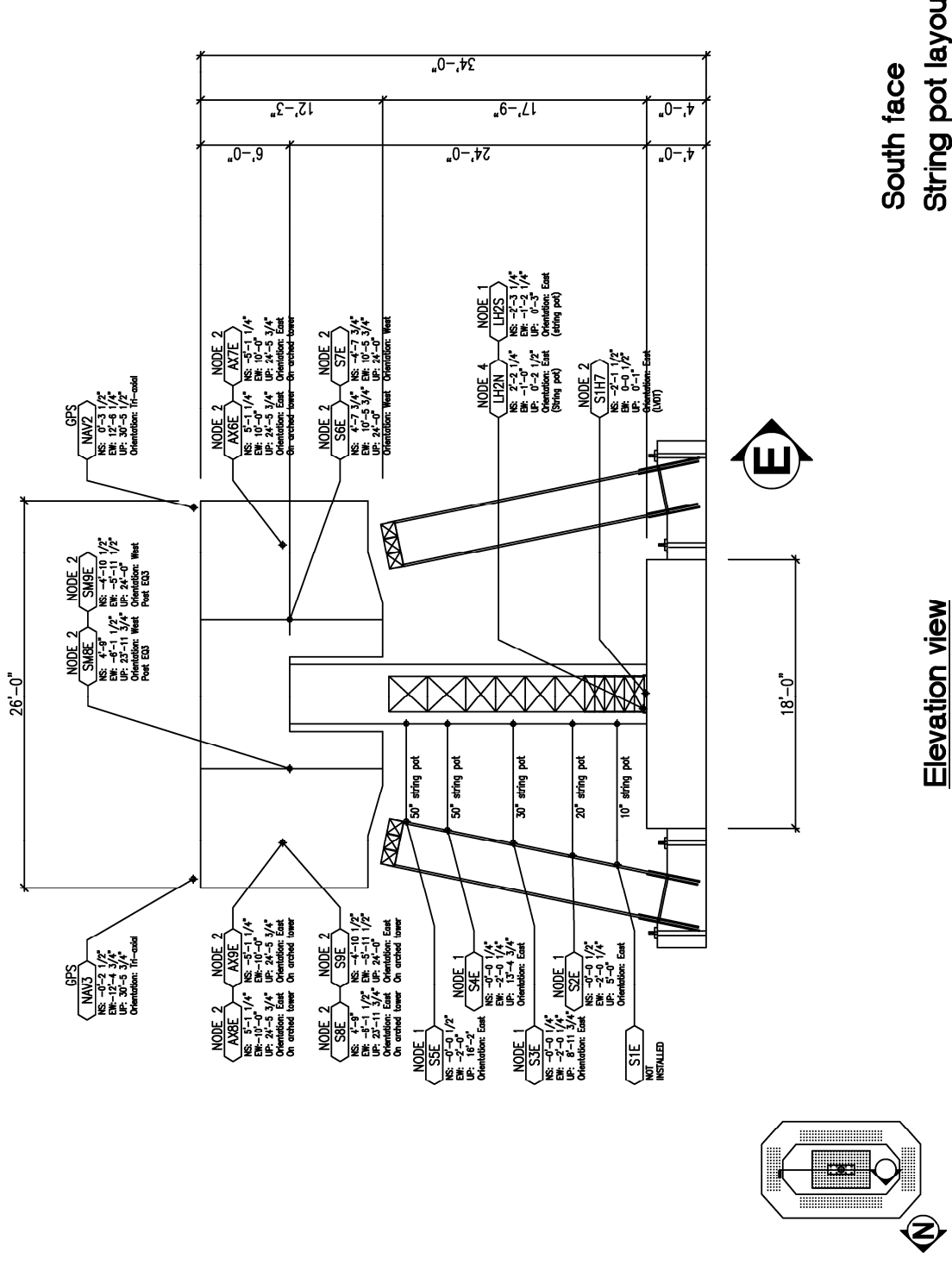


Figure A.11 Horizontal spring potentiometer and GPS antennae locations.

TEST DATES: 9/20/2010 - 9/21/2010

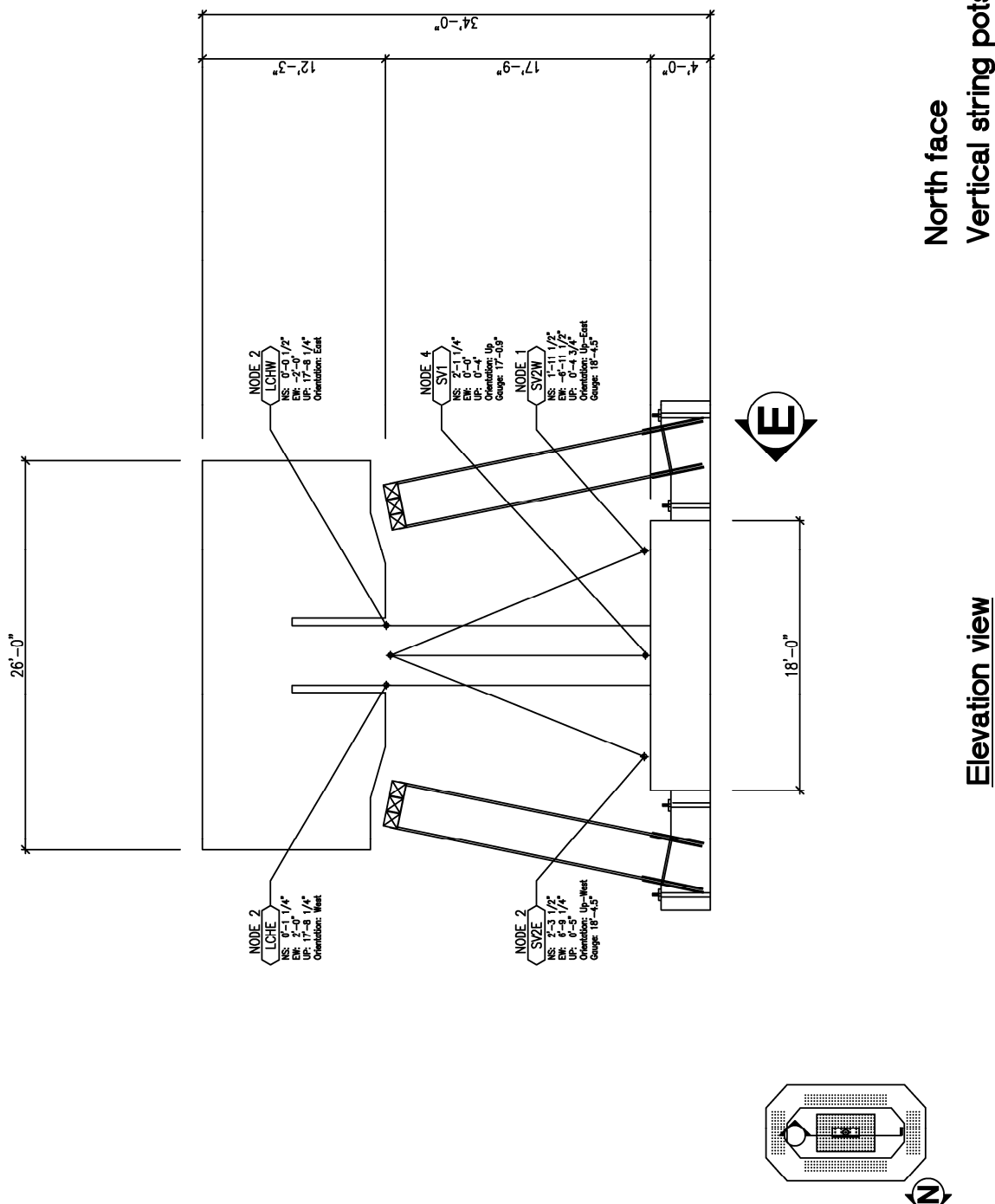
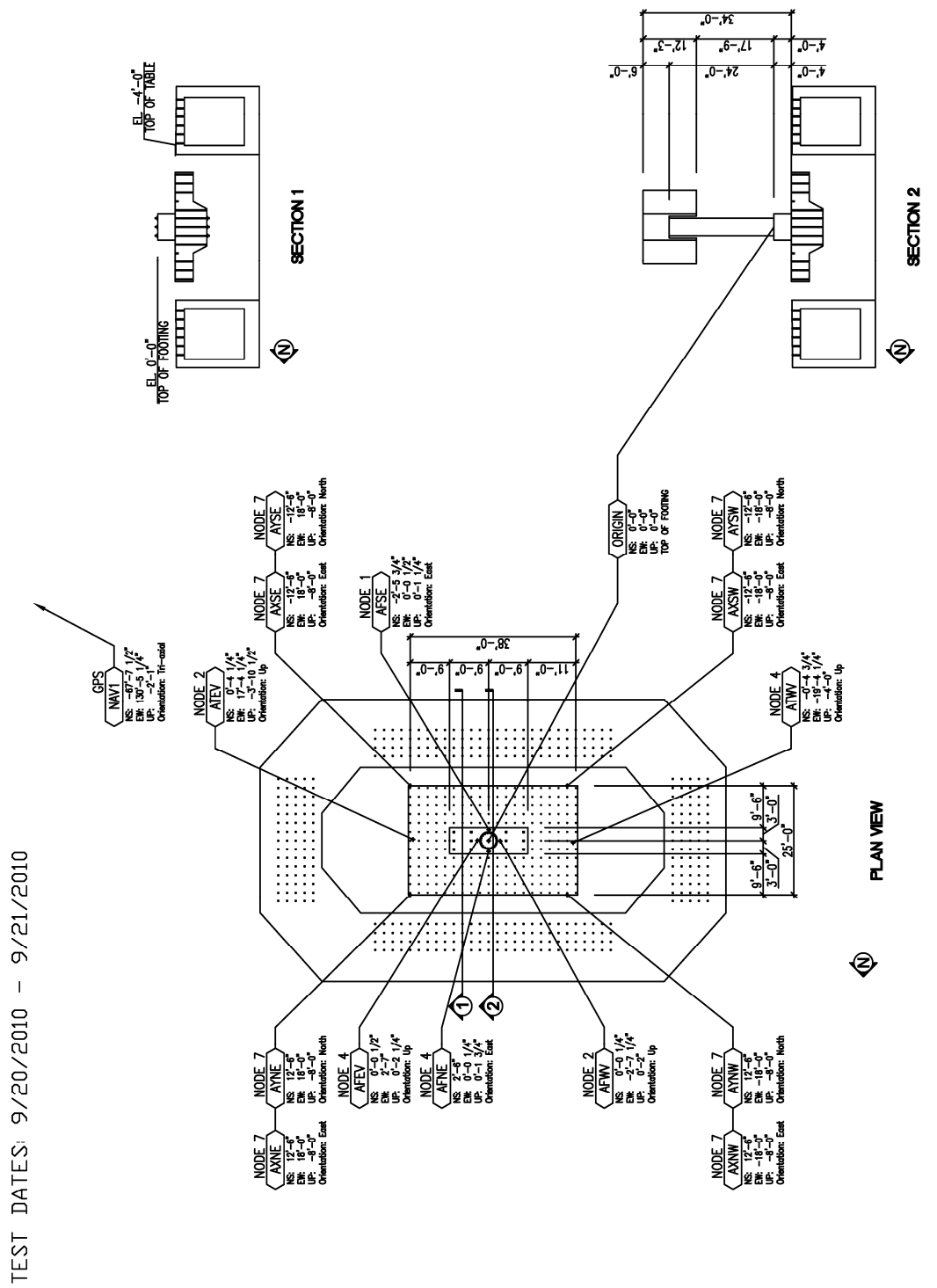


Figure A.12 Inclined spring potentiometer and column-to-top mass LVDT locations.

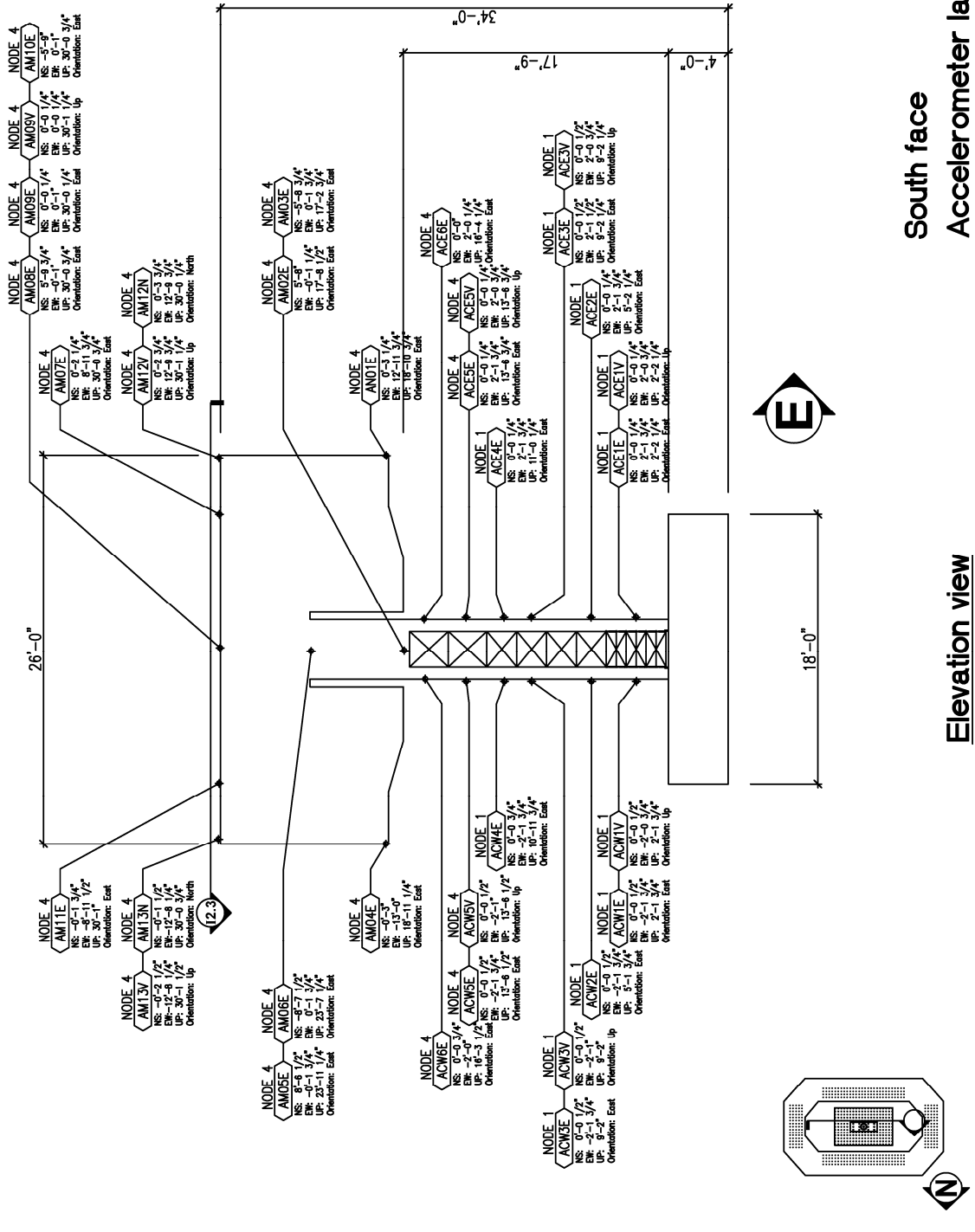
## A.4 ACCELEROMETERS



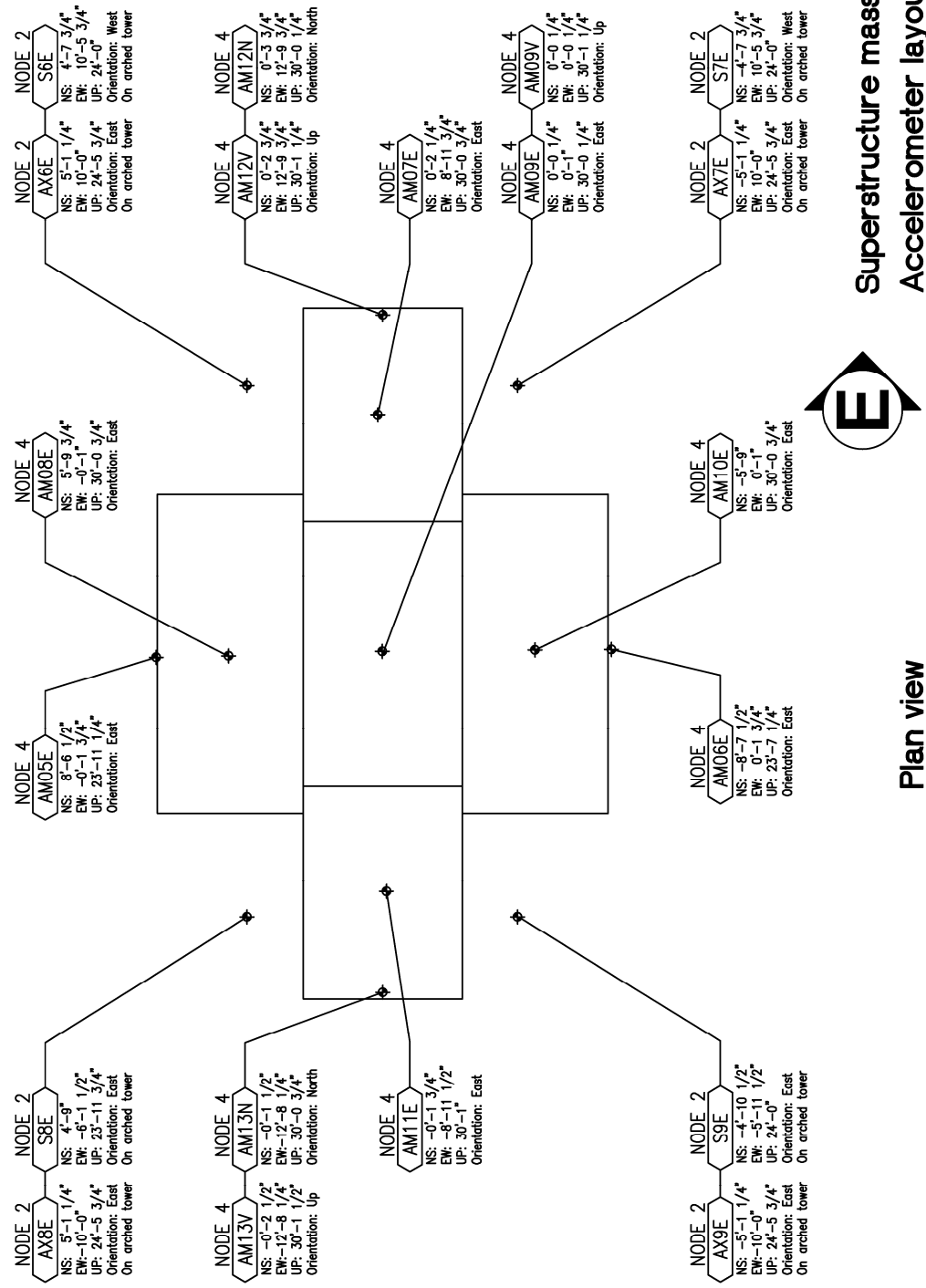
**FOUNDATION AND TABLE**

Figure A.13 Footing and table accelerometer locations and reference GPS antenna.

TEST DATES: 9/20/2010 – 9/21/2010



TEST DATE: 9/20/2010



**Figure A.15** Mass block accelerometer and wire pot locations for tests on 9/20/2010.

TEST DATE: 9/21/2010

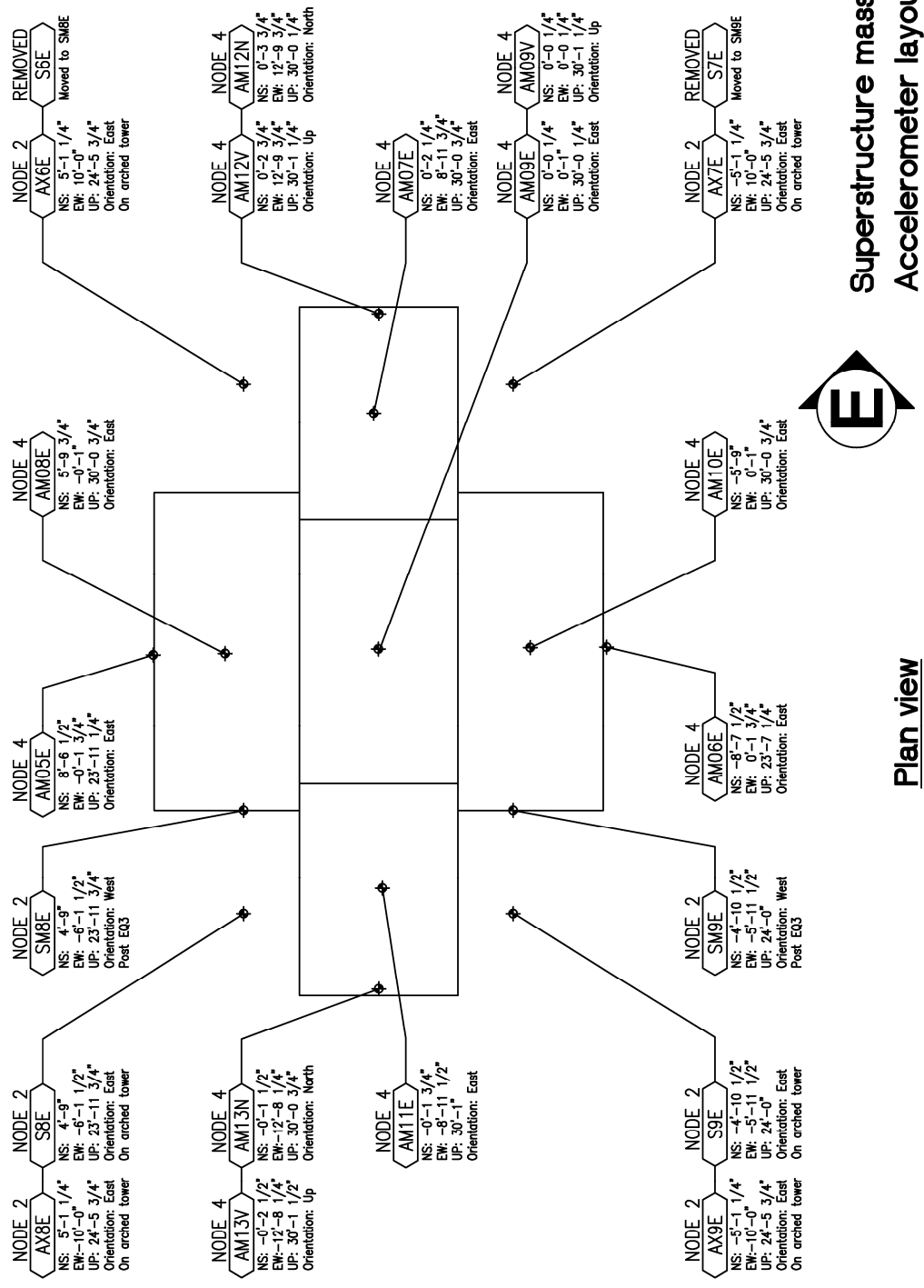


Figure A.16 Mass block accelerometer and wire pot locations for tests on 9/21/2010.

Superstructure mass  
Accelerometer layout

Plan view



TEST DATES: 9/20/2010 – 9/21/2010

## A.5 INCLINED SAFETY COLUMN INSTRUMENTATION AND BOND-SLIP LVDTS

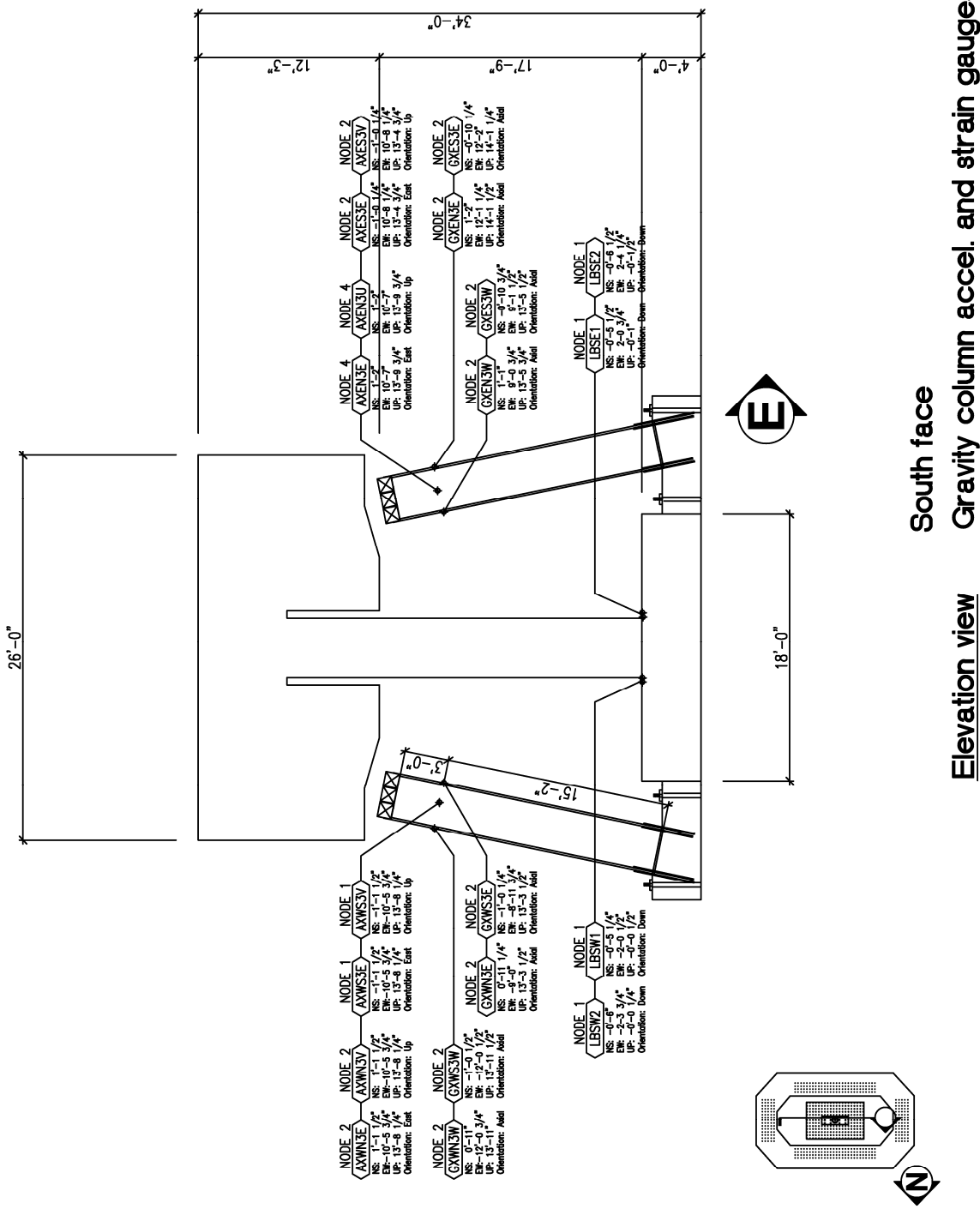


Figure A.17 Bond-slip LVDT locations and instrumentation locations on the inclined safety restraints.

 @Seismicisolation

## PEER REPORTS

PEER reports are available as a free PDF download from [http://peer.berkeley.edu/publications/peer\\_reports\\_complete.html](http://peer.berkeley.edu/publications/peer_reports_complete.html). Printed hard copies of PEER reports can be ordered directly from our printer by following the instructions at [http://peer.berkeley.edu/publications/peer\\_reports.html](http://peer.berkeley.edu/publications/peer_reports.html). For other related questions about the PEER Report Series, contact the Pacific Earthquake Engineering Research Center, 325 Davis Hall mail code 1792, Berkeley, CA 94720. Tel.: (510) 642-3437; Fax: (510) 665-1655; Email: [peer\\_editor@berkeley.edu](mailto:peer_editor@berkeley.edu)

- PEER 2015/02** *A Full-Scale, Single-Column Bridge Bent Tested by Shake-Table Excitation.* Matthew J. Schoettler, José I. Restrepo, Gabrielle Guerrini, David E. Duck, and Francesco Carrea. March 2015.
- PEER 2015/01** *Concrete Column Blind Prediction Contest 2010: Outcomes and Observations.* Vesna Terzic, Matthew J. Schoettler, José I. Restrepo, and Stephen A Mahin. March 2015.
- PEER 2014/20** *Stochastic Modeling and Simulation of Near-Fault Ground Motions for Performance-Based Earthquake Engineering.* Mayssa Dabaghi and Armen Der Kiureghian. December 2014.
- PEER 2014/19** *Seismic Response of a Hybrid Fiber-Reinforced Concrete Bridge Column Detailed for Accelerated Bridge Construction.* Wilson Nguyen, William Trono, Marios Panagiotou, and Claudia P. Ostertag. December 2014.
- PEER 2014/18** *Three-Dimensional Beam-Truss Model for Reinforced Concrete Walls and Slabs Subjected to Cyclic Static or Dynamic Loading.* Yuan Lu, Marios Panagiotou, and Ioannis Koutromanos. December 2014.
- PEER 2014/17** *PEER NGA-East Database.* Christine A. Goulet, Tadahiro Kishida, Timothy D. Ancheta, Chris H. Cramer, Robert B. Darragh, Walter J. Silva, Youssef M.A. Hashash, Joseph Harmon, Jonathan P. Stewart, Katie E. Wooddell, and Robert R. Youngs. October 2014.
- PEER 2014/16** *Guidelines for Performing Hazard-Consistent One-Dimensional Ground Response Analysis for Ground Motion Prediction.* Jonathan P. Stewart, Kioumars Afshari, and Youssef M.A. Hashash. October 2014.
- PEER 2014/15** *NGA-East Regionalization Report: Comparison of Four Crustal Regions within Central and Eastern North America using Waveform Modeling and 5%-Damped Pseudo-Spectral Acceleration Response.* Jennifer Dreiling, Marius P. Isken, Walter D. Mooney, Martin C. Chapman, and Richard W. Godbee. October 2014.
- PEER 2014/14** *Scaling Relations between Seismic Moment and Rupture Area of Earthquakes in Stable Continental Regions.* Paul Somerville. August 2014.
- PEER 2014/13** *PEER Preliminary Notes and Observations on the August 24, 2014, South Napa Earthquake.* Grace S. Kang (Editor), Stephen A. Mahin (Editors). September 2014.
- PEER 2014/12** *Reference-Rock Site Conditions for Central and Eastern North America: Part II – Attenuation (Kappa) Definition.* Kenneth W. Campbell, Youssef M.A. Hashash, Byungmin Kim, Albert R. Kottke, Ellen M. Rathje, Walter J. Silva, and Jonathan P. Stewart. August 2014.
- PEER 2014/11** *Reference-Rock Site Conditions for Central and Eastern North America: Part I - Velocity Definition.* Youssef M.A. Hashash, Albert R. Kottke, Jonathan P. Stewart, Kenneth W. Campbell, Byungmin Kim, Ellen M. Rathje, Walter J. Silva, Sissy Nikolaou, and Cheryl Moss. August 2014.
- PEER 2014/10** *Evaluation of Collapse and Non-Collapse of Parallel Bridges Affected by Liquefaction and Lateral Spreading.* Benjamin Turner, Scott J. Brandenberg, and Jonathan P. Stewart. August 2014.
- PEER 2014/09** *PEER Arizona Strong-Motion Database and GMPEs Evaluation.* Tadahiro Kishida, Robert E. Kayen, Olga-Joan Ktenidou, Walter J. Silva, Robert B. Darragh, and Jennie Watson-Lamprey. June 2014.
- PEER 2014/08** *Unbonded Pretensioned Bridge Columns with Rocking Detail.* Jeffrey A. Schaefer, Bryan Kennedy, Marc O. Eberhard, John F. Stanton. June 2014.
- PEER 2014/07** *Northridge 20 Symposium Summary Report: Impacts, Outcomes, and Next Steps.* May 2014.
- PEER 2014/06** *Report of the Tenth Planning Meeting of NEES/E-Defense Collaborative Research on Earthquake Engineering.* December 2013.
- PEER 2014/05** *Seismic Velocity Site Characterization of Thirty-One Chilean Seismometer Stations by Spectral Analysis of Surface Wave Dispersion.* Robert Kayen, Brad D. Carkin, Skye Corbet, Camilo Pinilla, Allan Ng, Edward Gorbis, and Christine Truong. April 2014.
- PEER 2014/04** *Effect of Vertical Acceleration on Shear Strength of Reinforced Concrete Columns.* Hyerin Lee and Khalid M. Mosalam. April 2014.
- PEER 2014/03** *Retest of Thirty-Year-Old Neoprene Isolation Bearings.* James M. Kelly and Niel C. Van Engelen. March 2014.

- PEER 2014/02** *Theoretical Development of Hybrid Simulation Applied to Plate Structures.* Ahmed A. Bakhaty, Khalid M. Mosalam, and Sanjay Govindjee. January 2014.
- PEER 2014/01** *Performance-Based Seismic Assessment of Skewed Bridges.* Peyman Kaviani, Farzin Zareian, and Ertugrul Taciroglu. January 2014.
- PEER 2013/26** *Urban Earthquake Engineering. Proceedings of the U.S.-Iran Seismic Workshop.* December 2013.
- PEER 2013/25** *Earthquake Engineering for Resilient Communities: 2013 PEER Internship Program Research Report Collection.* Heidi Tremayne (Editor), Stephen A. Mahin (Editor), Jorge Archbold Monterossa, Matt Brosman, Shelly Dean, Katherine deLaveaga, Curtis Fong, Donovan Holder, Rakeeb Khan, Elizabeth Jachens, David Lam, Daniela Martinez Lopez, Mara Minner, Geffen Oren, Julia Pavicic, Melissa Quinonez, Lorena Rodriguez, Sean Salazar, Kelli Slaven, Vivian Steyert, Jenny Taing, and Salvador Tena. December 2013.
- PEER 2013/24** *NGA-West2 Ground Motion Prediction Equations for Vertical Ground Motions.* September 2013.
- PEER 2013/23** *Coordinated Planning and Preparedness for Fire Following Major Earthquakes.* Charles Scawthorn. November 2013.
- PEER 2013/22** *GEM-PEER Task 3 Project: Selection of a Global Set of Ground Motion Prediction Equations.* Jonathan P. Stewart, John Douglas, Mohammad B. Javanbarg, Carola Di Alessandro, Yousef Bozorgnia, Norman A. Abrahamson, David M. Boore, Kenneth W. Campbell, Elise Delavaud, Mustafa Erdik and Peter J. Stafford. December 2013.
- PEER 2013/21** *Seismic Design and Performance of Bridges with Columns on Rocking Foundations.* Grigorios Antonellis and Marios Panagiotou. September 2013.
- PEER 2013/20** *Experimental and Analytical Studies on the Seismic Behavior of Conventional and Hybrid Braced Frames.* Jiun-Wei Lai and Stephen A. Mahin. September 2013.
- PEER 2013/19** *Toward Resilient Communities: A Performance-Based Engineering Framework for Design and Evaluation of the Built Environment.* Michael William Mieler, Bozidar Stojadinovic, Robert J. Budnitz, Stephen A. Mahin and Mary C. Comerio. September 2013.
- PEER 2013/18** *Identification of Site Parameters that Improve Predictions of Site Amplification.* Ellen M. Rathje and Sara Navidi. July 2013.
- PEER 2013/17** *Response Spectrum Analysis of Concrete Gravity Dams Including Dam-Water-Foundation Interaction.* Arnkjell Løkke and Anil K. Chopra. July 2013.
- PEER 2013/16** *Effect of hoop reinforcement spacing on the cyclic response of large reinforced concrete special moment frame beams.* Marios Panagiotou, Tea Visnjic, Grigorios Antonellis, Panagiotis Galanis, and Jack P. Moehle. June 2013.
- PEER 2013/15** *A Probabilistic Framework to Include the Effects of Near-Fault Directivity in Seismic Hazard Assessment.* Shrey Kumar Shahi, Jack W. Baker. October 2013.
- PEER 2013/14** *Hanging-Wall Scaling using Finite-Fault Simulations.* Jennifer L. Donahue and Norman A. Abrahamson. September 2013.
- PEER 2013/13** *Semi-Empirical Nonlinear Site Amplification and its Application in NEHRP Site Factors.* Jonathan P. Stewart and Emel Seyhan. November 2013.
- PEER 2013/12** *Nonlinear Horizontal Site Response for the NGA-West2 Project.* Ronnie Kamai, Norman A. Abramson, Walter J. Silva. May 2013.
- PEER 2013/11** *Epistemic Uncertainty for NGA-West2 Models.* Linda Al Atik and Robert R. Youngs. May 2013.
- PEER 2013/10** *NGA-West 2 Models for Ground-Motion Directionality.* Shrey K. Shahi and Jack W. Baker. May 2013.
- PEER 2013/09** *Final Report of the NGA-West2 Directivity Working Group.* Paul Spudich, Jeffrey R. Bayless, Jack W. Baker, Brian S.J. Chiou, Badie Rowshandel, Shrey Shahi, and Paul Somerville. May 2013.
- PEER 2013/08** *NGA-West2 Model for Estimating Average Horizontal Values of Pseudo-Absolute Spectral Accelerations Generated by Crustal Earthquakes.* I. M. Idriss. May 2013.
- PEER 2013/07** *Update of the Chiou and Youngs NGA Ground Motion Model for Average Horizontal Component of Peak Ground Motion and Response Spectra.* Brian Chiou and Robert Youngs. May 2013.
- PEER 2013/06** *NGA-West2 Campbell-Bozorgnia Ground Motion Model for the Horizontal Components of PGA, PGV, and 5%-Damped Elastic Pseudo-Acceleration Response Spectra for Periods Ranging from 0.01 to 10 sec.* Kenneth W. Campbell and Yousef Bozorgnia. May 2013.
- PEER 2013/05** *NGA-West 2 Equations for Predicting Response Spectral Accelerations for Shallow Crustal Earthquakes.* David M. Boore, Jonathan P. Stewart, Emel Seyhan, Gail M. Atkinson. May 2013.

- PEER 2013/04** *Update of the AS08 Ground-Motion Prediction Equations Based on the NGA-West2 Data Set.* Norman Abrahamson, Walter Silva, and Ronnie Kamai. May 2013.
- PEER 2013/03** *PEER NGA-West2 Database.* Timothy D. Ancheta, Robert B. Darragh, Jonathan P. Stewart, Emel Seyhan, Walter J. Silva, Brian S.J. Chiou, Katie E. Wooddell, Robert W. Graves, Albert R. Kottke, David M. Boore, Tadahiro Kishida, and Jennifer L. Donahue. May 2013.
- PEER 2013/02** *Hybrid Simulation of the Seismic Response of Squat Reinforced Concrete Shear Walls.* Catherine A. Whyte and Bozidar Stojadinovic. May 2013.
- PEER 2013/01** *Housing Recovery in Chile: A Qualitative Mid-program Review.* Mary C. Comerio. February 2013.
- PEER 2012/08** *Guidelines for Estimation of Shear Wave Velocity.* Bernard R. Wair, Jason T. DeJong, and Thomas Shantz. December 2012.
- PEER 2012/07** *Earthquake Engineering for Resilient Communities: 2012 PEER Internship Program Research Report Collection.* Heidi Tremayne (Editor), Stephen A. Mahin (Editor), Collin Anderson, Dustin Cook, Michael Erceg, Carlos Esparza, Jose Jimenez, Dorian Krausz, Andrew Lo, Stephanie Lopez, Nicole McCurdy, Paul Shipman, Alexander Strum, Eduardo Vega. December 2012.
- PEER 2012/06** *Fragilities for Precarious Rocks at Yucca Mountain.* Matthew D. Purvance, Rasool Anooshehpoor, and James N. Brune. December 2012.
- PEER 2012/05** *Development of Simplified Analysis Procedure for Piles in Laterally Spreading Layered Soils.* Christopher R. McGann, Pedro Arduino, and Peter Mackenzie-Helnwein. December 2012.
- PEER 2012/04** *Unbonded Pre-Tensioned Columns for Bridges in Seismic Regions.* Phillip M. Davis, Todd M. Janes, Marc O. Eberhard, and John F. Stanton. December 2012.
- PEER 2012/03** *Experimental and Analytical Studies on Reinforced Concrete Buildings with Seismically Vulnerable Beam-Column Joints.* Sangjoon Park and Khalid M. Mosalam. October 2012.
- PEER 2012/02** *Seismic Performance of Reinforced Concrete Bridges Allowed to Uplift during Multi-Directional Excitation.* Andres Oscar Espinoza and Stephen A. Mahin. July 2012.
- PEER 2012/01** *Spectral Damping Scaling Factors for Shallow Crustal Earthquakes in Active Tectonic Regions.* Sanaz Rezaeian, Yousef Bozorgnia, I. M. Idriss, Kenneth Campbell, Norman Abrahamson, and Walter Silva. July 2012.
- PEER 2011/10** *Earthquake Engineering for Resilient Communities: 2011 PEER Internship Program Research Report Collection.* Eds. Heidi Faison and Stephen A. Mahin. December 2011.
- PEER 2011/09** *Calibration of Semi-Stochastic Procedure for Simulating High-Frequency Ground Motions.* Jonathan P. Stewart, Emel Seyhan, and Robert W. Graves. December 2011.
- PEER 2011/08** *Water Supply in regard to Fire Following Earthquake.* Charles Scawthorn. November 2011.
- PEER 2011/07** *Seismic Risk Management in Urban Areas. Proceedings of a U.S.-Iran-Turkey Seismic Workshop.* September 2011.
- PEER 2011/06** *The Use of Base Isolation Systems to Achieve Complex Seismic Performance Objectives.* Troy A. Morgan and Stephen A. Mahin. July 2011.
- PEER 2011/05** *Case Studies of the Seismic Performance of Tall Buildings Designed by Alternative Means.* Task 12 Report for the Tall Buildings Initiative. Jack Moehle, Yousef Bozorgnia, Nirmal Jayaram, Pierson Jones, Mohsen Rahnama, Nilesh Shome, Zeynep Tuna, John Wallace, Tony Yang, and Farzin Zareian. July 2011.
- PEER 2011/04** *Recommended Design Practice for Pile Foundations in Laterally Spreading Ground.* Scott A. Ashford, Ross W. Boulanger, and Scott J. Brandenberg. June 2011.
- PEER 2011/03** *New Ground Motion Selection Procedures and Selected Motions for the PEER Transportation Research Program.* Jack W. Baker, Ting Lin, Shrey K. Shahi, and Nirmal Jayaram. March 2011.
- PEER 2011/02** *A Bayesian Network Methodology for Infrastructure Seismic Risk Assessment and Decision Support.* Michelle T. Bensi, Armen Der Kiureghian, and Daniel Straub. March 2011.
- PEER 2011/01** *Demand Fragility Surfaces for Bridges in Liquefied and Laterally Spreading Ground.* Scott J. Brandenberg, Jian Zhang, Pirooz Kashighandi, Yili Huo, and Minxing Zhao. March 2011.
- PEER 2010/05** *Guidelines for Performance-Based Seismic Design of Tall Buildings.* Developed by the Tall Buildings Initiative. November 2010.
- PEER 2010/04** *Application Guide for the Design of Flexible and Rigid Bus Connections between Substation Equipment Subjected to Earthquakes.* Jean-Bernard Dastous and Armen Der Kiureghian. September 2010.
- PEER 2010/03** *Shear Wave Velocity as a Statistical Function of Standard Penetration Test Resistance and Vertical Effective Stress at Caltrans Bridge Sites.* Scott J. Brandenberg, Naresh Bellana, and Thomas Shantz. June 2010.

- PEER 2010/02** *Stochastic Modeling and Simulation of Ground Motions for Performance-Based Earthquake Engineering.* Sanaz Rezaeian and Armen Der Kiureghian. June 2010.
- PEER 2010/01** *Structural Response and Cost Characterization of Bridge Construction Using Seismic Performance Enhancement Strategies.* Ady Aviram, Božidar Stojadinović, Gustavo J. Parra-Montesinos, and Kevin R. Mackie. March 2010.
- PEER 2009/03** *The Integration of Experimental and Simulation Data in the Study of Reinforced Concrete Bridge Systems Including Soil-Foundation-Structure Interaction.* Matthew Dryden and Gregory L. Fenves. November 2009.
- PEER 2009/02** *Improving Earthquake Mitigation through Innovations and Applications in Seismic Science, Engineering, Communication, and Response. Proceedings of a U.S.-Iran Seismic Workshop.* October 2009.
- PEER 2009/01** *Evaluation of Ground Motion Selection and Modification Methods: Predicting Median Interstory Drift Response of Buildings.* Curt B. Haselton, Ed. June 2009.
- PEER 2008/10** *Technical Manual for Strata.* Albert R. Kottke and Ellen M. Rathje. February 2009.
- PEER 2008/09** *NGA Model for Average Horizontal Component of Peak Ground Motion and Response Spectra.* Brian S.-J. Chiou and Robert R. Youngs. November 2008.
- PEER 2008/08** *Toward Earthquake-Resistant Design of Concentrically Braced Steel Structures.* Patxi Uriz and Stephen A. Mahin. November 2008.
- PEER 2008/07** *Using OpenSees for Performance-Based Evaluation of Bridges on Liquefiable Soils.* Stephen L. Kramer, Pedro Arduino, and HyungSuk Shin. November 2008.
- PEER 2008/06** *Shaking Table Tests and Numerical Investigation of Self-Centering Reinforced Concrete Bridge Columns.* Hyung IL Jeong, Junichi Sakai, and Stephen A. Mahin. September 2008.
- PEER 2008/05** *Performance-Based Earthquake Engineering Design Evaluation Procedure for Bridge Foundations Undergoing Liquefaction-Induced Lateral Ground Displacement.* Christian A. Ledezma and Jonathan D. Bray. August 2008.
- PEER 2008/04** *Benchmarking of Nonlinear Geotechnical Ground Response Analysis Procedures.* Jonathan P. Stewart, Annie On-Lei Kwok, Yousseff M. A. Hashash, Neven Matasovic, Robert Pyke, Zhiliang Wang, and Zhaohui Yang. August 2008.
- PEER 2008/03** *Guidelines for Nonlinear Analysis of Bridge Structures in California.* Ady Aviram, Kevin R. Mackie, and Božidar Stojadinović. August 2008.
- PEER 2008/02** *Treatment of Uncertainties in Seismic-Risk Analysis of Transportation Systems.* Evangelos Stergiou and Anne S. Kiremidjian. July 2008.
- PEER 2008/01** *Seismic Performance Objectives for Tall Buildings.* William T. Holmes, Charles Kircher, William Petak, and Nabih Youssef. August 2008.
- PEER 2007/12** *An Assessment to Benchmark the Seismic Performance of a Code-Conforming Reinforced Concrete Moment-Frame Building.* Curt Haselton, Christine A. Goulet, Judith Mitrani-Reiser, James L. Beck, Gregory G. Deierlein, Keith A. Porter, Jonathan P. Stewart, and Ertugrul Taciroglu. August 2008.
- PEER 2007/11** *Bar Buckling in Reinforced Concrete Bridge Columns.* Wayne A. Brown, Dawn E. Lehman, and John F. Stanton. February 2008.
- PEER 2007/10** *Computational Modeling of Progressive Collapse in Reinforced Concrete Frame Structures.* Mohamed M. Talaat and Khalid M. Mosalam. May 2008.
- PEER 2007/09** *Integrated Probabilistic Performance-Based Evaluation of Benchmark Reinforced Concrete Bridges.* Kevin R. Mackie, John-Michael Wong, and Božidar Stojadinović. January 2008.
- PEER 2007/08** *Assessing Seismic Collapse Safety of Modern Reinforced Concrete Moment-Frame Buildings.* Curt B. Haselton and Gregory G. Deierlein. February 2008.
- PEER 2007/07** *Performance Modeling Strategies for Modern Reinforced Concrete Bridge Columns.* Michael P. Berry and Marc O. Eberhard. April 2008.
- PEER 2007/06** *Development of Improved Procedures for Seismic Design of Buried and Partially Buried Structures.* Linda Al Atik and Nicholas Sitar. June 2007.
- PEER 2007/05** *Uncertainty and Correlation in Seismic Risk Assessment of Transportation Systems.* Renee G. Lee and Anne S. Kiremidjian. July 2007.
- PEER 2007/04** *Numerical Models for Analysis and Performance-Based Design of Shallow Foundations Subjected to Seismic Loading.* Sivapalan Gajan, Tara C. Hutchinson, Bruce L. Kutter, Prishati Raychowdhury, José A. Ugalde, and Jonathan P. Stewart. May 2008.
- PEER 2007/03** *Beam-Column Element Model Calibrated for Predicting Flexural Response Leading to Global Collapse of RC Frame Buildings.* Curt B. Haselton, Abbie B. Liel, Sarah Taylor Lange, and Gregory G. Deierlein. May 2008.

- PEER 2007/02** *Campbell-Bozorgnia NGA Ground Motion Relations for the Geometric Mean Horizontal Component of Peak and Spectral Ground Motion Parameters.* Kenneth W. Campbell and Yousef Bozorgnia. May 2007.
- PEER 2007/01** *Boore-Atkinson NGA Ground Motion Relations for the Geometric Mean Horizontal Component of Peak and Spectral Ground Motion Parameters.* David M. Boore and Gail M. Atkinson. May. May 2007.
- PEER 2006/12** *Societal Implications of Performance-Based Earthquake Engineering.* Peter J. May. May 2007.
- PEER 2006/11** *Probabilistic Seismic Demand Analysis Using Advanced Ground Motion Intensity Measures, Attenuation Relationships, and Near-Fault Effects.* Polsak Tothong and C. Allin Cornell. March 2007.
- PEER 2006/10** *Application of the PEER PBEE Methodology to the I-880 Viaduct.* Sashi Kunnath. February 2007.
- PEER 2006/09** *Quantifying Economic Losses from Travel Forgone Following a Large Metropolitan Earthquake.* James Moore, Sungbin Cho, Yue Yue Fan, and Stuart Werner. November 2006.
- PEER 2006/08** *Vector-Valued Ground Motion Intensity Measures for Probabilistic Seismic Demand Analysis.* Jack W. Baker and C. Allin Cornell. October 2006.
- PEER 2006/07** *Analytical Modeling of Reinforced Concrete Walls for Predicting Flexural and Coupled-Shear-Flexural Responses.* Kutay Orakcal, Leonardo M. Massone, and John W. Wallace. October 2006.
- PEER 2006/06** *Nonlinear Analysis of a Soil-Drilled Pier System under Static and Dynamic Axial Loading.* Gang Wang and Nicholas Sitar. November 2006.
- PEER 2006/05** *Advanced Seismic Assessment Guidelines.* Paolo Bazzurro, C. Allin Cornell, Charles Menun, Maziar Motahari, and Nicolas Luco. September 2006.
- PEER 2006/04** *Probabilistic Seismic Evaluation of Reinforced Concrete Structural Components and Systems.* Tae Hyung Lee and Khalid M. Mosalam. August 2006.
- PEER 2006/03** *Performance of Lifelines Subjected to Lateral Spreading.* Scott A. Ashford and Teerawut Juimarongrit. July 2006.
- PEER 2006/02** *Pacific Earthquake Engineering Research Center Highway Demonstration Project.* Anne Kiremidjian, James Moore, Yue Yue Fan, Nesrin Basoz, Ozgur Yazali, and Meredith Williams. April 2006.
- PEER 2006/01** *Bracing Berkeley. A Guide to Seismic Safety on the UC Berkeley Campus.* Mary C. Comerio, Stephen Tobriner, and Ariane Fehrenkamp. January 2006.
- PEER 2005/16** *Seismic Response and Reliability of Electrical Substation Equipment and Systems.* Junho Song, Armen Der Kiureghian, and Jerome L. Sackman. April 2006.
- PEER 2005/15** *CPT-Based Probabilistic Assessment of Seismic Soil Liquefaction Initiation.* R. E. S. Moss, R. B. Seed, R. E. Kayen, J. P. Stewart, and A. Der Kiureghian. April 2006.
- PEER 2005/14** *Workshop on Modeling of Nonlinear Cyclic Load-Deformation Behavior of Shallow Foundations.* Bruce L. Kutter, Geoffrey Martin, Tara Hutchinson, Chad Harden, Sivapalan Gajan, and Justin Phalen. March 2006.
- PEER 2005/13** *Stochastic Characterization and Decision Bases under Time-Dependent Aftershock Risk in Performance-Based Earthquake Engineering.* Gee Liek Yeo and C. Allin Cornell. July 2005.
- PEER 2005/12** *PEER Testbed Study on a Laboratory Building: Exercising Seismic Performance Assessment.* Mary C. Comerio, editor. November 2005.
- PEER 2005/11** *Van Nuys Hotel Building Testbed Report: Exercising Seismic Performance Assessment.* Helmut Krawinkler, editor. October 2005.
- PEER 2005/10** *First NEES/E-Defense Workshop on Collapse Simulation of Reinforced Concrete Building Structures.* September 2005.
- PEER 2005/09** *Test Applications of Advanced Seismic Assessment Guidelines.* Joe Maffei, Karl Telleen, Danya Mohr, William Holmes, and Yuki Nakayama. August 2006.
- PEER 2005/08** *Damage Accumulation in Lightly Confined Reinforced Concrete Bridge Columns.* R. Tyler Ranf, Jared M. Nelson, Zach Price, Marc O. Eberhard, and John F. Stanton. April 2006.
- PEER 2005/07** *Experimental and Analytical Studies on the Seismic Response of Freestanding and Anchored Laboratory Equipment.* Dimitrios Konstantinidis and Nicos Makris. January 2005.
- PEER 2005/06** *Global Collapse of Frame Structures under Seismic Excitations.* Luis F. Ibarra and Helmut Krawinkler. September 2005.
- PEER 2005/05** *Performance Characterization of Bench- and Shelf-Mounted Equipment.* Samit Ray Chaudhuri and Tara C. Hutchinson. May 2006.

- PEER 2005/04** *Numerical Modeling of the Nonlinear Cyclic Response of Shallow Foundations.* Chad Harden, Tara Hutchinson, Geoffrey R. Martin, and Bruce L. Kutter. August 2005.
- PEER 2005/03** *A Taxonomy of Building Components for Performance-Based Earthquake Engineering.* Keith A. Porter. September 2005.
- PEER 2005/02** *Fragility Basis for California Highway Overpass Bridge Seismic Decision Making.* Kevin R. Mackie and Božidar Stojadinović. June 2005.
- PEER 2005/01** *Empirical Characterization of Site Conditions on Strong Ground Motion.* Jonathan P. Stewart, Yoojoong Choi, and Robert W. Graves. June 2005.
- PEER 2004/09** *Electrical Substation Equipment Interaction: Experimental Rigid Conductor Studies.* Christopher Stearns and André Filiatrault. February 2005.
- PEER 2004/08** *Seismic Qualification and Fragility Testing of Line Break 550-kV Disconnect Switches.* Shakhzod M. Takhirov, Gregory L. Fenves, and Eric Fujisaki. January 2005.
- PEER 2004/07** *Ground Motions for Earthquake Simulator Qualification of Electrical Substation Equipment.* Shakhzod M. Takhirov, Gregory L. Fenves, Eric Fujisaki, and Don Clyde. January 2005.
- PEER 2004/06** *Performance-Based Regulation and Regulatory Regimes.* Peter J. May and Chris Koski. September 2004.
- PEER 2004/05** *Performance-Based Seismic Design Concepts and Implementation: Proceedings of an International Workshop.* Peter Fajfar and Helmut Krawinkler, editors. September 2004.
- PEER 2004/04** *Seismic Performance of an Instrumented Tilt-up Wall Building.* James C. Anderson and Vitelmo V. Bertero. July 2004.
- PEER 2004/03** *Evaluation and Application of Concrete Tilt-up Assessment Methodologies.* Timothy Graf and James O. Malley. October 2004.
- PEER 2004/02** *Analytical Investigations of New Methods for Reducing Residual Displacements of Reinforced Concrete Bridge Columns.* Junichi Sakai and Stephen A. Mahin. August 2004.
- PEER 2004/01** *Seismic Performance of Masonry Buildings and Design Implications.* Kerri Anne Taeko Tokoro, James C. Anderson, and Vitelmo V. Bertero. February 2004.
- PEER 2003/18** *Performance Models for Flexural Damage in Reinforced Concrete Columns.* Michael Berry and Marc Eberhard. August 2003.
- PEER 2003/17** *Predicting Earthquake Damage in Older Reinforced Concrete Beam-Column Joints.* Catherine Pagni and Laura Lowes. October 2004.
- PEER 2003/16** *Seismic Demands for Performance-Based Design of Bridges.* Kevin Mackie and Božidar Stojadinović. August 2003.
- PEER 2003/15** *Seismic Demands for Nondeteriorating Frame Structures and Their Dependence on Ground Motions.* Ricardo Antonio Medina and Helmut Krawinkler. May 2004.
- PEER 2003/14** *Finite Element Reliability and Sensitivity Methods for Performance-Based Earthquake Engineering.* Terje Haukaas and Armen Der Kiureghian. April 2004.
- PEER 2003/13** *Effects of Connection Hysteretic Degradation on the Seismic Behavior of Steel Moment-Resisting Frames.* Janise E. Rodgers and Stephen A. Mahin. March 2004.
- PEER 2003/12** *Implementation Manual for the Seismic Protection of Laboratory Contents: Format and Case Studies.* William T. Holmes and Mary C. Comerio. October 2003.
- PEER 2003/11** *Fifth U.S.-Japan Workshop on Performance-Based Earthquake Engineering Methodology for Reinforced Concrete Building Structures.* February 2004.
- PEER 2003/10** *A Beam-Column Joint Model for Simulating the Earthquake Response of Reinforced Concrete Frames.* Laura N. Lowes, Nilanjan Mitra, and Arash Altoontash. February 2004.
- PEER 2003/09** *Sequencing Repairs after an Earthquake: An Economic Approach.* Marco Casari and Simon J. Wilkie. April 2004.
- PEER 2003/08** *A Technical Framework for Probability-Based Demand and Capacity Factor Design (DCFD) Seismic Formats.* Fatemeh Jalayer and C. Allin Cornell. November 2003.
- PEER 2003/07** *Uncertainty Specification and Propagation for Loss Estimation Using FOSM Methods.* Jack W. Baker and C. Allin Cornell. September 2003.
- PEER 2003/06** *Performance of Circular Reinforced Concrete Bridge Columns under Bidirectional Earthquake Loading.* Mahmoud M. Hachem, Stephen A. Mahin, and Jack P. Moehle. February 2003.

- PEER 2003/05** *Response Assessment for Building-Specific Loss Estimation.* Eduardo Miranda and Shahram Taghavi. September 2003.
- PEER 2003/04** *Experimental Assessment of Columns with Short Lap Splices Subjected to Cyclic Loads.* Murat Melek, John W. Wallace, and Joel Conte. April 2003.
- PEER 2003/03** *Probabilistic Response Assessment for Building-Specific Loss Estimation.* Eduardo Miranda and Hesameddin Aslani. September 2003.
- PEER 2003/02** *Software Framework for Collaborative Development of Nonlinear Dynamic Analysis Program.* Jun Peng and Kincho H. Law. September 2003.
- PEER 2003/01** *Shake Table Tests and Analytical Studies on the Gravity Load Collapse of Reinforced Concrete Frames.* Kenneth John Elwood and Jack P. Moehle. November 2003.
- PEER 2002/24** *Performance of Beam to Column Bridge Joints Subjected to a Large Velocity Pulse.* Natalie Gibson, André Filiatrault, and Scott A. Ashford. April 2002.
- PEER 2002/23** *Effects of Large Velocity Pulses on Reinforced Concrete Bridge Columns.* Greg L. Orozco and Scott A. Ashford. April 2002.
- PEER 2002/22** *Characterization of Large Velocity Pulses for Laboratory Testing.* Kenneth E. Cox and Scott A. Ashford. April 2002.
- PEER 2002/21** *Fourth U.S.-Japan Workshop on Performance-Based Earthquake Engineering Methodology for Reinforced Concrete Building Structures.* December 2002.
- PEER 2002/20** *Barriers to Adoption and Implementation of PBEE Innovations.* Peter J. May. August 2002.
- PEER 2002/19** *Economic-Engineered Integrated Models for Earthquakes: Socioeconomic Impacts.* Peter Gordon, James E. Moore II, and Harry W. Richardson. July 2002.
- PEER 2002/18** *Assessment of Reinforced Concrete Building Exterior Joints with Substandard Details.* Chris P. Pantelides, Jon Hansen, Justin Nadauld, and Lawrence D. Reaveley. May 2002.
- PEER 2002/17** *Structural Characterization and Seismic Response Analysis of a Highway Overcrossing Equipped with Elastomeric Bearings and Fluid Dampers: A Case Study.* Nicos Makris and Jian Zhang. November 2002.
- PEER 2002/16** *Estimation of Uncertainty in Geotechnical Properties for Performance-Based Earthquake Engineering.* Allen L. Jones, Steven L. Kramer, and Pedro Arduino. December 2002.
- PEER 2002/15** *Seismic Behavior of Bridge Columns Subjected to Various Loading Patterns.* Asadollah Esmaeily-Gh. and Yan Xiao. December 2002.
- PEER 2002/14** *Inelastic Seismic Response of Extended Pile Shaft Supported Bridge Structures.* T.C. Hutchinson, R.W. Boulanger, Y.H. Chai, and I.M. Idriss. December 2002.
- PEER 2002/13** *Probabilistic Models and Fragility Estimates for Bridge Components and Systems.* Paolo Gardoni, Armen Der Kiureghian, and Khalid M. Mosalam. June 2002.
- PEER 2002/12** *Effects of Fault Dip and Slip Rake on Near-Source Ground Motions: Why Chi-Chi Was a Relatively Mild M7.6 Earthquake.* Brad T. Aagaard, John F. Hall, and Thomas H. Heaton. December 2002.
- PEER 2002/11** *Analytical and Experimental Study of Fiber-Reinforced Strip Isolators.* James M. Kelly and Shakhzod M. Takhirov. September 2002.
- PEER 2002/10** *Centrifuge Modeling of Settlement and Lateral Spreading with Comparisons to Numerical Analyses.* Sivapalan Gajan and Bruce L. Kutter. January 2003.
- PEER 2002/09** *Documentation and Analysis of Field Case Histories of Seismic Compression during the 1994 Northridge, California, Earthquake.* Jonathan P. Stewart, Patrick M. Smith, Daniel H. Whang, and Jonathan D. Bray. October 2002.
- PEER 2002/08** *Component Testing, Stability Analysis and Characterization of Buckling-Restrained Unbonded Braces<sup>TM</sup>.* Cameron Black, Nicos Makris, and Ian Aiken. September 2002.
- PEER 2002/07** *Seismic Performance of Pile-Wharf Connections.* Charles W. Roeder, Robert Graff, Jennifer Soderstrom, and Jun Han Yoo. December 2001.
- PEER 2002/06** *The Use of Benefit-Cost Analysis for Evaluation of Performance-Based Earthquake Engineering Decisions.* Richard O. Zerbe and Anthony Falit-Baimonte. September 2001.
- PEER 2002/05** *Guidelines, Specifications, and Seismic Performance Characterization of Nonstructural Building Components and Equipment.* André Filiatrault, Constantin Christopoulos, and Christopher Stearns. September 2001.

- PEER 2002/04** Consortium of Organizations for Strong-Motion Observation Systems and the Pacific Earthquake Engineering Research Center Lifelines Program: Invited Workshop on Archiving and Web Dissemination of Geotechnical Data, 4–5 October 2001. September 2002.
- PEER 2002/03** Investigation of Sensitivity of Building Loss Estimates to Major Uncertain Variables for the Van Nuys Testbed. Keith A. Porter, James L. Beck, and Rustem V. Shaikhutdinov. August 2002.
- PEER 2002/02** The Third U.S.-Japan Workshop on Performance-Based Earthquake Engineering Methodology for Reinforced Concrete Building Structures. July 2002.
- PEER 2002/01** Nonstructural Loss Estimation: The UC Berkeley Case Study. Mary C. Comerio and John C. Stallmeyer. December 2001.
- PEER 2001/16** Statistics of SDF-System Estimate of Roof Displacement for Pushover Analysis of Buildings. Anil K. Chopra, Rakesh K. Goel, and Chatpan Chintanapakdee. December 2001.
- PEER 2001/15** Damage to Bridges during the 2001 Nisqually Earthquake. R. Tyler Ranf, Marc O. Eberhard, and Michael P. Berry. November 2001.
- PEER 2001/14** Rocking Response of Equipment Anchored to a Base Foundation. Nicos Makris and Cameron J. Black. September 2001.
- PEER 2001/13** Modeling Soil Liquefaction Hazards for Performance-Based Earthquake Engineering. Steven L. Kramer and Ahmed-W. Elgamal. February 2001.
- PEER 2001/12** Development of Geotechnical Capabilities in OpenSees. Boris Jeremić. September 2001.
- PEER 2001/11** Analytical and Experimental Study of Fiber-Reinforced Elastomeric Isolators. James M. Kelly and Shakhzod M. Takhirov. September 2001.
- PEER 2001/10** Amplification Factors for Spectral Acceleration in Active Regions. Jonathan P. Stewart, Andrew H. Liu, Yoojoong Choi, and Mehmet B. Baturay. December 2001.
- PEER 2001/09** Ground Motion Evaluation Procedures for Performance-Based Design. Jonathan P. Stewart, Shyh-Jeng Chiou, Jonathan D. Bray, Robert W. Graves, Paul G. Somerville, and Norman A. Abrahamson. September 2001.
- PEER 2001/08** Experimental and Computational Evaluation of Reinforced Concrete Bridge Beam-Column Connections for Seismic Performance. Clay J. Naito, Jack P. Moehle, and Khalid M. Mosalam. November 2001.
- PEER 2001/07** The Rocking Spectrum and the Shortcomings of Design Guidelines. Nicos Makris and Dimitrios Konstantinidis. August 2001.
- PEER 2001/06** Development of an Electrical Substation Equipment Performance Database for Evaluation of Equipment Fragilities. Thalia Agnanos. April 1999.
- PEER 2001/05** Stiffness Analysis of Fiber-Reinforced Elastomeric Isolators. Hsiang-Chuan Tsai and James M. Kelly. May 2001.
- PEER 2001/04** Organizational and Societal Considerations for Performance-Based Earthquake Engineering. Peter J. May. April 2001.
- PEER 2001/03** A Modal Pushover Analysis Procedure to Estimate Seismic Demands for Buildings: Theory and Preliminary Evaluation. Anil K. Chopra and Rakesh K. Goel. January 2001.
- PEER 2001/02** Seismic Response Analysis of Highway Overcrossings Including Soil-Structure Interaction. Jian Zhang and Nicos Makris. March 2001.
- PEER 2001/01** Experimental Study of Large Seismic Steel Beam-to-Column Connections. Egor P. Popov and Shakhzod M. Takhirov. November 2000.
- PEER 2000/10** The Second U.S.-Japan Workshop on Performance-Based Earthquake Engineering Methodology for Reinforced Concrete Building Structures. March 2000.
- PEER 2000/09** Structural Engineering Reconnaissance of the August 17, 1999 Earthquake: Kocaeli (Izmit), Turkey. Halil Sezen, Kenneth J. Elwood, Andrew S. Whittaker, Khalid Mosalam, John J. Wallace, and John F. Stanton. December 2000.
- PEER 2000/08** Behavior of Reinforced Concrete Bridge Columns Having Varying Aspect Ratios and Varying Lengths of Confinement. Anthony J. Calderone, Dawn E. Lehman, and Jack P. Moehle. January 2001.
- PEER 2000/07** Cover-Plate and Flange-Plate Reinforced Steel Moment-Resisting Connections. Taejin Kim, Andrew S. Whittaker, Amir S. Gilani, Vitelmo V. Bertero, and Shakhzod M. Takhirov. September 2000.
- PEER 2000/06** Seismic Evaluation and Analysis of 230-kV Disconnect Switches. Amir S. J. Gilani, Andrew S. Whittaker, Gregory L. Fenves, Chun-Hao Chen, Henry Ho, and Eric Fujisaki. July 2000.

- PEER 2000/05** *Performance-Based Evaluation of Exterior Reinforced Concrete Building Joints for Seismic Excitation.* Chandra Clyde, Chris P. Pantelides, and Lawrence D. Reaveley. July 2000.
- PEER 2000/04** *An Evaluation of Seismic Energy Demand: An Attenuation Approach.* Chung-Che Chou and Chia-Ming Uang. July 1999.
- PEER 2000/03** *Framing Earthquake Retrofitting Decisions: The Case of Hillside Homes in Los Angeles.* Detlof von Winterfeldt, Nels Roselund, and Alicia Kitsuse. March 2000.
- PEER 2000/02** *U.S.-Japan Workshop on the Effects of Near-Field Earthquake Shaking.* Andrew Whittaker, ed. July 2000.
- PEER 2000/01** *Further Studies on Seismic Interaction in Interconnected Electrical Substation Equipment.* Armen Der Kiureghian, Kee-Jeung Hong, and Jerome L. Sackman. November 1999.
- PEER 1999/14** *Seismic Evaluation and Retrofit of 230-kV Porcelain Transformer Bushings.* Amir S. Gilani, Andrew S. Whittaker, Gregory L. Fenves, and Eric Fujisaki. December 1999.
- PEER 1999/13** *Building Vulnerability Studies: Modeling and Evaluation of Tilt-up and Steel Reinforced Concrete Buildings.* John W. Wallace, Jonathan P. Stewart, and Andrew S. Whittaker, editors. December 1999.
- PEER 1999/12** *Rehabilitation of Nonductile RC Frame Building Using Encasement Plates and Energy-Dissipating Devices.* Mehrdad Sasani, Vitelmo V. Bertero, James C. Anderson. December 1999.
- PEER 1999/11** *Performance Evaluation Database for Concrete Bridge Components and Systems under Simulated Seismic Loads.* Yael D. Hose and Frieder Seible. November 1999.
- PEER 1999/10** *U.S.-Japan Workshop on Performance-Based Earthquake Engineering Methodology for Reinforced Concrete Building Structures.* December 1999.
- PEER 1999/09** *Performance Improvement of Long Period Building Structures Subjected to Severe Pulse-Type Ground Motions.* James C. Anderson, Vitelmo V. Bertero, and Raul Bertero. October 1999.
- PEER 1999/08** *Envelopes for Seismic Response Vectors.* Charles Menun and Armen Der Kiureghian. July 1999.
- PEER 1999/07** *Documentation of Strengths and Weaknesses of Current Computer Analysis Methods for Seismic Performance of Reinforced Concrete Members.* William F. Cofer. November 1999.
- PEER 1999/06** *Rocking Response and Overturning of Anchored Equipment under Seismic Excitations.* Nicos Makris and Jian Zhang. November 1999.
- PEER 1999/05** *Seismic Evaluation of 550 kV Porcelain Transformer Bushings.* Amir S. Gilani, Andrew S. Whittaker, Gregory L. Fenves, and Eric Fujisaki. October 1999.
- PEER 1999/04** *Adoption and Enforcement of Earthquake Risk-Reduction Measures.* Peter J. May, Raymond J. Burby, T. Jens Feeley, and Robert Wood.
- PEER 1999/03** *Task 3 Characterization of Site Response General Site Categories.* Adrian Rodriguez-Marek, Jonathan D. Bray, and Norman Abrahamson. February 1999.
- PEER 1999/02** *Capacity-Demand-Diagram Methods for Estimating Seismic Deformation of Inelastic Structures: SDF Systems.* Anil K. Chopra and Rakesh Goel. April 1999.
- PEER 1999/01** *Interaction in Interconnected Electrical Substation Equipment Subjected to Earthquake Ground Motions.* Armen Der Kiureghian, Jerome L. Sackman, and Kee-Jeung Hong. February 1999.
- PEER 1998/08** *Behavior and Failure Analysis of a Multiple-Frame Highway Bridge in the 1994 Northridge Earthquake.* Gregory L. Fenves and Michael Ellery. December 1998.
- PEER 1998/07** *Empirical Evaluation of Inertial Soil-Structure Interaction Effects.* Jonathan P. Stewart, Raymond B. Seed, and Gregory L. Fenves. November 1998.
- PEER 1998/06** *Effect of Damping Mechanisms on the Response of Seismic Isolated Structures.* Nicos Makris and Shih-Po Chang. November 1998.
- PEER 1998/05** *Rocking Response and Overturning of Equipment under Horizontal Pulse-Type Motions.* Nicos Makris and Yiannis Roussos. October 1998.
- PEER 1998/04** *Pacific Earthquake Engineering Research Invitational Workshop Proceedings, May 14–15, 1998: Defining the Links between Planning, Policy Analysis, Economics and Earthquake Engineering.* Mary Comerio and Peter Gordon. September 1998.
- PEER 1998/03** *Repair/Upgrade Procedures for Welded Beam to Column Connections.* James C. Anderson and Xiaojing Duan. May 1998.
- PEER 1998/02** *Seismic Evaluation of 196 kV Porcelain Transformer Bushings.* Amir S. Gilani, Juan W. Chavez, Gregory L. Fenves, and Andrew S. Whittaker. May 1998.

**PEER 1998/01** *Seismic Performance of Well-Confining Concrete Bridge Columns.* Dawn E. Lehman and Jack P. Moehle. December 2000.

## ONLINE PEER REPORTS

The following PEER reports are available by Internet only at [http://peer.berkeley.edu/publications/peer\\_reports\\_complete.html](http://peer.berkeley.edu/publications/peer_reports_complete.html).

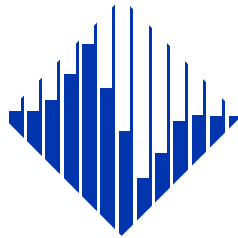
- PEER 2012/103** *Performance-Based Seismic Demand Assessment of Concentrically Braced Steel Frame Buildings.* Chui-Hsin Chen and Stephen A. Mahin. December 2012.
- PEER 2012/102** *Procedure to Restart an Interrupted Hybrid Simulation: Addendum to PEER Report 2010/103.* Vesna Terzic and Božidar Stojadinovic. October 2012.
- PEER 2012/101** *Mechanics of Fiber Reinforced Bearings.* James M. Kelly and Andrea Calabrese. February 2012.
- PEER 2011/107** *Nonlinear Site Response and Seismic Compression at Vertical Array Strongly Shaken by 2007 Niigata-ken Chuetsu-oki Earthquake.* Eric Yee, Jonathan P. Stewart, and Kohji Tokimatsu. December 2011.
- PEER 2011/106** *Self Compacting Hybrid Fiber Reinforced Concrete Composites for Bridge Columns.* Pardeep Kumar, Gabriel Jen, William Trono, Marios Panagiotou, and Claudia Ostertag. September 2011.
- PEER 2011/105** *Stochastic Dynamic Analysis of Bridges Subjected to Spatially Varying Ground Motions.* Katerina Konakli and Armen Der Kiureghian. August 2011.
- PEER 2011/104** *Design and Instrumentation of the 2010 E-Defense Four-Story Reinforced Concrete and Post-Tensioned Concrete Buildings.* Takuya Nagae, Kenichi Tahara, Taizo Matsumori, Hitoshi Shiohara, Toshimi Kabeyasawa, Susumu Kono, Minehiro Nishiyama (Japanese Research Team) and John Wallace, Wassim Ghannoum, Jack Moehle, Richard Sause, Wesley Keller, Zeynep Tuna (U.S. Research Team). June 2011.
- PEER 2011/103** *In-Situ Monitoring of the Force Output of Fluid Dampers: Experimental Investigation.* Dimitrios Konstantinidis, James M. Kelly, and Nicos Makris. April 2011.
- PEER 2011/102** *Ground-motion prediction equations 1964 - 2010.* John Douglas. April 2011.
- PEER 2011/101** *Report of the Eighth Planning Meeting of NEES/E-Defense Collaborative Research on Earthquake Engineering.* Convened by the Hyogo Earthquake Engineering Research Center (NIED), NEES Consortium, Inc. February 2011.
- PEER 2010/111** *Modeling and Acceptance Criteria for Seismic Design and Analysis of Tall Buildings.* Task 7 Report for the Tall Buildings Initiative - Published jointly by the Applied Technology Council. October 2010.
- PEER 2010/110** *Seismic Performance Assessment and Probabilistic Repair Cost Analysis of Precast Concrete Cladding Systems for Multistory Buildings.* Jeffrey P. Hunt and Božidar Stojadinovic. November 2010.
- PEER 2010/109** *Report of the Seventh Joint Planning Meeting of NEES/E-Defense Collaboration on Earthquake Engineering. Held at the E-Defense, Miki, and Shin-Kobe, Japan, September 18–19, 2009.* August 2010.
- PEER 2010/108** *Probabilistic Tsunami Hazard in California.* Hong Kie Thio, Paul Somerville, and Jascha Polet, preparers. October 2010.
- PEER 2010/107** *Performance and Reliability of Exposed Column Base Plate Connections for Steel Moment-Resisting Frames.* Ady Aviram, Božidar Stojadinovic, and Armen Der Kiureghian. August 2010.
- PEER 2010/106** *Verification of Probabilistic Seismic Hazard Analysis Computer Programs.* Patricia Thomas, Ivan Wong, and Norman Abrahamson. May 2010.
- PEER 2010/105** *Structural Engineering Reconnaissance of the April 6, 2009, Abruzzo, Italy, Earthquake, and Lessons Learned.* M. Selim Günay and Khalid M. Mosalam. April 2010.
- PEER 2010/104** *Simulating the Inelastic Seismic Behavior of Steel Braced Frames, Including the Effects of Low-Cycle Fatigue.* Yuli Huang and Stephen A. Mahin. April 2010.
- PEER 2010/103** *Post-Earthquake Traffic Capacity of Modern Bridges in California.* Vesna Terzic and Božidar Stojadinović. March 2010.
- PEER 2010/102** *Analysis of Cumulative Absolute Velocity (CAV) and JMA Instrumental Seismic Intensity ( $I_{JMA}$ ) Using the PEER-NGA Strong Motion Database.* Kenneth W. Campbell and Yousef Bozorgnia. February 2010.
- PEER 2010/101** *Rocking Response of Bridges on Shallow Foundations.* Jose A. Ugalde, Bruce L. Kutter, and Boris Jeremic. April 2010.
- PEER 2009/109** *Simulation and Performance-Based Earthquake Engineering Assessment of Self-Centering Post-Tensioned Concrete Bridge Systems.* Won K. Lee and Sarah L. Billington. December 2009.

- PEER 2009/108** *PEER Lifelines Geotechnical Virtual Data Center.* J. Carl Stepp, Daniel J. Ponti, Loren L. Turner, Jennifer N. Swift, Sean Devlin, Yang Zhu, Jean Benoit, and John Bobbitt. September 2009.
- PEER 2009/107** *Experimental and Computational Evaluation of Current and Innovative In-Span Hinge Details in Reinforced Concrete Box-Girder Bridges: Part 2: Post-Test Analysis and Design Recommendations.* Matias A. Hube and Khalid M. Mosalam. December 2009.
- PEER 2009/106** *Shear Strength Models of Exterior Beam-Column Joints without Transverse Reinforcement.* Sangjoon Park and Khalid M. Mosalam. November 2009.
- PEER 2009/105** *Reduced Uncertainty of Ground Motion Prediction Equations through Bayesian Variance Analysis.* Robb Eric S. Moss. November 2009.
- PEER 2009/104** *Advanced Implementation of Hybrid Simulation.* Andreas H. Schellenberg, Stephen A. Mahin, Gregory L. Fenves. November 2009.
- PEER 2009/103** *Performance Evaluation of Innovative Steel Braced Frames.* T. Y. Yang, Jack P. Moehle, and Božidar Stojadinovic. August 2009.
- PEER 2009/102** *Reinvestigation of Liquefaction and Nonliquefaction Case Histories from the 1976 Tangshan Earthquake.* Robb Eric Moss, Robert E. Kayen, Liyuan Tong, Songyu Liu, Guojun Cai, and Jiaer Wu. August 2009.
- PEER 2009/101** *Report of the First Joint Planning Meeting for the Second Phase of NEES/E-Defense Collaborative Research on Earthquake Engineering.* Stephen A. Mahin et al. July 2009.
- PEER 2008/104** *Experimental and Analytical Study of the Seismic Performance of Retaining Structures.* Linda Al Atik and Nicholas Sitar. January 2009.
- PEER 2008/103** *Experimental and Computational Evaluation of Current and Innovative In-Span Hinge Details in Reinforced Concrete Box-Girder Bridges. Part 1: Experimental Findings and Pre-Test Analysis.* Matias A. Hube and Khalid M. Mosalam. January 2009.
- PEER 2008/102** *Modeling of Unreinforced Masonry Infill Walls Considering In-Plane and Out-of-Plane Interaction.* Stephen Kadysiewski and Khalid M. Mosalam. January 2009.
- PEER 2008/101** *Seismic Performance Objectives for Tall Buildings.* William T. Holmes, Charles Kircher, William Petak, and Nabih Youssef. August 2008.
- PEER 2007/101** *Generalized Hybrid Simulation Framework for Structural Systems Subjected to Seismic Loading.* Tarek Elkhoraibi and Khalid M. Mosalam. July 2007.
- PEER 2007/100** *Seismic Evaluation of Reinforced Concrete Buildings Including Effects of Masonry Infill Walls.* Alidad Hashemi and Khalid M. Mosalam. July 2007.

The Pacific Earthquake Engineering Research Center (PEER) is a multi-institutional research and education center with headquarters at the University of California, Berkeley. Investigators from over 20 universities, several consulting companies, and researchers at various state and federal government agencies contribute to research programs focused on performance-based earthquake engineering.

These research programs aim to identify and reduce the risks from major earthquakes to life safety and to the economy by including research in a wide variety of disciplines including structural and geotechnical engineering, geology/seismology, lifelines, transportation, architecture, economics, risk management, and public policy.

PEER is supported by federal, state, local, and regional agencies, together with industry partners.



PEER Core Institutions:  
University of California, Berkeley (Lead Institution)  
California Institute of Technology  
Oregon State University  
Stanford University  
University of California, Davis  
University of California, Irvine  
University of California, Los Angeles  
University of California, San Diego  
University of Southern California  
University of Washington

PEER reports can be ordered at [http://peer.berkeley.edu/publications/peer\\_reports.html](http://peer.berkeley.edu/publications/peer_reports.html) or by contacting

Pacific Earthquake Engineering Research Center  
University of California, Berkeley  
325 Davis Hall, mail code 1792  
Berkeley, CA 94720-1792  
Tel: 510-642-3437  
Fax: 510-642-1655  
Email: [peer\\_editor@berkeley.edu](mailto:peer_editor@berkeley.edu)

ISSN 1547-0587X

@Seismicisolation